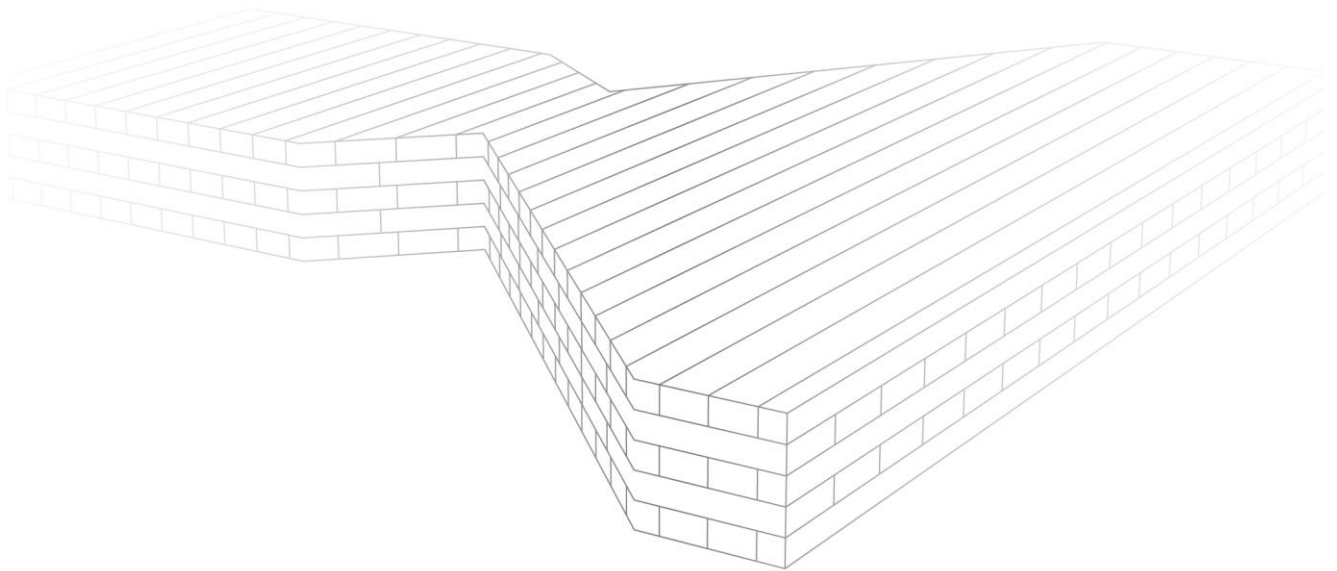


# Integral Design Process of CLT Structures and Robotic Fabrication

*An integral workflow for the preliminary structural design of CLT connection panels with the use of customized robotic fabrication*



G.J. Veldhuis

30-04-2020

MSc Thesis

# INTEGRAL DESIGN PROCESS OF CLT STRUCTURES AND ROBOTIC FABRICATION

An integral workflow for the preliminary structural design of CLT connection panels  
with the use of customized robotic fabrication

A thesis in

CIVIL ENGINEERING (CiTG), Master Building Engineering // Structural Design track

TU Delft

April 30, 2020

By

*Gerrit-Jan Veldhuis*

arjen\_gj@hotmail.com

Chair

*Prof. ir. R. Nijssen*

Thesis committee

*Dr. M. (Michela) Turrin*

*Ir. L.P.L. (Lennert) van der Linden*

*Ir. L. (Léon) Spikker*

*Ir. S. (Shibo) Ren (Supervisor)*

## Acknowledgement

This master's thesis defines the end of my studies at TU Delft. I had the privilege to not only gain knowledge in the field of structural design at this University, but also to enjoy my time as a student. The thesis is a collaboration of TU Delft, ARUP, and StudioRAP. Therefore, I thank these parties and the committee especially. Without their help I were not able to carry this graduation project to where it is right now.

I want to express my gratitude to Professor R. Nijse and Dr. M Turrin, who helped me deepening the scientific value of the research.

Also, I am grateful for the supervision of Shibo Ren. He always challenged me to explore different methodologies, choices, and techniques. It was not the first time to have him as a mentor, and his supervision always was of great value.

I thank Lennert van der Linden for his supervision regarding organizing the report properly and communicating messages clearly. Besides, he always was willing to help me out on technical issues. These lessons I will remind throughout my upcoming professional career.

Finally, I would like to thank StudioRAP for their collaboration with ARUP and TU Delft. They offered me unique opportunities to practically explore some of the processes of robotic fabrication. Special thanks I want to express to Léon Spikker, who triggered me to put this research in the proper perspective regarding robotic technologies.

Besides professional supervisors, I am firstly greatly indebted to my family, girlfriend, housemates and friends. Without their emotional and financial support, I never was able to complete my studies at TU Delft. Also, thanks to the kitchen of the Aida, Elzenlaan, and 'In de Bogaard'. The fresh meals in the train were great.

The One I thank in the last place deserves the first place. I thank God as my Father in heaven for all the strength, sharpness, energy and wisdom He provided each new day. To Him be the glory. Forever.

## Summary

Timber and complex designs are making a move in the building industry, as the building industry is on the brink of a significant change toward a 100% customized, more sustainable architecture. Robotic fabrication and Cross-Laminated Timber (CLT) can play an important role in this change, but there is a lot of uncertainty and ignorance about the design process of robotically fabricated CLT elements. This uncertainty is primarily caused by the application of linear workflows instead of integral ones. Within the fields of robotic fabrication and CLT, the research narrows down to the robotic milling process of CLT connection panels. Therefore, this research intends to answer the following question by means of four different parts:

*What does an integral workflow for robotically fabricated customized CLT connection panels look like, that promote exploration of the structural performance of CLT structures in the preliminary design phase?*

- Part I Literature Study
- Part II Pilot Study
- Part III Integral Workflow Development
- Part IV Discussions

The Literature Study focusses on two fields, namely the field of CLT and the field of robotic fabrication. In the final chapter of this part, the mutual affordances and constraints of these fields are discussed as these significantly influence the design space of the integral workflow. The second part concerns the production of a small mock-up to explore the process of robotic fabrication. The literature and pilot study together serve as input for the development of the integral workflow in the third part of the research. This workflow is developed in the parametric environment of Grasshopper and is divided in three modules.

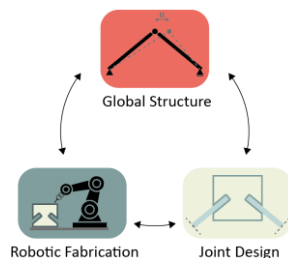


Figure i: Integral workflow with three integrated modules

Firstly, the Global Structure module focusses on the design of a CLT structure. Both the geometrical outline and Finite Element Method (FEM) models can be generated for a wide variety of geometries. An essential component of this module is the automated computation of the bending and shear stiffnesses of CLT plates in the strong and weak direction. Secondly, the Joint Design module explores the geometrical and structural modelling of a joint consisting of a CLT connection panel. The panel consists of slotted holes wherein the appending CLT structure is placed. This type of joint is derived from a commercial project in Alblasterdam where the initial design consisted of a CLT structure. Important components of the Joint Design module are the three-dimensional visualization of the CLT connection panel, an integrated tool to perform analytical Unity Check's (U.C.) to get a preliminar outline of the panel, and the generation of FEM models. Several methodologies with different accuracies were tested to determine the stiffness of the joints, and it was concluded from a higher level that the workflow can allow for a feedback loop to the Global Structure for the stiffness of the joints. However, a designer should ensure he is confident with the accuracy of the applicable methodology. No 100% accurate universal methodology was achieved, which is due to the large size of the panels ( $> 0.5\text{m} \times 0.5\text{m}$ ) and the orthotropic material properties.



Finally, the Robotic Fabrication module is discussed in this report. This module generates G-code for the robot to fabricate the customized CLT panel. The FEM models are validated by analytical calculations and relevant analytical U.C.'s. To keep the entire workflow inside the same software package, it was preferable if the Finite Element (FE) analyses were performed in Grasshopper by means of Karamba3D, a Grasshopper plugin to perform Finite Element Analyses (FEA). However, this software was not validated successfully and therefore the FEA are performed in GSA. Due to the parametric nature of the workflow, different FEM models can be generated effortlessly for both the Global Structure and Joint Design module. Subsequently, design graphs can be derived that inform a user about the influence of geometrical parameters on the structural performance of a structure or a joint. Each module consists of different components and each of these components are separately accessible, which increases the applicability of the integral workflow.

The main conclusions on the research question consist of the relationships and (in)dependencies between the different modules. Figure ii shows these relationships and (in)dependencies.

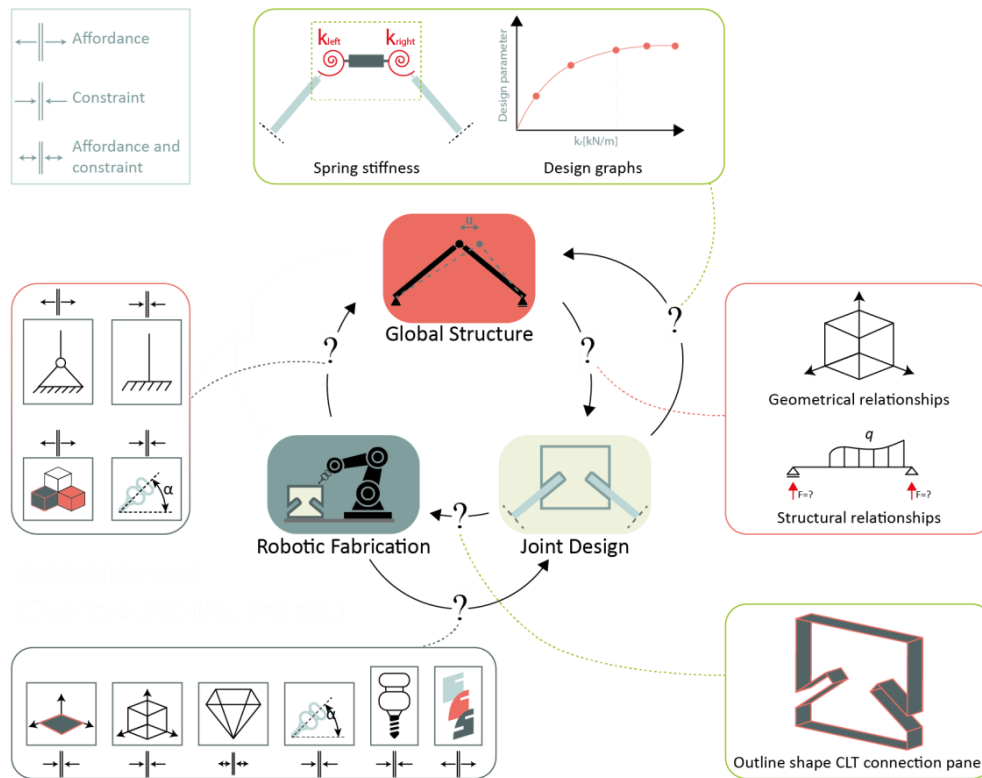


Figure ii: Relationships and (in)dependencies in the integral workflow

Another important conclusion is that one cannot apply CLT in the outdoor environment without applying shedding to ensure complete moisture control.

To increase the integrality of the workflow as developed in this research, more feedback loops across the three modules should be integrated. For instance, the affordances and constraints of the robotic fabrication process should be integrated within the relationships between the three modules. Hence, if doing so, this information was available in an early stage of the design process and would decrease the uncertainty of it. This implementation could be investigated by producing a mock-up study along the integral workflow.

**Keywords:** CLT, Robotic fabrication, integral workflow, CLT connection panel, preliminary design.

# TABLE OF CONTENTS

<b>INTRODUCTION</b>	<b>I. RESEARCH MOTIVATION</b>	<b>1</b>
	I.I ON CROSS-LAMINATED TIMBER STRUCTURES	1
	I.II ON CUSTOMIZED ROBOTIC FABRICATION	1
	<b>II. PROBLEM DEFINITION</b>	<b>2</b>
	<b>III. RESEARCH QUESTION</b>	<b>4</b>
	<b>IV. SCOPE AND OBJECTIVE</b>	<b>4</b>
	<b>V. RESEARCH METHODOLOGY</b>	<b>5</b>
<b>PART I: LITERATURE STUDY</b>	<b>1. CROSS-LAMINATED TIMBER</b>	<b>8</b>
	1.1 INTRODUCTION: WHAT IS CROSS-LAMINATED TIMBER?	8
	1.2 PRODUCTION AND SCALE	9
	1.3 DURABILITY	10
	1.4 FIRE SAFETY DESIGN	12
	1.5 MATERIAL PROPERTIES AND APPLICATIONS OF CLT	14
	1.6 STRUCTURAL DESIGN OF CLT	15
	1.7 POSSIBLE FAILURE MECHANISMS FOR CLT ELEMENTS	17
	1.8 POSSIBLE FAILURE MECHANISMS FOR CLT JOINTS	20
	1.9. CONCLUSION	23
	<b>2. CUSTOMIZED ROBOTIC FABRICATION</b>	<b>24</b>
	2.1 INTRODUCTION: WHAT IS A ROBOT?	24
	2.2 ROBOTIC SYSTEMS IN THE BUILDING INDUSTRY	25
	2.3 THE PROGRAM OF A ROBOTIC SYSTEM	28
	2.4 SCALE OF ROBOTIC FABRICATION IN THE BUILDING INDUSTRY	30
	2.5 SUITABLE MATERIALS FOR ROBOTIC OPERATIONS	31
	2.6 THE MAIN PURPOSE OF CUSTOMIZED ROBOTIC FABRICATION	32
	2.7 CONCLUSION	34
	<b>3. AFFORDANCES AND CONSTRAINTS OF CUSTOMIZED ROBOTICALLY FABRICATED CLT ELEMENTS</b>	<b>35</b>
	3.1 CROSS-LAMINATED TIMBER	35
	3.2 CUSTOMIZED ROBOTIC FABRICATION	36
	3.3 CUSTOMIZED ROBOTICALLY FABRICATED CLT PANELS	37

<b>PART II: PILOT STUDY</b>	<b>4. EXPLORING THE PROCESS OF ROBOTIC FABRICATION</b>	<b>40</b>
	4.1 INTRODUCTION	40
	4.2 SCOPE AND GOAL	41
	4.3 GEOMETRY	41
	4.4 SOFTWARE, HARDWARE, AND MATERIALS	42
	4.5 METHODOLOGY	43
	4.6. DISCUSSIONS AND CONCLUSIONS	45
<b>PART III: DEVELOPMENT OF THE INTEGRAL WORKFLOW</b>	<b>5. GLOBAL STRUCTURE MODULE</b>	<b>49</b>
	5.1 INTRODUCTION	49
	5.2 RELEVANT ORTHOGONAL MATERIAL PARAMETERS OF CLT IN THE FEM	50
	5.3 VARIABLES OF THE GLOBAL STRUCTURE MODULE	54
	5.4 COMPONENTS OF GLOBAL STRUCTURE MODULE	55
	5.5 FINITE ELEMENT MODELLING OF THE GLOBAL STRUCTURE	64
	5.6 RELATIONSHIPS WITH JOINT DESIGN	65
	5.7 POTENTIAL OF THE WORKFLOW: GLOBAL STRUCTURE	66
	5.8 CONCLUSION	71
	<b>6. JOINT DESIGN MODULE</b>	<b>72</b>
	6.1 INTRODUCTION	72
	6.2 BOUNDARY CONDITIONS AND DESIGN PHILOSOPHY	73
	6.3 VARIABLES OF THE JOINT DESIGN MODULE	76
	6.4 COMPONENTS OF THE JOINT DESIGN MODULE	77
	6.5 FINITE ELEMENT MODELLING OF THE JOINTS	85
	6.6 STRUCTURAL RELATIONSHIPS BETWEEN JOINT DESIGN AND GLOBAL STRUCTURE	88
	6.7 RELATIONSHIPS WITH GLOBAL STRUCTURE AND ROBOTIC FABRICATION	92
	6.8 POTENTIAL OF THE WORKFLOW: JOINT DESIGN	93
	6.9 CONCLUSION	98
	<b>7. ROBOTIC FABRICATION MODULE</b>	<b>99</b>
	7.1 INTRODUCTION	99
	7.2 VARIABLES OF THE ROBOTIC FABRICATION MODULE	100
	7.3 COMPONENTS OF THE ROBOTIC FABRICATION MODULE	101
	7.4 RELATIONSHIPS WITH GLOBAL STRUCTURE AND JOINT DESIGN	104
	7.5 POTENTIAL OF THE WORKFLOW: ENTIRE WORKFLOW	107
	7.6 CONCLUSION	110

<b>PART IV: DISCUSSIONS, CONCLUSIONS AND RECOMMENDATIONS</b>	<b>8. DISCUSSIONS</b>	<b>112</b>
	8.1 ANSWER TO THE RESEARCH QUESTION	112
	8.2 CRITICAL REFLECTIONS AND DISCUSSIONS	114
	8.3 CONCLUSIONS	117
	8.4 RECOMMENDATIONS AND FURTHER INVESTIGATIONS	120
<b>BIBLIOGRAPHY</b>	<b>BIBLIOGRAPHY</b>	<b>121</b>
<b>APPENDICES</b>	<b>APPENDIX A. DETERMINING <math>S_0</math></b>	<b>126</b>
	<b>APPENDIX B. BENDING- AND SHEAR STIFFNESSES OF CLT</b>	<b>127</b>
	<b>APPENDIX C. OVERVIEW OF ROBOTIC FABRICATION PURPOSES</b>	<b>128</b>
	<b>APPENDIX D. DESCRIPTION OF THE PROGRAM OF A ROBOTIC SYSTEM</b>	<b>129</b>
	<b>APPENDIX E. VALIDATION OF FINITE ELEMENT MODELLING OF CLT</b>	<b>134</b>
	<b>APPENDIX F. EXPLANATION OF VARIABLES FOR GLOBAL STRUCTURE</b>	<b>144</b>
	<b>APPENDIX G. PYTHON SCRIPT FOR ORTHOGONAL MATERIAL PROPERTIES</b>	<b>148</b>
	<b>APPENDIX H. INPUT FOR THE FEM OF GLOBAL STRUCTURE</b>	<b>153</b>
	<b>APPENDIX I. SCRIPT FOR GLOBAL STRUCTURE MODULE</b>	<b>154</b>
	<b>APPENDIX J. DESIGN GRAPHS GLOBAL STRUCTURE</b>	<b>155</b>
	<b>APPENDIX K. INSUFFICIENCIES OF GEOMETRYGYM</b>	<b>160</b>
	<b>APPENDIX L. EXPLANATION OF VARIABLES FOR JOINT DESIGN</b>	<b>161</b>
	<b>APPENDIX M. PYTHON SCRIPT FOR ANALYTICAL U.C. CROSS-SECTIONS</b>	<b>165</b>
	<b>APPENDIX N. PYTHON SCRIPT FOR ANALYTICAL U.C. SCREWS</b>	<b>170</b>
	<b>APPENDIX O. SPRING STIFFNESSES FOR SCREWS</b>	<b>172</b>
	<b>APPENDIX P. INPUT FOR THE FEM OF JOINT DESIGN</b>	<b>173</b>
	<b>APPENDIX Q. VALIDATION OF FEM JOINT MODELS</b>	<b>174</b>
	<b>APPENDIX R. METHODOLOGIES TO DETERMINE SPRING STIFFNESS</b>	<b>178</b>
	<b>APPENDIX S. SCRIPT FOR JOINT DESIGN MODULE</b>	<b>185</b>
	<b>APPENDIX T. DESIGN GRAPHS FOR JOINT DESIGN</b>	<b>186</b>
	<b>APPENDIX U. EXPLANATION OF VARIABLES FOR ROBOTIC FABRICATION</b>	<b>188</b>
	<b>APPENDIX V. SCRIPT FOR ROBOTIC FABRICATION</b>	<b>190</b>

# Introduction

# I. Research Motivation

## I.I ON CROSS-LAMINATED TIMBER STRUCTURES

Climate change is a trending topic nowadays. Last year, the Dutch parliament decided on severe measurements to reduce the emissions of carbon dioxide and nitrogen and to the environment. Builders are therefore forced to reduce their emissions while keeping the same production targets as before [1]. This requires exploration of new ways of producing and designing buildings and structures. Professors and scientists expect this measurement to be the engine of a breakthrough in the building industry to increase the use of timber [2]. A recent research of Drexel University states that timber is making a comeback as a construction material [3]. While it was one of the first and most common materials used to make things, timber has been on the outs for more than a century. Despite the high prices, a recent *New York Times* story suggests that a wave of timber construction is coming up [3]. One of the types of engineered timber that is upcoming is called Cross-Laminated Timber (CLT) [4]. This material is structurally efficient in two directions, instead of one. Therefore, it can significantly contribute to the exploration of new ways of applying timber design in buildings and structures, and subsequently meeting the emission criteria for the building industry.

An example of a current ongoing project that incorporates timber design is the bus transferium in Alblasterdam (NL), designed by StudioRAP [5]. This project forms part of the motivation for this research on the use CLT. Figure I.I shows an impression of the project.

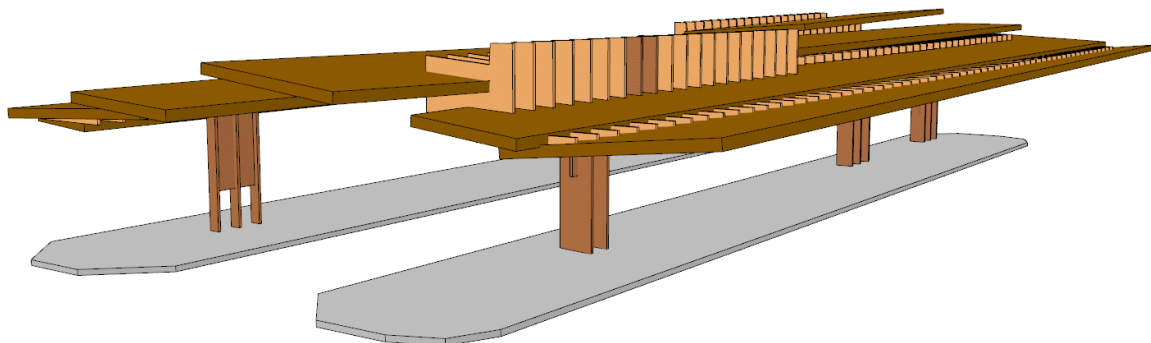


*Figure I.I: Illustration of the bus transferium Alblasterdam (NL) [5]*

## I.II ON CUSTOMIZED ROBOTIC FABRICATION

Besides the change referred to in the previous paragraph, the building industry is on the brink of another significant change, which is referred to as the fourth industrial revolution [6], [7]. This fourth industrial revolution let architects, engineers and builders aim for a 100% customized architecture. The reason for this is that they expect this to positively impact the quality and performance of the built environment [8]. To achieve this goal, it is of high importance to apply design and production technologies that can adapt to these customizations, for instance robotic fabrication, which opens opportunities to new ways of designing. Figures I.II - I.III show an example of the opportunities opened by robotic fabrication and timber. This project is called the 'Timber-wave' and is built up along a component-based design.

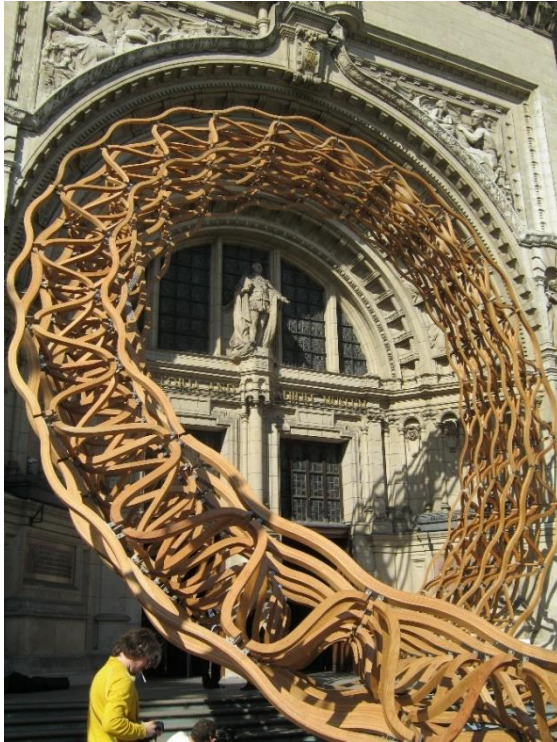


Figure I.II: Example of a project with robotic fabrication, component-based design – 'Timber Wave' [9]



Figure I.III: Foundation detail of the 'Timber Wave', near Victoria Albert Museum (London, U.K.) [9]

The two trends as described above about CLT and customized robotic fabrication are the motivation for this research, to contribute to the effort of architects, engineers, builders, designers and scientists to aim for a 100% customized building industry of sustainable buildings and structures.

## II. Problem Definition

On the one hand, one is aiming for a 100% customized sustainable building industry as stated above. For instance, with the help of robotic fabrication [10]. On the other hand, however, new manufacturing techniques with industrial robots are rarely used by the timber construction industry. The main reason for this paradox is that there is uncertainty and ignorance among designers about different aspects of robotic fabrication, such as economic efficiency, the relationships and (in)dependencies between the geometry of a structure and its structural behavior, the robotic fabrication process, and the ecological impact [11], [12].

Literature states that these uncertainties are strongly related to the type of workflow applied in the design process [12]. Right now, the building industry lacks in the efficiency to adapt to changes of the customer requirements due to the general application of traditional **linear** workflows. To increase this efficiency of adaptation, **integral**, flexible and reconfigurable workflows should replace the traditional linear ones [7]. Figures II.I - II.II show examples of generalized forms of both a linear and an integral workflow. The examples both consist of three general fragments: global structure, joint design, and robotic fabrication of the connection panels in the joints.

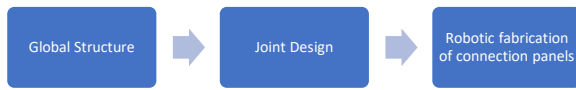


Figure II.I: Generalized representation of a traditional linear workflow

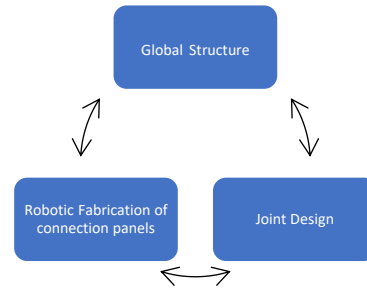


Figure II.II: Generalized representation of an integral workflow

The difference lies in the coherence of both workflows. As the traditional workflow is fragmented linearly, valuable and essential information is easily lost in between fragments. This makes the design and production process less efficient and more uncertain. The later in the process information is lost, the greater the error will be, see also Figure II.III [7]. The integral workflow however, reduces this loss of information by including front-end information loops, see also Figure II.IV [7]. Differently stated, front-end information loops will prevent severe design mistakes in different stages of the design process and so reduce the error.

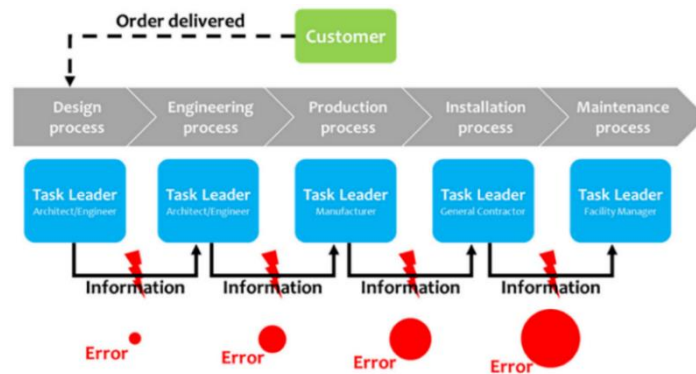


Figure II.III: Example of a traditional linear workflow [7]

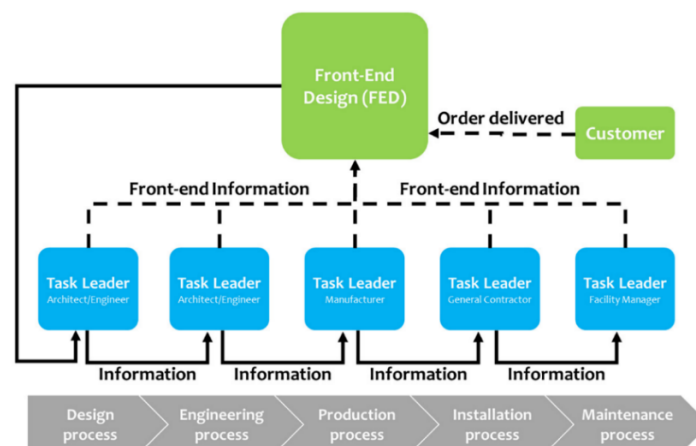


Figure II.IV: Example of an integral workflow [7]



### III. Research Question

There are many different domains in the fields of CLT structures and robotic fabrication. This research narrows down to the design of structural CLT connection panels that are robotically fabricated by means of milling. It specifically focusses on the integral design process of these connection panels. Investigating this process can contribute to the transformation process of the building industry towards a 100% customized, more sustainable architecture. Therefore, the main research question of this research is stated as follows:

*What does an integral workflow for robotically fabricated customized CLT connection panels look like, that promote exploration of the structural performance of CLT structures in the preliminary design phase?*

### IV. Scope and Objective

As described above, this research focusses on a specific type of CLT connection panel in CLT structures, and the robotic fabrication process by means of milling. The design principle of these panels is derived from the project in Alblasserdam, as described in the research motivation. Figure IV.I shows a generalized illustration of such a connection panel. The research leaves out of scope other types of connections in CLT structures, such as hold-down anchors or steel brackets. Likewise, the robotic assembling of elements and other robotic manufacturing methodologies, such as 3D printing or Computer Numerical Controlling (CNC) are left out of scope.

The research emphasizes on the relationships and (in)dependencies between the fragments of the integral workflow. At this moment, there are a lot of unanswered questions about this, which is one of the main reasons that causes uncertainty among designers about different aspects of robotic fabrication of CLT elements. Therefore, it is of high value to investigate these relationships and (in)dependencies. The research focusses on the relationships and (in)dependencies between the global shape of a CLT structure, its corresponding structural behavior, and the shape and fabrication process of the CLT connection panels. Various scientists set up reference projects and case studies to study similar relationships already for other types of structural timber (connections) [6], [13]. Herewith, it is essential to integrate the global shape and structural behavior, with its local shape and structural behavior [14]. In the last chapter of this research, an overview is given of conclusions specifically related to this research, and conclusions that are applicable in a broader sense as well.

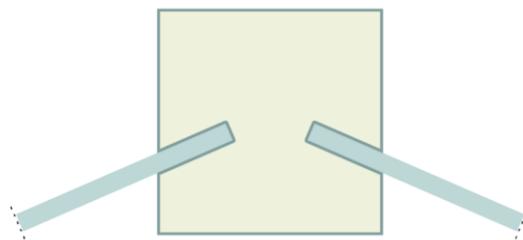


Figure IV.I: Generalized illustration of a CLT connection panel

## V. Research Methodology

The research methodology is divided in four parts, which are outlined in Table 1. The content of each part is then briefly elaborated thereafter.

Part	Description
Introduction	Research motivation, problem definition, research question, objective and scope.
I - Literature study	Cross-Laminated Timber. Robotic fabrication. The affordances and constraints of robotically fabricated CLT elements.
II - Pilot study	Production of a mock-up to explore the process of robotic fabrication of timber elements.
III - Development of the integral workflow	The development of an integral workflow in a parametric environment, that links the modules of the global structure, joint design, and robotic fabrication of the joints together.
IV - Discussions	Answer to the research question, critical reflections, conclusions, and recommendations for further research.

Table 1: Concise description of different parts of the research

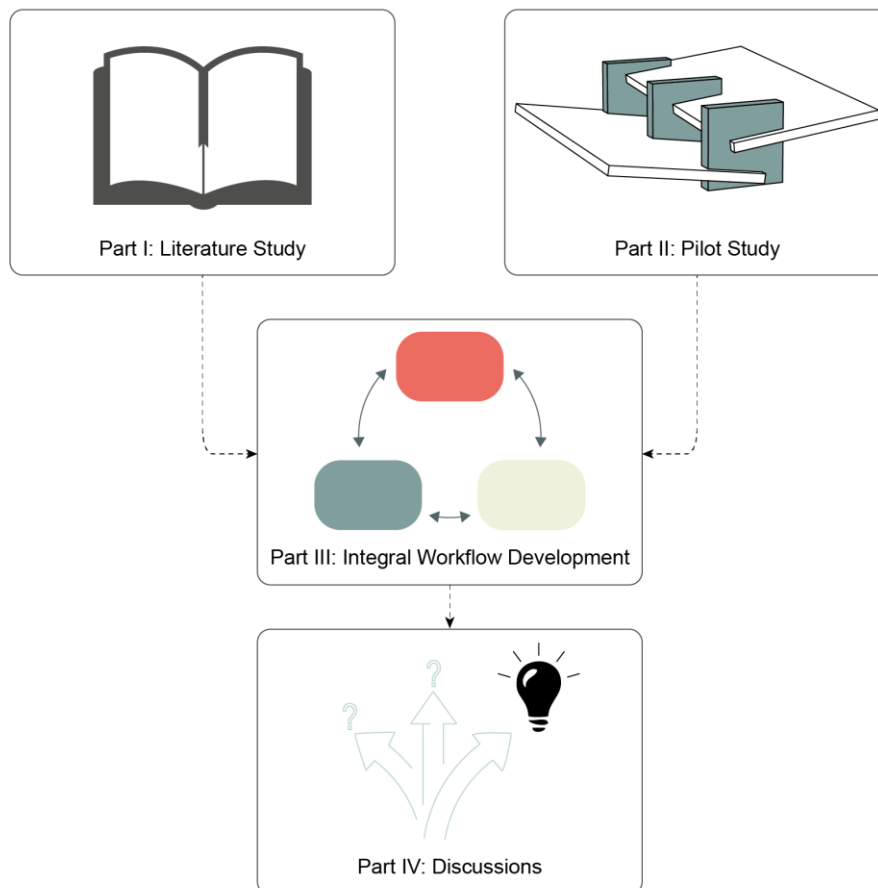


Figure V.1: Research diagram and correlations between different parts of the research

## Part I: Literature study

This research investigates the integral workflow for robotically fabricated CLT connection panels. The goal of the literature study is to shape the (theoretical) context where this workflow is developed in. Therefore, two main chapters answer the following questions.

### Chapter 1: Cross-Laminated Timber

- How is CLT produced?
- How can durability be considered in a CLT design?
- How does CLT behave in case of fire?
- What are the material properties and structural applications of CLT?
- How can CLT be structurally designed?
- What are the possible failure mechanisms of CLT elements?
- What are the possible failure mechanisms of CLT joints?

### Chapter 2: Customized Robotic Fabrication

- What type of robotic systems are applied in the building industry to produce customized elements?
- How does a robotic system perform a program of instructions?
- On what scale can a robot in the building industry perform operations?
- On what materials can a robot in the building industry perform operations?
- What main purpose does customized robotic fabrication in the building industry have?

For the integral workflow, several constraints and affordances apply regarding the robotic fabrication process. Although these are described spread over chapters one and two, chapter three explicitly lines out the actual constraints and affordances of robotically fabricated customized CLT elements. Therefore, the last chapter of the literature study answers the following questions.

### Chapter 3: Affordances and Constraints of customized robotically fabricated CLT elements

- What are the affordances and constraints of CLT structures? (based on Chapter 1)
- What are the affordances and constraints of customized robotic fabrication? (based on Chapter 2)
- What are the affordances and constraints of customized robotically fabricated CLT elements?

## Part II: Pilot study

The second part concerns a pilot study to explore the process of robotic fabrication for timber elements. The findings of this study are used as input for the development of the integral workflow.

## Part III: Development of the integral workflow

This part concerns the actual development of the integral workflow within the (theoretical) context that is drawn out by the literature study in *part I*. It also considers the findings of the pilot study in *part II*. The workflow is developed in Grasshopper3D, a graphical algorithm editor that enables users to model geometry in Rhino3D. Structural analyses are performed in GSA, a Finite Element Method (FEM) modelling program.

## Part IV: Discussions

Finally, the fourth part answers the research question and provides critical reflections on the research as well as conclusions that are drawn from the Literature Study (part I), the Pilot Study (part II), and the Development of the integral Workflow (part III). The last section of this part consists of several recommendations for further research.

# Part I

## Literature Study

# 1. Cross-Laminated Timber

## 1.1 INTRODUCTION: WHAT IS CROSS-LAMINATED TIMBER?

As stated in the introduction of this research, timber is an upcoming construction material. One of the upcoming structural timber types is Cross-Laminated Timber (CLT). Researchers and scientists are developing this type of structural timber since the early 1990's and it is applied in a wide range of applications nowadays [15]. It has its roots in Germany and Austria, and the NEN-EN 16351 defines CLT as follows:

*“CLT is a structural timber consisting of at least three layers of which a minimum of three are orthogonally bonded, which always comprise timber layers and may also comprise wood-based panel layers” [16]*

CLT is made of wood and therefore suitable to perform robotic operations on such as drilling, milling, and sawing. Customized elements can be robotically fabricated in a relative accurate way. As described in the objective and scope, this research focusses on the integral design process of robotically fabricated CLT connection panels. Therefore, two fields will be investigated regarding the material and manufacturing process:

- The field of CLT (current chapter)
- The field of customized Robotic Fabrication (Chapter 2)

This chapter focusses on the following domains and questions of CLT:

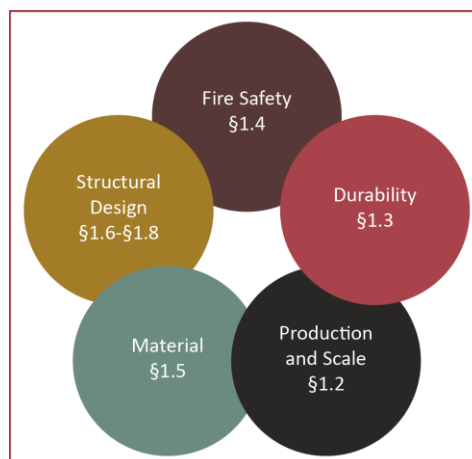


Figure 1.1: Domains of Chapter 1, Cross-Laminated Timber

- |  |        |
|--|--------|
| • How is CLT produced?   | • §1.2 |
| • How can durability be considered in a CLT design?                    | • §1.3 |
| • How does CLT behave in case of fire?                                 | • §1.4 |
| • What are the material properties and structural applications of CLT? | • §1.5 |
| • How can CLT be structurally designed?                                | • §1.6 |
| • What are the possible failure mechanisms of CLT elements?            | • §1.7 |
| • What are the possible failure mechanisms of CLT joints?              | • §1.8 |

The mutualities of this chapter and Chapter 2 will subsequently highlight the affordances and constraints of robotic fabrication of customized CLT elements. This is discussed in Chapter 3.

## 1.2 PRODUCTION AND SCALE

### 1.2.1 PRODUCTION PROCESS

The manufacturing process of CLT elements consists of multiple steps. Below, the manufacturing process is schematically shown.

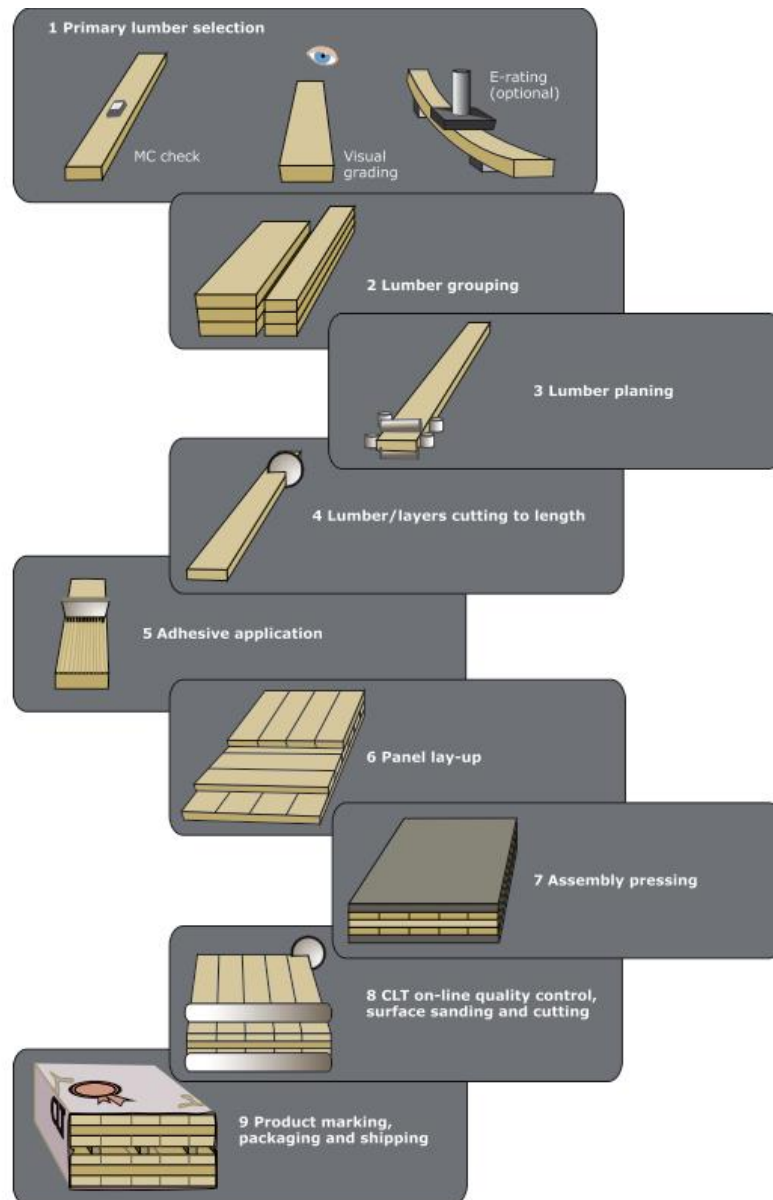


Figure 1.2: Production process of CLT [17]

The (structural) performance of the material is important, so the first step is to check the quality of the lumber. Moisture Content (MC) and visual grading are performed. Once the lumber is selected the elements are grouped based on dimension. Then the lumber is planed. This basically means the removal of a very thin surface layer to ensure better bonding between layers [17]. Now the lumber is selected and prepared to be cut to the right length. The adhesive is applied, and the panels are laid up. A minimum 'effective bonding area' of 80% of the lumber is recommended. This percentage depends on the final (structural) function of the panel and can be determined by the client. The next step is to press the assembly. This is a critical step of the manufacturing process. The goal of

pressing is to decrease the gaps in the material itself and between the layers. Finally, the quality is controlled, and the product is packed for shipping.

### 1.2.2 DIMENSIONS OF CLT

CLT panels are dimensionally stable. Therefore, a high precision of fabrication can be achieved using automated CNC machinery. CLT panels are available in dimensions up to 16m x 3m x 0.3m. At special request the thickness can be up to 0.5m [18]. The thickness of the individual layers should be between 6mm and 60mm. Manufacturers usually guarantee dimensional stability. Therefore, the following strict tolerances are applicable [15].

Thickness	±1.5mm
Width	±3.1mm
Length	±6.3mm
Squareness	±3.1mm
Straightness	±1.5mm

Table 2: Tolerances for the production CLT elements

## 1.3 DURABILITY

### 1.3.1 FOREST CERTIFICATION AND LIFE CYCLE ANALYSES

There are two factors that drive the ongoing development and utilization of CLT: its credentials as a sustainable material and the speed of construction [15]. However, something one needs to be keen on to ensure sustainable performance when applying timber or CLT as a construction material, is forest certification. The goal of forest certification is to enlarge the short life-span of wooden elements, by improving the technological performances related to the biodegradability of the woody material [19]. This improves the performance of the Life Cycle Analysis (LCA). Taking the environmental impact and LCA into account, CLT can be considered as a sustainable material, as the ecological and economic benefits outperform materials such concrete and steel [11]. A few key parameters of a standard LCA are highlighted in this paragraph. The base to identify critical aspects for each key parameter are the three main phases in the general life cycle of a building project. Figure 1.3 shows this generalized life cycle.

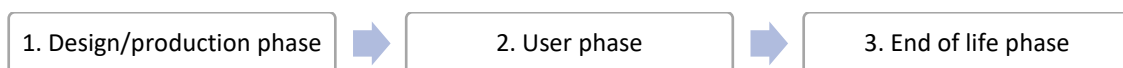


Figure 1.3: Three phases of a general Life Cycle of a building project

### 1.3.2 CIRCULAR ECONOMY AND CLT

The first critical parameter to improve the LCA of CLT is to look at CLT from the perspective of a circular economy instead of a linear economy. Figures 1.4-1.5 show generalized diagrams of these economies.

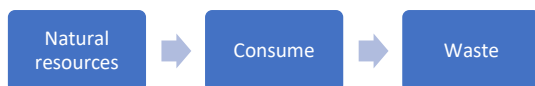


Figure 1.4: Generalized linear economy

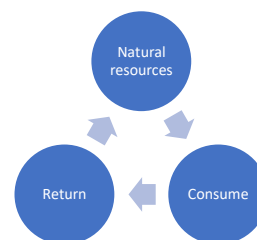


Figure 1.5: Generalized circular economy

The main difference between a linear and circular economy is that the circular economy enlarges the life-span of a product by *circulating* its life cycle. To transform the life cycle of CLT from linear to a circular, the end-of-life phase as illustrated in Figure 1.3 should focus on one of the following, or similar principles:

- Design a demountable structure and re-use as many CLT elements as possible.
- Use the CLT elements for bio-energy.

### 1.3.3 MOISTURE AND TEMPERATURE CONTROL OF CLT

Another critical key parameters in the LCA performance of CLT is the moisture control. The first step to rate this performance, is to identify in which climate class the CLT will be applied in. Upon this, measurements and design principles can be applied accordingly. Eurocode 5 states three different Climate Classes (CC) [20]:

- CC1: 20 degrees - relative humidity > 65% for only a few weeks per year.
- CC2: 20 degrees - relative humidity > 85% for only a few weeks per year.
- CC3: a higher relative humidity than climate class 1 or 2 for at least a few weeks per year.

In case the CLT will be applied in Climate Class 3, the material must be fully protected if possible [21]. It is then strongly recommended to apply several precautions to sufficiently protect the structure from moisture penetration and mold forming. The moisture control of a CLT structure must be carefully analyzed for the following phases of the life cycle.

#### 1.3.3.1 Design Phase

- *Moisture Detailing.*
  - **Interface material detailing.** Separate CLT from other construction materials such as concrete. This will prevent moisture from entering the CLT elements by accumulation and sorption.
  - **Allow drying.** Design details and elements in such a way that the design allows for drying in case wetting occurs. This can be achieved by not placing a potential vapor barrier/retard on both sides of the element for instance.
- *Green roof.* Consider the design of a green roof on top the CLT roof plates. This green roof will avoid water accumulation and protect CLT roof plates from direct contact with rain.
- *Durable wood.* Apply durable wood species with a low penetrability. Typical types of wood for CLT and their natural durability are shown below [22]. Species outside of Europe are not listed below to avoid CO<sub>2</sub> emissions due to transport. It is recommended to apply either European pine or European Larch.
  - Spruce      4    (1= very resistant, 4=poorly resistant)
  - Pine        2-3 (1= very resistant, 4=poorly resistant)
  - Larch       2-3 (1= very resistant, 4=poorly resistant)
- *Water management system.* In the design of the water management drainage system it is important to design according the 4D strategy [23].
  - **Deflection:**      Divert water off the structure as soon as possible.
  - **Drainage:**        Remove water that tends to stay at the structure.
  - **Drying:**          Facilitate drying of the wood as good as possible.
  - **Durable wood:**   Apply treated or naturally durable wood.



### 1.3.3.2 Production Phase

- *Assemble off-site.* Assemble as many elements as possible off-site, to minimize the execution time and so avoid moisture entering the material during construction [11].
- *Penetrative Wood Treatment.* A treatment can be applied that avoids moisture from entering the CLT elements. However, post-planing can remove or damage such a treatment easily.
- *Coating.* A coating can be applied that avoids moisture from entering the CLT elements.
- *Membrane.* A membrane can be applied that avoids moisture from entering the CLT elements.

### 1.3.3.3 Construction Phase

- *Dry environment.* The construction of a project could be situated in a dry environment. For instance, a temporary tent with heating inside.
- *Construction time.* The design should be set up in such a way that the construction time is minimized. For instance, apply BIM models to simulate the construction sequence and set up the planning accordingly.

Different from concrete and steel, wood is more sensitive to expansion and shrinkage due to temperature changes. Therefore, it is important to consider this material property during the design phase to avoid unwanted temperature stresses in the material. This can be achieved by movement joints for instance.

## 1.4 FIRE SAFETY DESIGN

One of the behaviors that should be studied carefully for a timber design, is the material behavior during fire, as well as protective measurements that can be taken accordingly. There are several codes and guidelines available for wooden structures in buildings, such as the Eurocode and the Bouwbesluit.

### 1.4.1 MATERIAL BEHAVIOR OF CLT ELEMENTS SUBJECTED TO FIRE

In case of fire, CLT shows a different behavior than monogenetic structural timber elements. The main differences between CLT elements and monogenetic timber element subjected to fire are:

- 1) Norms and guidelines to set up a fire safety design for monogenetic timber elements are present. However, for CLT there is no Eurocode provided at the moment of writing. Therefore, the fire safety of CLT structures should be determined by product sheets of CLT manufacturers and the Technical Guideline for Europe for fire safety in timber buildings [24].
- 2) The orthogonal orientation between the layers that induces jerky strength reductions.

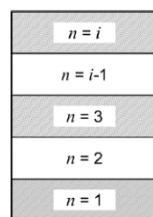


Figure 1.6: Cross-section at ambient temperature [24]

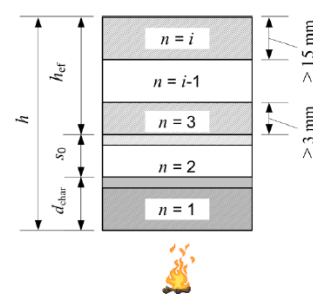


Figure 1.7: Residual cross-section, char layer and zero-strength layer of cross-section exposed to fire on one side [24]

- 3) The seams between the layers results in a higher charring rate.
  - Depending on the type of glue applied, there is a danger of layers falling off structural elements, especially in case of lateral oriented elements. These layers can deliberately be considered as protection layers for the remaining cross-section.

To consider fire safety in the design, the one-dimensional charring depth for seamless CLT is:

$$d_{char,0} = \beta_0 * t \quad (1)$$

- $d_{char,0}$  = Charring depth for seamless CLT
- $\beta_0$  = Charring rate in mm/min. 0.65 for softwoods [20]
- $t$  = Total thickness of the CLT element

In case seams are present, the influence of the seams should be considered by the factor  $k_n$ :

$$d_{char,n} = \beta_n * t \quad (2)$$

- $d_{char,n}$  = Charring depth for seamed CLT
- $\beta_n$  =  $k_n * \beta_0$
- $k_n$  = Correction factor for two-dimensional charring. For CLT,  $k_n = 1.2$ .
- $\beta_0$  = Charring rate in mm/min. 0.65 for softwoods [20]
- $t$  = Total thickness of the CLT element

The next step is to determine the effective charring depth of the CLT members. For seamless CLT the effective charring depth can be determined as follows:

$$d_{ef} = d_{char} + k_0 * s_0, \text{ where:} \quad (3)$$

- $d_{ef}$  = Effective charring depth for CLT
- $d_{char}$  = Charring depth of CLT, derived from Formula (1) or (2)

$$k_0 = \begin{cases} \frac{t}{20} & \text{for unprotected members} \\ \frac{t}{t_{ch}} & \text{for protected members} \end{cases} \quad (4)$$

- $k_0$  = Correction factor that considers the fact that the zero-strength layer is not fully effective during the first twenty minutes of initially unprotected members, or until the start of charring of protected members.

- $t$  = Total thickness of the CLT element.

- $t_{ch}$  = Total protected thickness,  $t_{ch} = \sum t_{prot,i}$

- $s_0$  = A virtual compensating layer for CLT [mm]. See Appendix A.

Once the effective charring depth is determined, the effective cross-section that is structurally operational in case of fire, can be calculated by subtracting the effective charring depth from the cross-sectional dimensions of the members:

- Height  $h$ :  $h_{ef} = h - d_{ef}$
- Width  $w$ :  $w_{ef} = w - d_{ef}$
- Thickness  $t$ :  $t_{ef} = t - d_{ef}$

In fact, the design philosophy of CLT members subjected to fire is to count the outer layer as a protective layer. By doing so, the following correlation between time  $t$  and charring depth  $d_{\text{char}}$  holds as shown in Figure 1.8.

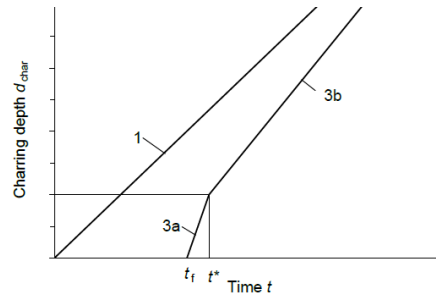


Figure 1.8: Correlation between charring depth  $d_{\text{char}}$  and time  $t$  [24]

Graph	Description
1	Relationship for initially unprotected members
3a	Increased charring rate after failure of ceiling lining
3b	Charring after consolidation at time $t^*$

#### 1.4.2 PROTECTIVE MEASUREMENTS FOR CLT STRUCTURES AGAINST FIRE

Besides adding extra layers to the CLT element as a protective measurement, other treatments can be applied to increase the fire resistance of CLT members:

- *Fire protection and insulation boards.*
- *Fire protection spray.*
- *Impregnating wood.* The options as stated above may not be desirable for visible elements as it strongly affects the aesthetical performance. Therefore, one can choose to impregnate the wood. An example of this measurement is SafeWood from Foreco [25]. The wood is impregnated and besides increasing the fire resistance, the impregnation also avoids moisture from penetrating the wood. This is a significant advantage, as moisture has a large impact on the durability of the CLT elements. However, one should be keen on possible damage of the impregnation due to post-planing of the CLT.

### 1.5 MATERIAL PROPERTIES AND APPLICATIONS OF CLT

#### 1.5.1 STRUCTURAL MATERIAL PROPERTIES

CLT is generally made of typical construction wood species, such as conifers, spruce, pine, Scots pine, larch or Douglas fir tree [26]. These types of wood have a larger stiffness than the types of wood applied in non-structural applications, such as sheeting material or finishing layers. In the Netherlands, CLT is generally produced of pine.

The unique property of CLT elements compared to homogeneous timber elements is that layers are arranged orthogonally to the grain, which creates stiffness in two perpendicular dimensions. This structural efficiency illustrates the main advantage of this type of timber elements [27]. As the layers are compressed and glued on top of each other, CLT can be considered as a 'mass timber' type. The structural efficiency of the material offers the opportunity to apply CLT as a structural material. CLT can be loaded perpendicular to the plane and in-plane. In case of loading *perpendicular to the plane*, CLT elements can take bending either parallel or perpendicular to the grain of the external layer. In case of loading *in-plane*, CLT elements can take bending, compression, and tension in plane and parallel or perpendicular to the grain of the external layers [27].

For the structural material parameters, the following values as shown below are generally applied [18]. These values can be used as input for structural calculations of CLT elements.

<i>Material parameter</i>	<i>Symbol</i>	<i>Magnitude</i>	<i>Unity</i>
Modulus of Elasticity*	$E_0$	11.000	N/mm <sup>2</sup>
	$E_{90}$	370	N/mm <sup>2</sup>
Shear modulus*	$G_0$	690	N/mm <sup>2</sup>
	$G_{90}$	50	N/mm <sup>2</sup>
Characteristic bulk density	$\rho_k$	400	kg/m <sup>3</sup>

Table 3: Orthogonal material parameters for CLT where  $0$  is considered as the strong direction and  $90$  as the weak direction

### 1.5.2 STRUCTURAL APPLICATIONS OF CLT

Since wood is an anisotropic material, the stiffness ratio of a CLT panel transverse and parallel to the span direction is as little as 1:6. For floors, CLT is therefore suited to be used as a one-way spanning floor. The structural scheme is comparable to a precast concrete panel or hollow-core plank. Recent researches, however, show the potential and opportunity to apply CLT panels as a two-way spanning floor [15].

Besides applying CLT as floors, other applications of CLT are (structural) walls, beams, and roofs. From an aesthetical point of view, CLT elements can be either fabricated with a 100% fill of material, or a <100% fill. As CLT has a good structural performance, the weak link in this system will be the wall to floor connection. These connections should be stiffened by wall-to-floor fasteners or screws. Throughout the past years, CLT is suited to more and more markets. It is applied in mid-rise residential buildings, schools, warehouses, pedestrian bridges, and bus stops.



Figure 1.9: CLT walls [28]



Figure 1.10: CLT floors [29]

## 1.6 STRUCTURAL DESIGN OF CLT

### 1.6.1 NORMS AND DESIGN GUIDES

There are multiple (local) norms that can be applied for the structural design of CLT, such as the NEN, proHolz CLT design guide, and the CLT Handbooks of Canada and America. However, this research only considers the norms and design guides shown below, as these cover the fundamentals of CLT design sufficiently. After all, they are internationally recognized and applied.

- NEN-EN 1995-1-1 Eurocode 5: Design of timber structures [20]
- NEN-EN 16351 Cross-Laminated Timber Structures – requirements [16]
- Cross-Laminated Timber Structural Design [18]

These norms form the basis for the remaining part of this chapter. For designing CLT structures, bending- and shear stiffness properties of elements should be obtained to perform analytical calculations and set up structural analyses of a CLT structure. The NEN-EN 16351 states that these properties shall be obtained by either:

- Determination and declaration of geometrical data and relevant properties of layers
- Testing of CLT

As testing of CLT is not in the scope of this research, the first method shall be applied, using the three norms mentioned above. The main part of the design principles will be obtained from the Cross-Laminated Timber Structural Design guide from proHolz [18]. This guide offers clear guidelines for CLT design based on Eurocodes. General design principles will be applied from the NEN-EN 1991-1-1 and NEN-EN 16351 [16], [30].

### 1.6.2 OVERVIEW OF RELEVANT DESIGN PARAMETERS

The focus of this research is on the relation between the global shape and structural behavior of a CLT structure, with its local shape and structural behavior. Therefore, design criteria, parameters and factors such as official deflection criteria, load combinations, and load factors are left out of the scope of this research. These can be found in the proHolz design guide [18]. However, the cross-sectional stiffness parameters should be determined according the applicable norms and design guides. The relevant cross-sectional parameters required for these calculations are highlighted below.

Manufacturer	BSP
Element thickness	150
Orientation of top layers	L
Number of board layers	5
Element build-up: symmetrical or asymmetrical	s
Thickness and orientation of individual layers	(30l-30w-30l-30w-30l)

Table 4: Data for the notation of CLT cross-sectional build-up

For CLT elements, a specific notation is generally used for the cross-sectional build-up, which includes geometrical data for the input of structural analyses. The official notation for the element described above is BSP 150 L5s (30l-30w-30l-30w-30l). Figure 1.11 shows the corresponding cross-sectional build-up. Given the cross-sectional build-up, the structural properties that are required for design checks of failure mechanisms for CLT as stated in Chapter 1.7 can be determined accordingly.

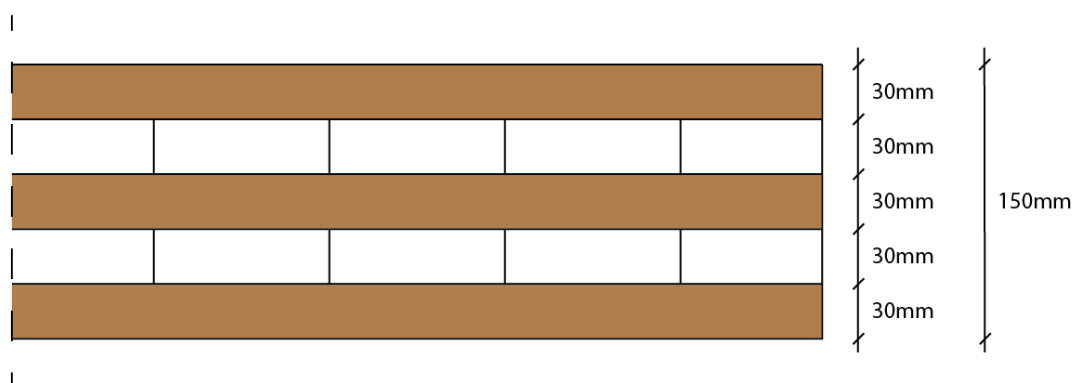


Figure 1.11: Cross-sectional build-up for BSP 150 L5s (30l-30w-30l-30w-30l)

### 1.6.3 DESIGN PHILOSOPHY

For the calculation of CLT members different methods can be applied. The most common calculation methods are the gamma method, the shear-flexible Timoshenko beam, the shear analogy method, the laminate theory and the calculation according to the Finite Element Method. The gamma method and the shear-flexible Timoshenko beam are widely applied and included in general design standard. Therefore, these two design philosophies as well as their differences are briefly highlighted.

- 1) The *gamma method* only considers one direction of the layers of the CLT element as load-bearing elements. So, either the load-bearing capacity in the main- or the ancillary load-bearing direction is considered. Thus, the layers transverse to the load-bearing direction are purely considered as spacers and are only subject to shear. The bending stiffness is reduced accordingly by adding a  $\gamma$ -factor for each layer. This is called the *Gamma method*.
- 2) The *shear-flexible beam method*, based on the Timoshenko beam theory, considers both directions of the layers as load-bearing elements. However, different bending- and shear stiffnesses apply for the elements in the transverse and ancillary direction according their orientation and position in the cross-sectional geometry. The shear stiffness however, is reduced with a shear correction factor  $\kappa$ . This is called the *shear-flexible beam method*.

Both methods are suitable for analytical calculations and numerical modelling of CLT structures in a Finite Element Method (FEM) model. However, in case of the gamma method the  $\gamma$ -factor must be determined for each layer individually. This can lead to complex matrix system as an equation must be set up for each layer separately. Therefore, the shear-flexible beam method, will be applied in this research. The effective bending stiffness  $(EI)_{ef}$  and shear stiffness  $(GA)_{ef}$  can be determined according the generalized Formulas (6) and (7). Appendix B presents an extended explanation of the formulas for both the weak and strong direction.

$$\text{Bending Stiffness } (EI)_{ef} \text{ [Nmm}^2\text{]} \quad (EI)_{ef} = \sum_{i=1}^n E_i * \frac{b * d_i^3}{12} + \sum_{i=1}^n E_i * b * d_i * a_i^2 \quad (6)$$

$$\text{Shear Stiffness } (GA)_{ef} \text{ [N]} \quad (GA_s)_{ef} = \kappa \left( \sum_{i=1}^n G_i * b * d_i + \sum_{i=1}^n G_i * b * d_i \right) \quad (7)$$

## 1.7 POSSIBLE FAILURE MECHANISMS FOR CLT ELEMENTS

Once the structural properties of CLT are determined, the failure mechanisms of a CLT structure should be checked. There are three different principles the failure mechanisms can be divided into: rolling shear, failure of the CLT, failure the connections.

### 1.7.1 ROLLING SHEAR

The failure mechanism that is typical for CLT is rolling shear. If shear occurs, then normally a break tangential to the annual ring areas of the transverse layers can be observed. This break is called *rolling shear failure* and it is induced by exceeding the *rolling shear strength*  $f_{V,R,k}$ . Therefore, it is essential to check whether a CLT element will exceed the shear strength in case it is loaded.



Figure 1: Rolling shear failure [31]

### 1.7.2 GENERAL FAILURE MECHANISMS

The other failure mechanisms that should be verified are the resistances against tension, compression, bending, and shear. These resistances of a CLT structure should be greater than the impact on it. Below, the relevant Unity Checks are presented.

<b>Loading in plane</b>		
	$\sigma_{t,0,d} \leq f_{t,0,d}$ (8)	
Tension parallel	$\frac{N_{0,d}}{A_{0,net}} \leq k_{mod} * k_{sys} * \frac{f_{t,0,k}}{\gamma_m}$ (9)	
	$\sigma_{t,90,d} \leq f_{t,90,d}$ (10)	
Tension transverse	$\frac{N_{90,d}}{A_{90,net}} \leq k_{mod} * k_{sys} * \frac{f_{t,90,k}}{\gamma_m}$ (11)	
	$\sigma_{c,0,d} \leq f_{c,0,d}$ (12)	
Compression parallel	$\frac{N_{0,d}}{A_{0,net}} \leq k_{mod} * \frac{f_{c,0,k}}{\gamma_m}$ (13)	
	$A_{0,net} = b * d_{0,net}$ (14)	
Compression transverse	$\frac{N_{90,d}}{A_{90,net}} \leq k_{mod} * \frac{f_{c,90,k}}{\gamma_m}$ (16)	
	$A_{90,net} = b * d_{90,net}$ (17)	

	$\sigma_{m,z,d} \leq f_{m,d}$	(18)	
<i>Bending parallel</i>	$\frac{M_{z,d}}{W_{z,0,net}} \leq k_{mod} * \frac{f_{m,k}}{\gamma_m}$	(19)	
	$W_{z,0,net} = \frac{\sum d_0 * h^2}{6}$	(20)	
	$\sigma_{m,z,d} \leq f_{m,d}$	(21)	
<i>Bending transverse</i>	$\frac{M_{z,d}}{W_{z,90,net}} \leq k_{mod} * \frac{f_{m,k}}{\gamma_m}$	(22)	
	$W_{z,90,net} = \frac{\sum d_{90} * h^2}{6}$	(23)	
<b>Loading out-of-plane</b>			
	$\sigma_{c,90,d} \leq f_{c,90,d}$	(24)	
<i>Compression transverse</i>	$\frac{N_{90,d}}{k_{c,90}} \leq k_{mod} * \frac{f_{c,90,k}}{\gamma_m}$	(25)	
	$\sigma_{m,d} \leq f_{m,d}$	(26)	
<i>Bending parallel</i>	$\frac{M_{0,d}}{W_{0,net}} \leq k_{mod} * k_{sys} * \frac{f_{m,k}}{\gamma_m}$	(27)	
	$\sigma_{m,d} \leq f_{m,d}$	(28)	
<i>Bending transverse</i>	$\frac{M_{90,d}}{W_{90,net}} \leq k_{mod} * k_{sys} * \frac{f_{m,k}}{\gamma_m}$	(29)	
	$\tau_{V,d} \leq f_{V,d}$	(30)	
<i>Shear parallel</i>	$\frac{V_{0,d} * S_{0,V,net}}{I_{0,net} * b} \leq k_{mod} * \frac{f_{V,k}}{\gamma_m}$	(31)	
	$\tau_{V,R,d} \leq f_{V,R,d}$	(32)	
<i>Shear transverse</i>	$\frac{V_{90,d} * S_{90,R,net}}{I_{90,net} * b} \leq k_{mod} * \frac{f_{V,R,k}}{\gamma_m}$	(33)	

\*Parallel/transverse = the direction of the force relative to the load-bearing direction.



**Flat versus curved CLT elements.** All the above checks should be applied at planar CLT elements. On the other hand, recent research shows the potential of curved CLT elements [32], [33]. However, this requires much expertise and is generally more complicated to design than planar CLT element.



Figure 1.12: Curved CLT elements [32]



Figure 1.13: The Smile – curved CLT elements [33]

## 1.8 POSSIBLE FAILURE MECHANISMS FOR CLT JOINTS

There are many different types of connections for CLT structures. Figures 1.14-1.17 show some examples of connections in CLT.



Figure 1.14: Hold down brackets for base connection of CLT (shear) walls [34]



Figure 1.15: X-rad connection to connect a CLT wall to another wall [34]

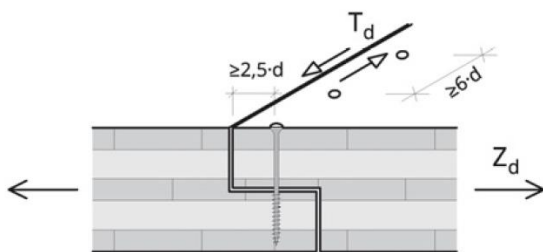


Figure 1.16: Rabbet edge connection between CLT plates loaded in tension [18]

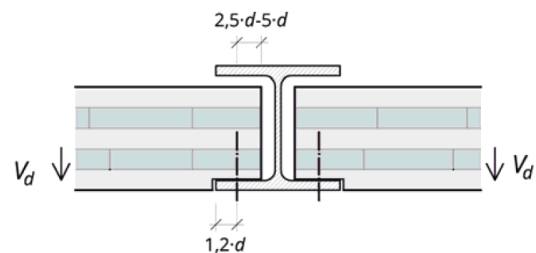


Figure 1.17: Flush joists with a steel profile in between CLT plates loaded in shear [18]

Considering several types of connections derived from literature, of which a few are shown above, it can be stated many additional structural provisions must be made to ensure a clamped connection. For instance, for 'The Smile', as illustrated in the previous paragraph, a glulam beam is added to the roof-wall connection to ensure a clamped connection. One should carefully consider whether a clamped connection is desired, or a pinned or semi-rigid connection can fulfil the purpose of a design as well.

As described in the scope of this research, only one type of connection will be investigated which is a CLT connection panel; a connection where planar CLT elements are connected to each other by screws. Therefore, this Chapter explicitly focusses on screwed connections between planar CLT elements and the corresponding failure mechanisms. Regarding the design of screwed connections between CLT members, four situations should be verified against failure according the proHolz design guide.



Figure 1.18: Situation 1. In-plane withdrawal of screws  
[18]

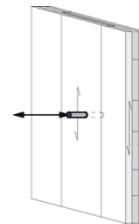


Figure 1.19: Situation 2. Out-of-plane withdrawal of screws  
[18]



Figure 1.20: Situation 3. In-plane shearing off screws  
[18]

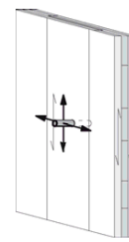


Figure 1.21: Situation 4. Out-of-plane shearing off screws  
[18]

Generally, the screw capacity against withdrawal and shearing off is verified according Formulas (34) and (35):

$$\text{Withdrawal resistance } F_{ax,k} \quad F_{ax,k} = \frac{31 * d^{0.8} * l_{ef}^{0.9}}{1.5 * \cos(\varepsilon)^2 + \sin(\varepsilon)^2} \quad (34)$$

$$\text{Shear resistance } R_{Vd} \quad R_{Vd} = F_{v,Rk,d} + 0.25 * F_{ax,Rk,d} \quad (35)$$

Extended calculations are required to determine the values of these resistances. However, these resistances are usually delivered by product sheets of the manufacturers. Therefore, for this research data from product sheets of manufacturers will be used to verify the resistance against shearing off and withdrawal of screws. Besides determining the capacities of the screwed connections, there are minimum geometrical distances that should be considered during the design of screwed connections between CLT elements, which are shown in Figure 1.22.

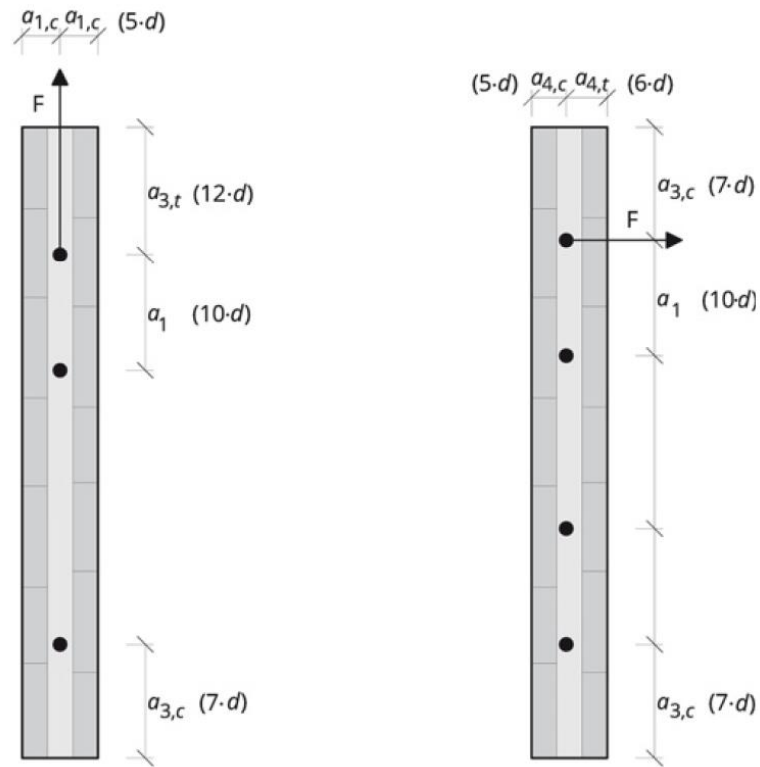


Figure 1.22: Situation 3. Minimum distance for screwed connections in CLT [18]

Distance	In the direction of the element side	$a_1$	$10 \cdot d$
	Transverse to the element surface	$a_2$	$3 \cdot d$
Edge distance	Stressed edge	$a_{3,t}$	$12 \cdot d$
	Non-stressed edge of the top layer	$a_{3,c}$	$7 \cdot d$
	Stressed edge to the element surface	$a_{4,t}$	$6 \cdot d$
	Non-stressed edge to the element surface	$a_{4,c}$	$5 \cdot d$

Table 5: Minimum distances of self-tapping woodscrews in the narrow side [18]

## 1.9. CONCLUSION

This chapter answers the following questions:

- How is CLT produced?
- How can durability be considered in a CLT design?
- How does CLT behave in case of fire?
- What are the material properties and structural applications of CLT?
- How can CLT be structurally designed?
- What are the possible failure mechanisms of CLT elements?
- What are the possible failure mechanisms of CLT joints?

The production process of CLT is briefly explained in this chapter. The different steps of this process are highlighted, as well as one of the main advantages of this type of structural timber, namely its dimensional stability. Another advantage is the stiffness in two directions, as the layers of a CLT panel are oriented perpendicularly to their adjacent ones.

Moisture control should be carefully considered to increase the sustainability performance of CLT. At the moment of writing, CLT is not suited to be applied unprotected in the outdoor environment. In case of fire, extra layers or additional measurements to increase the fire resistance should be added to CLT elements.

CLT can be produced of different types of wood, but generally it is produced of pine. The material properties of the type of wood are used as input parameters for the calculation of the bending- and shear stiffness in both directions of a CLT panel. The panels are used for several structural applications, such as floors, walls, beams, and roofs.

For a structural design it is important to determine the bending- and shear stiffness in both directions. These cross-sectional structural properties can be used as input parameters for analytical calculations or the FEM. There are three different principles of failure that apply to CLT structures: rolling shear, failure of the CLT element itself, and failure of the connections. Regarding connections in a CLT structure, if one desires to design a clamped connection between CLT elements, additional structural provisions must be made to ensure structural safety. This research focusses particularly on screwed connections between CLT elements, and different failure mechanisms for this type of connection are described in this chapter.

As stated in the introduction of this chapter, the focus of this research is on the integral design process of robotically fabricated CLT connection panels. This integral design process has several affordances and constraints in it that can be divided within two fields:

- The field of CLT
- The field of customized Robotic Fabrication

This chapter highlights several affordances and constraints within the field of CLT, that are elaborated in Chapter 3. The next chapter explores the field of customized robotic fabrication.

## 2. Customized Robotic Fabrication

### 2.1 INTRODUCTION: WHAT IS A ROBOT?

A robot is defined as an electromechanical device with multiple Degrees-Of-Freedom (DOF) that is programmable to accomplish a variety of tasks [35]. They are programmed by a Computer Numerical Control (CNC) system. This implies they facilitate the possibility to perform customized, non-standard fabrication processes, which are also more accurate and flexible than traditional fabrication processes [6]. Robots do not only offer opportunities to explore new ways of designing and accurate fabrication processes, they also open the possibility of giving designers and engineers insight and control of all aspects from design to operation. This raises the efficiency and flexibility of the file to factory process immensely and make them an effective tool in the design along an integral workflow [36]. As described in the objective and scope, this research focusses on the integral design process of customized robotically fabricated CLT connection panels. Therefore, two fields will be investigated regarding the material and manufacturing process:

- The field of CLT (Chapter 1)
- The field of customized Robotic Fabrication (current chapter)

This chapter focusses on the field of robotic fabrication, by highlighting the following domains of it:

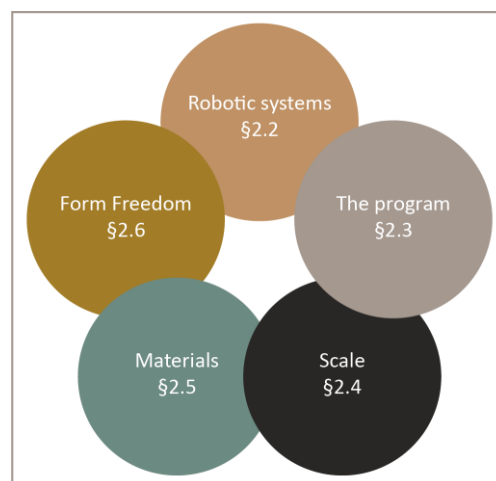


Figure 2.1: Domains of Chapter 2, Robotic Fabrication

Along these five domains, the following questions will be answered:

- |   |      |
|---|------|
| • What type of robotic systems are applied in the building industry to produce customized elements? | §2.2 |
| • How does a robotic system perform a program of instructions?                                      | §2.3 |
| • On what scale can a robot in the building industry perform operations?                            | §2.4 |
| • On what materials can a robot in the building industry perform operations?                        | §2.5 |
| • What main purpose does customized robotic fabrication in the building industry have?              | §2.6 |

The mutualities of this chapter and Chapter 1 will subsequently highlight the affordances and constraints of robotic fabrication of customized CLT elements. This is discussed in Chapter 3.

## 2.2 ROBOTIC SYSTEMS IN THE BUILDING INDUSTRY

The past decade robots have become a more accessible multifunctional tool, open to any kind of task [32]. Schematically generalized, the system of a robot consists of three components. Figure 2.2 shows these components and this paragraph describes each component concisely.

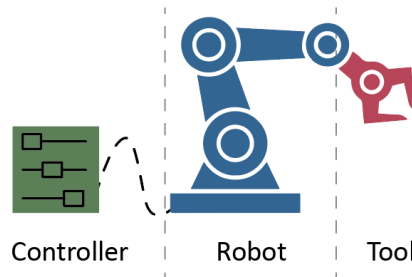


Figure 2.2: The three components of a robot

### 2.2.1 ROBOTS

The first component of a robotic system is the robot itself. There are different kinds of robots available for different industries. Well-known examples of robots are CNC machines, drones, androids, self-driving cars and many more. This research explicitly focusses on architectural robots for customized fabrication. This type of robots is accessible to many kinds of actors within the building industry, from architects to manufacturers. The three main common types of robots applied in the building industry are KUKA, ABB, and FANUC [32], [37].



Figure 2.3: KUKA robot [38]



Figure 2.4: ABB robot [39]



Figure 2.5: FANUC robot [40]

KUKA is one of the world's leading specialists in automation. Through the past 40 years they have developed their technologies and are known especially by their lightweight 6-axis robots. ABB is another supplier in robots and robot software. ABB robots can be equipped with features such as advanced vision systems, which enables the robot to assemble elements on moving objects. Through past decades till now, ABB keeps developing new innovations for both hardware and software. This enables them to act in a wide field of applications, including the automotive and building industry. FANUC robots are the last type of robot highlighted in this research. They offer a diverse range of applications and industries, such as automotive and the building industry. One of the remarkable products of FANUC are their collaborative robots. These are robots that can collaborate with a human operator during the fabrication process.

## 2.2.2 CONTROLLERS

The second component in a robotic system is the robot controller. In a broad sense, a robot controller is a combination of *software* and *hardware* to program and control single or multiple robots.

**Controlling software.** There are different tools and programs available to control robots of the three brands as described in the previous paragraph. Many of them share one main principle in common: they are a software tool that can be used parametrically by means of visual or scriptural programming. An example of controlling software is KUKAprc [41]. KUKAprc is developed by a split-off association of TU Vienna and is easily accessible and applicable [37], [41]. Another example is RapCam. This controlling software enables a user to control either a KUKA, ABB, or FANUC robot [42]. The code generated on a computer, is finally sent to the controller itself. Besides the programs named above, another example of controlling software is RoboDK, which makes use of scriptural programming [43].

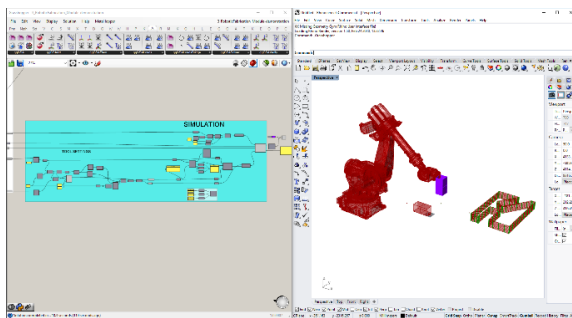


Figure 2.6: Rapcam interface – example of controlling software by visual programming (1)

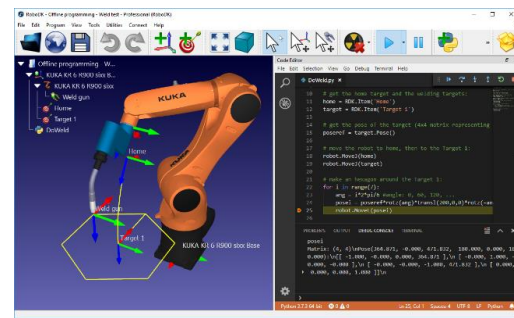


Figure 2.7: RoboDK interface – example of controlling software by python coding (2) [43]

**Controlling hardware.** Figure 2.8 shows an example of a robot controller's hardware.



Figure 2.8: Hardware of a robot controller [38]

The controller enables a user to physically control the robot. The user can control the robot via the pendant by adjusting the speed of the robot, aborting a certain operation, or calibrating the robot correctly according to the program to be executed. Another feature of the controller is to load certain program modules that are defined beforehand. Program modules are a set of instructions in a specific sequence that the robot should execute, which is described in Chapter 2.3

### 2.2.3 TOOLING

The last component of a robotic system in the building industry is the tooling. Tooling refers to the tool that is used to operate on the material, which can have five different fabrication purposes [12], [44].

- Subtraction
- Addition
- Joining
- Forming
- Generating

Table 6 shows a concise overview of the different fabrication purposes related to wood [12]. Appendix C shows a more extended overview of fabrication purposes related to wood and other materials.

Fabrication purpose	Technique	Examples of materials it could be applied on
<i>Subtraction</i>	Milling	Foam, wood, metal
	Cutting	Foam, stone, wood
	Drilling	Wood, stone, metal
<i>Joining</i>	Gluing	Plastic, wood
<i>Forming</i>	Bending	Metal, wood
	Punching	Plywood
<i>Generating</i>	Assembling/Gripping	Stone, wood

Table 6: Concise overview of different fabrication purposes related to wood

Depending on budget, application, payload, available tooling and preference of manufacturer, designers can choose the robotic system that fits to their design task. Some examples of fabrication techniques and tools for different materials are shown below.



Figure 2.9: Subtraction – milling [45]

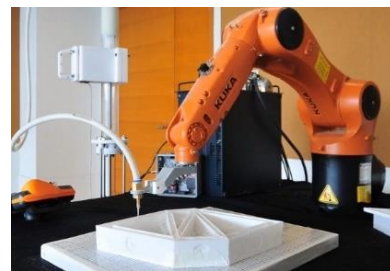


Figure 2.10: Addition - 3D printing [46]



Figure 2.11: Joining – welding [47]

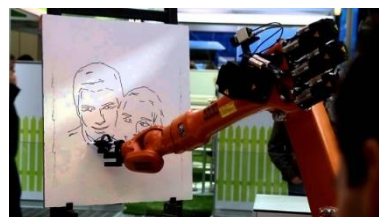


Figure 2.12: Generating – drawing [48]



Figure 2.13: Forming – bending [49]



## 2.3 THE PROGRAM OF A ROBOTIC SYSTEM

The second domain that should be investigated regarding robotic fabrication, is the program of a robot. The program of a robot is the entire set of instructions that instruct the robot to perform a sequence of operations. This paragraph highlights the following aspects of a program briefly: the components of a robotic program, the instructions of it, and how a robot physically performs these instructions. An extended description of these aspects can be found in Appendix D.

### 2.3.1 COMPONENTS OF A ROBOTIC PROGRAM

A program consists of different programming elements. The ABB robot manual is used to retrieve information from about how to set up a program for a robot. However, the information is reported in a general way that is applicable to most common types of robots [50]. Figure 2.14 shows an overview of the relationships between the different programming elements and their corresponding scales.

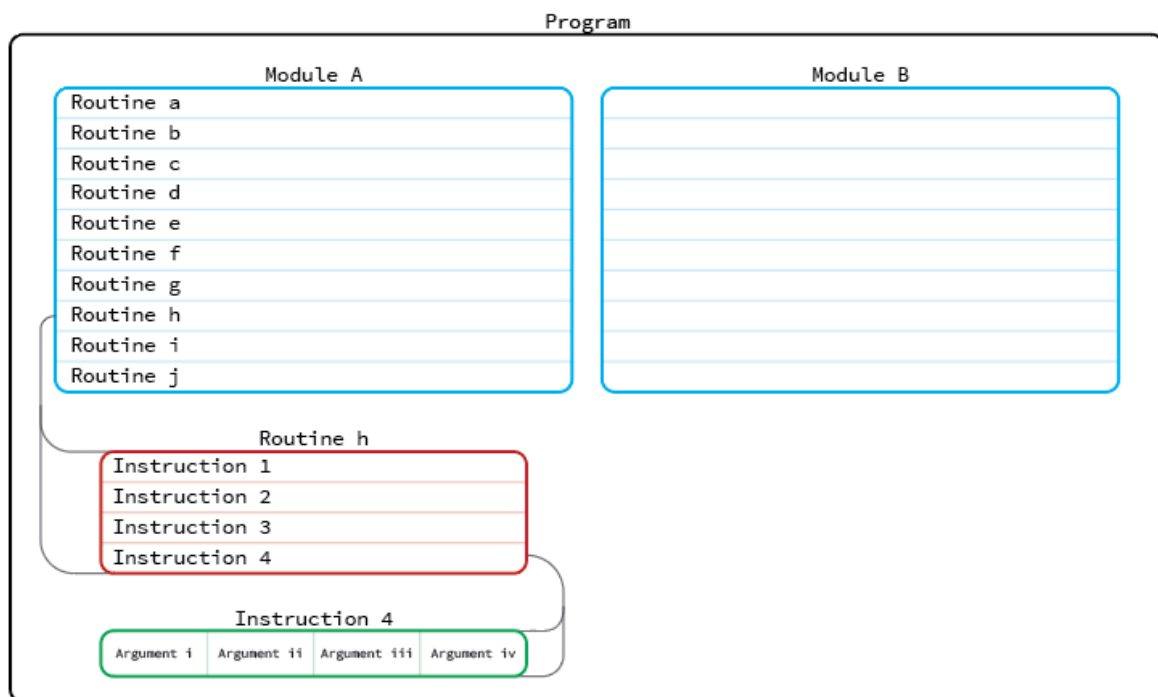


Figure 2.14: Overview of the components of a robotic program: Arguments, Instructions, Routines, and Modules

The components of a program of a robot are arguments, instructions, routines and modules. An instruction consists of arguments, a routine consists of instructions, a module consists of routines, and a program consists of modules. By combining these elements on their corresponding scales, several tasks can be repeated, combined and prioritized to form the program of a robot. As a matter of course, by setting up the right arguments and combinations within and between different elements, a wide range of customized programs can be set up.

### 2.3.2 INSTRUCTIONS OF A ROBOTIC PROGRAM

The first step to let a robot perform a certain program, is to write instructions. These instructions tell the robot *what* to do. Within the program, different combinations of instructions can be generated if tasks need to be performed repeatedly. These combinations tell the robot what to do *when* and are called routines. Besides different combinations, also different sequences can be applied on the order of instructions.

By putting tasks either to the fore- or background, the priority of tasks can be set. The background tasks will only execute when the foreground tasks are waiting for other tasks to be performed or have stopped the execution (idle). Figure 2.15 shows an example of task priorities.

Round robin chain 1:

- Tasks 0, 1, and 8 are busy

Round robin chain 2:

- Tasks 0, 3, 4, 5 and 8 are busy tasks 1 and 2 are idle

Round robin chain 3:

- Tasks 2, 4 and 5 are busy tasks 1, 2, 9 and 10 are idle.

Round robin chain 4:

- Tasks 6 and 7 are busy tasks 0, 1, 2, 3 4, 5, 8 and 9 are idle

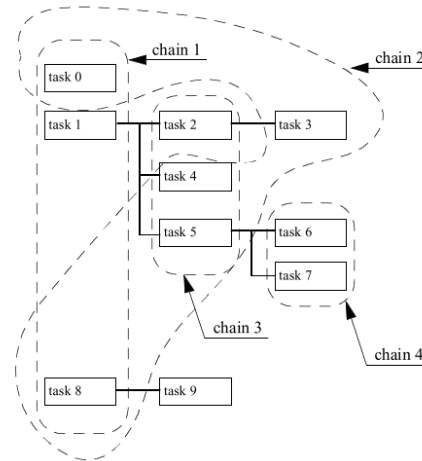


Figure 2.15: Prioritizing tasks by chains [50]

### 2.3.3 PHYSICAL PERFORMANCE OF INSTRUCTIONS BY A ROBOT

Once the program is setup with its instructions and ordered as desired, the next step is to analyze how a robot physically processes and performs the program. It moves with the Tool Center Point (TCP) that the robot is calibrated at, from one point to another. The TCP is the location on the end effector or tool of a robot manipulator whose position and orientation define the coordinates of the controlled object. During motion there are different types of motion that a robot can apply. Figures 2.16-2.18 show these different types of motion.

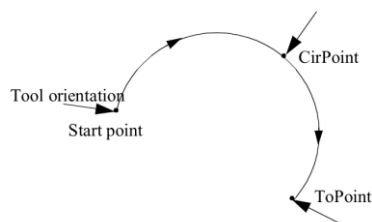


Figure 2.16: Circular movement [50]

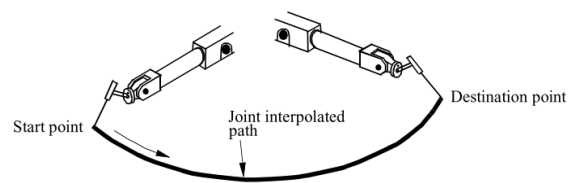


Figure 2.17: (Absolute) joint movement [50]

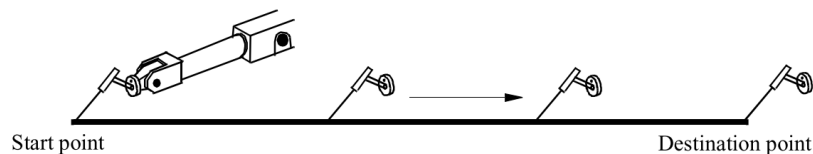


Figure 2.18: Linear movement without reorientation of the tool [50]

During this movement, a robot uses a coordinate system to orient its position upon. There are seven different coordinate systems a robot can apply for its orientation: the base coordinate system, the world coordinate system, the user coordinate system, the object coordinate system, the displacement coordinate system, the external axes based on the user coordinate system, and the external axes based on the object coordinate system. Figures 2.19 - 2.20 show the base- and world coordinate systems. Appendix D presents an extended overview and explanation.

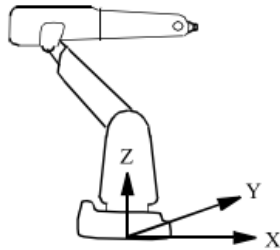


Figure 2.19: Base coordinate system [50]

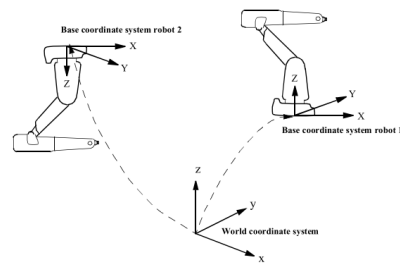


Figure 2.20: World coordinate system [50]

## 2.4 SCALE OF ROBOTIC FABRICATION IN THE BUILDING INDUSTRY

### 2.4.1 SCALE IN GENERAL

The motion range of a 6-axis robot generally is not more than 7 meters by 7 meters [51], [52], [53]. This implies there is a constraint regarding the size of robotically fabricated elements. Robots cannot always produce an element of any order of scale in one go.

However, the scale can be upgraded. The ETH Institute of Technology in Architecture performed experiments with robots on portal frames [54]. This setup could possibly double the scale of motion range of a robot. Besides constructing robots on a portal frame, they could also be installed on a track. This enables the robots to move along the element they fabricate. Another way to increase the scale of robots is to construct robots on a drone. In this way the scale is theoretically limitless. Nevertheless, this research explicitly focusses on customized robotic fabrication in the building industry and leaves drones out of its scope, as well as robotic assembling or fabrication of elements performed by robots on a track or portal frame.

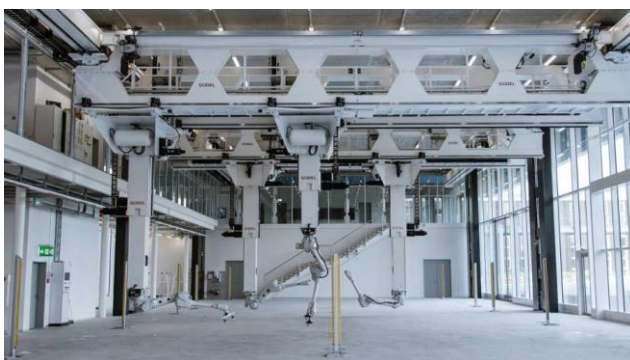


Figure 2.21: Robots on portal frames at ETH Zurich [54]



Figure 2.22: Robot on a track [55]

### 2.4.2 SCALE AND ACCURACY

Accuracy in the robotic world is relative, as it depends on many different factors such as scale, material, and calibration technology. The size of elements that are produced in the building industry is larger than for instance in the electronic industry. Even though robotics in the building industry are accurate, they will not be as accurate as robot that produce Intel chips for example. In case the architectural design requires high accuracy ( $\leq 1\text{mm}$ ), CNC machines will be more suitable instead of architectural robotics [56], [57].

## 2.5 SUITABLE MATERIALS FOR ROBOTIC OPERATIONS

### 2.5.1 MATERIALS IN GENERAL

Robots can perform operations on a wide range of materials with a diverse collection of tools, as described in Chapter 2.2. Materials such as steel, metal, wood, concrete, stone, plastic, foam, clay, resin, ceramic, and brick can be produced or operated on by robots. One thriving affordance regarding architectural robotics and materials worth mentioning, is the technique of morphogenetic design. This technique investigates possible convergences of computational form generation and computer-aided materialization in architecture through integrative design computation [58]. The material characteristics and robotic production method are integrated along the design process.

Specific types of robots can also process material feedback during the fabrication process. This feedback control replaces fixed instructions with decision rules, making the process responsive to material information. The robot can measure the force that is executed on the material and determine whether it should increase or decrease the force to achieve optimal accuracy. This is included in the program of the robot by setting one axis as a soft-servo, which makes the axis act as a mechanical spring. The force from the robot on the work object will increase as a function of the distance between the programmed position and the contact position ( $F=k*u$ ). Soft servo is of value when high precision is required [50].



Figure 2.23: Morphogenetic design by Achim Menges et al. [59]

### 2.5.2 MATERIALS AND ACCURACY

Among other factors, the accuracy of an architectural robot strongly depends on the type of material. When a robot starts to operate on a material, the material will start to vibrate, to move, or become fragile. For instance, friction will arise between the tool and the material in case of milling. The amount of vibration, movement, fragility and friction is different for each material. Wood is better at resisting high forces than polystyrene for example. Therefore, a designer should carefully consider which combination of robotic techniques and materials one will apply in the fabrication process. The affordances are not endless, and accuracy cannot be achieved at the same level as robots from other industries, such as the electronic industry.

## 2.6 THE MAIN PURPOSE OF CUSTOMIZED ROBOTIC FABRICATION

### 2.6.1 FORM FREEDOM IN GENERAL

Customized robotic fabrication in the building industry offers the affordance to produce or form elements of many kinds of forms and materials. Factors such as the type of robotic system, scale, and material determine the way to which extend the designer has form freedom in a design. It is not in the scope of this research to give a complete overview of all freeform affordances, but below a few examples of reference projects are shown. These examples exhibit a small representation out of the spectrum of form freedom in the field of customized robotic fabrication.



Figure 2.24: Robotic sensing mechanisms of tailored thin wooden shell elements [60]



Figure 2.25: AA/ETH Pavilion, bent panels of lightweight plywood [61]

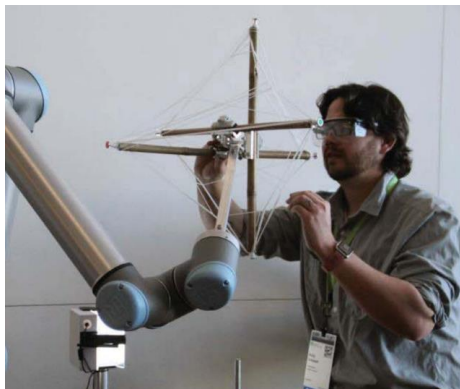


Figure 2.26: Human collaboration with robots for wire-based structures [62]



Figure 2.27: Honeycomb bricks [8]



Figure 2.28: Self-shaping CLT (1) [63]



Figure 2.29: Self-shaping CLT (2) [63]



*Figure 2.30: Milled wooden parametric inflections based on fabrication logic [8]*



*Figure 2.31: Organic design balancing program constraints, digital load-bearing optimization and fabrication affordances [64]*

## 2.6.2 FORM FREEDOM AND ACCURACY

As illustrated in this paragraph, there is a wide spectrum of form freedom. All types of freeform fabricated structures share one mutual aspect: architectural robotics have the purpose to fabricate customized elements. This implies to fabricate unique elements that can be optimized towards one or more objectives. As described in the introduction, the building industry is aiming for a 100% customized architecture, and robots can certainly contribute to achieving this goal.

One should carefully consider that customized elements are not as accurately fabricated as mass produced elements. If a designer is looking for mass production, CNC machines would fit the purpose better for instance. These robots generally have a higher accuracy and faster production speed. However, robots with the purpose of customized fabrication should be utilized at their strength, which is the production of unique elements.



## 2.7 CONCLUSION

This chapter answers the following questions:

- What type of robotic systems are applied in the building industry to produce customized elements?
- How does a robotic system perform a program of instructions?
- On what scale can a robot in the building industry perform operations?
- On what materials can a robot in the building industry perform operations?
- What main purpose does customized robotic fabrication in the building industry have?

This chapter describes the components of a robotic system, which are the controller, the robot itself, and the tooling. Not every robotic system is suited for every operation in the building industry. The main types of robots that are applied in this industry are the ABB, KUKA, and FANUC robots. They each have their own specific controlling system and available tooling. The choice of the robotic system highly depends on the purpose of fabrication, material, and scale.

A robot performs operations by interpreting a program that consists of instructions. These instructions can be ordered along customized combinations and priorities. As a matter of course, one can setup a completely customized program that the robot must perform.

The accuracy of a robot highly depends on the scale it is acting at, and the material it is performing operations on. For robotic systems in the building industry, customized robotic fabrication generally is limited to a scale of 7m x 7m, unless the scale is upgraded by a portal frame for instance or a track the robot can move along. The materials a robot can perform operations on, can be of a wide variety, such as steel, metal, wood, concrete, stone, plastic, et cetera.

The main purpose of customized robotic fabrication is form freedom. Highly customized elements can be produced of any kind of form. This stimulates the building industry to move towards a 100% customized industry. Even material-feedback can be included in an integral design process to form the shape of an element or structure.

As stated in the introduction of this chapter, the focus of this research is on the integral design process of robotically fabricated CLT connection panels. This integral design process has several affordances and constraints in it that can be divided within two fields:

- The field of CLT
- The field of customized Robotic Fabrication

This chapter highlights several affordances and constraints within the field of customized robotic fabrication, that are elaborated in the next chapter. That chapter combines the two fields and analyzes the mutual affordances and constraints of customized robotically fabricated CLT elements.

### 3. Affordances and Constraints of Customized Robotically Fabricated CLT Elements

This chapter lines out the affordances and constraints of customized robotically fabricated CLT elements. First, the field of CLT is discussed, followed by the field of customized robotic fabrication. Finally, the mutual constraints and affordances are laid out. The constraints and affordances as presented in this chapter are retrieved from Chapters 1 and 2.

#### 3.1 CROSS-LAMINATED TIMBER

This paragraph answers the following question:

*What are the affordances and constraints of CLT (structures)?*

From Chapter 1 the following affordances and constraints can be retrieved:

##### **Affordances.**

- CLT has a high dimensional stability: pre-fabrication allows for high-tolerance and a high-quality product.
- CLT can be made in dimensions up to 16m x 3m x 0.3m.
- CLT can transfer loads biaxially and is therefore suitable for structural applications
- CLT can be applied as lightweight (structural) walls, floors, beams and roofs.
- CLT can withstand tension, compression, bending, and shear both in-plane and out-of-plane.
- CLT has a high design flexibility due to the nature of the material.
- CLT is suitable to perform robotic fabrication methods on such as milling, drilling, and sawing.
- Screwed connections are relatively easy to materialize and can ensure a pinned or semi-rigid connection without additional structural provisions.

##### **Constraints.**

- Forest certification should be applied at the timber elements of a project.
- One should carefully design a moisture- and temperature control system for a CLT structure.
- At this moment, the material is not suited, and it is not common to apply CLT unprotected in the outdoor environment.
- Extra weight is added to a CLT structure by fire protection sheeting or extra layers to ensure fire safety.
- The material is delivered in the format of plates only with maximum dimensions of 16m x 3m x 0.3m.
- As CLT is an upcoming structural type of timber, there is a lack of experience in engineering compared to more common materials, such as concrete and steel.
- It is recommended to stick to planar CLT elements when designing a CLT structure. However, recent researches show the potential of curved CLT elements.
- Many structural provisions must be made to ensure a clamped connection. A designer should critically reflect whether a pinned or semi-rigid connection can fulfil the design's purpose.

Besides the affordances and constraints of CLT that are retrieved from a literature point of view, this research investigates these from a practical point of view as well, along the development of the digital integral workflow (part III).



### 3.2 CUSTOMIZED ROBOTIC FABRICATION

This paragraph particularly focusses on the affordances and constraints of customized robotic fabrication. It therefore answers the following question:

*What are the affordances and constraints of customized robotic fabrication?*

From Chapter 2, the following affordances and constraints can be retrieved:

#### **Affordances**

- There are five different types of robotic fabrication:
  - o Subtraction
  - o Addition
  - o Joining
  - o Forming
  - o Generating
- Instructions that a robot should execute can be ordered along customized combinations and priorities. As a matter of course, one can setup a completely customized program that the robot must perform.
- A robot can use several coordinate systems to base its orientation and position upon.
- The maximum motion range or scale of a robot can be enlarged by installing the robot on a track or portal frame.
- Generally, the maximum motion range of a robot is about 7m x 7m.
- Customized robotic fabrication in the building industry offers the opportunity to produce a wide variety of customized forms of many kinds of materials.
- Specific types of robots can process material feedback during the fabrication process.

#### **Constraints**

- The working dimensions of robots in the building industry are not wider than 7m x 7m without installing the robot on a track or portal frame.
- In case of assembling or gripping, the designer should consider the maximum payload of the robot.
- Customized robotic fabrication in the building industry is not suited to acquire a high level of accuracy compared to CNC machines for instance.

Besides the affordances and constraints of robotic fabrication that are retrieved from a literature point of view, this research investigates these from a practical point of view as well, in the pilot study (part II), and the development of the digital integral workflow (part III). Finally, one should consider that the technological developments are part of an ongoing evolution. The affordances and constraints of this year will be different from next year or the next decennium to come.

### 3.3 CUSTOMIZED ROBOTICALLY FABRICATED CLT PANELS

The previous two paragraphs analyze the affordances and constraints of robotic fabrication and CLT within several domains. The mutualities of these paragraphs will answer the following question more into depth:

*What are the affordances and constraints of customized robotically fabricated CLT elements?*

Below a graphical representation is shown of the mutualities between the domains of CLT and robotic fabrication, which are elaborated more into depth in the consecutive section. These affordances and constraints will define the design space of the Pilot Study (part II) and the Development of the integral Workflow (part III).

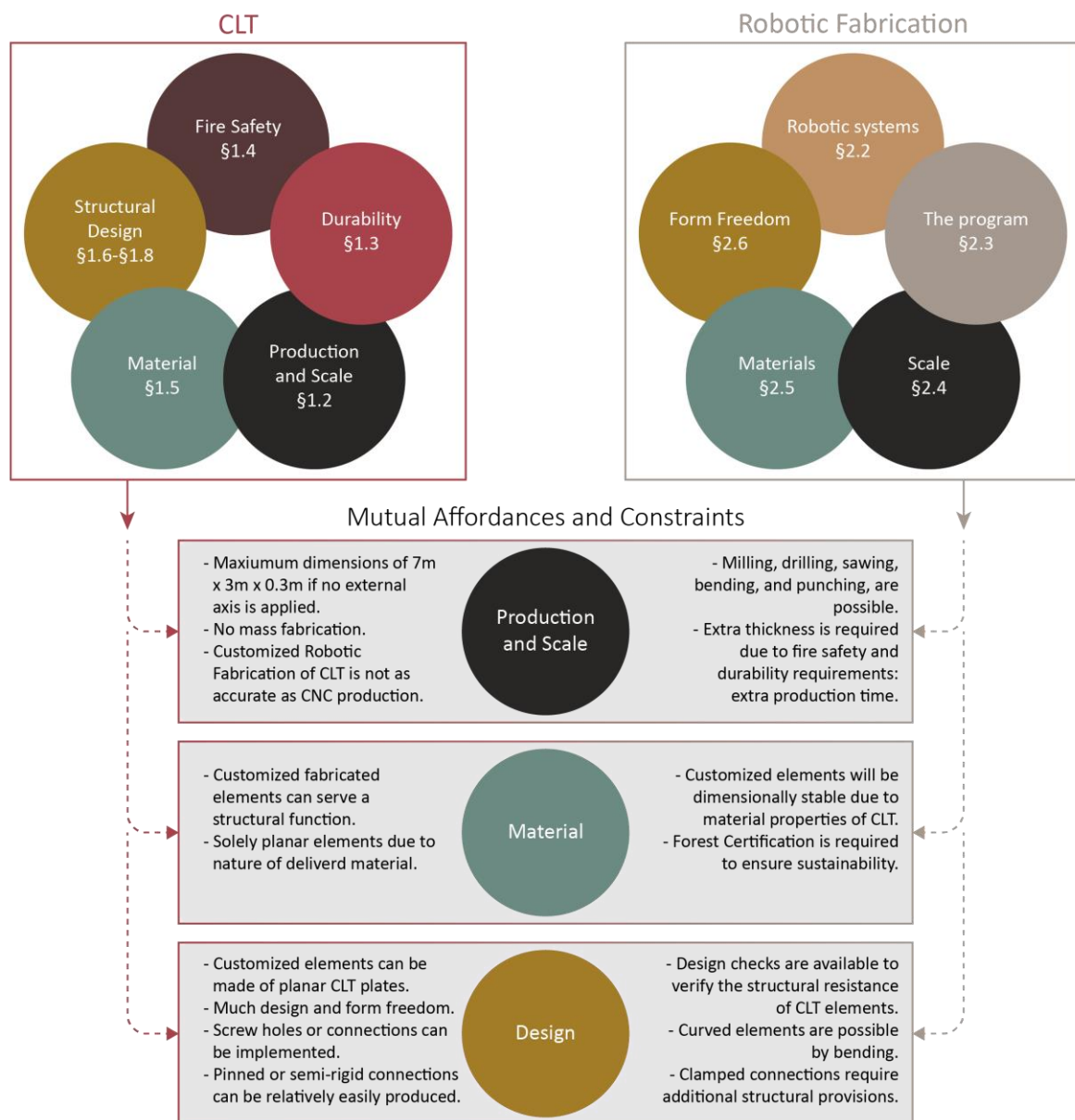


Figure 3.1: Mutualities of Robotic Fabrication and CLT

### 3.3.1 CONCLUSIONS ON ROBOTIC FABRICATION OF CLT CONNECTION PANELS

#### ... the Affordances of CLT connection panels and robotic fabrication

- Robotically fabricated CLT elements have a *high dimensional stability* and therefore allow for high-tolerance and high-quality products.
- Monolithic CLT elements can be robotically fabricated up to average *dimensions* of 3m x 3m x 0.3m, depending on the domain of the robot and delivered CLT elements. Assuming the domain of the robot is not upgraded by means of a portal frame or track.

<i>Maximum domain</i>	<i>Length [m]</i>	<i>Width [m]</i>	<i>Height [m]</i>
CLT element	16	3	0.3
Robot	7	7	3

- CLT elements can be robotically fabricated through the fabrication process of *subtracting* by means of milling, drilling, sawing, bending and punching.
- CLT is suitable for *customized* robotic fabrication and this technique opens opportunities to produce a wide variety of customized forms of structural timber due to the nature of the material. This contributes to the significant change the building industry is on the brink of, namely the move towards a *100% customized more sustainable architecture*.
- Robotic fabrication of CLT connection panels opens opportunities to a *modular* or *component-based design*.
- The CLT connection panels can represent either a *pinned* or *semi-rigid connection*.

#### ... the Constraints of CLT connection panels and robotic fabrication

- The *thickness of CLT elements* is mainly influenced by structural requirements, fire safety, and desired durability of a structure. This thickness has significant influence on the robotic production time and therefore must be carefully considered in the early design process. Besides, these additional layers also add extra self-weight which should be considered in the structural analyses.
- *Forest certification* should be applied at CLT elements of a project, to ensure contribution to a more sustainable architecture.
- CLT elements are *always* delivered in *plates* and therefore no curved CLT connection panels can be produced by means of subtraction.
- CLT connection panels can be robotically fabricated up to *dimensions of 3m x 3m x 0.3m*.
- Robotically fabricated CLT connection panels will *not* be *as accurately* produced as CNC produced CLT elements for instance.
- To acquire sufficient *accuracy* ( $\pm 1\text{mm}$  tolerance), one should carefully consider the type of termination, termination speed of the robot, the angle of the mill, type and hardness of the material, and scale of the object.
- *No clamped connection* can be produced of a CLT connection panel without additional structural provisions, which is mainly due to the accuracy of the fabrication process.

## Part II

### Pilot Study

## 4. Exploring the Process of Robotic Fabrication

### 4.1 INTRODUCTION

The second part of this research, the pilot study, serves one main purpose: exploring the process of robotic fabrication. The knowledge gained during this study will be used as upfront input for the design process of the integral workflow in the third part of the research. As the integral workflow will integrate the global shape of a CLT structure with the design of CLT connection panels, the pilot study will focus on the design and robotic fabrication connection panels.

The project of the bus transferium in Alblasterdam (NL) as introduced in the introduction of this report, serves as an inspiration of the pilot study. The project exists of planar CLT roof plates that shed the bus platform from rain, snow and sunlight. These roof plates each have a unique angle and orientation to both serve the architectural concept, and to not block off the bus platform from daylight entirely. As the shape of the connection panels is a result of the orientation and position of the roof plates, each connection panel will have a unique shape. Figure 4.1 shows an architectural impression.

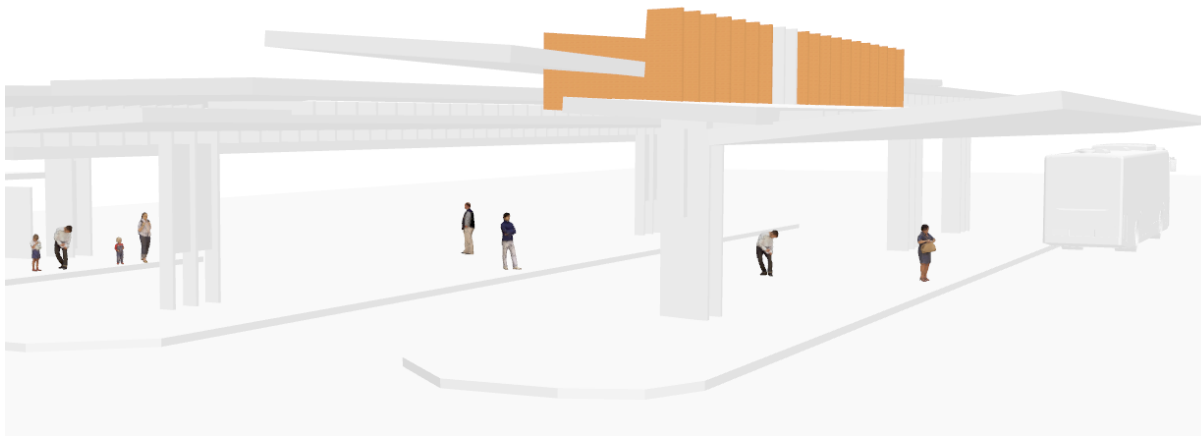


*Figure 4.1: CLT connection panels highlighted in the preliminary architectural impression of the bus transferium [5]*

As shown in the architectural impression, the CLT connection panels connect the CLT roof plates together. The roof plates are connected to the connection panels by slotted holes. Screws will be added to transfer forces properly. This concept of CLT connections panels with slotted holes is represented in the pilot study.

## 4.2 SCOPE AND GOAL

**Scope.** This pilot study explicitly investigates the robotic fabrication process of milling. It does not include assembling elements or drilling holes for instance. No optimization or structural analyses are involved.

**Objective.** The goal of this pilot study is to explore the process of robotic fabrication from digital design to physical manufacturing. Therefore, this chapter includes the main steps involved in this process.

## 4.3 GEOMETRY

This study only includes a simple geometry consisting of two planar multiplex plates and three multiplex joints. The geometry as modelled is shown below with the joints in red, the plates in green.

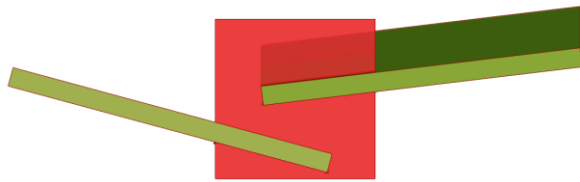


Figure 4.2: Front view

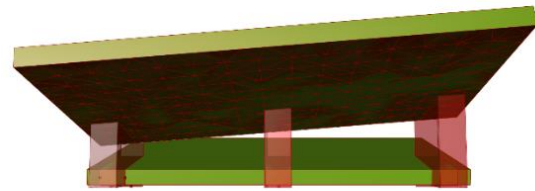


Figure 4.3: Side view

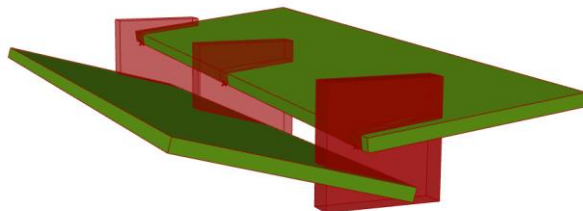


Figure 4.4: Perspective view

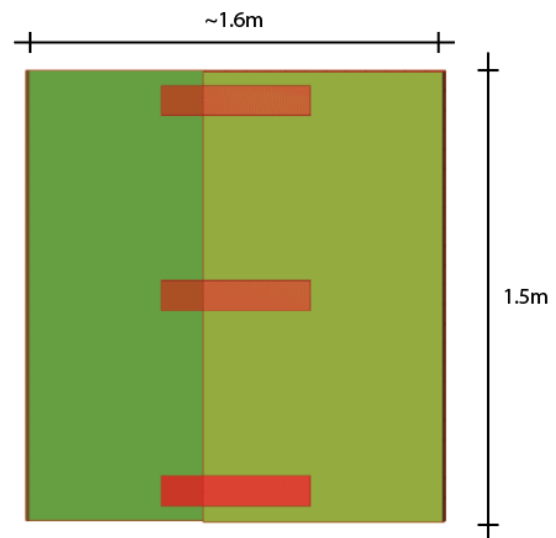


Figure 4.5: Top view

#### 4.4 SOFTWARE, HARDWARE, AND MATERIALS

The following software, hardware, and materials are used during the pilot study:

##### Software:

<i>Component</i>	<i>Purpose:</i>
Rhino3D	Model the geometry in 3D.
Grasshopper3d	Graphically setup of algorithms to model geometry in Rhino3D.
Rapcam	Simulate the robotic fabrication process and generate robotic code.
Python	Translate robotic code from Grasshopper to binary code.

##### Hardware:

<i>Component</i>	<i>Purpose:</i>
FANUC robot	Mill the three connection panels, highlighted in red in Figure 4.2-4.5.
Drilling machine	Attach the objects to the table, to avoid severe vibration during production.
Circular saw	Cut the multiplex plates that will be assembled in the connection panels.

##### Materials:

<i>Component</i>	<i>Purpose:</i>
Multiplex wood (t=34mm, $\rho=488.3\text{kg/m}^3$ )	Material for the plates and connection panels

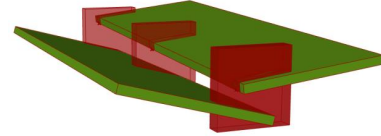
## 4.5 METHODOLOGY

The methodology is listed below in the consecutive sequence of steps involved in the pilot study.

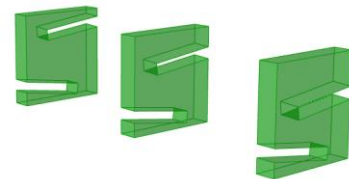
*Step*      *Description*

*Outcome*

**1**            **Modelling of geometry in Grasshopper**

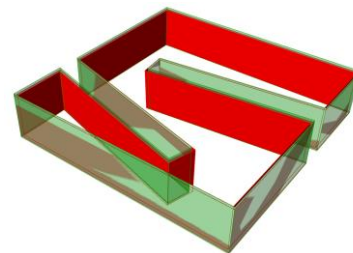


**2**            **Isolate elements for robotic fabrication: the connection panels**

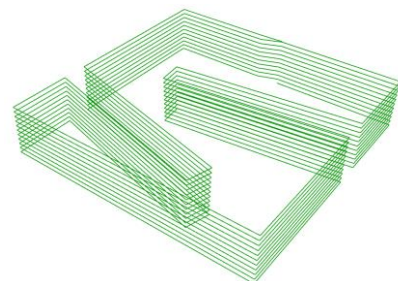


**3**            **Prepare geometry for robotic fabrication**

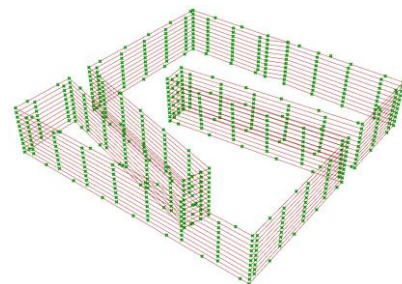
a) Offset of the side faces of the original BREP. At these faces the toolpath will be constructed.



b) Create a toolpath around the offset faces by 'slicing' the faces of the BREP vertically.

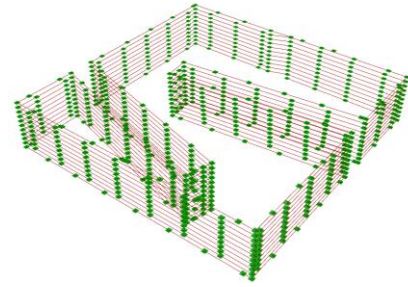


c) Construct points on the toolpath that the tool should move along.

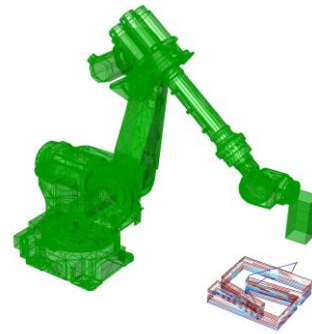




- d) Construct planes perpendicular to the toolpath on the defined points of the previous step to model the correct orientation of the robot.



- e) Simulate the robotic fabrication process with RapCam to check for potential errors. [42]



#### 4 Generate G-code with python

```

g20[mm] G0 X100 Y100 Z10 F1000 ;
g21 G1 X100 Y100 Z10 F1000 ;
g22 G1 X100 Y100 Z10 F1000 ;
g23 G1 X100 Y100 Z10 F1000 ;
g24 G1 X100 Y100 Z10 F1000 ;
g25 G1 X100 Y100 Z10 F1000 ;
g26 G1 X100 Y100 Z10 F1000 ;
g27 G1 X100 Y100 Z10 F1000 ;
g28 G1 X100 Y100 Z10 F1000 ;
g29 G1 X100 Y100 Z10 F1000 ;
g30 G1 X100 Y100 Z10 F1000 ;
g31 G1 X100 Y100 Z10 F1000 ;
g32 G1 X100 Y100 Z10 F1000 ;
g33 G1 X100 Y100 Z10 F1000 ;
g34 G1 X100 Y100 Z10 F1000 ;
g35 G1 X100 Y100 Z10 F1000 ;
g36 G1 X100 Y100 Z10 F1000 ;
g37 G1 X100 Y100 Z10 F1000 ;
g38 G1 X100 Y100 Z10 F1000 ;
g39 G1 X100 Y100 Z10 F1000 ;
g40 G1 X100 Y100 Z10 F1000 ;
g41 G1 X100 Y100 Z10 F1000 ;
g42 G1 X100 Y100 Z10 F1000 ;
g43 G1 X100 Y100 Z10 F1000 ;
g44 G1 X100 Y100 Z10 F1000 ;
g45 G1 X100 Y100 Z10 F1000 ;
g46 G1 X100 Y100 Z10 F1000 ;
g47 G1 X100 Y100 Z10 F1000 ;
g48 G1 X100 Y100 Z10 F1000 ;
g49 G1 X100 Y100 Z10 F1000 ;
g50 G1 X100 Y100 Z10 F1000 ;
g51 G1 X100 Y100 Z10 F1000 ;
g52 G1 X100 Y100 Z10 F1000 ;
g53 G1 X100 Y100 Z10 F1000 ;
g54 G1 X100 Y100 Z10 F1000 ;
g55 G1 X100 Y100 Z10 F1000 ;
g56 G1 X100 Y100 Z10 F1000 ;
g57 G1 X100 Y100 Z10 F1000 ;
g58 G1 X100 Y100 Z10 F1000 ;
g59 G1 X100 Y100 Z10 F1000 ;
g60 G1 X100 Y100 Z10 F1000 ;
g61 G1 X100 Y100 Z10 F1000 ;
g62 G1 X100 Y100 Z10 F1000 ;
g63 G1 X100 Y100 Z10 F1000 ;
g64 G1 X100 Y100 Z10 F1000 ;
g65 G1 X100 Y100 Z10 F1000 ;
g66 G1 X100 Y100 Z10 F1000 ;
g67 G1 X100 Y100 Z10 F1000 ;
g68 G1 X100 Y100 Z10 F1000 ;
g69 G1 X100 Y100 Z10 F1000 ;
g70 G1 X100 Y100 Z10 F1000 ;
g71 G1 X100 Y100 Z10 F1000 ;
g72 G1 X100 Y100 Z10 F1000 ;
g73 G1 X100 Y100 Z10 F1000 ;
g74 G1 X100 Y100 Z10 F1000 ;
g75 G1 X100 Y100 Z10 F1000 ;
g76 G1 X100 Y100 Z10 F1000 ;
g77 G1 X100 Y100 Z10 F1000 ;
g78 G1 X100 Y100 Z10 F1000 ;
g79 G1 X100 Y100 Z10 F1000 ;
g80 G1 X100 Y100 Z10 F1000 ;
g81 G1 X100 Y100 Z10 F1000 ;
g82 G1 X100 Y100 Z10 F1000 ;
g83 G1 X100 Y100 Z10 F1000 ;
g84 G1 X100 Y100 Z10 F1000 ;
g85 G1 X100 Y100 Z10 F1000 ;
g86 G1 X100 Y100 Z10 F1000 ;
g87 G1 X100 Y100 Z10 F1000 ;
g88 G1 X100 Y100 Z10 F1000 ;
g89 G1 X100 Y100 Z10 F1000 ;
g90 G1 X100 Y100 Z10 F1000 ;
g91 G1 X100 Y100 Z10 F1000 ;
g92 G1 X100 Y100 Z10 F1000 ;
g93 G1 X100 Y100 Z10 F1000 ;
g94 G1 X100 Y100 Z10 F1000 ;
g95 G1 X100 Y100 Z10 F1000 ;
g96 G1 X100 Y100 Z10 F1000 ;
g97 G1 X100 Y100 Z10 F1000 ;
g98 G1 X100 Y100 Z10 F1000 ;
g99 G1 X100 Y100 Z10 F1000 ;

```

#### 5 Robotic fabrication



#### 6 Assembling



## 4.6. DISCUSSIONS AND CONCLUSIONS

### 4.6.1 DISCUSSIONS

#### Automation and optimization

This pilot study showed the particular steps involved in the process of robotic fabrication by means of milling wooden elements. The third step of this process involved the preparation of geometry for robotic fabrication. This is quite a circuitous process as it involves extra steps besides the setup of the 3D geometry. These steps are described in the previous paragraph. However, the entire process from plain geometry to generating the correct G-code could possibly be automated and optimized to reduce human intervention. Below the main challenges are described that were encountered, which are controlling of the accuracy in general and controlling of the accuracy in case of angular milling.

#### Accuracy in general

To control the accuracy of the milling process, several parameters should be carefully considered:

- The diameter of the mill.
- The type of wood applied.
- The vibration of the object.
- The amount of slices the toolpath is divided into, see also step 3b.
- The number of planes on the tool path to orient the tool's position upon, see also step 3d.
- The length of the exploded toolpath segments. The smaller the segment, the more points are needed to acquire sufficient accuracy. The underlying reason for this is that the TCP moves along a circular movement from one point to the next point. So, the denser the amount of points on a small segment, the smaller the circular movement, and the higher the accuracy. An example is shown below.

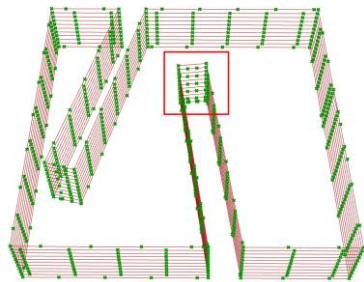


Figure 4.6: Small segments highlighted

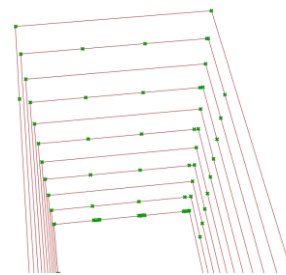


Figure 4.7: Two intermediate points constructed on the small segments



Figure 4.8: Result without intermediate points – lower accuracy



Figure 4.9: Result with intermediate points – higher accuracy

### Accuracy of angular milling

One remarkability of the pilot study is the milling of the slotted holes. As shown in the digital geometry they should be milled under a specific angle out-of-plane. This can be shown by the top view of the wooden joint.

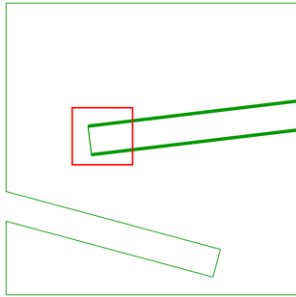


Figure 4.10: Digital geometry of wooden joint (top view)

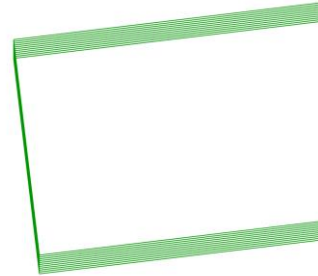


Figure 4.11: Zoomed section of paths to show the slope in the slotted holes of the joint (top view)

This pilot study showed however, that the angle of the physical model was milled under a smaller angle than modelled digitally. The assumption is that this has to do with several factors:

- The number of slices the faces of the BREP is divided into, see also step 3b of Chapter 4.5.
- The accuracy and calibration of the robot itself.
- The diameter of the mill.
- The power of the robot.

The reason why these assumptions are made, is that during the milling of the slotted holes extra noise was noticed. Probably too much friction and heat arose between the mill and the wood as the number of slices was insufficient. Consequently, the mill had to mill away too much wood in one go.

#### 4.6.1 CONCLUSIONS

- Sufficient accuracy should be considered by carefully managing the amount of constructed points on small toolpath segments. However, the accuracy of the connection panels is not sufficient to guarantee a perfect fitting connection with the plates. This eliminates the possibility to let the connection panels function as a clamped connection.
- The process of preparing geometry for robotic fabrication should be automated and optimized if possible.
- In case of angular milling, the number of slices along the thickness of a connection panel should be sufficient to avoid too much friction between the mill and the wood.
- The accuracy on small segments of the toolpath highly depends on the number of orientation planes constructed on these segments. The more planes on a segment, the higher the accuracy.

## Part III

# Integral Workflow Development

# Introduction

## Integral Workflow Development

This third part of the research concerns the development of the integral workflow for robotically fabricated customized CLT connection panels. The workflow is built up along three modules, which are shown in Figure III.I, and is based on the Literature study (part I) and the Pilot study (part II). The goal of this part of the research is to study the relationships and (in)dependencies between the three modules of the workflow. Doing so, one should be able to quickly explore the structural performance of CLT structures on a global and local level in the preliminary design phase. As a matter of course, this aligns with the main research question as stated in the introduction of this report. Different geometries are developed in Grasshopper, and Finite Element (FE) analyses are performed in GSA.

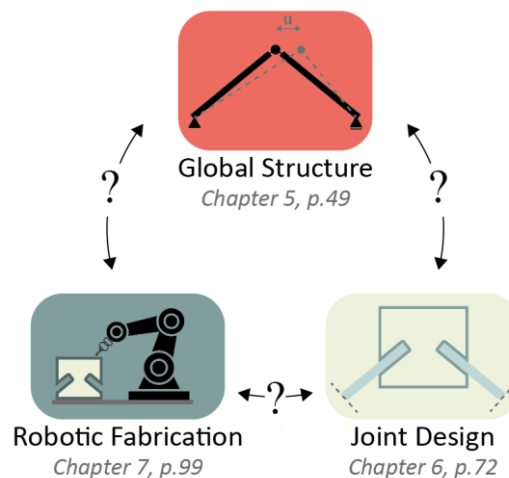


Figure III.I: Three components of the integral workflow and the corresponding chapters

### **Main research question:**

*What does an integral workflow for robotically fabricated customized CLT connection panels look like, that promote exploration of the structural performance of CLT structures in the preliminary design phase?*

## 5. Global Structure Module

### 5.1 INTRODUCTION

This chapter deals with the structural modelling and exploration of a CLT structure on a global level and concerns the first module of the integral workflow. The goal of this chapter is to develop a module that enables users to quickly explore the structural performance of a CLT structure on a global level in the preliminary design phase. Therefore, the following question is answered in this chapter:

What does a workflow for CLT structures look like, that promote exploration of the structural performance of CLT structures on a *global* level in the preliminary design phase?

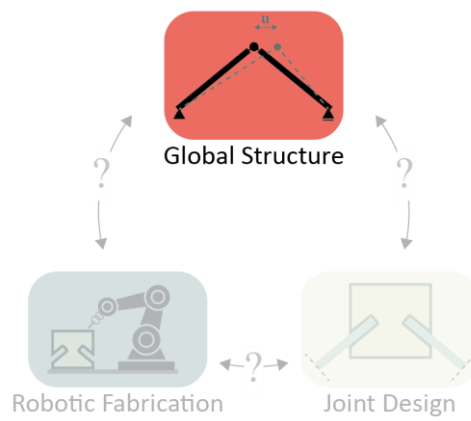


Figure 5.1: Focus of this chapter - the Global Structure module

The answer is formulated by first describing the relevant orthogonal material properties of CLT. This concerns the bending- and shear stiffness in the weak and strong directions of a CLT element. In the third and fourth paragraph, different variables are described that should be integrated in the workflow to model different geometries of CLT structures. The fifth paragraph shows how these structures can be transformed into FEM models to perform Finite Element Analyses (FEA) on it. Thereafter, the relationships with the joint design are described, which are geometrical and structural relationships. The closing paragraphs of this chapter briefly demonstrate the protentional of the Global Structure module by showing different geometries of CLT structures processed by the workflow. Correlations are derived that describe the influence of geometrical parameters of a structure on the structural performance of it.

## 5.2 RELEVANT ORTHOGONAL MATERIAL PARAMETERS OF CLT IN THE FEM

As CLT is an orthotropic material, it is of importance to carefully pay attention to the bi-directional material properties in FEM programs. The literature study of this report explains the design philosophy of CLT. Concisely stated, a designer derives effective parameters of the bending- and shear stiffnesses for both the strong and weak directions of the element. This paragraph describes the application of this design philosophy for the required input parameters of the FEM, consecutively the Young's moduli, shear moduli, and remaining material parameters.

### 5.2.1 YOUNG'S MODULI

According to the proHolz design guide, the effective bending stiffness of a CLT cross-section can be calculated based on the cross-sectional geometry, see Chapter 1.6. [18] This results in the following parameters:

$(EI)_{ef,strong}$	$[Nmm^2]$	<i>Effective bending stiffness in strong direction</i>
$(EI)_{ef,weak}$	$[Nmm^2]$	<i>Effective bending stiffness in weak direction</i>

Once the effective bending stiffnesses are derived, these parameters need to be translated into effective Young's moduli  $E_{ef}$  [N/mm<sup>2</sup>], as the input parameters for the material properties of a FEM model cannot consist of an EI-factor. The effective Young's moduli can be calculated by the Formulas (36) and (37):

$$E_{ef,strong} = \frac{(EI)_{ef,strong}}{I_{tot}} \quad [Nmm^2] \quad (36)$$

$$E_{ef,weak} = \frac{(EI)_{ef,weak}}{I_{tot}} \quad [Nmm^2] \quad (37)$$

For orthotropic materials in the FEM, the Young's modulus can be defined in the x-, y-, and z-direction of the element, by  $E_x$ ,  $E_y$ , and  $E_z$ . Figures 5.2-5.3 show a graphical overview of the required Young's moduli in the local x- and y-direction that are provided as input parameters to model an orthotropic material in a FEM model. The third direction, the local z-direction, is not relevant as plates are modelled as two-dimensional mesh elements. The third dimension can therefore be ignored.

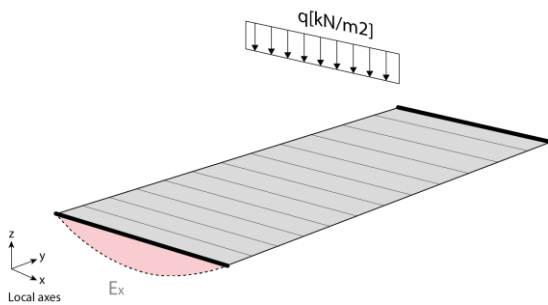


Figure 5.2:  $E_x$  is governing for bending around y-axis – supports situated at thick edges

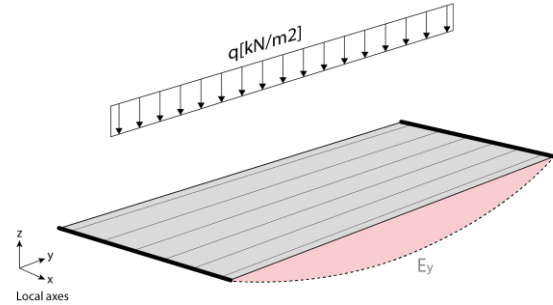


Figure 5.3:  $E_y$  is governing for bending around x-axis – supports situated at thick edges

### 5.2.1 SHEAR MODULI

The effective shear modulus  $G$  [Nmm<sup>2</sup>] in both directions can be calculated in the same way as the effective Young's modulus. Based on the proHolz design guide, Chapter 1.6 describes how the effective shear stiffness can be calculated, which results in the following parameters [18]:

$(GA)_{ef,strong}$	[N]	Effective shear stiffness in strong direction
$(GA)_{ef,weak}$	[N]	Effective shear stiffness in weak direction

Once the effective shear stiffnesses are derived, these parameters need to be translated into effective shear moduli  $G_{xy}$  [N/mm<sup>2</sup>], as the input parameters for the material properties of a FEM model cannot consist of a GA-factor. The effective shear moduli can be calculated by Formulas (38) and (39). For rectangular cross-sections,  $k=5/6$  according the proHolz design guide.[18]

$$G_{ef,strong} = \frac{(GA)_{ef,strong}}{k * A_{tot}} \quad [\text{Nmm}^2] \quad (38)$$

$$G_{ef,weak} = \frac{(GA)_{ef,weak}}{k * A_{tot}} \quad [\text{Nmm}^2] \quad (39)$$

For orthotropic materials, the shear moduli can be defined in the xy-, yz-, and xz-plane by  $G_{xy}$ ,  $G_{yz}$ , and  $G_{zx}$ . Therefore, the following general notation applies:

$G_{ij}$  shows the face  $G$  is acting at ( $i$ ) and the direction  $G$  is acting in ( $j$ ).

Figure 5.4 shows a general representation of shear moduli acting in different planes. These should be provided as input parameters to model an orthotropic material in a FEM model.

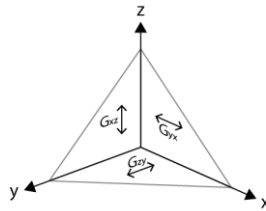


Figure 5.4: General notation of shear moduli

If applying this theory at a simply supported plate, a distinction between the strong and weak direction should be made. The strong direction concerns the direction with the largest shear area (blue), whereas the weak direction has the smallest shear area (yellow). Figure 5.5 shows this.

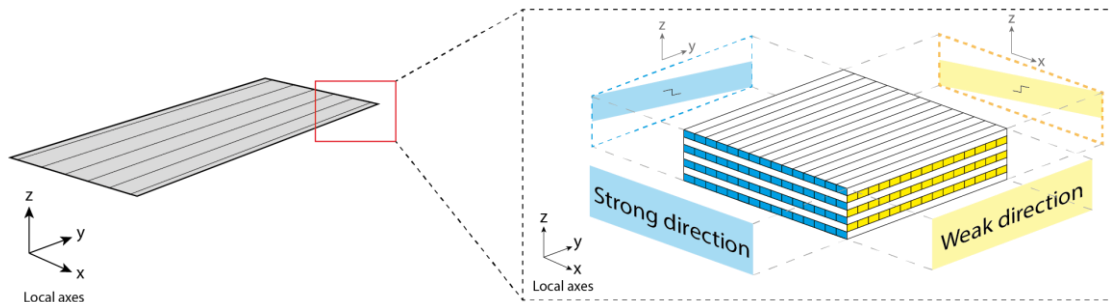


Figure 5.5: Graphical representation of shear planes in the strong and weak direction of a CLT element.



Ordering the faces- and directions of the shear moduli in the weak and strong direction results in an overview as presented in Table 7. The shear deformation of the strong direction is acting in the yz-plane and at the face of the x-axis, whereas the shear deformation of the weak direction is acting in the xz-plane, at the face of the y-axis. Finally, the shear deformation in the xy-plane, the in-plane-shear, is not governing in case of loading out-of-plane. However,  $G_{xy}$  were governing if in-plane loading occurred, which for instance is the case with shear walls. Literature states that  $G_{xy} = 0.36 \cdot G_0$  with  $G_0 = 690 \text{ N/mm}^2$  for pine [65].

	Face G is acting at (i)	Direction G is acting in (j)	Shear modulus $G_{ij}$
Strong direction	x	z	$G_{xz}$
Weak direction	y	z	$G_{yz}$
In-pane	-	-	$G_{xy}$

Table 7: Overview of faces and directions of shear moduli in weak and strong direction

Once the weak and strong shear planes are defined, the general shear planes as defined in Figure 5.4 should be transformed to the local axes of the element. This results in the shear moduli as shown in Figures 5.6-5.8.

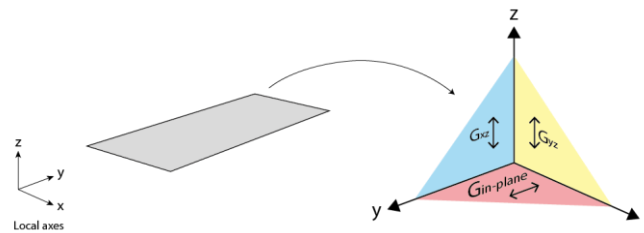


Figure 5.6: Graphical representation of shear moduli according to the local axes system of a CLT element

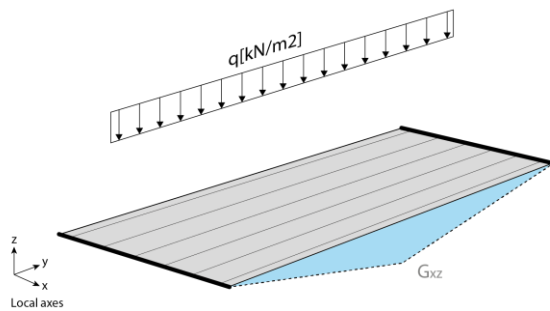


Figure 5.7: Graphical representation of shear deformation in the strong direction due to loading in the z-direction – supports situated at thick edges

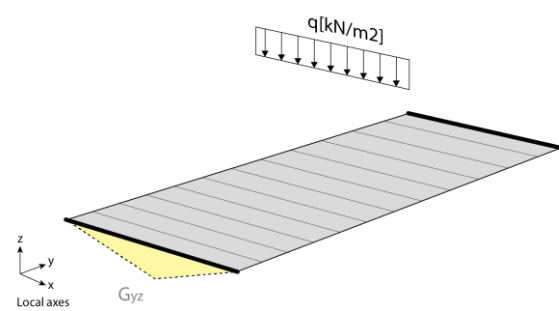
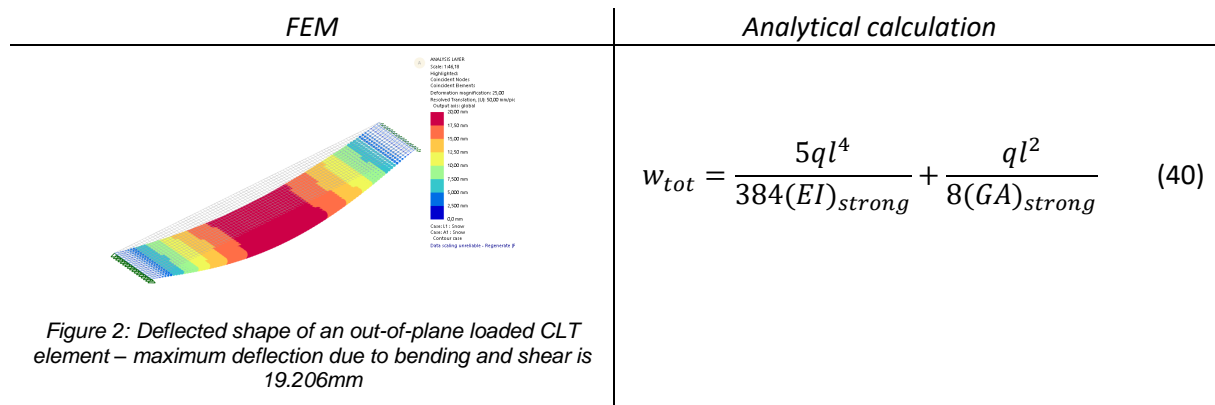


Figure 5.8: Graphical representation of shear deformation in the weak direction due to loading in the z-direction – supports situated at thick edges

### 5.2.3 VALIDATION AND REMAINING MATERIAL PARAMETERS

Appendix E shows an overview of all required orthogonal material properties for the FEM including the Young's- and shear moduli as described in this paragraph. Besides, this Appendix shows a numerical validation of the FEM as well, to assure the orthogonal material properties are correctly applied. The result of this appendix is shown below.

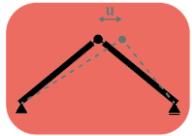


	Bending	Shear	Bending and Shear
FEM	18,6mm	0,606mm	19,206mm
Analytical calculation	18,61mm	0,607mm	19,217mm
Deviation	0,053%	0,06%	0,057%

**Conclusion validation.** The maximum deviation between the FEM and the analytical calculation is 0.0057%. The FEM is therefore successfully validated.

### 5.3 VARIABLES OF THE GLOBAL STRUCTURE MODULE

Once the relevant orthogonal material properties are determined, the actual workflow of the Global Structure module can be set up. This paragraph presents all variables that are required for this module. Below an overview is shown of the variables and output of the Global Structure module.

Input Variable		Type	Global Structure module	Output
a	Surface	Geometry		* Relevant data for a FEM model of the Global Structure * Numerical data as input for the Joint Design Module
b	Width of joints	Integer		
c	Joined or separated surface	Integer		
d	Number of joints along edge	Integer		
e	Scaled length for joint division	Number		
f	Joint orientation	Integer		
g	Joint to analyze	Integer		
h	Cross-sectional build-up	List		
i	Wood properties	Numbers		
j	Orientation of first layer	Integer		

All variables as presented above are explained and illustrated in Appendix F. Figure 5.9 shows the components of the simplified workflow of the Global Structure module. Each component is explained more into depth in the consecutive paragraphs.

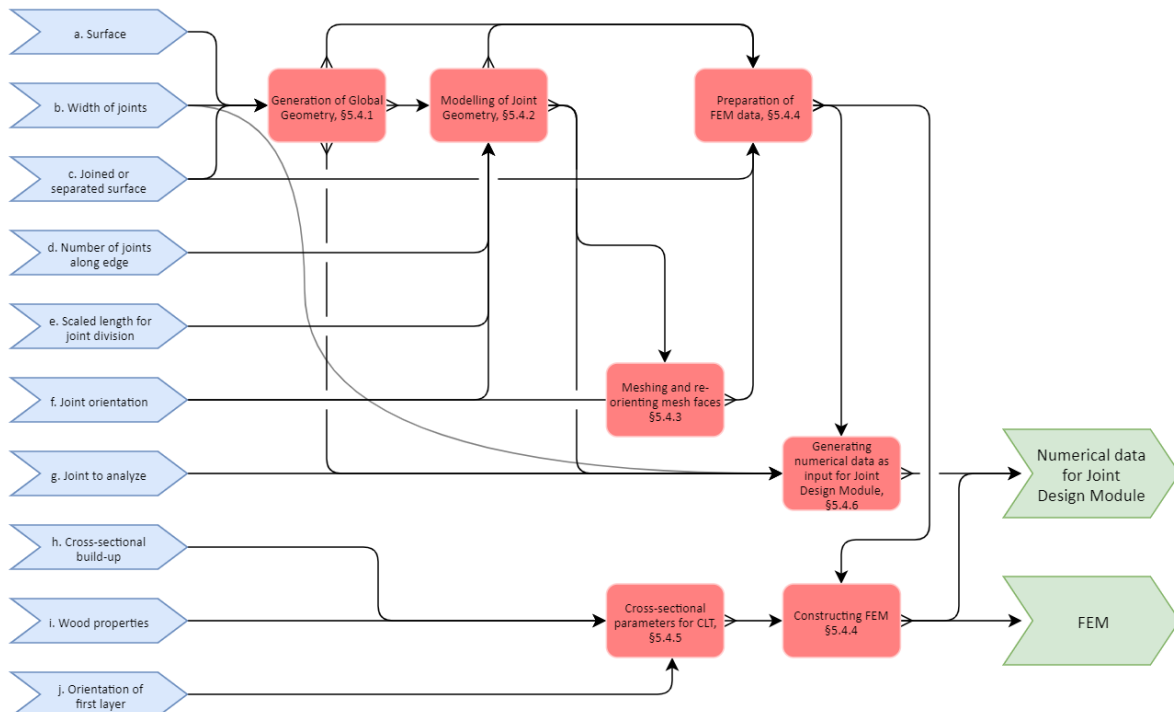


Figure 5.9: Simplified representation of the Global Structure module

(Blue: input variables, Red: processing by the Global Structure module, Green: output of the Global Structure module)

## 5.4 COMPONENTS OF GLOBAL STRUCTURE MODULE

### 5.4.1 GENERATION OF GLOBAL GEOMETRY

Figure 5.10 shows a simplified workflow of the first component of the global structure module, which is the generation of global geometry. The output of this component of the module is discussed hereafter.

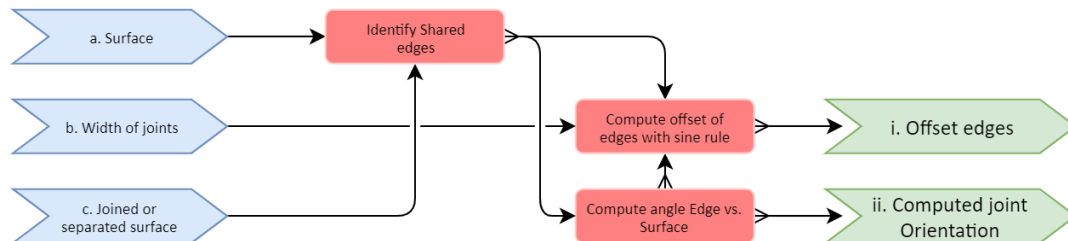


Figure 5.10: Simplified workflow of Generation of Global Geometry

(Blue: input variables, Red: processing, Green: output)

#### i. Offset Edges

##### Goal

To create offset edges that will split the originally joined surface into the actual surfaces that represent the planar CLT plates, which will be connected by the CLT connection panels in the Joint Design module.

##### Methodology

The offset edges are computed by isolating the shared edges between planar surfaces. These edges or lines represent the domain where potential connection panels can be placed and therefore are the first step in this module. Secondly the offset vector of these edges is computed by means of the sine rule between the offset edge and its original position. Both a joined surface or separated surfaces can be provided as input. In case of the separated surfaces, the joint width is already set as the surfaces are already placed at a set distance from each other. Figures 5.11-5.14 show examples of the different types of surfaces and the identified shared edges. The rest of this chapter will take the joined surface as an example to demonstrate the workflow.



Figure 5.11: Separated surface – set distance between connection panels

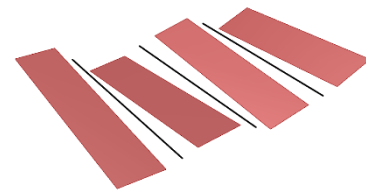


Figure 5.12: Separated surface – identified 'shared' edges

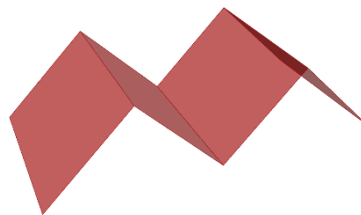


Figure 5.13: Joined surface – variable width for connection panels

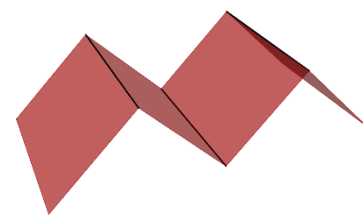


Figure 5.14: Joined surface – identified shared edges

### i. Offset Edges (continued)

**State of the art** The sine rule is applied as this mathematical rule can compute the length of an edge with only providing two angles and one length of a triangle. In this case, the provided length represents the width of the joints. This lets the width of the joints act as a variable, which is important since this also will be a variable for the design of the CLT connection panels in the Joint Design module.

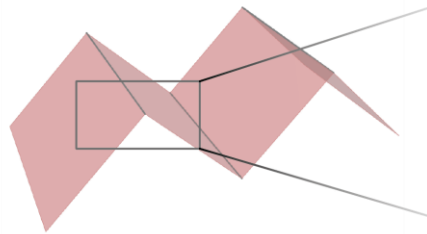


Figure 5.15: Identified shared edges (black) of a joined surface

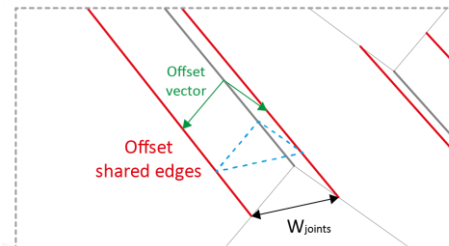


Figure 5.16: Sine rule applied on the blue triangle to compute the offset of the shared edges.

### ii. Computed Joint Orientation

**Goal** To compute the joint orientation relative to the adjacent surfaces.

**Methodology** A perpendicular frame is placed on each shared edge, since this constructs the correct orientation for the joints within the domain that is determined by identifying the shared edges

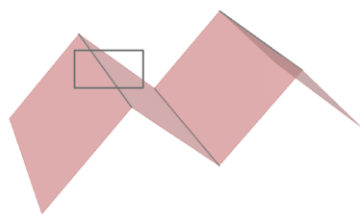


Figure 5.17: Shared edges (black) of a joined surface

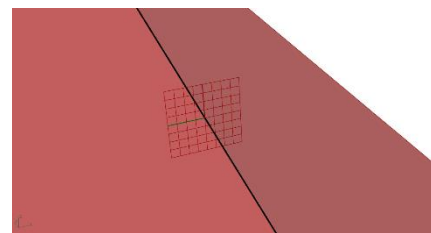


Figure 5.18: Perpendicular Frame constructed on shared edge

## 5.4.2 MODELLING OF JOINT GEOMETRY

Figure 5.19 shows a simplified workflow of the second component of the global structure module, which is the modelling of joint geometry. The output of this component of the module is discussed hereafter.

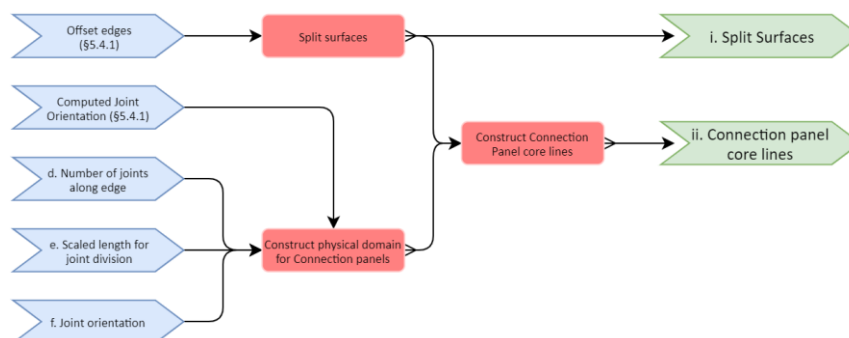


Figure 5.19: Simplified workflow of Modelling of Joint Geometry

(Blue: input variables, Red: processing, Green: output)

### i. Split surfaces

- Goal** To split the originally joined surface into separate surfaces that represent the planar CLT plates, which will be connected by the connection panels in the Joint Design module.
- Methodology** The joined surface is split by curves, which are the offset edges as described in Chapter 5.4.1.

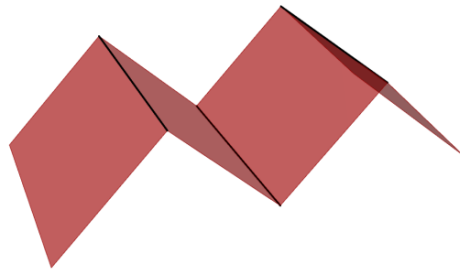


Figure 5.20: Shared edges (black) of a joined surface



Figure 5.21: Surfaces split by the offset edges as defined in the previous step

### ii. Connection panel core lines

- Goal** To generate the core lines of the connection panels according to the desired number of panels, position and orientation.
- Methodology** The shared edges are divided in a number of points. These points are pulled to the nearest surface from where the core lines of the connection panels are constructed. This methodology ensures that each point is pulled to the right surface since the pulled points are sorted on their pulled distance. By sorting the points and surfaces along the sorted pulled distances, the first point of the list always corresponds with the nearest surface.

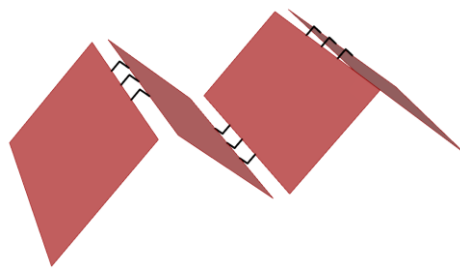


Figure 5.22: Three panels positioned in the middle

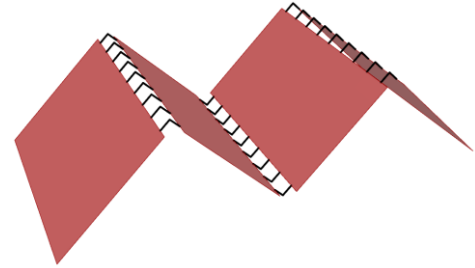


Figure 5.23: Nine panels positioned over the entire shared edge

- State of the art** The script allows for choosing different orientations for the connection panels. The orientation can be either aligned to the adjacent surface or to the global z-axis. See also Appendix F.

### 5.4.3 MESHING AND RE-ORIENTING MESH FACES

Figure 5.24 shows a simplified workflow of the third component of the global structure module, which is the meshing and re-orienting the mesh face orientation. The output of this component of the module is discussed hereafter.

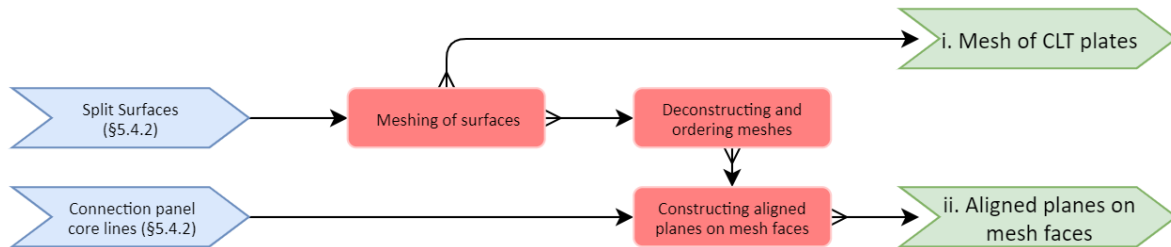


Figure 5.24: Simplified workflow of meshing of the CLT plates and orientation of mesh faces

(Blue: input variables, Red: processing, Green: output)

#### i. Mesh of CLT plates

**Goal** To mesh the surfaces that represent planar CLT plates.

**Methodology** The surfaces are meshed by the Karamba3D mesh component, since the points where the core-lines of the connection panels connect to the surfaces should also be included in the meshes. Other mesh methodologies could have been applied, which would result in better distributed meshes. However, the karamba3D meshing component allows for including points in meshes. Since this research is not about optimizing meshes, this simple though not ideal meshing methodology is applied.

#### ii. Aligned planes on mesh faces

**Goal** To construct planes on each individual mesh face that are aligned to the initial strong direction of the CLT plates. The initial strong direction is determined by the longest span of the plate, see also Appendix F for more information on this topic. The strong and weak direction can be manually switched if desired.

**Methodology** First, one aligned plane is constructed on each plate. Subsequently the aligned plane is moved to each individual mesh face. Hence, aligned planes are constructed on each mesh face. By constructing the planes in this sequence, no error can occur in constructing the planes along the wrong alignment as they all automatically will have the same orientation.

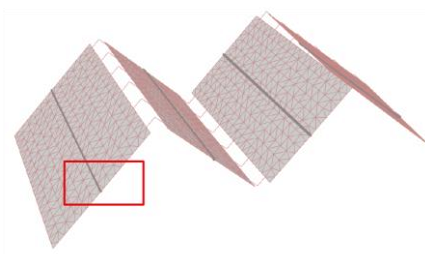


Figure 5.25: Strong direction (black) of a meshed CLT plate, to construct a plane along

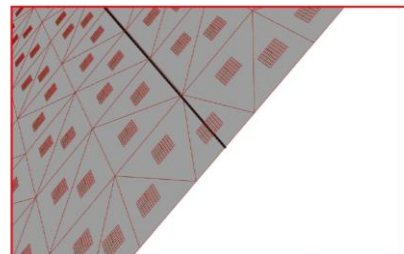


Figure 5.26: Individual mesh face orientations aligned to the strong direction (black)

#### 5.4.4 FEM MODEL OF GLOBAL STRUCTURE

Figure 5.27 shows a simplified workflow of the fourth component of the global structure module, which is the FEM modelling of the global structure. The output of this component of the module is discussed hereafter.

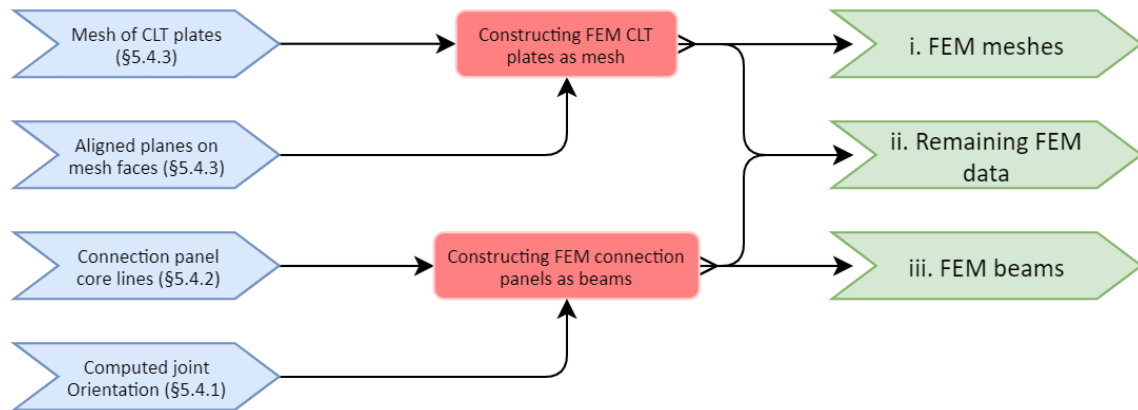


Figure 5.27: Simplified workflow of FEM modelling of the global structure  
(Blue: input variables, Red: processing, Green: output)

##### i. FEM meshes

**Goal** To create meshes with the correct face orientation according to the strong and weak direction of the CLT plates. The script automatically generates the FE meshes and can process a variety of geometries.

**Methodology** The FE mesh is built up along random mesh face orientations. Therefore, the FE mesh must be destructed first and subsequently be re-aligned to the planes as constructed in the previous paragraph. Figures 5.28 - 5.29 show these reoriented mesh faces for different geometries. The mesh faces are aligned along the strong direction of the plates.

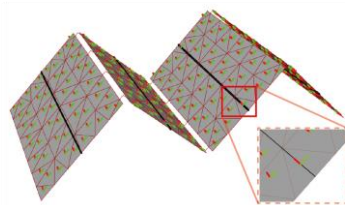


Figure 5.28: Strong (red) and weak (green) directions of mesh faces from a 1D folded surface with a sparse mesh density

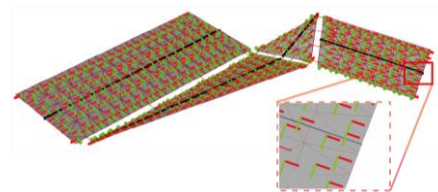


Figure 5.29: Strong (red) and weak (green) directions of mesh faces from a random surface with a sparse mesh density

##### ii. Remaining FEM data

**Goal** To provide all information for the FE model except the geometry. Information such as load cases, loading, supporting conditions, and analyses cases.

**Methodology** The FEM data is generated by GeometryGym components. GeometryGym is a plugin in Grasshopper that enables users to transfer geometry to a FE package, i.e. GSA.



### iii. FEM beams

**Goal** To create FEM beams that represent the connection panels and CLT plates, which will be designed in the Joint Design module in Chapter 6. By representing the connection panels by beams, the results of the FEM will meet the goal of the Global Structure module. Namely, to analyze the structural behavior of a CLT structure on a global level in the preliminary design phase.

**Methodology** As the connection panels will be represented by beams in the global structural model, these beams should approach the model as if the joints were there. Figures 5.30-5.31 represent these situations. Therefore, the following simplifications are applied:

- The structural joints between these beams are assumed as hinges. This will nullify the stiffness of the connection panels and therefore be a conservative simplification.
- The connection panels are represented by structural beams:
  - o That have the same dimensions as the CLT plates (Figure 5.30).
  - o That have the same structural properties as the CLT plates (Figure 5.33).

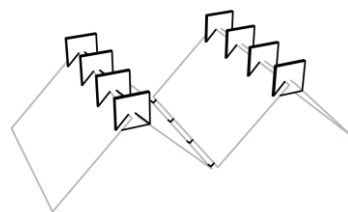


Figure 5.30: Geometry with physical connection panels present

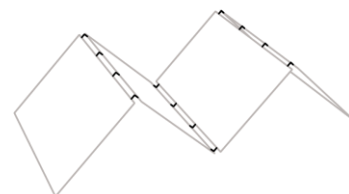


Figure 5.31: Simplified geometry with representative beams for the Global Structure module

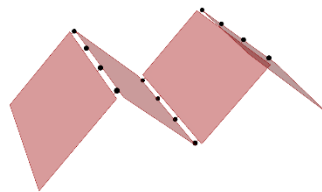


Figure 5.32: Representative beams that are assumed and modelled as hinges

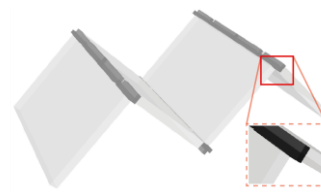


Figure 5.33: Structural beams – with the same (structural) properties as the CLT plates – to represent the connection panels

**State of the art** The cross-sections of the beams that represent the connection panels, depend on the number of joints along an edge to avoid overlapping or gaps between the beams. So, the load distribution between the panels aligns with the corresponding cross-sections of each beam. Figure 5.34-5.35 show this principle.

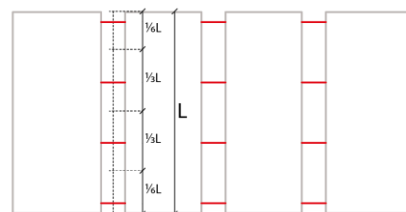


Figure 5.34: Distributed length (top view) of a geometry to generate the corresponding cross-sections – 4 joints

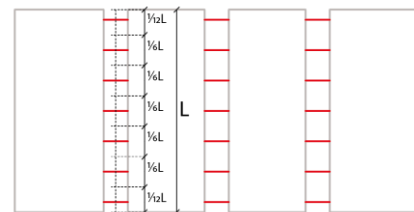


Figure 5.35: Distributed length (top view) of a geometry to generate the corresponding cross-sections – 8 joints

		{0}
0	312.5	
1	625	
2	312.5	
		{1}
0	312.5	
1	625	
2	312.5	
		{2}
0	312.5	
1	625	
2	312.5	

Figure 5.36: Affective length per joint, ordered per shared edge

		{0}
0	STD R 313 70	
1	STD R 313 70	
2	STD R 313 70	
3	STD R 313 70	
4	STD R 313 70	
5	STD R 313 70	
6	STD R 625 70	
7	STD R 625 70	
8	STD R 625 70	

Figure 5.37: Parametrically generated cross-sections list for the FEM with a CLT thickness of 70mm

#### 5.4.5 CROSS-SECTIONAL PARAMETERS OF CLT

Figure 5.38 shows a simplified workflow of the fifth component of the global structure module, which is the computation of the cross-sectional parameters of CLT. The output of this component of the module is discussed hereafter.

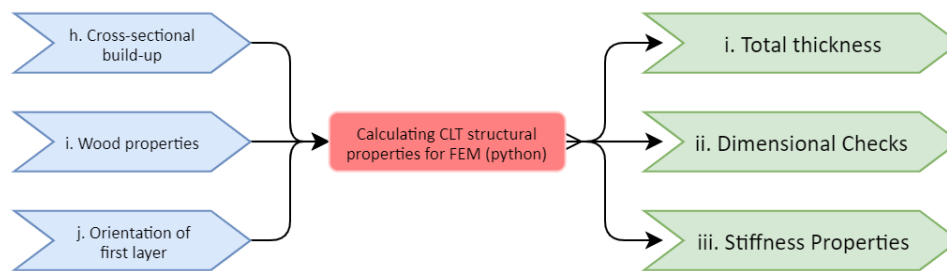


Figure 5.38: Simplified workflow of the computation of Cross-sectional parameters for CLT  
(Blue: input variables, Red: processing, Green: output)

This component makes use of a python script. Appendix G shows this script. The script performs several checks and computes all relevant orthogonal material properties of CLT that are required as input for the FE model. This is explained more into depth below. Python is applied as this allows for the inclusion of several loops along parameters, which is the case with a CLT panel. Each property must be analyzed and calculated for each layer individually, to finally compose the effective orthogonal material properties.

##### i. Total Thickness

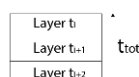
**Goal** To calculate the total thickness of the CLT panel.

**Methodology** The total thickness of the CLT panel is calculated by summing the individual layer's thicknesses. This calculation is performed in python.

##### ii. Dimensional checks

**Goal** To verify whether the CLT panel is within the boundaries of fabrication restraints. The following dimensional checks are performed according applicable codes.[18]

- $t_{tot} < 300\text{mm?}$
- $t_i < 60\text{mm?}$



**Methodology** The checks are performed in python.

### iii. Stiffness Properties

**Goal** To retrieve the orthogonal material properties from the cross-sectional geometry that are required for FE modelling. The following (structural) orthogonal material properties are automatically computed:

$E_{\text{strong}}$	[N/mm <sup>2</sup> ]
$E_{\text{weak}}$	[N/mm <sup>2</sup> ]
$G_{\text{strong}}$	[N/mm <sup>2</sup> ]
$G_{\text{weak}}$	[N/mm <sup>2</sup> ]
$G_{\text{in-plane}}$	[N/mm <sup>2</sup> ]
$\rho$	[kg/m <sup>3</sup> ]

**Methodology** The calculations are based on the theory as presented in the literature study, Chapter 5.2, and performed in python.

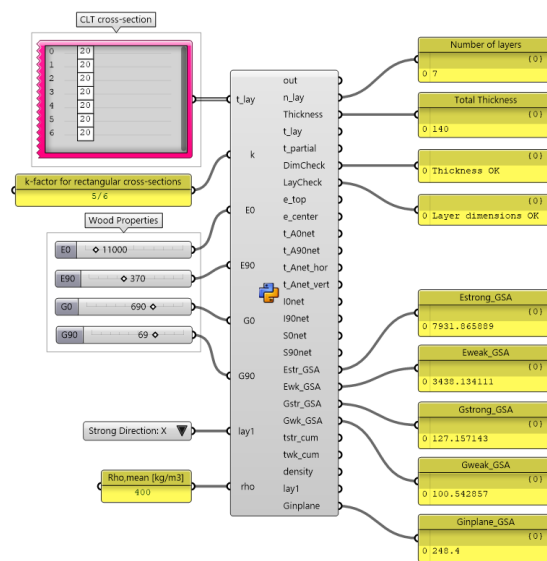


Figure 39: (Python) component to compute relevant material properties

### 5.4.6 GENERATING NUMERICAL DATA FOR JOINT DESIGN MODULE

Figure 5.40 shows a simplified workflow of the sixth component of the global structure module, which is the generation of numerical as input for the Joint Design module. The output of this component of the module is discussed hereafter.

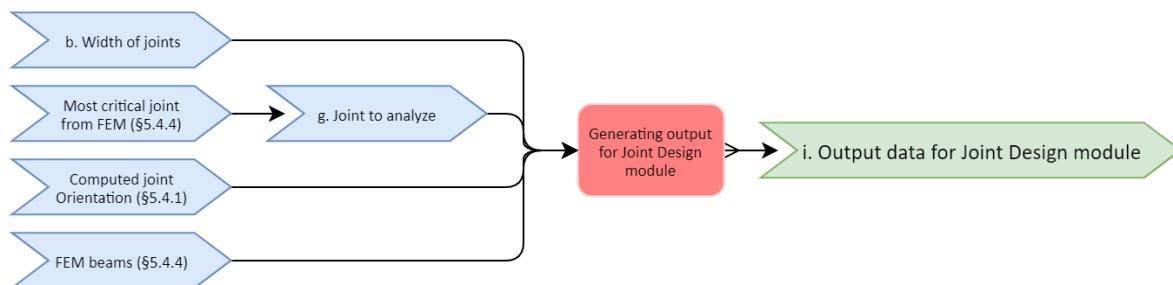


Figure 5.40: Simplified workflow of generating numerical data for the Joint Design module

(Blue: input variables, Red: processing, Green: output)

### i. Output data for Joint module

**Goal** To collect all relevant data from the global structure (FE) model that should serve as input for the Joint Design Module, see Chapter 6.

**Methodology** First, a FEM calculation should be performed, which is described in Chapter 5.5. This will enable a user to identify the most critical joint by retrieving the beam element with the highest occurring forces. Next, the user can select the joint from the geometrical model in Grasshopper. From this joint, all relevant data will be retrieved such as angle, load, applied forces et cetera will be collected. Figures 5.13-5.14 show the following parameters:

- Length appending structure on left side
- Length appending structure on right side
- Width between the plates
- Distributed loading area on the left side
- Angle with appending structure on the left side
- Angle with appending structure on the right side

Besides these parameters there are more relevant parameters, which are elaborated in Chapters 5.6 and 6. Figure 5.43 shows some example parameters that are collected in this component from the global structure module.

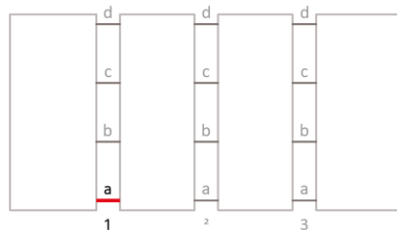


Figure 5.41: Top view – Joint selection with joint 1.a selected

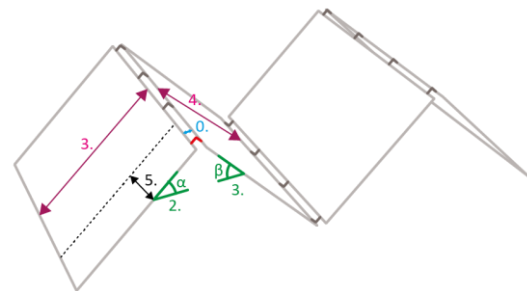


Figure 5.42: Parameters from geometrical model for Joint Design module

Data for Joint module	
	{ 0 }
0	Width Joint: 150
1	Angle left: 45°
2	Angle right: 45°
3	Length pending structure left: 884mm
4	Length pending structure right: 884mm
5	Spanning distance for q: 312.5m

Figure 5.43: Geometrical data collected from the global structure module.

## 5.5 FINITE ELEMENT MODELLING OF THE GLOBAL STRUCTURE

### 5.5.1 INPUT FOR THE FEM

From the geometry that is generated along the workflow from the Global Structure module as presented in the previous paragraph, a FEM model can automatically be retrieved. The only parameter that must be manually set is the supporting conditions. This could be automated; however, the supporting conditions are variable to offer design variability to the user. To demonstrate the FEA, the 1-D folded geometry is taken as an example. Figure 5.44 shows the geometrical input, whereas Appendix H shows the entire input that is used for this model.

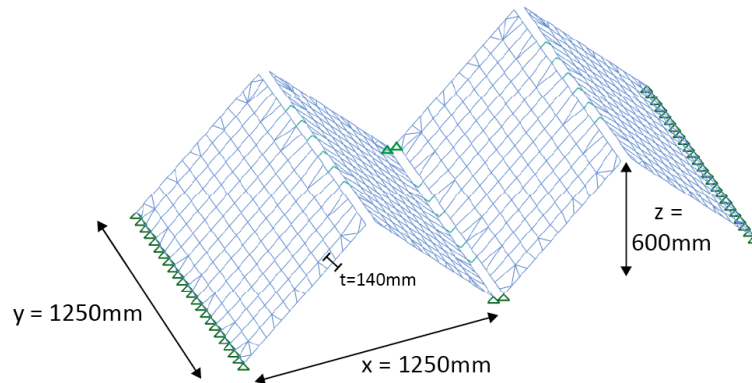


Figure 5.44: GSA geometrical input

### 5.5.2 OUTPUT FROM THE FEM

The results from the FEA are shown below.

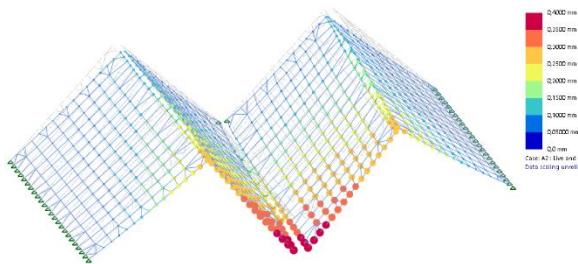


Figure 5.45: Deflected shape of the structure.  $u_{max} = 0.4\text{mm}$

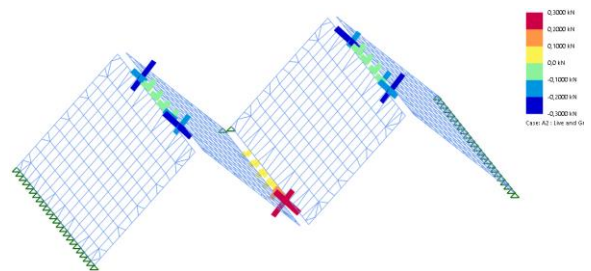


Figure 5.46: Beam force  $F_x$  in the joints.  $F_{x,max} = 0.25\text{kN}$

Figure 5.46 shows reaction forces that occur in the joints. One should notice that these forces can be used as input for the Joint Design module, which is described in Chapter 6.

This structure is an example to demonstrate the potential of the global structure module related to Finite Element Analyses (FEA). The maximum deflection for example, is low (0.4mm) due to the low loading, small dimensions of the structure, and relative thick CLT panel sizes. However, a user can quickly generate any FE model he wants to analyze by providing the script with the variables as discussed in the beginning of this chapter.

## 5.6 RELATIONSHIPS WITH JOINT DESIGN

The goal of this research is to investigate an integral workflow for robotically fabricated customized CLT connection panels. Figure 5.47 shows the three components on the highest level of this workflow. This paragraph focusses on the relationships that can be derived from the Global Structure module.

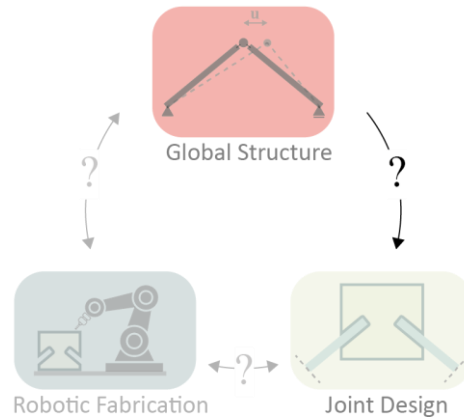


Figure 5.47: Relationships between Global Structure and Joint Design in the integral workflow

Summarized, there are two types of parameters that describe the relationships and (in)dependencies that flow from the Global Structure to the Joint Design module:

- Geometrical relationships
- Structural relationships

Figure 5.47 describes these relationships, which are already (partly) discussed in the previous paragraph. The common denominator of all **geometrical relationships** is that they explicitly determine the initial outlined shape of the connection panel. They concern the following parameters:

- 1) Width of the joints. This parameter is a variable that can be set by the user.
- 2) Thickness of the appending CLT plates.
- 3) Angle  $\alpha$  of the appending structure on the left side of the connection panel.
- 4) Angle  $\beta$  of the appending structure right side of the connection panel.

The **structural parameters** can both be retrieved from the geometrical model and the FEA. Chapter 6 explains how they form the boundary conditions for the Joint Design module. They concern the following parameters.

- The area that is distributed to the connection panel is determined by the length of the appending structure (i, ii) and the width of this area (iii). This area determines the magnitude of the load applied on the panel.
- $F_x, F_y, F_z, M_{yy}$  of the representative beams. These forces are retrieved from the FEM model and result in horizontal, vertical, and torsional forces that form the boundary conditions for the Joint Design module.

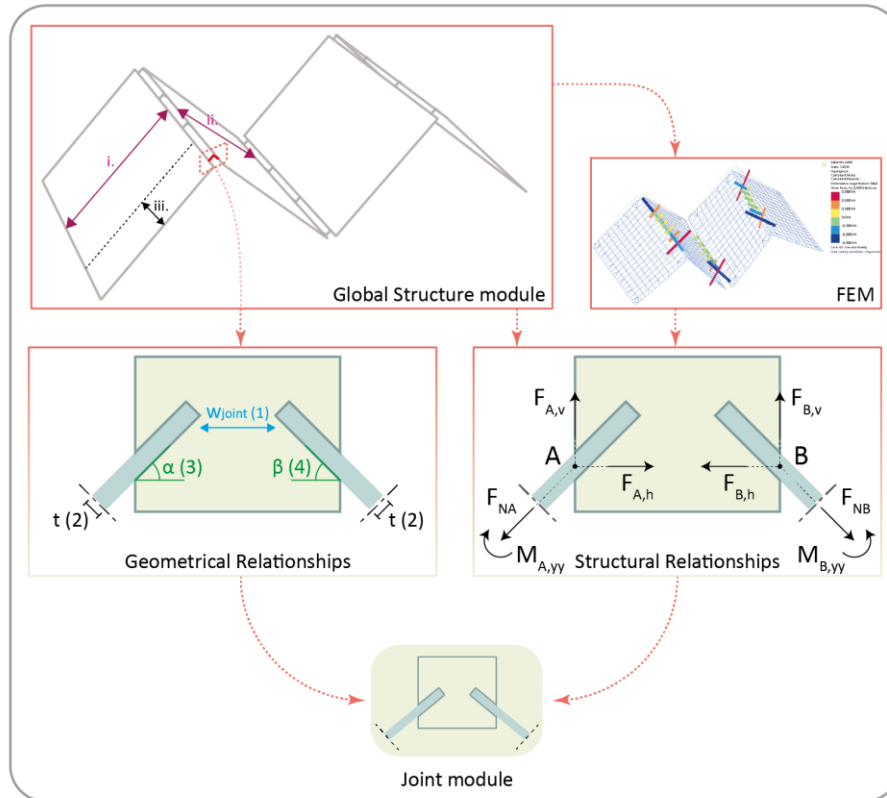


Figure 5.48: Diagram with geometrical and structural relationships from Global Structure to Joint Design module

## 5.7 POTENTIAL OF THE WORKFLOW: GLOBAL STRUCTURE

This paragraph demonstrates the potential of the workflow as described in this chapter. The potential is demonstrated by showing possibilities regarding different geometries the workflow can handle. Finally, design graphs are derived, to show the potential for a designer to get quick insight in the influence of geometrical parameters on the structural performance of a structure. This will help a designer to make reliable judgments on the structural behavior of a CLT structure in the preliminary design phase. Appendix H shows an overview of the script that represents this workflow.

### 5.7.1 GEOMETRICAL MODELLING

Figures 5.49-5.53 show different geometries the workflow can handle, including the correctly aligned meshes and finite elements.

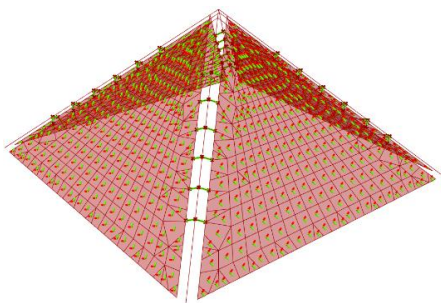


Figure 5.49: Pyramidal geometry – geometrical model and aligned meshes

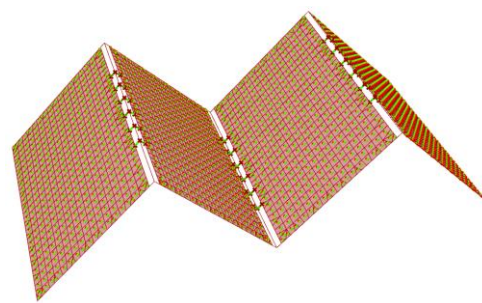


Figure 5.50: 1-D folded geometry - geometrical model and aligned meshes



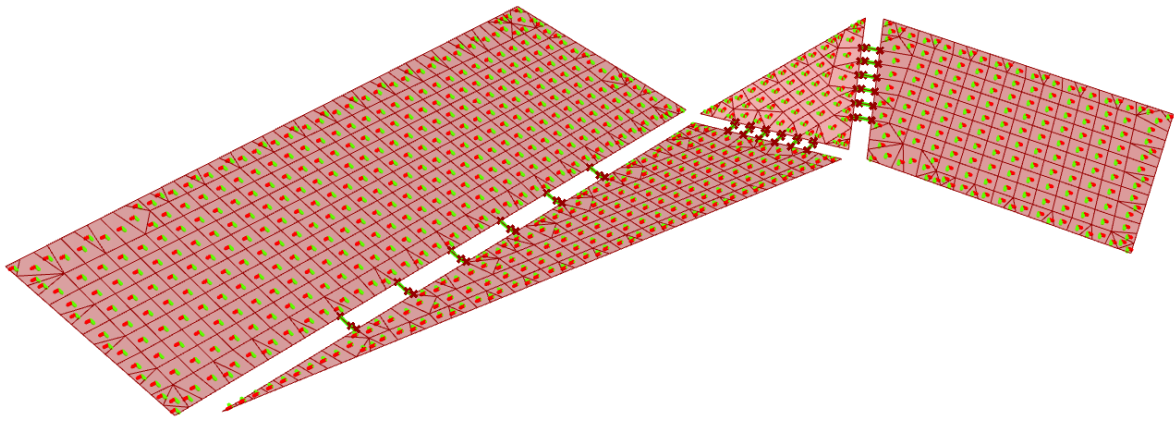


Figure 5.51: A random geometry – geometrical model and aligned meshes

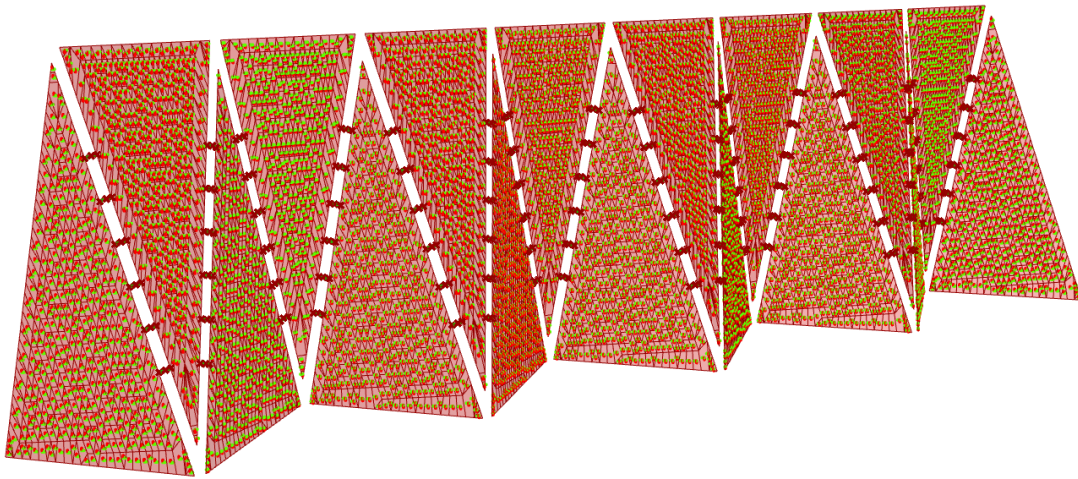


Figure 5.52: Double Folded wall structure – geometrical model and aligned meshes

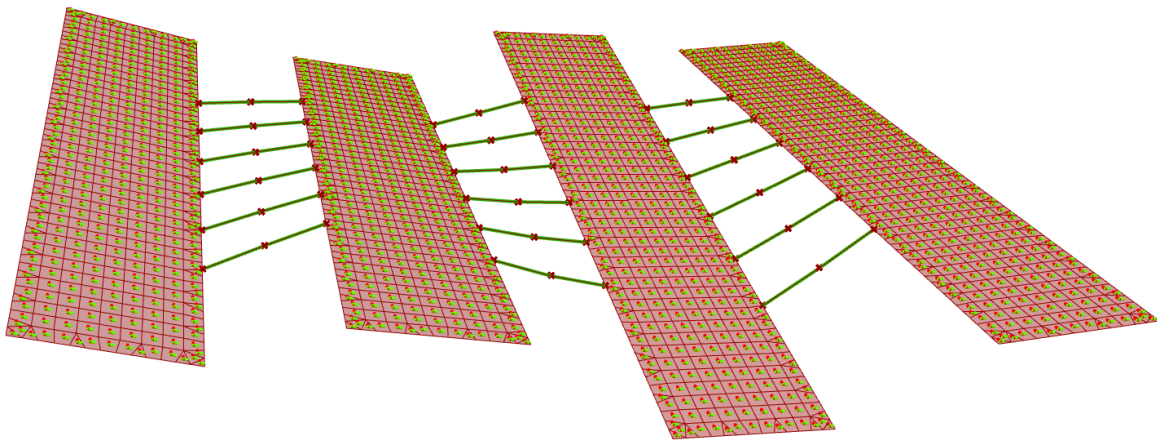


Figure 5.53: Floating separate CLT panels with representative beams in between – geometrical model and aligned meshes



### 5.7.2 FINITE ELEMENT MODELLING – POTENTIAL

Figures 5.54-5.58 show the corresponding FEM models of the geometry as presented above. Arbitrary distributed loading is applied, and no numerical results are presented since the purpose of the figures below is to show the potential of the workflow.

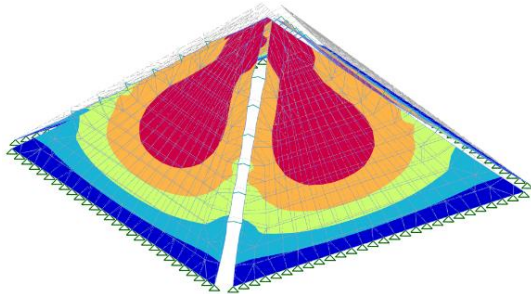


Figure 5.54: Pyramidal geometry – Deflected shape

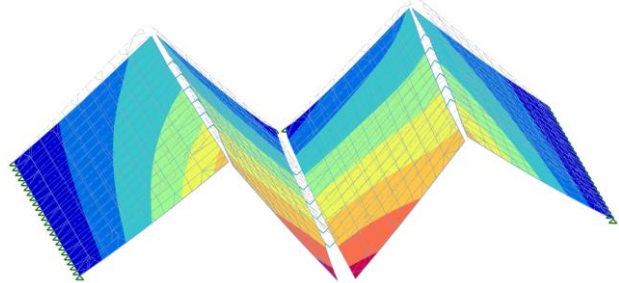


Figure 5.55: 1-D folded geometry – Deflected shape

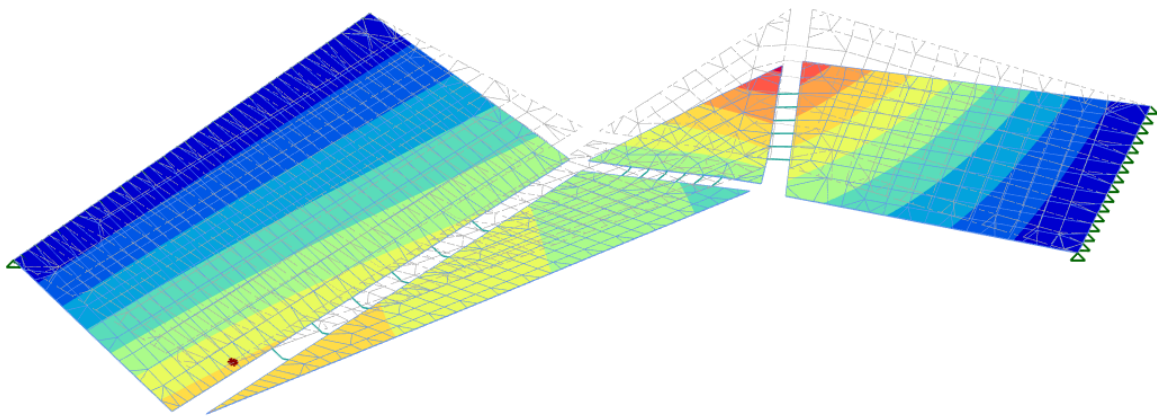


Figure 5.56: A random geometry – Deflected shape

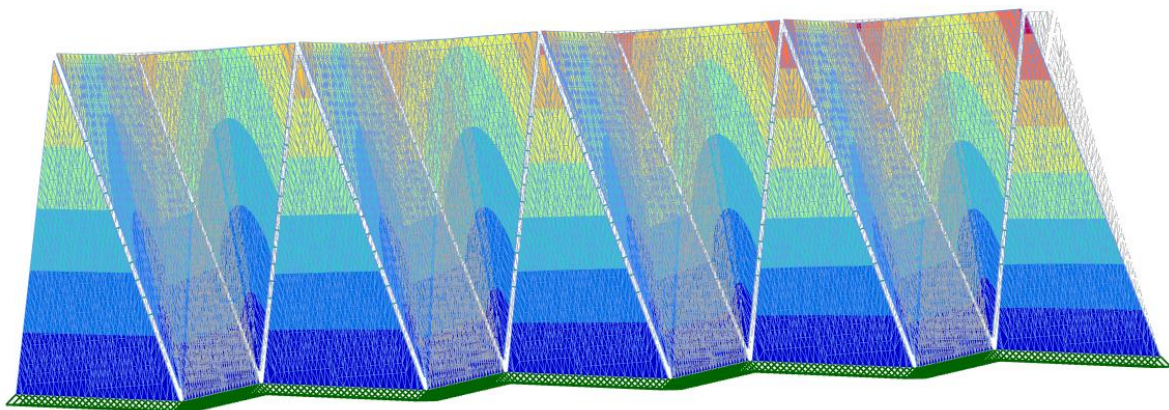


Figure 5.57: Double Folded structure – Deflected shape

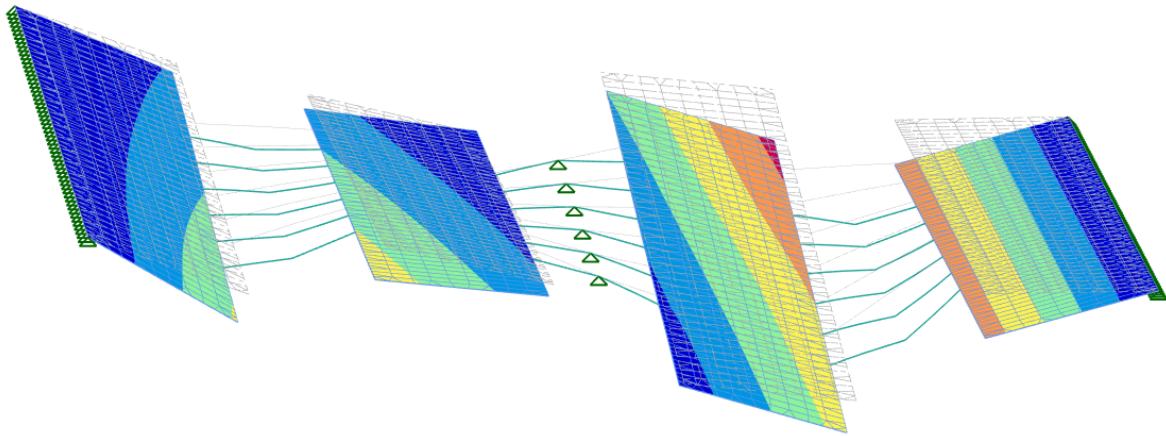


Figure 5.58: Floating separate CLT panels with representative beams in between – Deflected shape

### 5.7.3 FINITE ELEMENT MODELLING – DESIGN GRAPHS

From the FE results, different design graphs can be derived to get insight in the influence of geometrical parameters on the structural performance of a structure. The 1-D folded geometry is taken as an example for the design graphs as presented below, and the graphs are derived from the FE results. The resulting (reaction) forces and deflections are low due to the thick CLT-panel sizes and the low load that is applied. However, the goal of these results is to show the potential of the workflow, not to explicitly create a FE model that fits into an existing project. More design graphs are presented in Appendix J.

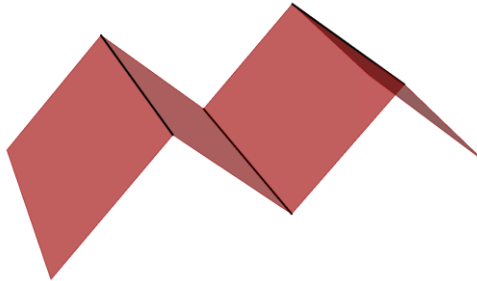


Figure 5.59: Input geometry of the reference model

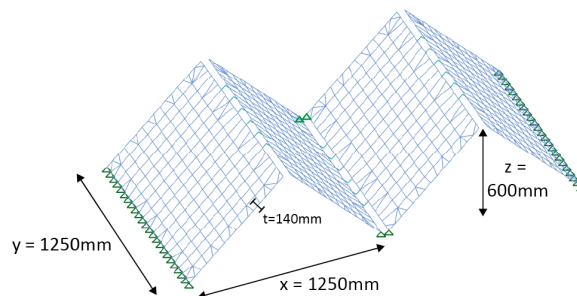


Figure 5.60: Reference FE model with variables

### Varying parameter

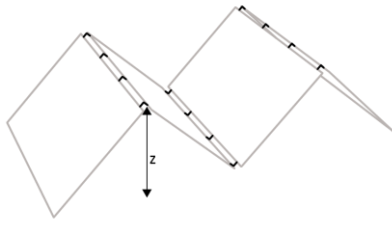


Figure 5.61: Varying parameter  $z$

As one can see, increasing the height ( $z$ ) of the 1-D folded geometry results in lower deflections. This is a compelling correlation as increasing the height results in a stiffer structure. However, an interesting phenomenon is that after  $z \geq 600\text{mm}$  not much extra stiffness is gained compared to the extra height that is added between  $z = 400\text{mm} - 600\text{mm}$ .

### Derived design graph from FE

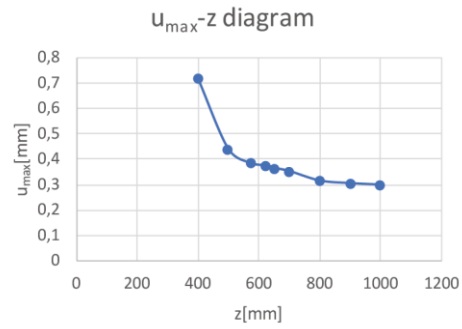


Figure 5.62: Design graph for varying parameter  $z$ [mm] versus the maximum displacement[mm] in the FE model

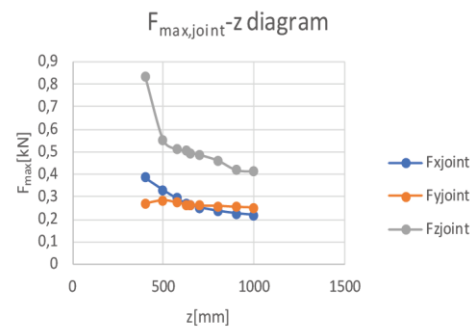


Figure 5.63: Design graph for varying parameter  $z$ [mm] versus the maximum occurring force  $F_x$ ,  $F_y$ ,  $F_z$  [kN] in the joints

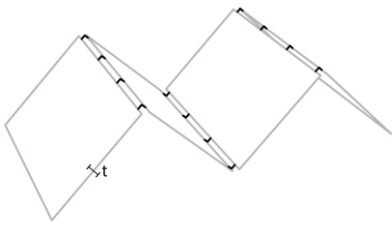


Figure 5.64: Varying parameter  $t$

Increasing the thickness of the CLT plates results in lower deflections. The same phenomenon as with varying the height ( $z$ ) of the structure occurs. Increasing the thickness up to  $z = 100\text{mm}$  results in much lower deflection. However, increasing  $z \geq 100\text{mm}$  might not be beneficial for a designer.

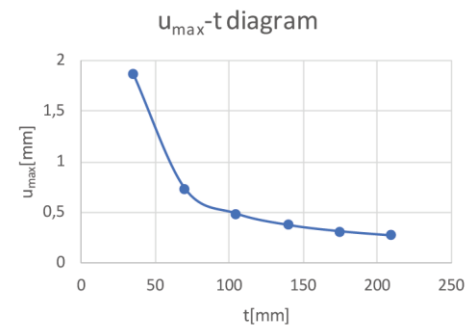


Figure 5.65: Design graph for varying parameter  $t$ [mm] versus the maximum displacement[mm] in the FE model

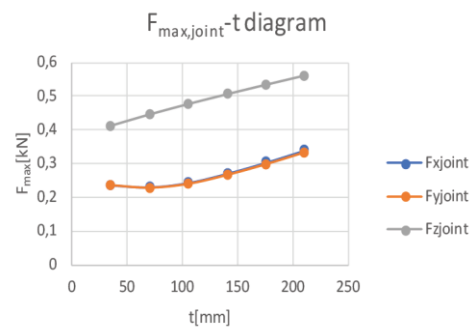


Figure 5.66: Design graph for varying parameter  $t$ [mm] versus the maximum occurring force  $F_x$ ,  $F_y$ ,  $F_z$  [kN] in the joints

## 5.8 CONCLUSION

This chapter focused on the Global structure module of the integral workflow as presented in Figure 5.67 and answers the following question.

What does a workflow for CLT structures look like, that promote exploration of the structural performance of CLT structures on a *global* level in the preliminary design phase?

For this module, a workflow was developed to answer the question as stated above. Besides, it focusses on the relationships and (in) dependencies between the Global Structure and the Joint Design. The workflow consists of different components, of which one is the computation of the orthogonal material properties of CLT for the FEM. This computation is automated by a python script. One important aspect is the alignment of mesh faces along the strong directions of planar CLT plates. This aspect is included in the workflow. To link the Global Structure to the Joint Design, numerical data was retrieved that can be used as input for the second module, the Joint Design. There are two types of relationships found that flow from the Global Structure to the Joint Design, which are geometrical and structural relationships. Geometrical relationships inform about the size of the appending structure, while structural relationships inform about the occurring forces in the joints. These relationships together form the boundary conditions for the joint design. Figure 5.67 shows this schematically.

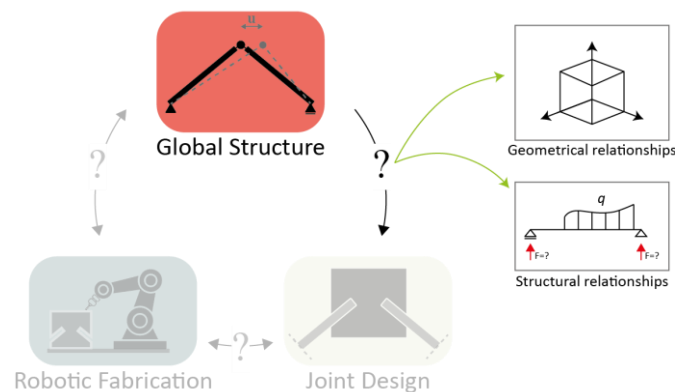


Figure 5.67: Relationships between the Global Structure and the Joint Design

**Further improvements and development.** The workflow as presented in this chapter, can be further developed and improved on at least the following aspects:

- Meshing. Right now, the Karamba3D meshing component is integrated in the workflow. However, this often results in unequal distributed meshes with overlapping or too slender mesh faces. This could be solved by using other meshing technologies. However, the difficulty is to connect the beam elements that represents the connection panels in the mesh. This increases the complexity of the meshing process. One technology that is worth mentioning, is to mesh geometry in the FE program. However, this is not possible with the current software of GeometryGym that transfers geometry to a FEM program. Finally, exploring meshing technologies is not in the scope of this research.
- The workflow is set up in such a way that it is suitable for the implementation of a User Interface (UI), for instance by Human UI, which is a plugin for Grasshopper. This will increase the user-friendliness.
- The workflow is set up in such a way that the variables as described in this chapter and Appendix F, are suitable to perform (evolutionary) optimization on. For instance, one could optimize the joint width along an edge towards a minimum occurring force.

## 6. Joint Design module

### 6.1 INTRODUCTION

Once the global structure is developed in the first component of the integral workflow, the next component should be investigated, which is the Joint Design module. The boundary conditions of the Global Structure module as discussed in the previous chapter serve as input for the Joint Design module. This chapter therefore deals with the structural modelling and exploration of a CLT structure on a local level. The goal of this chapter is to develop a module that enables users to quickly explore the structural performance of a CLT structure on this level in the preliminary design phase. Therefore, the following question is answered in this chapter:

What does a workflow for CLT structures look like, that promote exploration of the structural performance of CLT structures on a *local* level in the preliminary design phase?

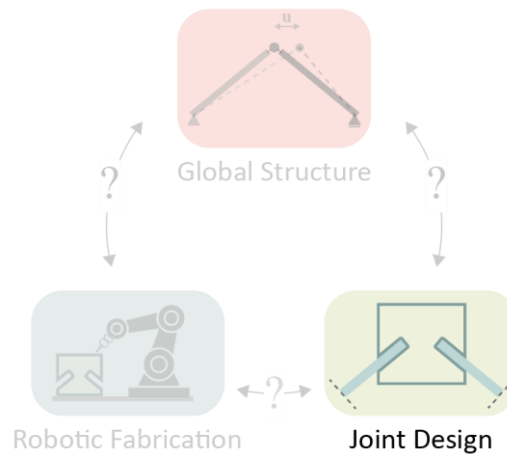


Figure 6.1: Focus of this chapter - the Joint Design module

The answer is formulated by investigating a type joint that consists of a CLT connection panel with slotted holes, which is derived from the project as described in the motivation of this research. Inside these slotted holes, CLT plates of a (global) structure are placed. Through this connection panel these plates are connected. A workflow to set up a joint design along this concept is developed, which is described in this chapter. Different methodologies to get an understanding of the structural performance of the joint in the preliminar design phase are incorporated in this workflow. The workflow can both process the modelling of a CLT panel on a geometrical level, as well as the determination of the structural performance by means of an analytical Unity Check or a FEM model. The closing paragraphs of this chapter briefly demonstrate the protentional of the Joint Design module by showing different geometries of joints processed by the workflow, and structural correlations that are derived from these models. Especially influential geometrical parameters are investigated that influence the stiffness of this type of joint. Finally, the relationships are described between the Joint Design and the other modules, namely the Global Structure and Robotic Fabrication module.

## 6.2 BOUNDARY CONDITIONS AND DESIGN PHILOSOPHY

### 6.2.1 BOUNDARY CONDITIONS FROM GLOBAL STRUCTURE MODULE

The first step for the Joint Design is to determine the correct boundary conditions. These boundary conditions are set values that form the design space of the Joint Design. These conditions can be retrieved from the relationships between the Joint Design module and the Global Structure module, which are described in Chapter 5.6. Figure 6.2 shows a two-dimensional schematized model derived from the Global Structural module, from which the joint should be designed.

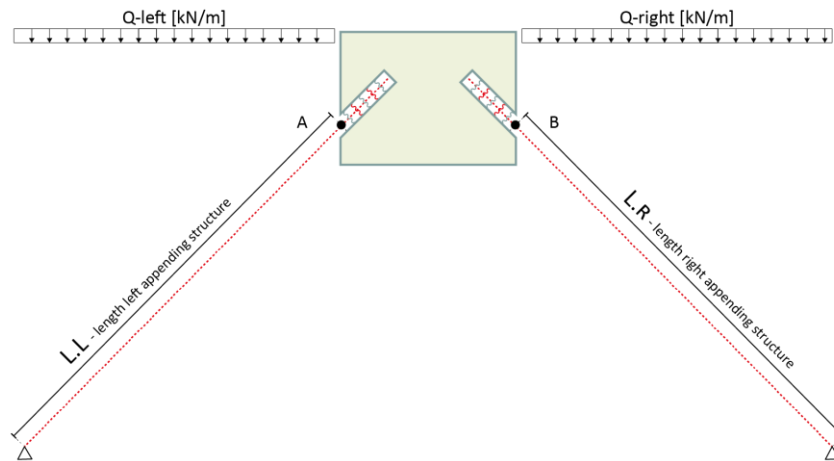


Figure 6.2: Two-dimensional schematization of a global structure and corresponding CLT Connection panel  
(Note: in the Global Structure module the connection panels are represented by FE beam elements)

Hence, from the global structure the following boundary conditions apply:

- **Geometrical** boundary conditions
- **Structural** boundary conditions, where point A and B correspond to the position of point A and B in Figure 6.2 above.

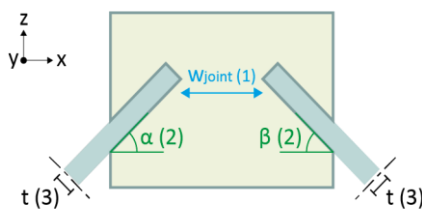


Figure 6.3: Geometrical boundary conditions

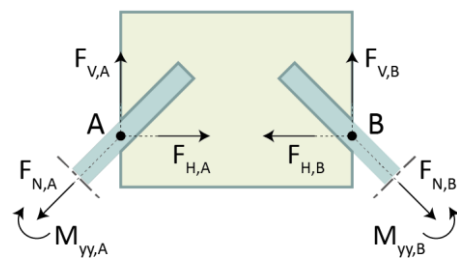


Figure 6.4: Structural boundary conditions

		Boundary Condition	Symbol
Geometrical	1)	Width that the joint should span between the CLT plates	$W_{\text{joint}}$
	2)	Angles between appending structure and global xy-plane	$\alpha, \beta$
	3)	Thickness of appending structure	$t$
Structural	4)	Horizontal reaction forces from the Global structure	$F_{H,\dots}$
	5)	Vertical reaction forces from the Global structure	$F_{V,\dots}$
	6)	Normal reaction forces from the Global structure	$F_{N,\dots}$
	7)	Momentum reaction forces from the Global structure	$M_{yy,\dots}$



### 6.2.2 DESIGN VARIANTS

Now the boundary conditions for the Joint Design are set, the design philosophy of the joints should be developed. Looking at the shape of the connection panel, two design variants are discussed below, variant a and variant b.

Variant a

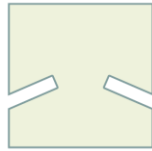


Figure 6.5: Step 1 – CLT connection panel

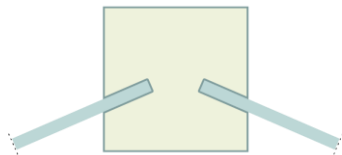


Figure 6.7: Step 2 – Plates placed in slotted holes of CLT panel

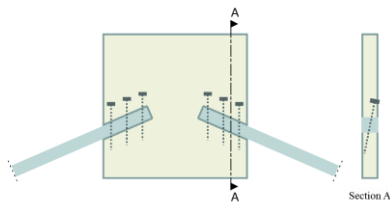


Figure 6.9: Step 3 – Plates connected to CLT connection panel by screws under a tilted angle. Final situation.

Variant b

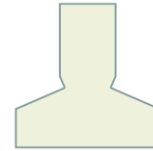


Figure 6.6: Step 1 – CLT connection panel

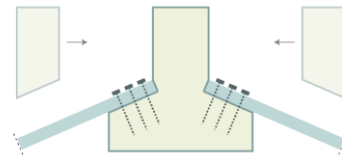


Figure 6.8: Step 2 – Plates attached to the CLT panel by screws perpendicular to the plates

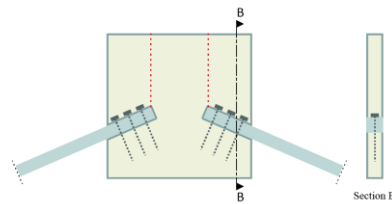


Figure 6.10: Step 3 – Upper wings of the CLT connection panel constructed. Final situation.

Considering the two design variants above, the following Multi-Criteria Analysis (MCA) is made.

		Variant a	Variant b
Executability	Pros (+)	* No extra operations required to construct the connection panel	* Straightforward assembly procedure
	Cons (-)	* Difficult assembling of screws	* Extra connection required in the connection panel (step 3)
Structural performance	Pros (+)	* Monolithic connection panel; stiffer behavior and structural contribution * Therefore, reduction in loading on the screws	* Clear load-distribution * Less complex to model reliably in a FEM model
	Cons (-)	* Complex to model reliably in a FEM model * Unclear load-distribution in the slotted hole	* Non-monolithic connection panel * Due to the non-monolithic connection panel, higher loading on the screws

Considering the pros and cons of both design variants, one argument stands out of the others for variant b, which is the reliable load-distribution. Once the load-distribution in the panel is clear, a reliable (FE) design can be set up. The load distribution can be divided between the screws and the connection panel. Figure 6.11 shows this load distribution:

- Screws: Shear, tension
- Connection panel: Compression, bending

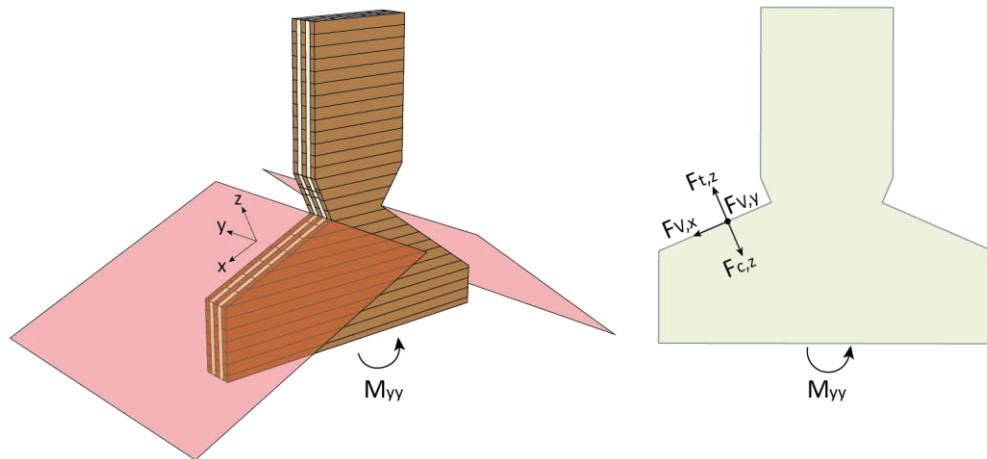


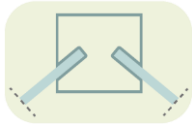
Figure 6.11: Tension ( $F_{t,z}$ ) and in-plane shear ( $F_{v,x}$  and  $F_{v,y}$ ) in the local  $x$ -,  $y$ -, and  $z$ -direction of the appending CLT plates are taken by the screws. Compression ( $F_{c,z}$ ) and bending ( $M_{yy}$ ) are taken by the CLT connection panel.

Concluding, despite the structural advantage of *variant a* with the monolithic CLT connection panel, from here on *variant b* will be discussed in this report.



### 6.3 VARIABLES OF THE JOINT DESIGN MODULE

Now the design philosophy is determined, the actual workflow of the Joint Design module can be explained. This paragraph presents all variables that are required for this module. Below an overview is shown of the variables and output of the Joint Design module.

Input Variable		Type	Global Structure module	Output
a	Inclined angle CLT plates	Integer		* Shape for Robotic Fabrication * Visualized three-dimensional geometry Relevant data for a FEM model of the Global Structure
b	Visualization settings	Integers		
c	Connection panel sizes	Integers		
d	Cross-sectional parameters	Integers		
e	Derived forces from the FEM	Numbers		
f	Spring settings	Integers		
g	Diameter screws	Integer		
h	Q-loading	Number		
i	Length appending structure	Numbers		

All variables as presented above are explained and illustrated in Appendix L. Figure 6.12 shows the components of the simplified workflow of the Joint Design module. Each component is explained more into depth in the consecutive paragraphs. The red highlighted variables below are derived from the Global Structure module, whereas the blue ones are provided as new variables in the current module

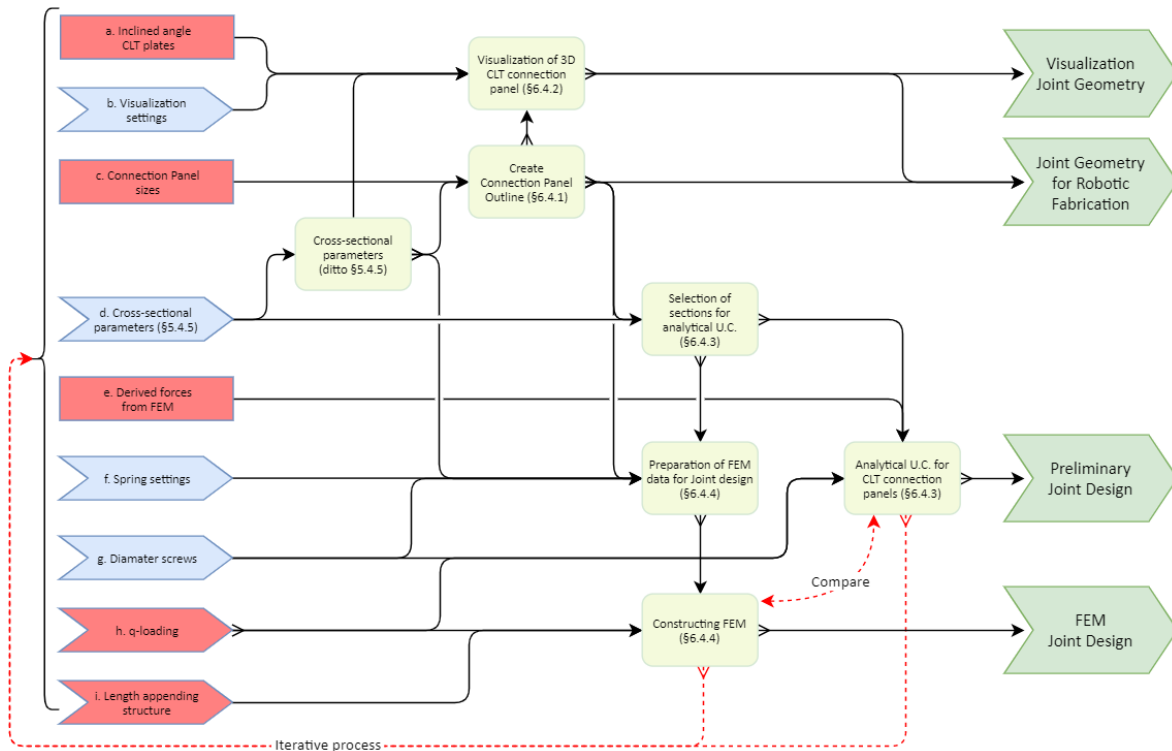


Figure 6.12: Simplified representation of the Joint Design module

(Blue: input variables, Red: input derived from the Global Structure module, Light yellow: processing by the Joint Design module, Green: output of the Joint Design module)

## 6.4 COMPONENTS OF THE JOINT DESIGN MODULE

### 6.4.1 GENERATION OF CLT CONNECTION PANEL GEOMETRY

Figure 6.13 shows a simplified workflow of the first component of the Joint Design module, which is the generation of connection panel geometry. The output of this component of the module is discussed hereafter.



Figure 6.13: Simplified workflow of Generation of CLT connection panel geometry

(Blue: input variables, Red: input derived from the Global Structure module, Light yellow: processing, Green: output)

#### i. Outline Structural area of connection panel

**Goal** To create the outline of the structural area of the connection panel as described in Chapter 6.2.

**Methodology** The outline is created by subtracting different areas from a rectangular base. The dimensions of these areas can be controlled by different variables. Figure 6.14 shows these variables, such as the width of the joint ( $w_{\text{joint}}$ ). It is of importance to set this width as a variable to integrate the Joint Design with the dimensions of the Global Structure. The final outline is created by a region difference. Figures 6.15-6.17 show these different steps.

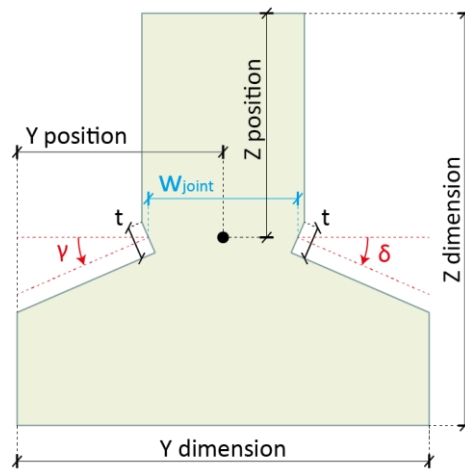


Figure 6.14: Variables for the outline of the CLT connection panel sizes

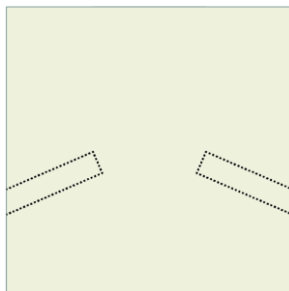


Figure 6.15: Rectangular outline with positioned slotted holes

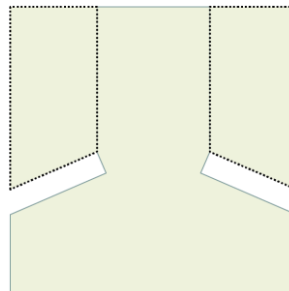


Figure 6.16: Extracting the non-structural area from panel

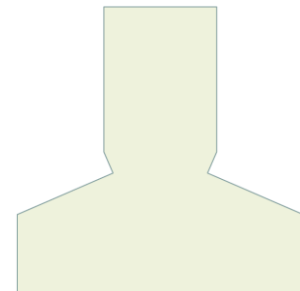


Figure 6.17: Final outline of the structural area of the CLT connection panel

## 6.4.2 VISUALIZATION OF THE 3D CLT CONNECTION PANEL

Figure 6.18 shows a simplified workflow of the second component of the Joint Design module, which is the visualization of the 3D connection panel. The output of this component of the module is discussed hereafter.

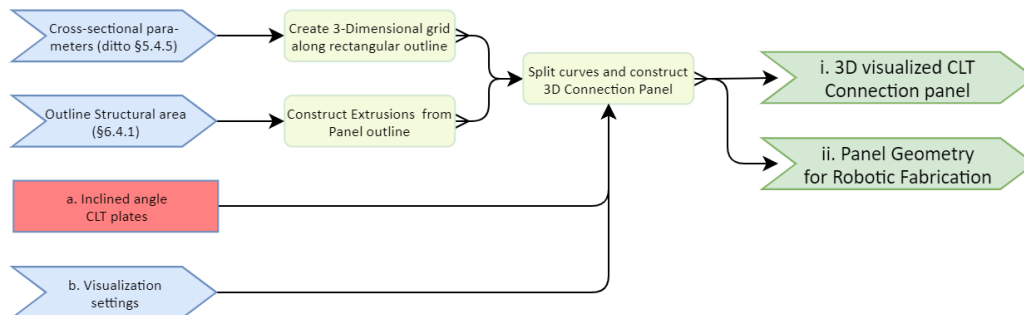


Figure 6.18: Simplified workflow of the visualization of the 3D Connection Panel

(Blue: input variables, Red: input derived from the Global Structure module, Light yellow: processing, Green: output)

### i. Visualized 3D Connection Panel

**Goal** To construct a three-dimensional visualized CLT connection panel to give the user insight in the shape of it. This visualized shape should also serve as an input for the Robotic Fabrication module to produce the physical CLT connection panel.

**Methodology** First, a three-dimensional grid is constructed within the rectangular outline of the joint, its sizes based on the sizes of the lumber and panel thickness. Consecutively, the outline of the panel is extruded and this BREP is split by the three-dimensional grid. Hence, the visualized joint and shape to be delivered for robotic fabrication is generated. Figures 6.19-6.21 show this process schematically.

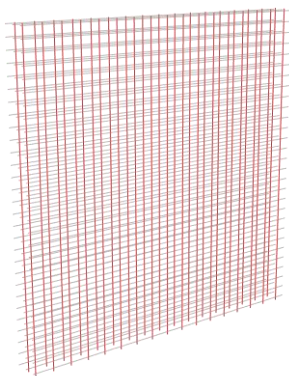


Figure 6.19: 3D grid based on the sizes of the lumber and panel thickness

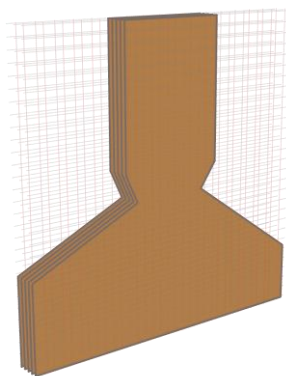


Figure 6.20: Extruded outline of the Connection panel

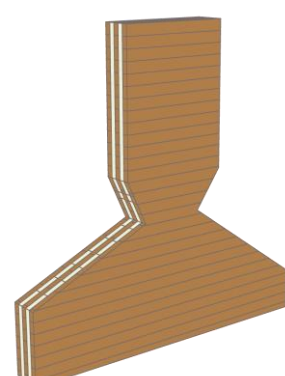


Figure 6.21: 3D Visualized Connection panel, constructed by a split BREP.

### ii. Joint Geometry for Robotic Fabrication

**Goal** To create the outline shape of the CLT connection panel in a BREP format, so that it can be robotically fabricated. This output is based on the findings in the Pilot study.

**Methodology** The outline is generated from the split curves and the visualized 3D connection panel, by subtracting the outer contour of it. As a result, the exact outline shape of a connection panel can be derived.

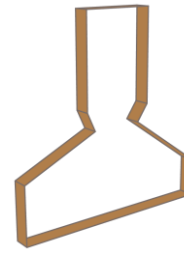


Figure 6.22: Outlined shape for Robotic Fabrication

### 6.4.3 ANALYTICAL UNITY CHECKS FOR CLT CONNECTION PANELS

Figure 6.23 shows a simplified workflow of the third component of the Joint Design module, which is the Analytical Unity Check (U.C.'s) for the connection panels. The output of this component of the module is discussed hereafter.

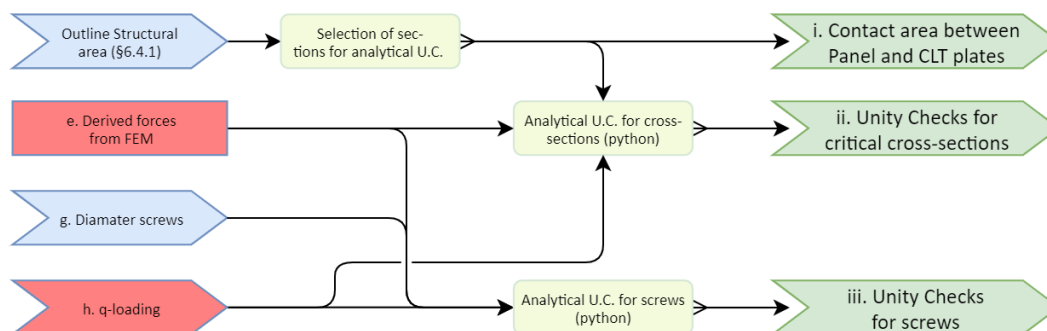


Figure 6.23: Simplified workflow of the Analytical Unity Checks for Connection Panels

(Blue: input variables, Red: input derived from the Global Structure module, Light yellow: processing, Green: output)

#### i. Contact area between Panel and CLT plates

**Goal** To select the cross-sections that represent the contact areas between the CLT connection panel and the appending CLT plates.

**Methodology** By selecting the segment of the exploded outline with the corresponding index number. Figure 6.24 shows the segment of the contact area for the left appending CLT plate.

#### ii. Unity Checks for critical cross-sections

**Goal** To get insight in the structural performance of the preliminar outline of a connection panel, that is modelled by the user. The relevant cross-sections of the initial outline are tested against U.C.'s as described in Chapter 1.7. These checks should give a user a preliminar indication about the structural performance of the panel.

**Methodology** As described in Chapter 6.2, the screws will take all tensional forces and in-plane shear forces. The CLT connection panel should therefore be checked on the cross-sections and cases as shown in Figures 6.42-6.26.

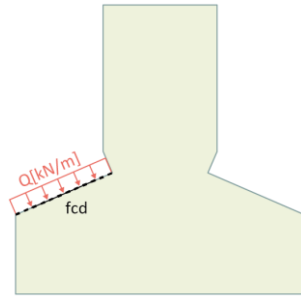


Figure 6.24: Section to check for compression resistance

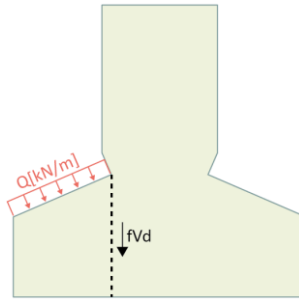


Figure 6.25: Section to check for Shear resistance

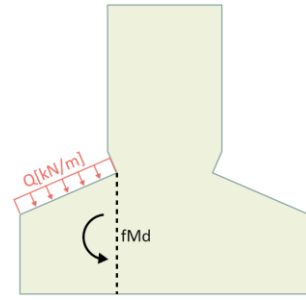


Figure 6.26: Section to check for bending resistance

State of  
the art

All U.C.'s are automatically performed by a python script. This script is presented in Appendix M. It also tells a user the rate of how much the cross-section meets the U.C. criterium. Figure 6.28 shows the outcome of a U.C. against compression. The U.C. is low in this case, due to the optimal orientation of the strong- and weak direction of the CLT connection panel. A user can change the initial size of the panel accordingly to get a first outline, to evolve along the integral workflow. Besides, the script of the U.C.'s is set up parametrically to enable it to process different geometries of connection panels.

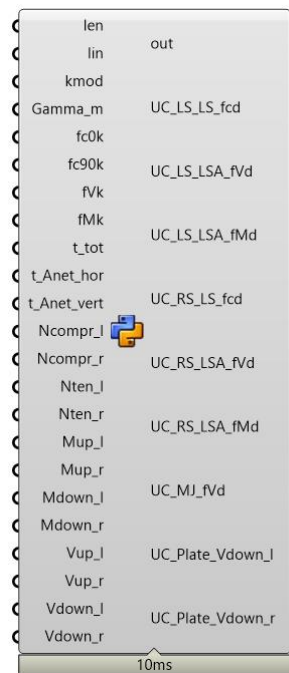


Figure 6.27: Python component to perform relevant U.C.'s.

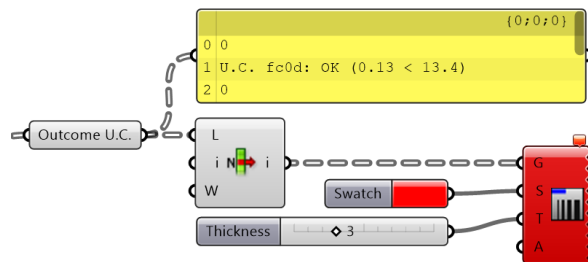


Figure 6.28: The outcome of a the U.C. against compression. Result. Corresponding cross-section shows up if U.C. > 1.0.

### iii. Unity Checks for screws

Goal

To verify whether the screws will fail under a certain load or not.

Methodology

By retrieving information from screw manufactures, the following information is retrieved from product sheets.

- Diameter of screws
- Resistance against shear,  $R_{V,k}$
- Resistance against withdrawal,  $R_{ax,k}$



### i. FEM meshes

<i>Goal</i>	To mesh surfaces that represent the CLT connection panels.
<i>Methodology</i>	The surfaces are meshed by the Karamba3D mesh component, since the points where the appending CLT plates meet the panels should be included in the mesh. The same consideration is made as described for the meshing process of the CLT plates from the global structure, see Chapter 5.4.3-5.4.4. The cross-sectional parameters are provided by the same python script as applied for the CLT plate meshes. No correct alignment of the strong- and weak direction of the mesh faces is required, since the panels are modelled as two-dimensional elements in the global yz-plane. Therefore, the strong- and weak directions are aligned along the global y- and z-axes.

### ii. FEM springs

<i>Goal</i>	To create representative springs for: <ol style="list-style-type: none"> <li>1) Screws that connect the CLT plates with the connection panel</li> <li>2) Contact area between the CLT plates and the connection panel</li> </ol>
<i>Methodology</i>	<p>For the <b>screws</b>, resistances in the following local directions are modelled:</p> <ul style="list-style-type: none"> <li>▪ x-direction: withdrawal resistance [kN]</li> <li>▪ y-direction: shear resistance [kN]</li> <li>▪ z-direction: shear resistance [kN]</li> </ul> <p>The resistances are retrieved from product sheets of manufacturers. An example is the VGS fully threaded screw from Rothoblaas [66]. In case the shear resistances <math>k_{ser,V}</math> are not provided in the product sheet, these are calculated by Formula (41), according Eurocode 5 [20]. Appendix O shows an overview of possible stiffnesses that can be applied at the springs that represent screws.</p>

$$K_{ser,V} = k_y = k_z = \frac{\rho_m^{1.5} * d}{23} \quad [N/mm] \quad (41)$$

$\rho_m$	=	Density of CLT	[kg/m <sup>3</sup> ]
$d$	=	Diameter of the screw	[mm]

For the **contact area**, springs are modelled as compression-only springs. The total contact area between the CLT plates and the connection panel is divided by the number of modelled springs. As the contact area is represented by compression-only springs, the stiffness can be derived from Formula (42).

$$K_{compr} = k_x = \frac{E_{CLT} * A_{spring}}{l_{spring}} \quad [N/mm] \quad (42)$$

$E_{CLT}$	=	E-modulus of CLT	[N/mm <sup>2</sup> ]
$A_{spring}$	=	Area distributed to spring	[mm <sup>2</sup> ]
$l_{spring}$	=	Length of the spring	[mm]

The contact area between the appending CLT plates and the CLT connection panel can only take compression and no tension or shear. Therefore, as soon as tension or shear forces occur in the spring, the stiffness is reduced to zero. Figure 6.32 shows illustrations of the FEM principles of springs that represent the screws and the contact area.

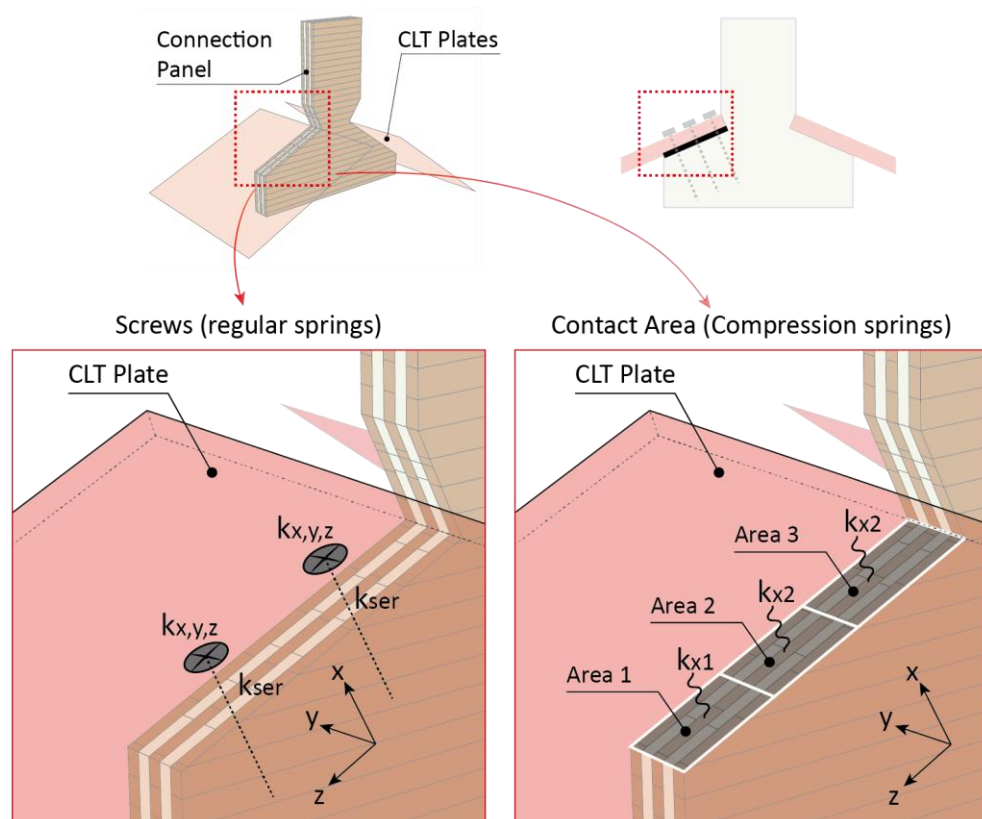


Figure 6.32: Left: local axes of screws (2 pc.). Right: Distributed area per compression spring in case of three compression-only springs.

#### State of the art

The spring properties are automatically computed. A user can define how many compression springs, and how many screws should be modelled. The stiffness properties are automatically determined based on the parameters as discussed above. Standard Grasshopper components are combined with a python component to integrate modelling of springs in the integral workflow in a parametric way.

#### iii. FEM beams

##### Goal

To represent the CLT plates of the appending structure by beams.

##### Methodology

As the joints will be two-dimensionally modelled, the CLT plates should be represented by beams. Therefore, representative beams with similar orthogonal material properties as the CLT plates will be modelled. The length of the beams depends on the geometrical information derived from the Global Structure module.



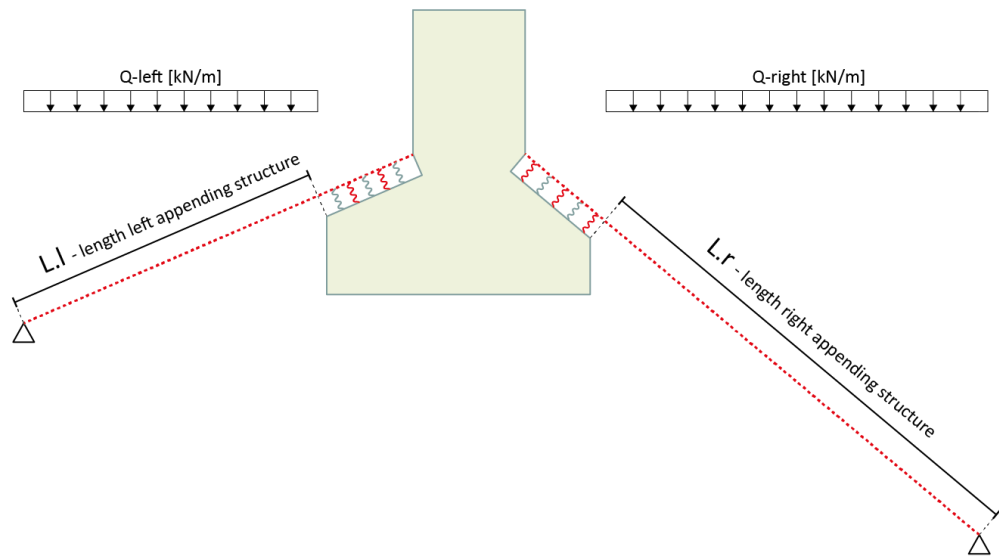


Figure 6.33: Two-dimensional representation of appending CLT plates and fully modelled joint

#### iv. Remaining FEM data

<i>Goal</i>	To provide all information for the FE model except the geometry. Information such as load cases, loading, supporting conditions, and analyses cases.
<i>Methodology</i>	The q-load should be of the same magnitude as the q-load that is applied on the appending structure in the FEM model of the global structural model. Therefore, this input is retrieved from the Global Structure module. The FEM data is generated by GeometryGym components.

## 6.5 FINITE ELEMENT MODELLING OF THE JOINTS

### 6.5.1 FINITE ELEMENT MODELLING SOFTWARE

**Karamba vs. GSA verification.** As this research is about an integral workflow, it is preferable to link the Global Structure module and the Joint Design within the same software package. The entire geometry of the global structure is modelled in Grasshopper, and therefore it was investigated to set up the FE models of the Joint Design in Grasshopper as well. This could be achieved with the use of Karamba3D, which is a FE software package and can be installed as a plugin for Grasshopper. However, to verify the accuracy and correctness of Karamba3D handling orthogonal material properties, a validation was made between Karamba and GSA models from an out-of-plane loaded element. From the GSA model, it is given this result was successfully validated by an analytical calculation, see Chapter 5.2.3 and Appendix E. Therefore, the GSA model is valid apart from the results from the Karamba model. Figures 6.34-6.37 show the results.

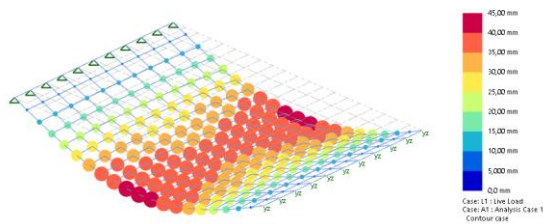


Figure 6.34: GSA FEM model, 3-D impression of deflected shape

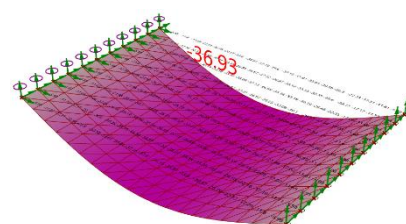


Figure 6.35: Karamba3D FEM model, 3-D impression of deflected shape

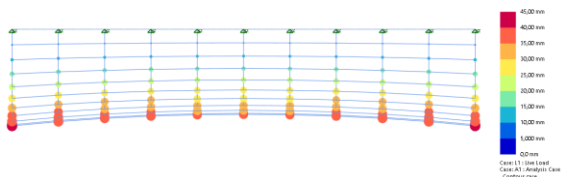


Figure 6.36: GSA FEM model.

$$W_{middle,max} = 36.48mm, W_{edge,max} = 41.45mm$$

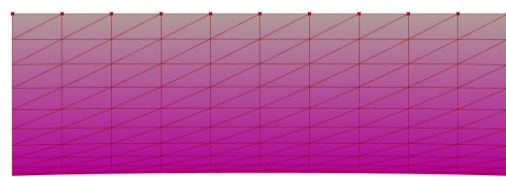


Figure 6.37: Karamba3D FEM model.

$$W_{middle,max} = 36.93mm, W_{edge,max} = 37.32mm$$

**Results.** From these results the conclusion can be drawn that the Karamba model shows a deviation from the GSA model, especially at the edge of the simply supported out-of-plane loaded element. After all, the following considerations apply as well:

- Post-processing of FE results is possible from Karamba but requires additional operations.
- GSA is better suited for non-linear and more advanced FE calculations, which might be required considering the spring properties present in the joint models.
- The orthogonal material component of Karamba is a new component since the latest update. Therefore, the reliability of this component, which is essential for the modelling of CLT, is questionable as the validation study shows. This concise study showed that the in-plane shear  $G_{xy}$  was governing the deflection of the FE model in Karamba, whereas the bending stiffness  $EI$  should be governing since the element was loaded out-of-plane. In the GSA model the bending stiffness  $EI$  was governing.

**Conclusion.** Considering the validation results and considerations as stated above, the FEM model will be modelled in GSA.

### 6.5.2 INPUT FOR THE FEM

From the geometry that is generated along the workflow from the Joint Design module as presented in Chapter 6.4, a FEM model in GSA can automatically be retrieved. Figure 6.38 shows an impression of a joint as modelled according the FEM, whereas Appendix P describes the full input for this model. The fictive joint is setup in a symmetrical way. The purpose is to verify the FEM by analytical Unity Checks (U.C.) to ensure correct modelling of the joint. The geometry is not retrieved from a Global Structure model or an existing project.

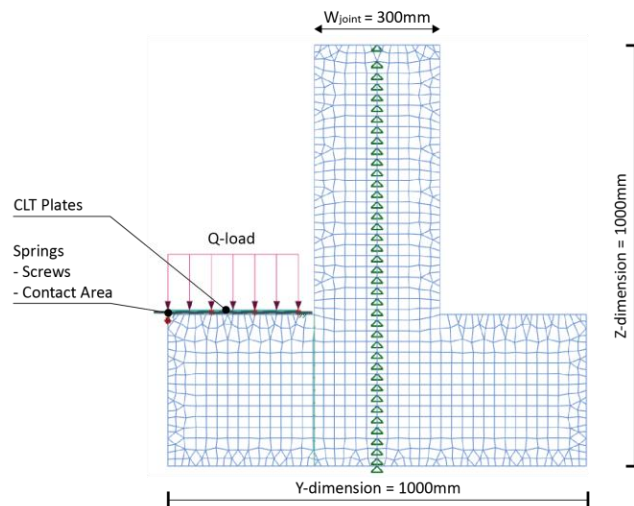


Figure 6.38: GSA geometrical input

### 6.5.3 OUTPUT FROM THE FEM

The results from the FEA are shown below.

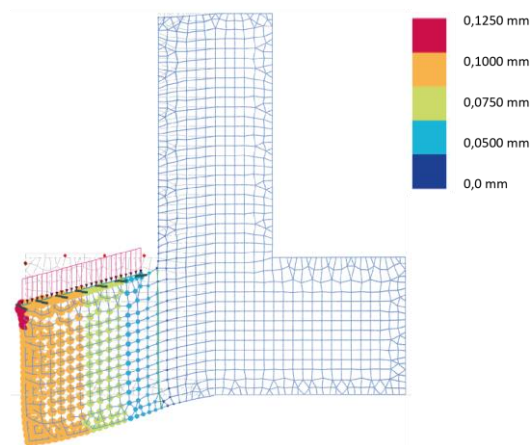


Figure 6.39: Deflected shape of the structure.  $u_{max} = 0.11\text{mm}$

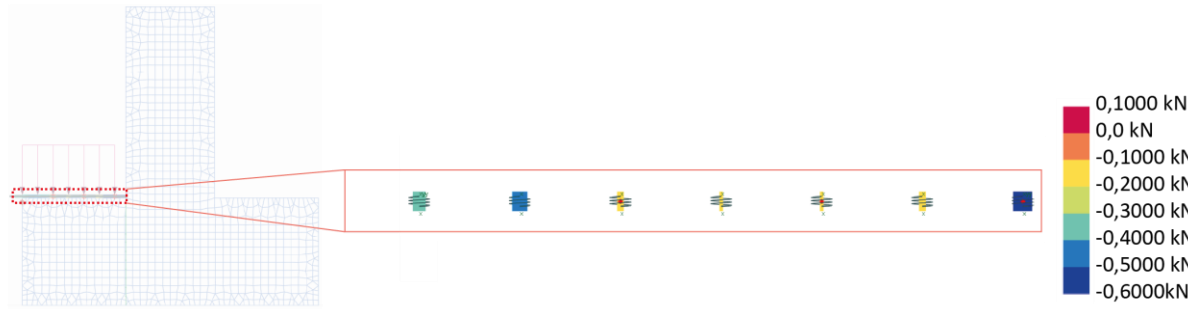


Figure 6.40: Spring forces  $F_x$  in the springs.  $F_{x,max} = 0.6\text{kN}$  (compression). No tension ( $>0\text{kN}$ ) occurs

#### 6.5.4 VERIFICATION

As stated in the introduction of this paragraph, the joint geometry was set up in such a way that the results could be easily verified by an analytical calculation. Therefore, the joint is supported along the vertical symmetry axis. Figure 6.41 shows the red highlighted cross-section where the shear force and -stress is measured. These values were compared against the shear force and -stress computed through the analytical U.C.'s, see Chapter 1.7 and 6.4.3. The results are presented hereafter.

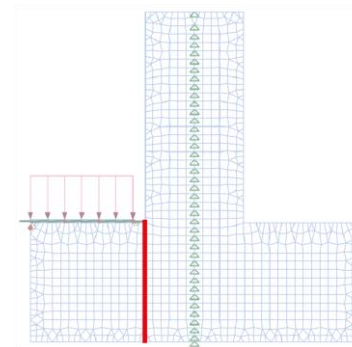


Figure 6.41: Cross-section of the joint along which the shear force and -stress are measured

**Results.** The net area  $A_{net}$  of the cross-section is  $28.800\text{mm}^2$ . For the analytical U.C., the shear force and -stress are calculated by Formulas (43) and (44).

$$F_V = q * l_{beam} \quad (43)$$

$$\sigma_\tau = \frac{F_V}{A_{net}} \quad (44)$$

Model	Shear Force $F_V$	Shear stress $\sigma_\tau$
Analytical U.C.	1,872 kN	0.065 N/mm <sup>2</sup>
FEM	1,79963 kN	0,062487153 N/mm <sup>2</sup>
Deviation		4.02% %

**Conclusion.** The results deviate with 3.87%. Therefore, it can be concluded the FEM model is modelled correctly. The deviation is probably caused by the fact that the FEA are performed along multiple iterations due to the compression-only springs in the FE model. For every iteration, the FE software analyses whether the compression force in a compression-only spring  $\leq 0\text{kN}$ , till an equilibrium is found. This process of iterations results in a redistribution of forces which are not considered in case of the analytical U.C.. Another reason can be the mesh density, and subsequently the accuracy of determining the sectional force in the FEM model. Appendix Q shows more geometrical variations of a joint that are validated to ensure correct modelling in the FE software.

From the integral workflow of the Joint Design module, an important component is the comparison and alignment between the FEM model and the Analytical U.C.. Figure 6.42 shows a call-out of the workflow where this comparison is shown. It proves that the analytical U.C. component can serve as an initial joint design tool get a reliable preliminar outline of a joint, given the geometrical and structural boundary conditions of the Global structure module.

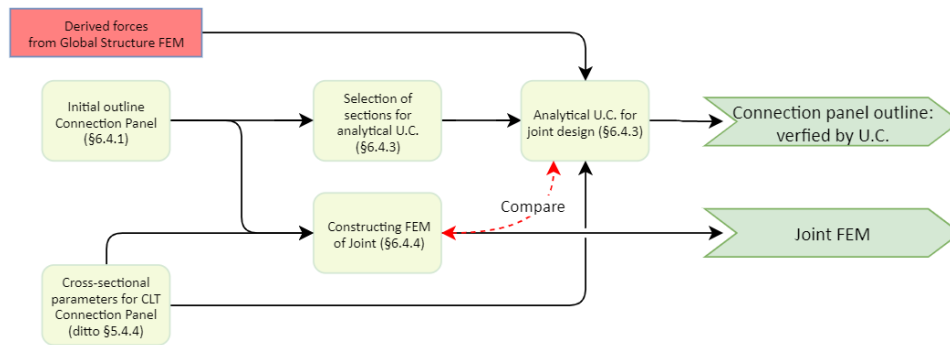


Figure 6.42: Call-out of workflow to show the design loop between the analytical U.C. and FE modelling

## 6.6 STRUCTURAL RELATIONSHIPS BETWEEN JOINT DESIGN AND GLOBAL STRUCTURE

### 6.6.1 STRUCTURAL PERFORMANCE OF A JOINT

The purpose of this research is to investigate what an integral workflow looks like for robotically fabricated customized CLT connection panels. Therefore, it is of importance to link the Joint Design as discussed in this chapter, with the Global Structure and the robotic fabrication process. This paragraph focusses on the link from the Joint Design back to the Global structure. Figure 6.43 shows this link.

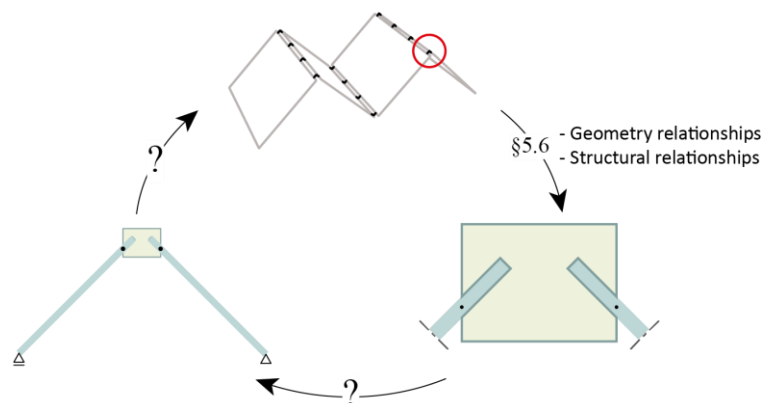


Figure 6.43: Link from the Joint design back to the global structure module, highlighted with question marks

The parameter that should be fed back to the global structure, is a parameter that represents the structural behavior of the joint. A (rotational spring) stiffness reflects this structural behavior. Therefore, this paragraph focusses on determining the (rotational spring) stiffness of a joint and the desired output of the Joint Design module, to link the Joint Design with the Global Structure module.

### 6.6.2 REPRESENTATIVE ROTATIONAL SPRING STIFFNESS OF JOINTS

The principle of determining the rotational spring stiffness of a joint, is to measure its resistance against rotation. Formula (45) shows this principle in the most simplistic form.

$$k_r = \frac{M}{\Phi} \quad (45)$$

Once the stiffness is determined, rotational springs with corresponding stiffnesses should replace the joints in the global structural model. This representative spring model should subsequently be verified by comparing it to a full model of the global structure. In this model both the joint and appending structure are detailly modelled. Figure 6.44 shows this process.

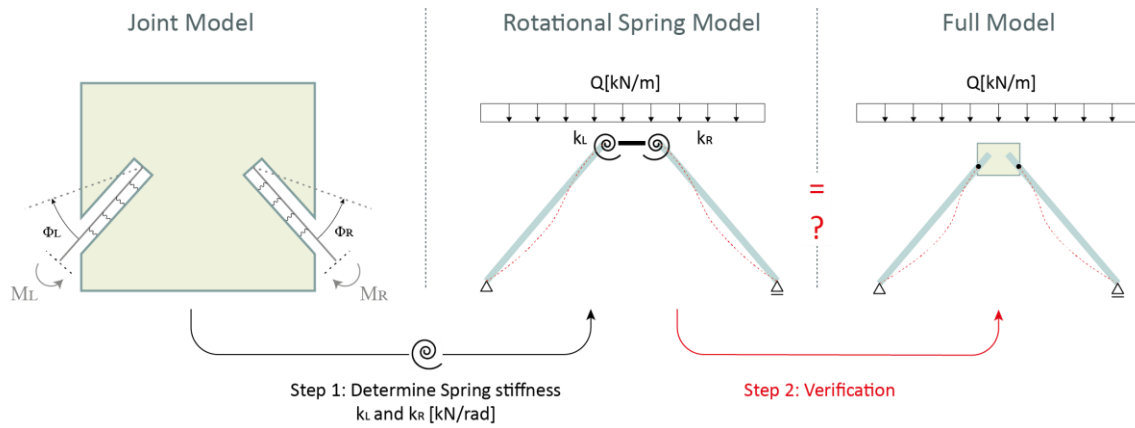


Figure 6.44: Verification process of the rotational spring model. Step 1) Feeding back the spring stiffness to the global structure. Step 2) Verification with full model

In this research, different methodologies are investigated that determine the (spring) stiffness of the joints. The methodologies apply different loadings to rotate the joint, as well as different supporting conditions to resist this rotation. Figure 6.45 shows these methodologies.

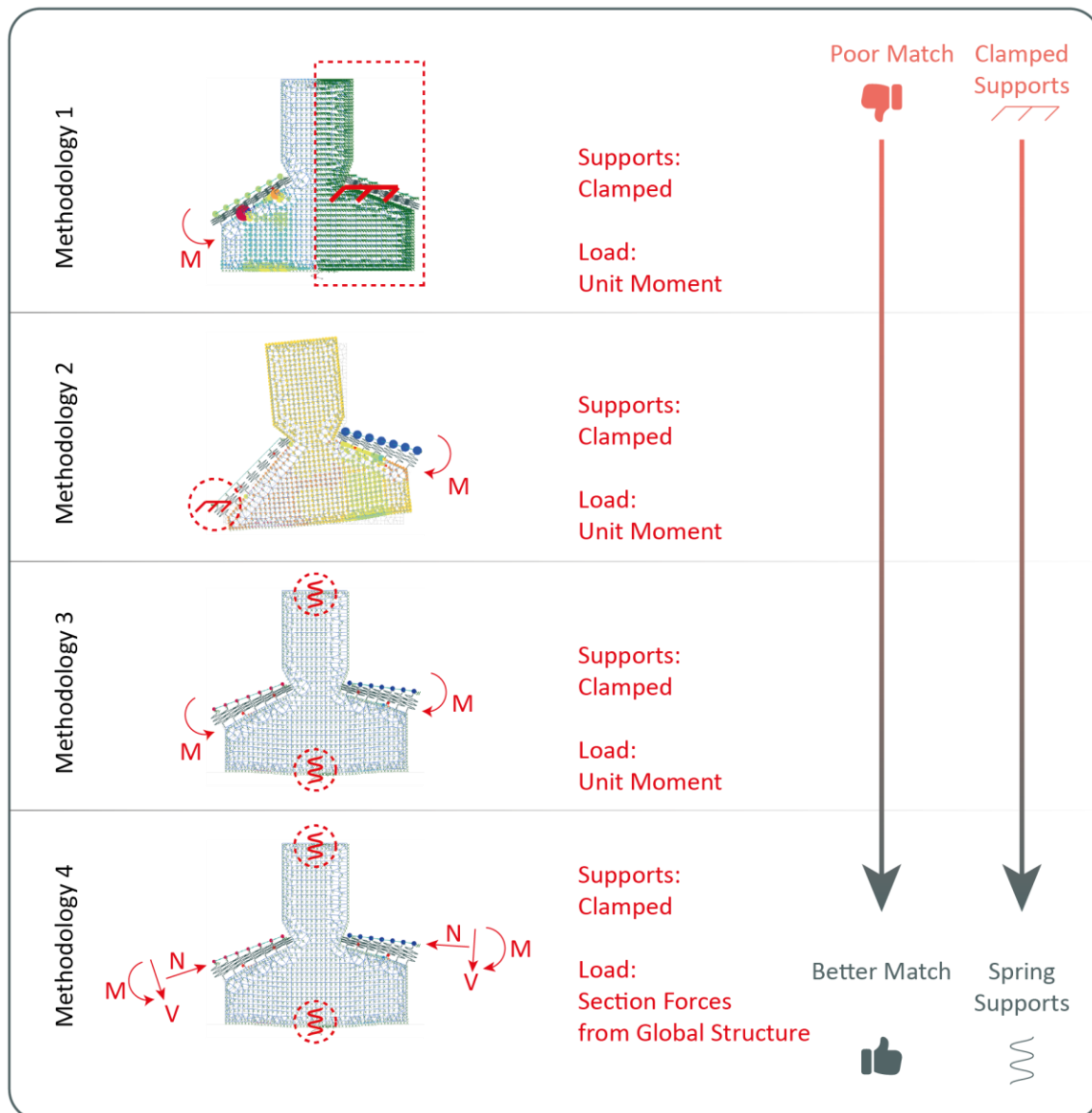


Figure 6.45: Four methodologies to investigate the representative spring stiffness of joints

In this report, only the results of fourth methodology are shown hereafter, as this methodology matches the verification with full model of the global structure the finest. Appendix R shows the elaborated results of all methodologies.

**Methodology 4.** As the fourth methodology showed the best results determining the rotational spring stiffness, different variants were set up to validate the methodology along the following steps:

1. Retrieve sectional force from the Global structure, as described in Chapter 5.6
2. Induce these forces as loading on a separate joint model and determine the rotational stiffness by  $k_r$   

$$= M_{\text{Global structure}} / \Phi$$
3. Feed the stiffness back to the rotational spring model
4. Verify with the full model

**Results.** Across different models, the results from the rotational spring models did show a deviation from the full models. Figure 6.46 shows a boxplot distribution of the deviation.

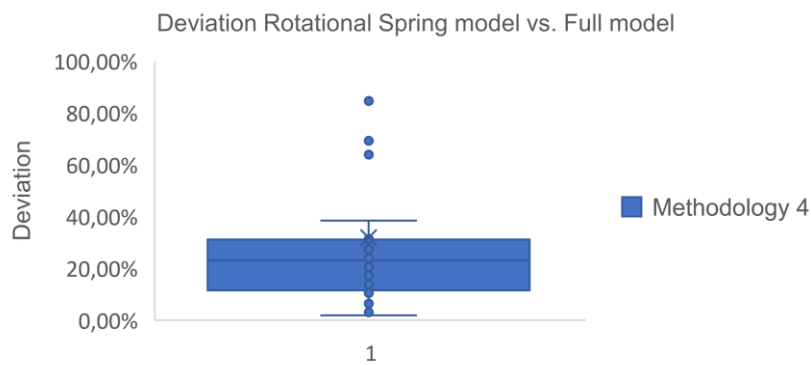


Figure 6.46: Deviation between the rotational spring model vs. the full model according the fourth methodology

**Conclusion.** After analyzing the results and applying different methodologies, it was concluded there is no universal methodology with 100% accuracy found, to determine the exact representative (spring) stiffness. This presumably relates to the following reasons:

- The size of the joint is too large to catch the entire behavior in one or two rotational springs.
- The appending CLT plates can barely bend and rotate in the slotted hole of the connection panel, in case of the full model. However, in the representative spring model, they are only restricted to bend or rotate by the rotational springs.
- The iterations the full model undergoes due to the modelling of the compression-only springs. This behavior and result cannot be covered or simulated in a representative spring model.

After all, the workflow does allow for a feedback loop of the spring stiffness back to the Global Structure module. However, different methodologies relate to different levels of accuracy. At this moment, no universal method is found with 100% accuracy. Therefore, a designer should carefully evaluate the desired level of accuracy to implement a feedback loop with the spring stiffness, to get a more reliable understanding of the global structural performance. Besides, determining the stiffness of joints should be utilized to determine correlations between the normalized magnitude of the stiffness of the joints and different design parameters of the connection panel. Chapter 6.7 and 6.8 illustrate these correlations.



### 6.6.3 FEM OUTPUT OF THE JOINT DESIGN MODULE

The FEM output of the Joint Design module consists of the three models as discussed in this paragraph. Figures 6.47-6.49 show these models.

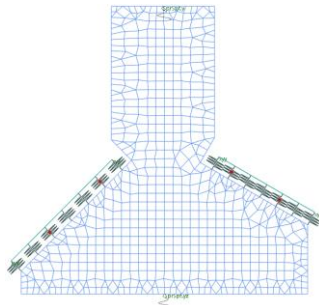


Figure 6.47: Detailed Joint Model

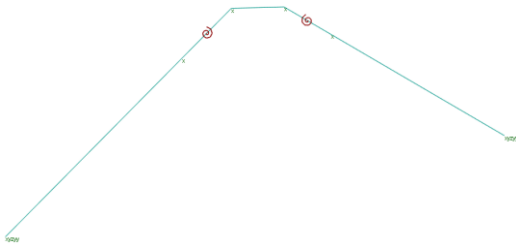


Figure 6.48: Rotational spring model that represents the full model of the figure on the right. The red springs represent the joint of Figure 6.47.

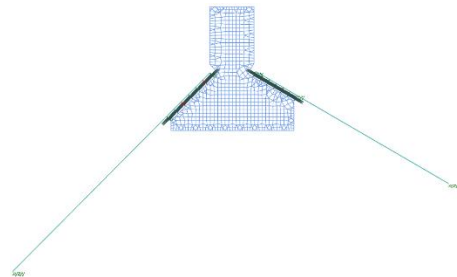


Figure 6.49: Full model with the entire appending structure and detailed modelled joint.

## 6.7 RELATIONSHIPS WITH GLOBAL STRUCTURE AND ROBOTIC FABRICATION

This chapter focusses on the relationships of the Joint Design with the other two modules of the integral workflow, namely the Global Structure and the Robotic Fabrication. Figure 6.50 shows these relationships among the three components on the highest level of the integral workflow.

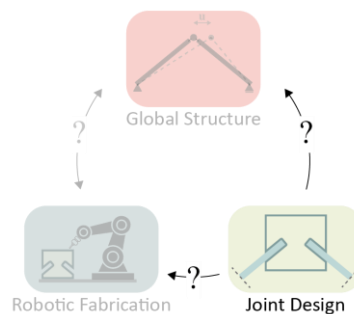


Figure 6.50: Relationships of the Joint Design with the Global Structure and Robotic Fabrication

**Joint Design → Global Structure.** From the Joint Design back to the global structure, there is one main parameter that can be fed back, which is the representative (spring) stiffness of the joints. However, as described in the previous paragraph, yet there is no universal methodology found that determines this stiffness accurately. Several methodologies with different accuracies were tested to determine the stiffness of the joints, and it was concluded from a higher level that the workflow can allow for a feedback loop for the stiffness of the joints. However, a designer should ensure he is confident with the accuracy of the applicable methodology. Therefore, the fourth methodology should be integrated in the Joint Design module and be utilized to quickly retrieve design graphs for

CLT connection panels. These design graphs can clarify correlations between geometrical parameters of a CLT panel and the corresponding structural performance.

**Joint Design → Robotic Fabrication.** From the Joint Design module there is one main component that relates strongly to the Robotic Fabrication module, namely the outline shape of the CLT connection panel. This shape only concerns the two-dimensional outline as the third dimension is set, given the fact that CLT plates are delivered in planar elements always. Figure 6.51 shows the relationships that flow from the Joint Design to the other modules of the integral workflow.

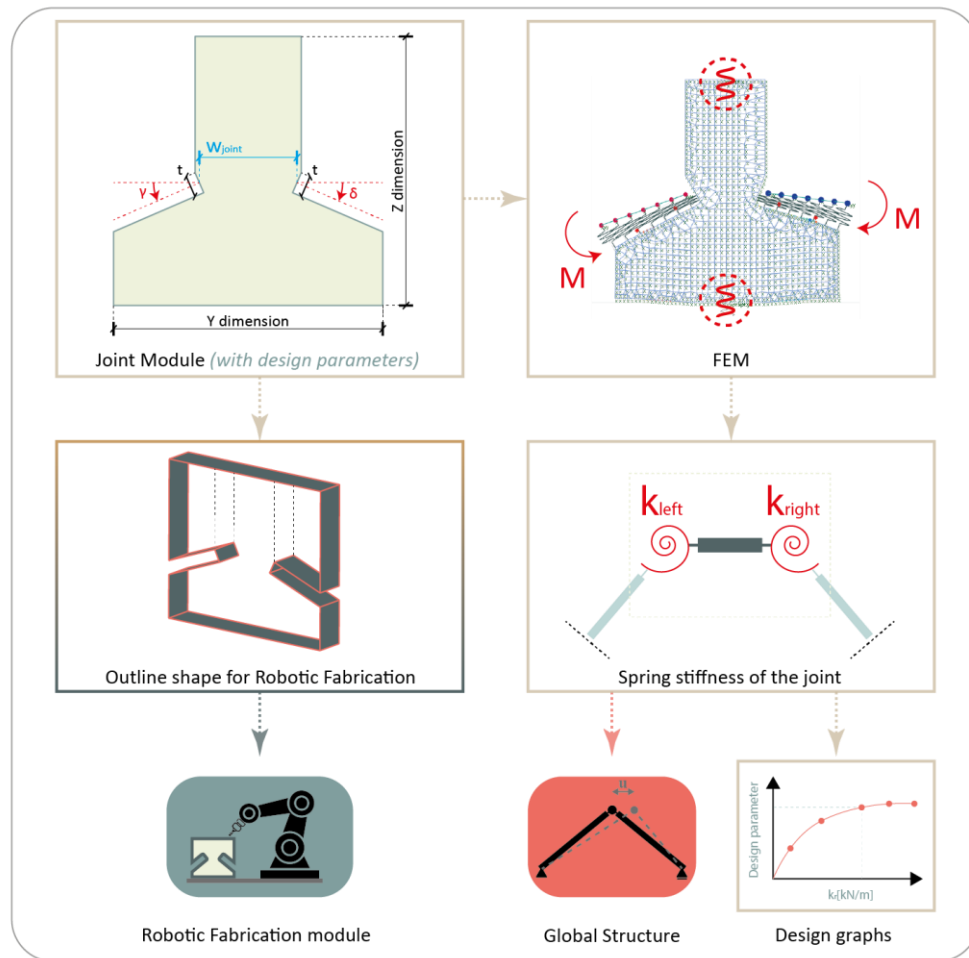


Figure 6.51: Relationships of the Joint Design with other modules

## 6.8 POTENTIAL OF THE WORKFLOW: JOINT DESIGN

This paragraph demonstrates the potential of the workflow as described in this chapter. The potential is demonstrated by showing different joint geometries the workflow can handle. Finally, design graphs are derived, to show the potential for a designer to get quick insight in the correlations between dimensional parameters and structural performance of a joint. This will help a designer to make reliable judgments on the structural behavior of a CLT structure on a local level in the preliminary design phase. Appendix S shows an overview of the script that represents this workflow.

## 6.8.1 GEOMETRICAL MODELLING

Figure 6.52-6.54 show different geometries the workflow can handle.

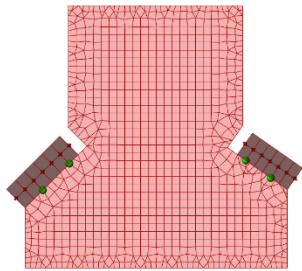


Figure 6.52: Geometry 1. Small slotted holes and rotated appending structure

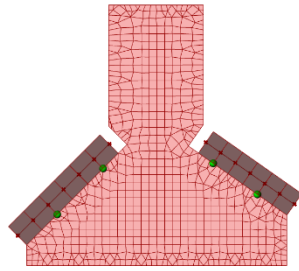


Figure 6.53: Geometry 2. Large slotted holes and horizontal appending structure

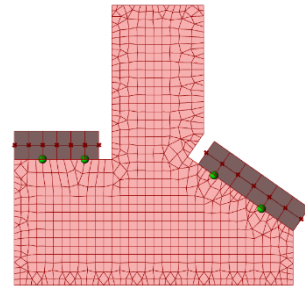


Figure 6.54: Geometry 3. Variable angles left and right and rotated appending structure



Figure 6.55: Geometry 1. Corresponding shape for robotic fabrication



Figure 6.56: Geometry 2. Corresponding shape for robotic fabrication

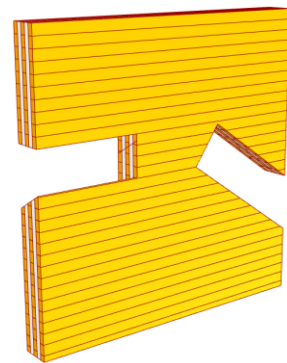


Figure 6.57: Geometry 3. Corresponding shape for robotic fabrication

Figure 6.58 shows the failure of the contact area between the appending CLT plates and the CLT connection panel. This section fails on tension with U.C. = 1.28, which is due to the few number of screws present (3pc.).

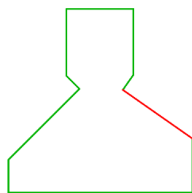


Figure 6.58: Geometry 2. Outline and result of analytical U.C. (1) - screws

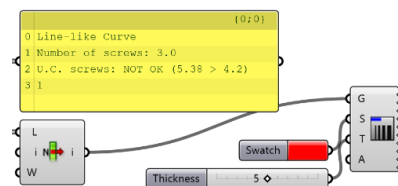


Figure 6.59: Result of analytical U.C. (screws)

Figure 6.59 shows the failure of the section on shear with U.C. = 1.025, which is due to the shear area that is modelled too small. These examples only show the potential of the workflow. They are not derived from an existing project or situation from practice.

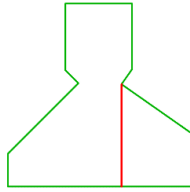


Figure 6.60: Geometry 2. Outline and result of analytical U.C. (2) - shear

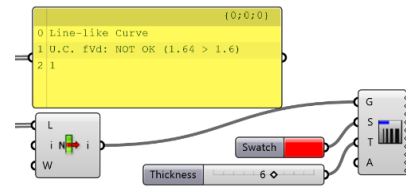


Figure 6.61: Result of analytical U.C. (shear)

## 6.8.2 FINITE ELEMENT MODELLING

From the FE results, different design graphs for the joint stiffness can be derived to get insight in the correlations between (structural) design parameters. Besides, the workflow also automatically generates the hinged and fixed model of the global structure, which form the lower and upper limit of the rotational spring model. Figure 6.62-6.66 show these models. This paragraph presents three design graphs, more graphs are presented in Appendix T.

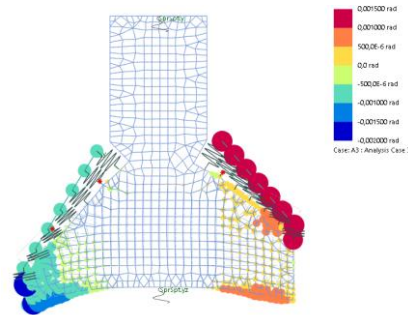


Figure 6.62: FEM model a. Joint model to determine rotational stiffness with measuring the rotation of the plates (rad)

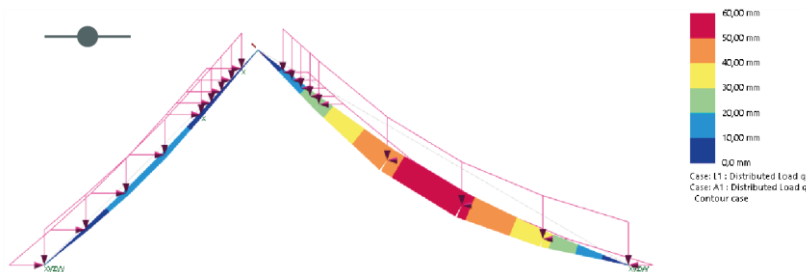


Figure 6.63: FEM model b. Hinged model, lower limit for the rotational spring model

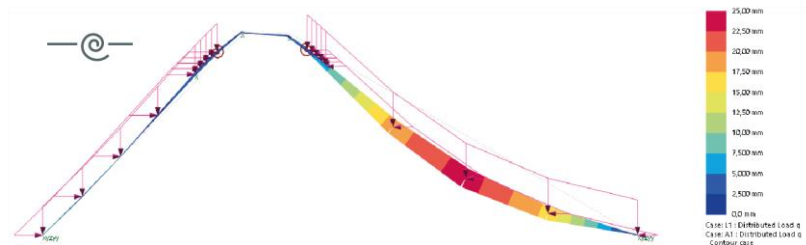


Figure 6.64: FEM model c. Rotational spring model with rotational springs. Derived according Chapter 6.6

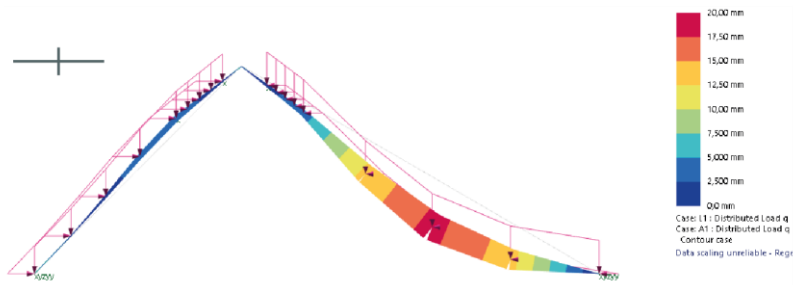


Figure 6.65: FEM model d. Fixed model, upper limit for the rotational spring model

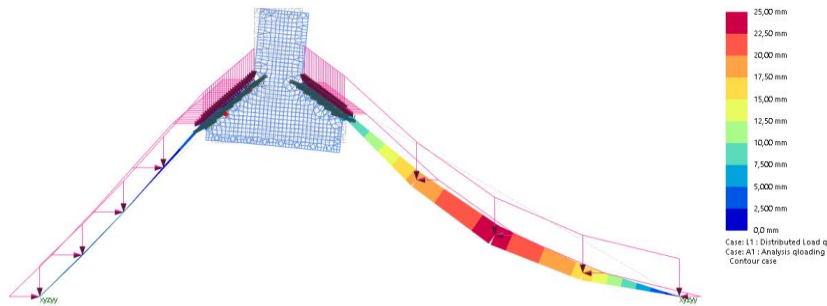


Figure 6.66: FEM model e. Full model to verify the structural behavior of the rotational spring model

### Explanation

As shown in the design graph on the right, the  $H$  of the joint influences the stiffness especially in the lower dimensions. For  $H \geq \pm 500\text{mm}$ , not much extra stiffness is gained. The larger the  $H$ , the stiffer the joint. This is caused by the size of the area of material through which the forces can be redistributed in case the joint is loaded under a bending moment.

### Derived design graph from FE and varying parameter

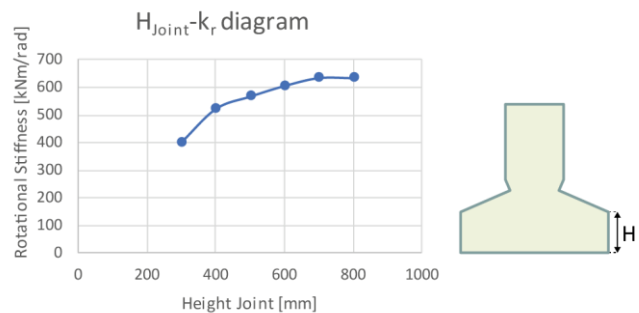


Figure 6.67: Design graph for varying parameter  $H$  [mm] versus the corresponding spring stiffness of the joint

The angle of the slotted hole influences the stiffness significantly after  $25^\circ < \alpha_{\text{slot}} < 30^\circ$ . This seems to be compelling as a larger  $\alpha_{\text{slot}}$  results in a steeper and so stiffer structure. It is interesting that especially in the domain of  $0 < \alpha_{\text{slot}} < 20^\circ$  not much extra stiffness of the joint is gained. This is due to the fact that if  $\alpha_{\text{slot}} < 20^\circ$  almost all forces are taken by the screws.

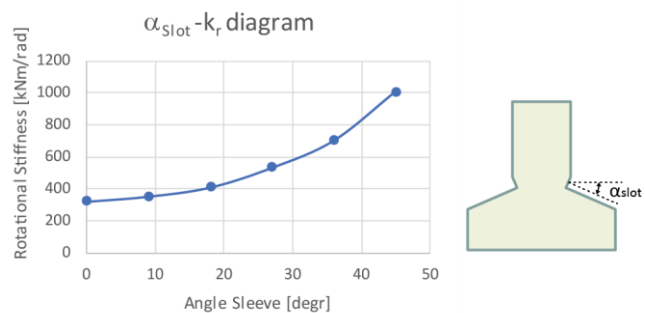


Figure 6.68: Design graph for varying parameter  $\alpha_{\text{slot}}$  [mm] versus the corresponding spring stiffness of the joint

If the thickness is increased, the stiffness is increased non-linearly. From the design graph on the right it can be concluded that for  $t \geq \pm 180\text{mm}$ , not much stiffness is gained. This is related to the moment of inertia. Simply stated,  $I = 1/12 \cdot b \cdot h^3$  shows that if  $h=t$ , the moment of inertia does not increase linearly but cubically. This phenomenon apparently also applies to CLT plates.

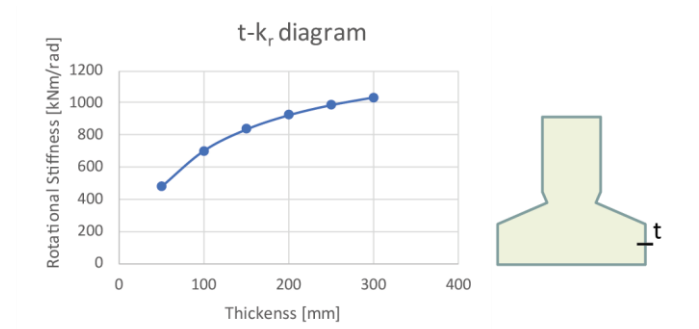


Figure 6.69: Design graph for varying parameter thickness [mm] versus the corresponding spring stiffness of the joint

## 6.9 CONCLUSION

This chapter focused on the Joint Design module of the integral workflow as presented in Figure 6.70 and answers the following question.

What does a workflow for CLT structures look like, that promote exploration of the structural performance of CLT structures on a *local* level in the preliminary design phase?

For this module, a workflow was developed to investigate the design process of a joint in a CLT structure. The type of joint that is discussed in this chapter consists of a CLT panel with slotted holes, to connect CLT plates from a structure together. For this type of joint two design variants were analyzed. The one with the most straightforward executability philosophy and clear load distribution was further elaborated in this chapter. Besides, the chapter focused on the relationships and (in)dependencies between the Joint Design and the Global Structure and Robotic Fabrication. The main relationship from the Joint Design to the global structure is the stiffness of the joints. In this research, several methodologies with different accuracies were tested to determine the stiffness of the joints, and it was concluded from a higher level that the workflow can allow for a feedback loop for the stiffness of the joints. However, a designer should ensure he is confident with the accuracy of the applicable methodology. No 100% accurate universal methodology was achieved. Determining the stiffness can be utilized to retrieve design graphs, to investigate the influence of different geometrical parameters of the joint geometry on the structural performance of it. The relationship between the Joint Design and the robotic fabrication process is the geometrical three-dimensional outline of the joint to be fabricated. This relationship was included in the workflow, and the outline of a joint could be extracted to send to a robot. Figure 6.70 shows the relationships as described above.

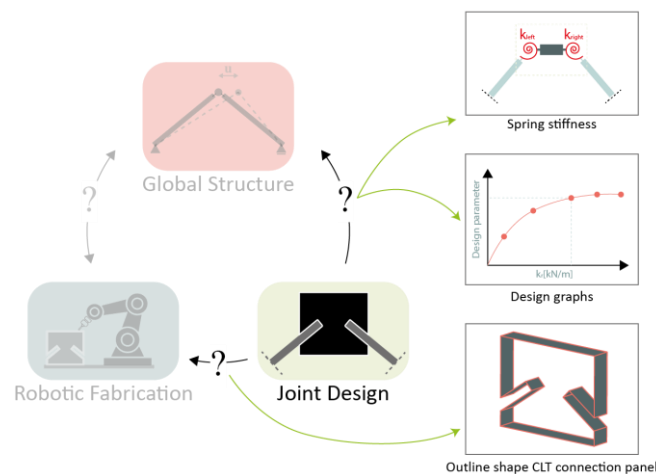


Figure 6.70: Relationships between the Joint Design and the Global Structure and Robotic Fabrication

Regarding software, a trade-off was made to perform the FEA in GSA instead of Karamba3D. The workflow of the Joint Design also includes a tool that enables users to quickly explore the structural performance of a CLT connection based on only the geometrical outline. This tool also served as a successful validation of the FEM models of different joints. Finally, the developed workflow showed potential for a user to quickly explore the structural behavior and performance of joint in a CLT structure. Different geometries could be handled effortlessly.

**Further improvements and development.** The main thing that should be improved on this module of the integral workflow is the methodology to determine the stiffness of the joints. Once this is implemented in the workflow, the integrality will increase as well. Right now, the Global Structure module will stick to model the joints as hinges, as described in Chapter 5.

## 7. Robotic Fabrication Module

### 7.1 INTRODUCTION

From the Joint Design, the three-dimensional outline of the CLT connection panel can be derived, which is described in the previous chapter. The goal of this chapter is to investigate how this panel can be robotically fabricated based on this three-dimensional outline. Therefore, the following question is answered in this chapter.

How can a customized CLT connection panel be robotically fabricated?

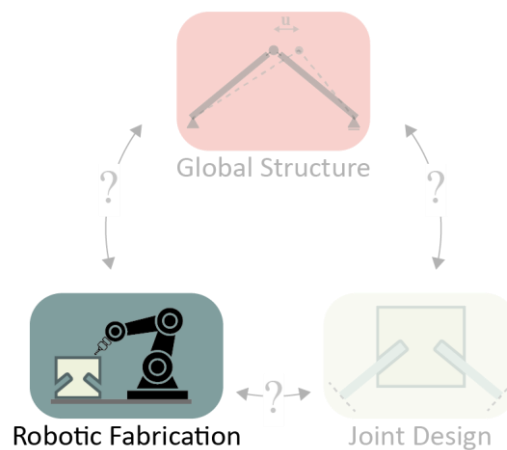



Figure 7.1: Focus of this chapter - the Robotic Fabrication module

The workflow as presented in this chapter, is based on a workflow and corresponding Grasshopper script for robotic milling developed by StudioRAP. Therefore, this chapter will only highlight the main design steps of this module and not go into technical details of it due to confidentiality. However, the design philosophy and steps as presented in this chapter are generally applicable to other projects as well. In the closing chapters, the relevant affordances and constraints are discussed, followed by a concise overview and demonstration of the potential of the entire integral workflow. A fictive structure is taken as an example to demonstrate this.



## 7.2 VARIABLES OF THE ROBOTIC FABRICATION MODULE

This paragraph presents all variables that are required for the Robotic Fabrication module. Below an overview is shown of the variables and output of this module.

Input Variable		Type	Global Structure module	Output
a	Geometry of connection panel	Geometry		* Milled CLT connection panel * Simulation of robotic fabrication
b	Milling diameter	Number		
c	Layer height for toolpath	Number		
d	Ramp length start/stop toolpath	Number		
e	Simulation settings	-Numbers -Planes		

All variables as presented above are explained and illustrated in Appendix U. The light yellow highlighted variables are derived from the Joint Design module, whereas the blue ones are provided as new variables in the current module. Figure 7.2 shows the components of the simplified workflow of the Robotic Fabrication module. Each component is explained more into depth in the consecutive paragraphs.

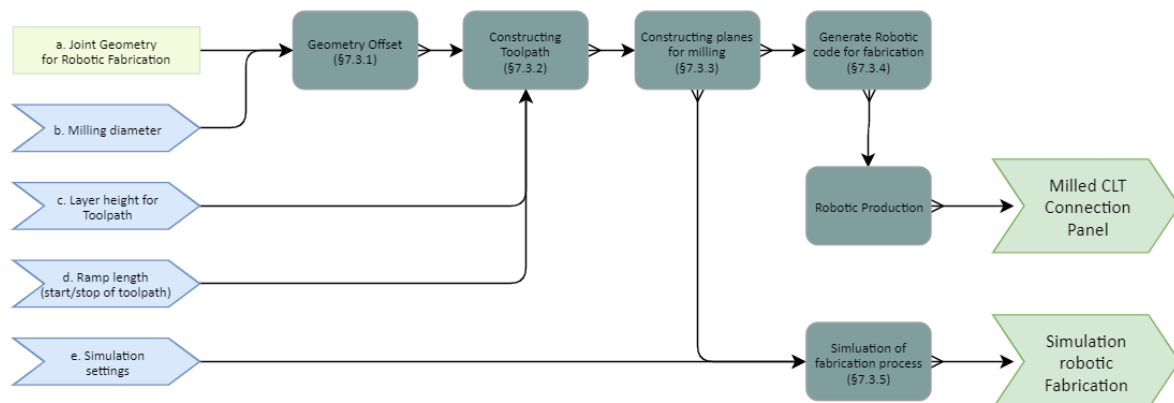


Figure 7.2: Simplified representation of the Robotic Fabrication module

(Blue: input variables, Light yellow: input derived from the Joint Design module, Dark grey: processing by the Robotic Fabrication module, Green: output of the Robotic Fabrication module)

## 7.3 COMPONENTS OF THE ROBOTIC FABRICATION MODULE

### 7.3.1 GEOMETRY OFFSET

Figure 7.3 shows a simplified workflow of the first component of the Robotic Fabrication module, which is the generation of the offset of the geometry. The output of this component of the module is discussed hereafter.

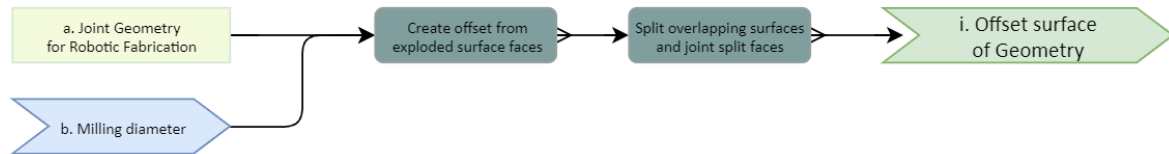


Figure 7.3: Simplified workflow of Geometry Offset

(Blue: input variables, Light yellow: input derived from the Joint Design module, Dark grey: processing, Green: output)

#### i. Offset surface of Geometry

**Goal** To retrieve the offset surface of the geometry and to integrate the milling diameter in the toolpath.

**Methodology** As the mill has a certain diameter and the toolpath of the mill is aligned in the center of the mill, the diameter divided by two should be integrated in the modelling of the toolpath. This is achieved by constructing the toolpath on the offset geometry.

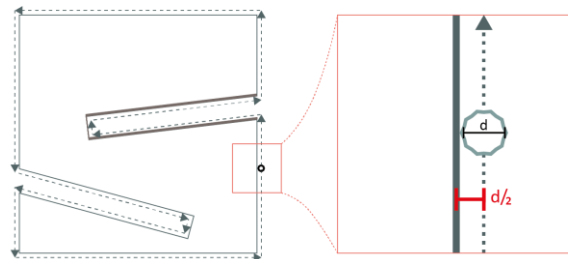


Figure 7.4: Diameter of the mill offset of the original geometry

### 7.3.2 CONSTRUCTING TOOLPATH

Figure 7.5 shows a simplified workflow of the second component of the Robotic Fabrication module, which is the construction of the toolpath on the offset BREP. The output of this component of the module is discussed hereafter.

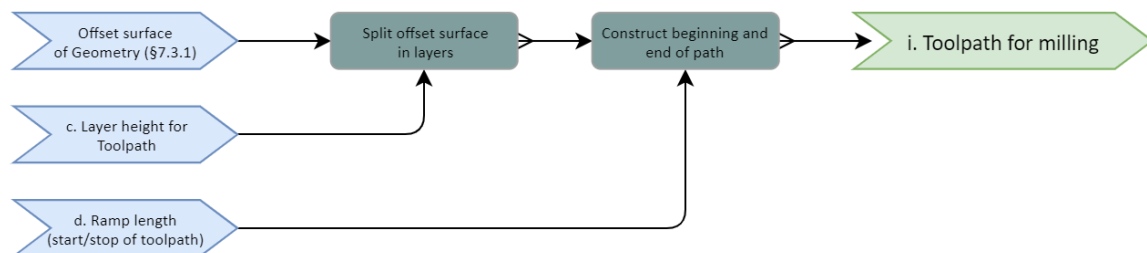


Figure 7.5: Simplified workflow of constructing the toolpath

(Blue: input variables, Dark grey: processing, Green: output)

### i. Toolpath for milling

<b>Goal</b>	To construct the toolpath for milling on the offset BREP of the previous step. The toolpath is the path the mill on the robot will move along to mill the CLT connection panel.
<b>Methodology</b>	A path is constructed on the offset BREP by slicing the BREP vertically by the layer height. The layer height determines how many times the mill will move around the geometry to cut through the material: the harder a material, the more layers are required. The start and stop of the path are constructed by considering the ramp length that is set by the user. This variable determines the slope and length of the start and stop of the toolpath.

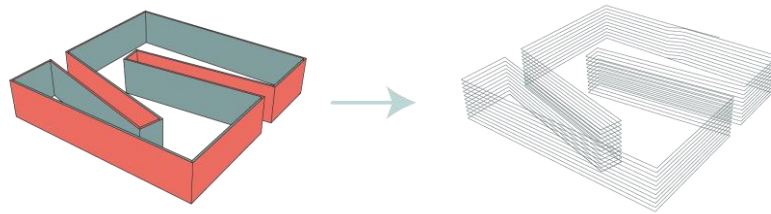


Figure 7.6: The offset BREP (red) and the toolpath on the right, derived from offset BREP geometry

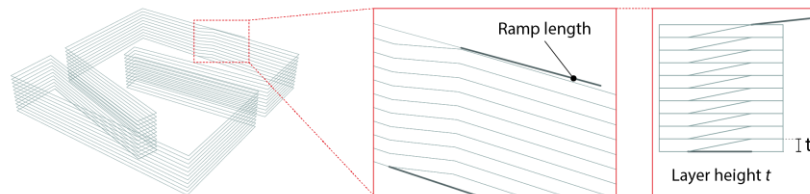


Figure 7.7: The ramp length and layer height  $t$  as variables to construct the toolpath

## 7.3.3 CONSTRUCTING ORIENTATION PLANES ON THE TOOLPATH FOR MILLING

Figure 7.8 shows a simplified workflow of the third component of the Robotic Fabrication module, which is the construction of orientation planes on the toolpath for milling. The output of this component of the module is discussed hereafter.

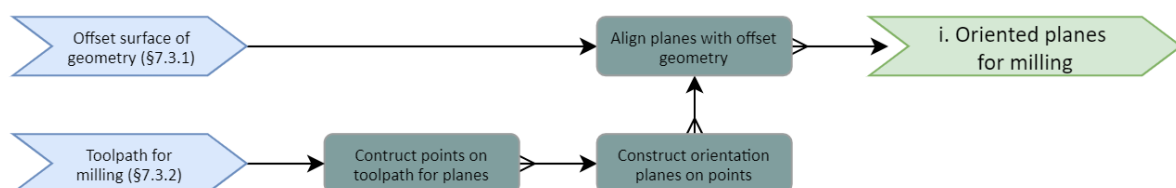


Figure 7.8: Simplified workflow of constructing orientation planes on the toolpath for milling

(Blue: input variables, Dark grey: processing, Green: output)

### i. Oriented planes for milling

<b>Goal</b>	To construct planes on the toolpath for the correct orientation of the mill.
<b>Methodology</b>	The toolpath is divided in different points on which the planes are constructed. The orientation is retrieved from the three-dimensional offset BREP outline. The Pilot Study (part II) shows that the smaller a segment of the toolpath, the more planes per length of the segment are needed to acquire better accuracy, see Chapter 4.5-4.6.

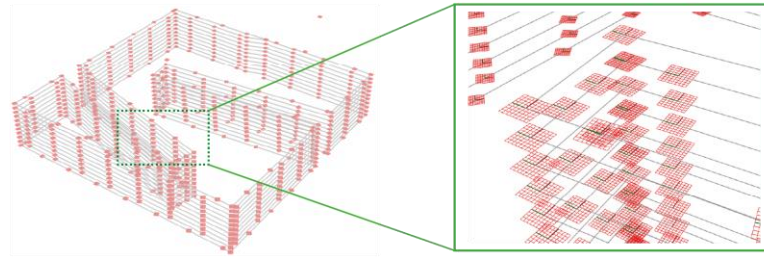


Figure 7.9: Planes for the mill to orient upon

### 7.3.4 GENERATE CODE FOR ROBOTIC FABRICATION

Figure 7.10 shows a simplified workflow of the fourth component of the Robotic Fabrication module, which is the generation of robotic code for fabrication. The output of this component of the module is discussed hereafter.



Figure 7.10: Simplified workflow of generating robotic code for fabrication

(Blue: input variables, Dark grey: processing, Green: output)

#### i. Robotic code for fabrication

**Goal** To generate code that can be read by the robot to fabricate the geometry.

**Methodology** The code consists of several components, whereof the most important ones are listed below:

1. The sorted coordinates and corresponding orientations along the toolpath, which are derived from the orientation planes.
2. The type of termination. This implies the way that a robot moves from one point to another. For instance, CNT100 means that the robot will come as close as it can to the point while maintaining 100% of its speed. The accuracy decreases in this way, compared to CNT0 for instance. This means the robot exactly will meet each point of the toolpath but will reduce the speed from point to point.
3. Preferred speed of the robot.

Besides these three parameters more parameters are linked to a python script, such as the type of user frame. This script generates the code that is sent to the controller of the robot.

*NOTE: the above aspects apply to a FANUC robot and are derived from the Pilot Study (part II). They are not generally applicable to any type of robot.*

### 7.3.5 SIMULATION OF ROBOTIC FABRICATION PROCESS

Figure 7.11 shows a simplified workflow of the fifth component of the Robotic Fabrication module, which is the simulation of the robotic fabrication process. The output of this component of the module is discussed hereafter.

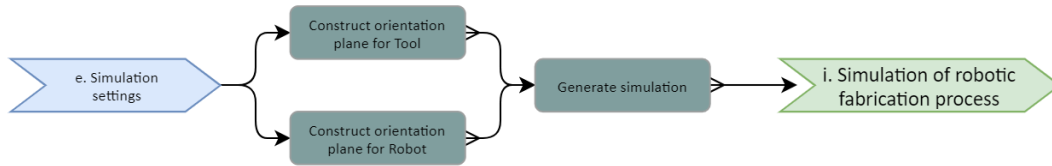


Figure 7.11: Simplified workflow of the simulation of the robotic fabrication process  
(Blue: input variables, Dark grey: processing, Green: output)

#### i. Simulation of robotic fabrication process

**Goal** To simulate the robotic fabrication process.

**Methodology** For the simulation of the robotic fabrication process, several settings are required that need to be defined by the user.

- The orientation plane for the tool.
- The orientation plane for the robot.
- The distance between the Tool Center Point (TCP) and the object. The TCP is the point on which the robot is calibrated at.
- The simulation step  $x$   $[(0 < x < 1)]$ .

Finally, the settings are processed by Rapcam. Rapcam is a plugin for Grasshopper that enables users to robotically fabricate geometries.[42]

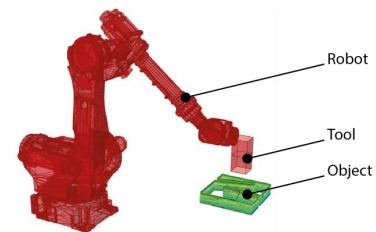


Figure 7.12: Example of a simulation of a robotic fabrication process in a parametric environment

## 7.4 RELATIONSHIPS WITH GLOBAL STRUCTURE AND JOINT DESIGN

To investigate the relationships between the Robotic Fabrication module and the Global Structure and Joint Design module, one should carefully consider the affordances and constraints of robotic fabrication for CLT. The reason theretofore is that the final product, a customized robotically fabricated CLT element, does not form any clear relation with the other modules since this is the outcome of the entire workflow. However, it is of value to investigate the affordances and constraints of the fabrication method as these imply relationships and design principles for the design of the global structure and its joints. The affordances and constraints as described below are derived from the Literature Study (part I) and Pilot Study (part II).

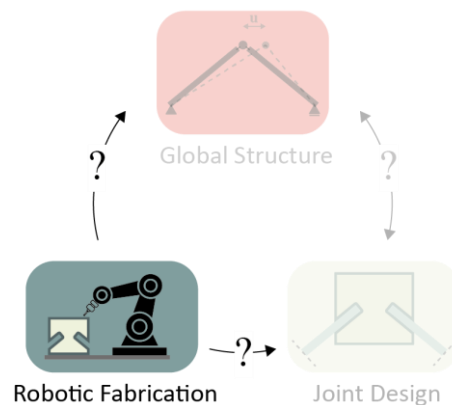




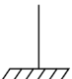
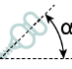






Figure 7.13: Relationships of Robotic Fabrication with the Global Structure and Joint Design

	Name	Description
Affordances	 Pinned or semi-rigid connection	From the Pilot Study (part II), it appeared that the process of robotic fabrication is suitable to produce pinned or semi-rigid connections. This implies that a global structure and its joints, designed along the integral workflow as described in this report, can either consist of a pinned or semi-rigid connection.
	 Customizations (geometry)	Robotic fabrication opens opportunities to produce customized complex three-dimensional geometries and apply (structural) optimizations between design and fabrication if desired. This enlarges the possibilities for the joint design of a CLT structure.
	 Hardness of material	CLT has a high dimensional stability due to its hardness. Therefore, complex dimensional stable geometries can be produced that serve as structural panels in a CLT structure.
	 Modular design	Modular design is possible with the use of robotic fabrication. This opens opportunities to set up a joint design that consists of certain modules, that are individually repeated or in a group.
Constraints	 No clamped connection	The accuracy of customized robotic fabrication is not high enough to fabricate CLT connection panels that form a clamped connection. Only pinned or semi-rigid connections can be included in the design of the global structure and its joints, if no additional structural provisions are made.
	 Maximum milling angle	Due to the length of the mill and the hardness of the material, the mill can only fabricate CLT connection panels while milling up to an angle of $\alpha \leq \pm 45^\circ$ . This implies a restriction for the angle of the appending CLT structures in the joint.
	 Hardness of material	The hardness of the material results in dimension stable geometry at one hand, but on the other hand this implies that it takes a longer time for a robot to mill. A lower layer height should be considered and a lower speed to acquire sufficient accuracy as well.
	 Physical dimensions	The physical dimensions of the CLT element relate to: <ul style="list-style-type: none"> <li>- The domain of robot (7m x 7m on average)</li> <li>- The dimensions of the CLT plate (16m x 3m x 0.3m)</li> </ul> This implies that CLT connection panels cannot be larger than 3m x 3m unless a non-monolithic panel is fabricated, or the domain of the robot is upgraded by means of a track or portal frame.
	 Planar elements only	CLT elements are always delivered as planar element. This is an important constraint that should be considered while setting up the design of the global structure and its joints.
	 Available tooling	The only technique of customized robotic fabrication that applies to CLT is subtraction by milling, drilling or sawing. One should carefully consider this in an early stage of the design process of a CLT structure.

Note that affordances and constraints related to assembling of elements are left out of the list as presented above since this is out of the scope of this research. The constraints are incorporated in the integral workflow. Figure 7.14 shows an overview of the relationships between the Robotic Fabrication module and the Joint Design and Global Structure module, whereas Figures 7.15-7.16 show an example of the incorporated constraint of maximum dimensions in the integral workflow. Appendix V shows the script that represents the module of Robotic Fabrication.

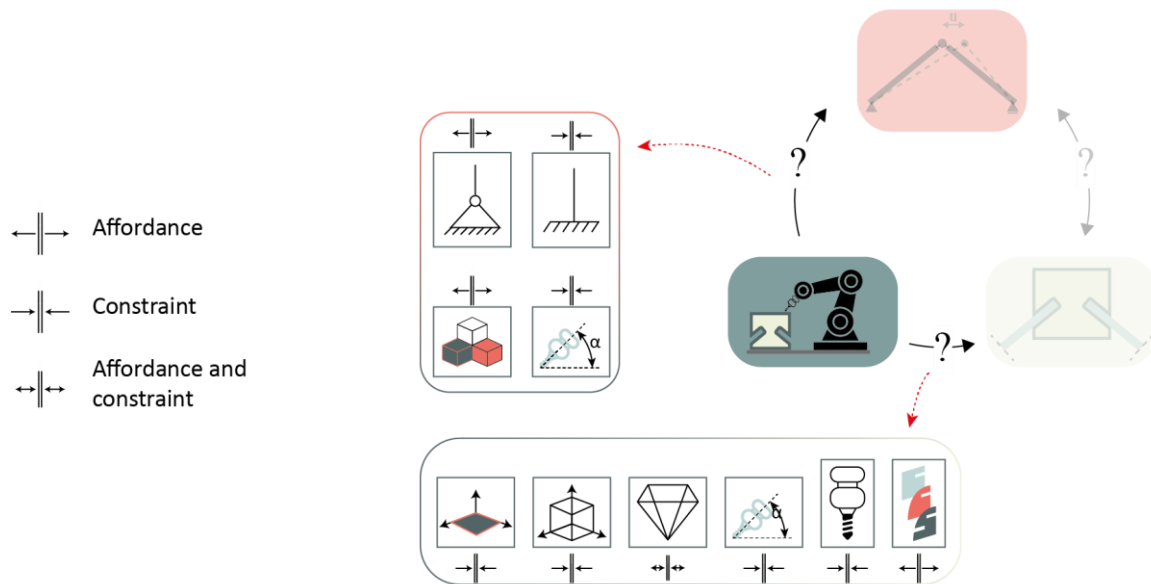


Figure 7.14: Relationships between the Robotic Fabrication module and the Global Structure and Joint Design module by means of implying affordances and constraints of robotically fabricated CLT elements

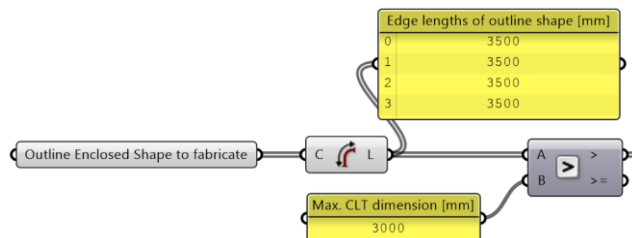


Figure 7.15: The integral workflow allows for a maximum size of a CLT connection panel to be fabricated

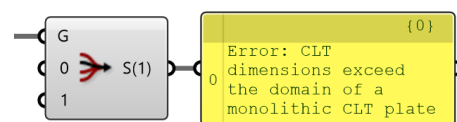


Figure 7.16: An Error is given if the maximum dimensions are exceeded

## 7.5 POTENTIAL OF THE WORKFLOW: ENTIRE WORKFLOW

This paragraph concisely shows the most important steps of the entire workflow by means of a fictive geometry that is developed along the three modules of this workflow: Global Structure, Joint Design, and Robotic Fabrication. The geometry could be a roof for instance, where the client desires a certain amount of daylight going through the roof.

### 7.5.1 GLOBAL STRUCTURE MODULE

Figure 7.17 shows the surface that is provided as input for the Global Structure. This results in the aligned FE mesh and beams that represent the connection panels as shown in Figure 7.18. The width of the joints (gap between the CLT plates) is set to 200mm.

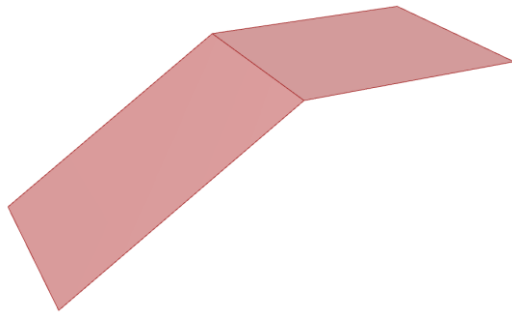


Figure 7.17: Surface as input for Global Structure

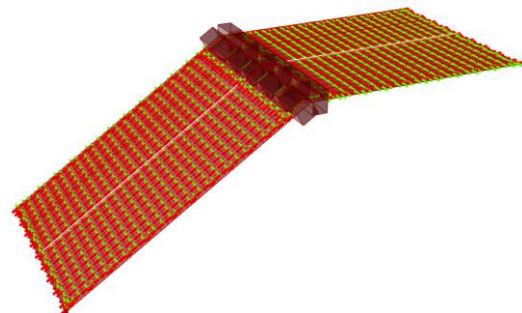


Figure 7.18: Aligned FE mesh for CLT and beams that represent the CLT connection panels

Figure 7.19 shows the results of the corresponding FEM model. The following supporting conditions and material property are applied:

- Pinned supports on the edges of the CLT plates in the y-direction
- $t_{CLT} = 140\text{mm}$  (7 x 20mm)

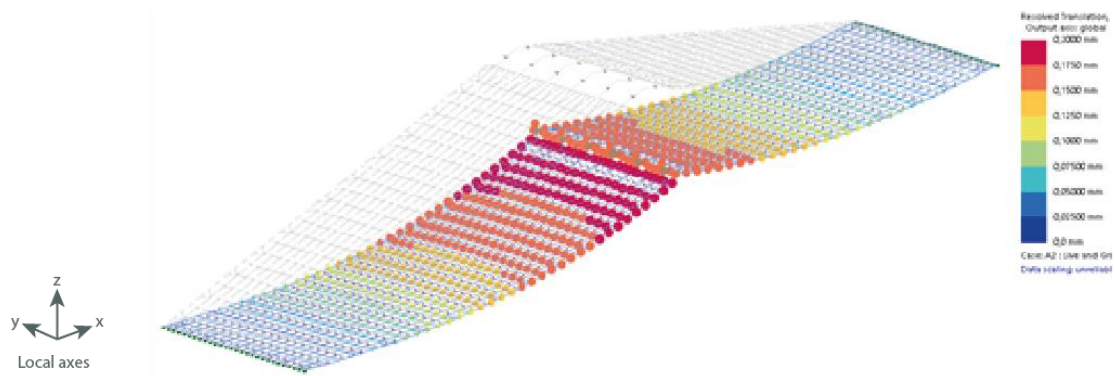


Figure 7.19: Maximum deflection of the corresponding FEM model due to variable loading (1.5kN/m) and gravity,  $u_{max} = 0.4\text{mm}$

The deflections are low due to the thick CLT plates (140mm) and the symmetrical supporting conditions. However, the deflected shape looks compelling looking at the geometry, loading and supporting conditions.



### 7.5.2 JOINT DESIGN MODULE

For the Joint Design module, the most important parameters that serve as input are derived from the Global Structure module. Figure 7.20 shows these parameters.

OUTPUT FOR JOINT DESIGN	
	{ 0 }
0	Width Joint: 200
1	Ydim,min: 800
2	Zdim,min: 300
3	Angle left: 34°
4	Angle right: 90°
5	Length pending structure left: 1803mm
6	Length pending structure right: 1500mm
7	Angle left pending structure: 180°
8	Angle right pending structure: 180°
9	Spanning distance for q: 175m

Figure 7.20: Input parameters for Joint Design, derived from Global Structure

These parameters serve as input for the generation of the joint geometry and FEM model as shown in Figures 7.21-7.22. A user can explore the geometry by the three-dimensional visualization of the joint, included in the integral workflow.

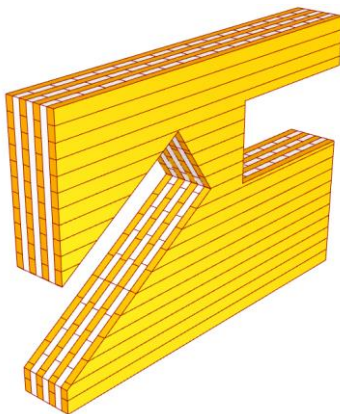


Figure 7.21: Visualized three-dimensional geometry. The non-structural wings are included in the visualization

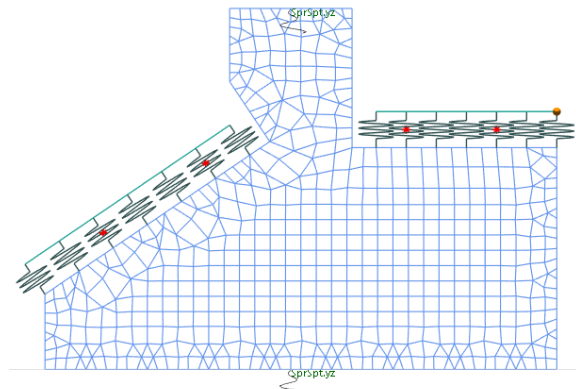


Figure 7.22: FEM of the structural part of the CLT connection panel

For the structural design, several analytical U.C.'s can be performed to get a first indication of the preliminar outline of the CLT connection panel. Beam forces from the FEM model of the global structure serve as input for the forces for the U.C.'s. Figures 7.23-7.24 show examples of this process.

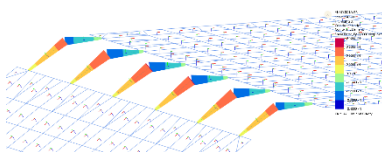


Figure 7.23: Maximum beam force from the FEM model  
 $F_{y,max} = 0.75kN$

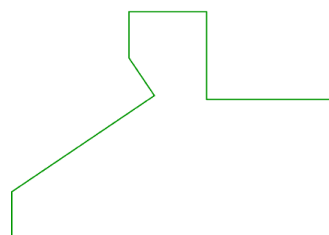


Figure 7.24: Analytical U.C. – no failure of screws or cross-sections

Also, the two-dimensional hinge, rotational spring, and fixed models of the structure can be generated by the Joint Design module. However, this is only relevant for the structural verification of the CLT connection panels and these models do not provide any physical output for the last module, which is the Robotic Fabrication module.

### 7.5.3 ROBOTIC FABRICATION MODULE

Figure 7.25 shows the relevant output this module, which is the three-dimensional BREP outline. This shape is generated as output from the Joint Design module.

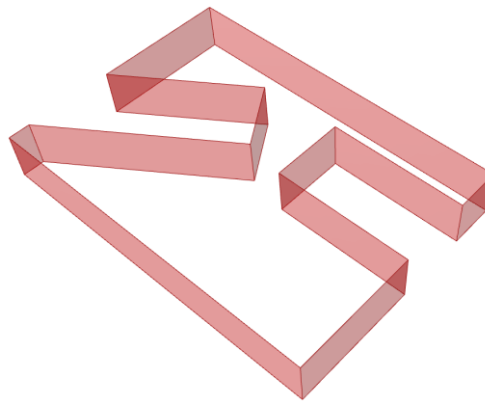


Figure 7.25: Three-dimensional outline as input for the Robotic Fabrication module

From the shape as shown above, the toolpath and robotic code can be derived. Figures 7.26-7.27 show a few steps from the generation of robotic code for fabrication.



Figure 7.26: Constructed toolpath for robotic fabrication

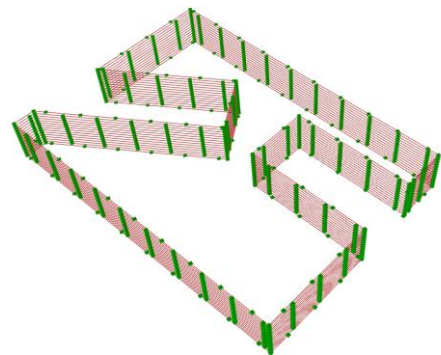


Figure 7.27: Planes for orientation that the robot can orient along. Planes are constructed on the toolpath

The shape can now be robotically fabricated by means of robotic milling. Note that different shapes and structural explorations are possible with this parametric workflow, as changes are effortlessly processed. This is demonstrated in the preceding three chapters.

## 7.6 CONCLUSION

This chapter focused on the Robotic Fabrication module of the integral workflow and answers the following question.

How can a customized CLT connection panel be robotically fabricated?

First, the parametric process is described to generate code for robotic fabrication. This is a relative linear process and only requires one input variable: the three-dimensional outline BREP from the CLT connection panel, derived from the Joint Design module. Subsequently a toolpath with corresponding orientation planes is constructed to finally generate the robotic code. For the code additional information is required, such as the speed of the robot and type of termination. The workflow of this module is based on the Pilot Study (part II) as described in Chapter 4.

After investigating the Robotic Fabrication module, several affordances and constraints were found, which are described in Chapter 7.4. The most important affordance is that with the use of robotic fabrication, many customized shapes can be produced. This increases the form-freedom and design opportunities immensely. The most prominent constraint found in this research, is that the accuracy of robotic fabrication of CLT elements is not suitable to produce clamped CLT connection panels. Besides, one must consider the maximum possible milling angle and the maximum thickness of the CLT panel that should be milled, due to the constraining length of the mill. All affordances and constraints should be considered in the earliest design stage of both the global structure and joint design.

**Further improvement.** Several improvements can be made in this module. Especially a feedback loop of the affordances and constraints would improve the quality of the workflow. Right now, several constraints are implemented already, but in a linear way. The maximum dimensions of CLT elements for instance, are incorporated in the workflow, whereas the influence of production time due to the element thickness is not included in the workflow. All these aspects should be clear as early as possible in the design process.

Another aspect that could be improved is the linearity of the workflow. Whereas the Global Structure and the Joint Design modules are linked with multiple parameters and in- and outputs, the Robotic Fabrication module is only linked with a three-dimensional outline of a CLT connection panel.

## Part IV

# Discussions

## 8. Discussions

### 8.1 ANSWER TO THE RESEARCH QUESTION

The building industry faces the challenge to contribute to a more sustainable world by reducing the nitrogen and carbon emissions. On the other hand, the building industry is on the brink of a significant change towards a 100% customized architecture. Therefore, timber and customized robotic fabrication are trending topics nowadays. The main difficulty in moving towards a customized and more sustainable building industry, lies in the uncertainty and ignorance about the design process. This is primarily caused by the application of linear workflows instead of integral ones. Integral workflows tend to relate the modules of geometry, structure, and robotic fabrication process cross-modularly, instead of relating these three modules linearly. Considering these current trends and the stated problem, this thesis intends to answer the following research question:

*What does an integral workflow for robotically fabricated customized CLT connection panels look like, that promote exploration of the structural performance of CLT structures in the preliminary design phase?*

To answer the research question, this thesis consists of a literature study, pilot study and the development of an integral workflow. The workflow consists of three modules: Global Structure, Joint Design, and Robotic Fabrication. To come to a successful exploration of the structural performance of CLT structures, one should integrate the relationships and (in)dependencies across the modules of the integral workflow. These relationships and (in)dependencies can decrease the level of uncertainty in the design process of customized CLT structures. Decreasing this uncertainty can subsequently stimulate the move towards a 100% customized and more sustainable building industry. Figure 8.1 shows the relationships and (in)dependencies as identified in this research.

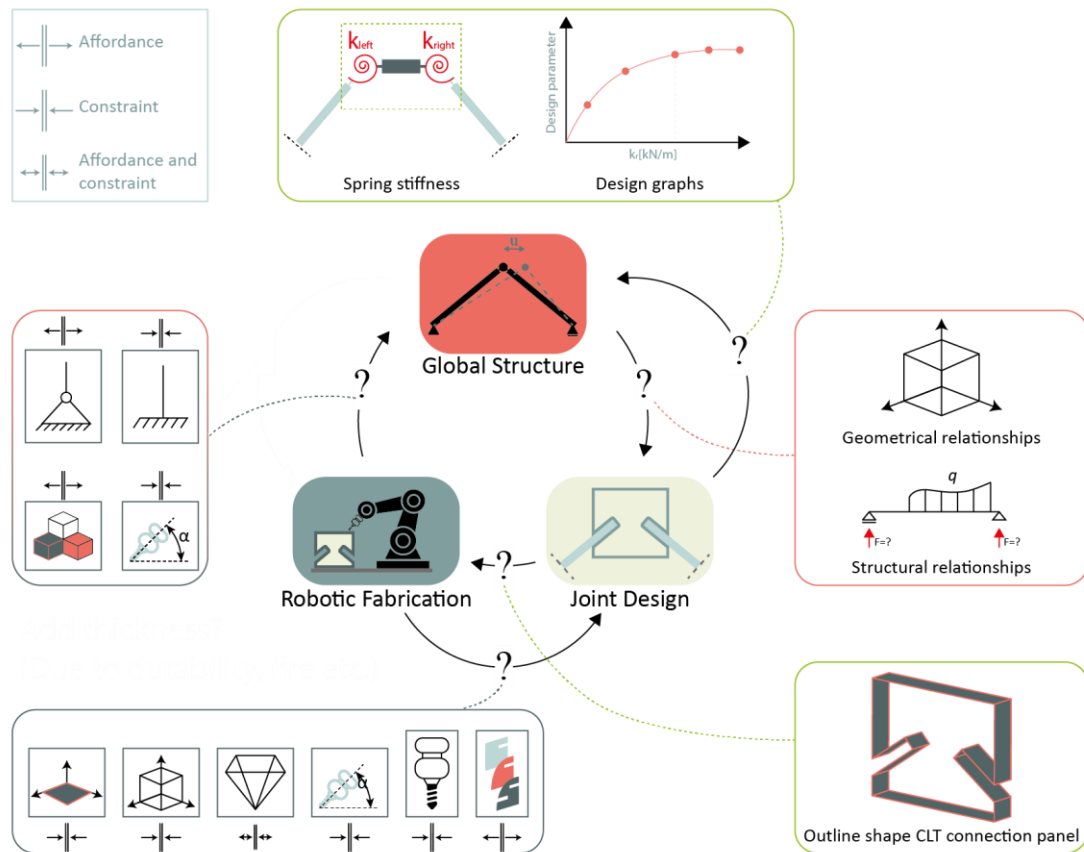


Figure 8.1: Relationships and (in)dependencies across the three modules of the integral workflow

One of the most prominent findings was that robotically fabricated CLT connection panels can hardly function as a clamped connection, without additional structural provisions beside screws. This finding influenced the development of the integral workflow significantly, as joints in structural models either had to be modelled as hinges or semi-rigid connections with a certain spring stiffness. The fact that a clamped connection is difficult to realize was mainly due to the accuracy of the robot fabrication process.

Especially the structural performance of the CLT connection panels in a CLT structure and the affordances and constraints of the applicable type of robot(ic fabrication process) can provide a designer valuable information upfront in the preliminar design phase. For instance, the thicker a CLT panel, the higher the structural performance, but the longer the production time and the more expensive the panel. All these relationships and (in)dependencies should be carefully considered in each stage of the design process.

Some of the findings are also considered in the development of the reference project as described in the motivation of this research, the bus transferium in Alblasterdam. The most prominent finding for this project, is that at this moment CLT is not suitable to apply unprotected in the outdoor environment. Additional provisions regarding shedding and/or impregnation of the timber against moisture and temperature changes must be applied.

## 8.2 CRITICAL REFLECTIONS AND DISCUSSIONS

This research situates itself as part of the broad efforts to stimulate the building industry moving towards a 100% customized more sustainable architecture. However, it is only part of the broad efforts, and does not cover every relevant aspect of an integral workflow for the design of CLT structures in the preliminar design phase. Therefore, the following section consists of critical reflections and discussions on the scope of the research, the pilot study, the development of the integral workflow, and achieved ambitions.

### 8.2.1 ON THE SCOPE OF THE RESEARCH

The scope of the research included the exploration of the structural performance of CLT structures on both a global and local level. Besides, it integrated the process of robotic fabrication in the development of the integral workflow as well.

However, as described in the introduction, within the fields of CLT and robotic fabrication the research narrows down to one type of connection, which is the customized CLT connection panel with slotted holes. The CLT plates of a structure are placed inside these slotted holes and assembled by screws. Other types of connections, such as glued or anchored connections are not investigated. The research therefore does not apply to every type of CLT structure or connection. Regarding the robotic fabrication process, the research only focusses on the technology of robotic subtraction by means of milling. It does not cover any aspect of robotic processes such as drilling, screwing or assembling. The integrality of the workflow would increase if these aspects were included in the scope of the research, whereas the design freedom and automation of the design process would improve accordingly.

Considering the critical reflections on the scope, this research situates itself as a small part of the efforts that can contribute to a 100% customized sustainable architecture. The conclusions are therefore partly narrowed down within the defined scope of the research on one hand. On the other hand, however, some conclusions are broadened up to apply them in a broader sense as well.

### 8.2.2 ON THE PILOT STUDY

During the pilot study a mock-up was produced that consisted of two plates and three unique customized connection panels. The design of the mock-up was based on the geometrical principle of the CLT connection panel as presented in this research. In this pilot study however, multiplex was applied instead of CLT. As the literature study shows, the hardness of material is one of the parameters that influences the accuracy of the robotic fabrication process. Therefore, the pilot study cannot be considered as a representative mock-up for CLT structures and explicitly serves as an exploration of the process of robotic fabrication. Besides the material applied, also the scale is not representative for commercial reference projects as the scale of the mock-up was small (1m x 1.5m x 0.4m). Finally, no structural modelling or testing was performed, which as a matter of course leaves out the integration of the robotic fabrication process with structural verification. Aside from all these drawbacks, much insight was gained in the process of robotic fabrication, which provided valuable input for the development of the workflow.

### 8.2.3 ON THE DEVELOPED WORKFLOW

**Integral workflow.** For the development of the integral workflow, three modules are integrated which are the Global Structure, Joint Design, and Robotic Fabrication. To model a CLT structure's geometry properly in according the FEM, correct modelling of the orthogonal material properties is required. One of these properties are the bending- and shear stiffnesses, which are calculated according the shear-flexible beam method, based on the Timoshenko beam theory. However, more theories are available and might result in higher stiffnesses of the orthogonal material. The reason why this theory was applied, is that it is straightforward and commonly applied among designers. Nevertheless, one should consider there are more procedures to compute the structural

orthogonal material properties of CLT. Also, a Eurocode specified on CLT will be published in the coming year or the year after.

The workflow only forms a tool for designers to explore the structural performance of CLT structures in the *preliminary* design phase. A final structural design set up along this workflow should be further verified and elaborated. However, the integral workflow provides insight in the initial structural performance of a CLT structure. The integrality however, were increased if more information about the robotic fabrication process was available upfront. Only constraints of the fabrication process related to the FANUC robot as applied in the pilot study are implemented in the workflow. Besides, the FEM models are generated in GSA whereas users may not have the availability of this software package. Therefore, the geometry and parametric models of the three modules are set up in such a way that with minor adjustments a link can be constructed to another FE software package.

As stated in the answer to the research question, focus is laid on the relationships and (in)dependencies across the three modules of the integral workflow. Therefore, the relationships, (in)dependencies and design of each module are briefly discussed hereafter.

**Global Structure.** The Global Structure module can handle the modelling of different geometries effortlessly. However, regarding the meshing of CLT plates, improvements could be made. As discussed in the fifth chapter, the Karamba3D meshing component is integrated in the workflow. However, this sometimes can result in overlapping or (too) slender mesh faces. Besides, the joints between the plates are modelled as hinges whereas they certainly should have a certain stiffness. Considering all these aspects, it is strongly recommended to not apply this module of the workflow for a final design, but explicitly to retrieve an initial understanding about the structural behavior of a CLT structure.

The relationships that flow from the Global Structure module to the Joint Design module consist of geometrical and structural relationships. The structural relationships are the forces that occur in the joints. However, a user must derive the forces from the most critical joint in the FEM models manually, whereas these also could be pulled back automatically to the parametric environment where the geometry is modelled. This would also open opportunities for structural optimization. To carry this out a quick validation was made to perform the FEA in Karamba3D. Nevertheless, this software package was not validated successfully for the modelling of CLT structures.

**Joint Design.** The Joint Design module generates the joint geometry and corresponding FEM models, based on the geometrical and structural relationships from the Global Structure module. However, these parameters still must be manually set by the user. This 'data flow' or relationship between modules could be automated to reduce the amount of human intervention while exploring a design. The output of the Joint Design module is the three-dimensional outline of a connection panel to be fabricated. This output forms the relationship with the Robotic Fabrication module and is retrieved automatically.

The main aspect of the Joint Design module that should be critically analyzed is the methodology to determine the (spring)stiffness of a joint. Once this stiffness can be determined accurately, the stiffness could be fed back to the Global Structure module and subsequently result in a more reliable structural design of the CLT structure. However, after validation with other models, no universal methodology was found to determine the accurate stiffness of joints. A designer should therefore carefully consider accuracy level he desires to derive the joint's stiffness, and hence, a feedback loop could be set up. Given this fact, one should also be careful with deriving design graphs from the FEM models of the joints. Nevertheless, they do provide clear insight in the structural performance related to several geometrical parameters.



Besides determining the stiffness of a joint, also the meshing methodology should be improved. Now, the same component is implemented as for the Global Structure module. The main difficulty of meshing joints lies in the fact that the end points of the springs need be included in the mesh as well.

**Robotic Fabrication.** The part of the integral workflow that belongs to the Robotic Fabrication module is mainly from a script of StudioRAP. Therefore, this script is not shared in this report due to confidentiality. However, the design philosophy of this module as presented in this thesis is generally applicable to other robotic fabrication processes by means of milling as well. The module is set up in a linear way and no feedback of structural performance is implemented for instance. This decreases the integrality and weakens the relationships and (in)dependencies with the other two modules.

From the Literature Study (part I) and Pilot Study (part II), several affordances and constraints are identified. It is of value to implement the constraints across all modules especially. For instance, the maximum milling angle of a robot implies a maximum angle between the appending CLT structure and the CLT connection panel. Most of the constraints are implemented in the workflow, but within each module separately and not across the three modules.

#### *8.2.4 ON THE ACHIEVED AND UNACHIEVED AMBITIONS*

**Achieved ambitions.** A successful integral workflow was developed that enables users to explore the structural performance of CLT structures in the preliminary design phase. The relationships and (in)dependencies are analyzed clearly and implemented in the workflow. The workflow can also provide a user quick insight in the influence of geometrical parameters on the structural performance of the structure or its joints. However, ...

**Unachieved ambitions.** The ambition at the beginning of the research was to setup a (structural) design for the bus transferium in Alblasterdam. This simply was not feasible at this moment, since CLT is proved to be unsuitable to be applied unprotected in an outdoor environment. Besides, the workflow is not validated by means of a case-study. Beforehand, it was intended to build a mock-up of a CLT structure along the developed workflow. Also, no optimization is implemented which would increase the integrality of the workflow. Finally, the CLT connection panels are not structurally tested to verify their stiffness. The possible implementation of these aspects should be considered if applying or using the integral workflow as developed in this thesis.

## 8.3 CONCLUSIONS

As described in the introduction, this research narrows down to a specific type of connection in CLT structures and to the robotic fabrication process of milling. Therefore, the conclusions are divided in three parts: conclusions on CLT structures and CLT connection panels, conclusions on robotic milling of CLT connection panels, and conclusions on the integral design process of robotically fabricated CLT elements. Each part is subdivided in conclusions specifically related to this research, and conclusions that apply in a broader sense.

### 8.3.1 ON CLT STRUCTURES AND CLT CONNECTION PANELS

#### 8.3.1.1 Research Specific Conclusions on CLT Connection Panels

- Without additional structural provisions besides screws, a *clamped connection is hardly feasible* with the application of CLT connection panels. Therefore, one should carefully look at the design of a cantilevering structure connected to these type of panels, by means of a roof for instance.

#### 8.3.1.2 On CLT Structures in general

- Along the reference project of the bus transferium, this research shows that it is *not common to apply CLT unprotected* in the outdoor environment. After contacting several CLT manufacturers across Europe, it turned out that the CLT market does not deliver CLT for this purpose at this moment.
- If one wants to apply CLT that is visible in the outdoor environment, *impregnating the CLT* is required. However, there is large risk on damaging the impregnation layer due to planing in the post-processing of the material production.
- Extra attention should be paid to the design of a *moisture- and temperature control system* for a CLT structure.

### 8.3.2 ON ROBOTIC MILLING OF CLT CONNECTION PANELS

#### 8.3.2.1 Conclusions on the Robotic Milling of CLT Connection Panels

- The accuracy of customized robotic milling is insufficient to produce *clamped CLT connection panels* without additional structural provisions besides screws.

#### 8.3.2.2 Conclusions on Robotic Milling in general

- The *physical affordances and constraints* of the fabrication process must be considered as early as possible in the design process. An important governing constraint of robotic milling is the maximum milling angle that the robot allows for.
- In general, the *maximum dimensions* of *monolithic CLT elements* that allow for robotic milling, are 3m x 3m x 0.3m. This is related to the domain of the robot and the maximum dimensions of CLT elements produced by manufacturers.
- Only *planar elements* can be produced by robotic milling. To produce curved elements, the production process should start from scratch and the lumbers should be bend individually.
- The main *advantage of robotic milling by a 6-axis robot* compared to CNC machines or 3-axis robots, is the affordance to produce different customized elements instead of mass produced batches of elements. This opens opportunities to modular designs and increases the form-freedom of designs.
- The accuracy of robotic milling is determined by several factors. Important ones that are found in this research are the speed of the robot, the type of termination, the material, and the scale of the object and robot.

### 8.3.3 ON THE INTEGRAL DESIGN PROCESS OF ROBOTICALLY FABRICATED CLT ELEMENTS

#### 8.3.3.1 Qualitative conclusions on the developed workflow

- The integral workflow is developed successfully in sense of that it forms a tool that enables users to *quickly explore* the structural performance of a CLT structure on a global and local level. FEM models are effortlessly generated, and the computation time is low for both generation of the geometry and FEM calculations (<1.5sec.).
- The integral workflow consists of three different modules, which each consist of associated components. Each component or module is separately applicable as well, to increase the modularity of the integral workflow. For instance, if one only needs to translate the bending stiffnesses of CLT for the FEM, only the variables or input of this component are required to compute these stiffnesses. This modelling approach of the integral workflow increases the *applicability among users* based on their specific request. Users are supposed to have knowledge about Grasshopper and Finite Element modelling.
- Between modules human intervention is required. Even though the number of steps of intervention could be decreased, this should never be reduced to zero human intervention. This, to *avoid* the concept of a 'black-box', where a user cannot trace of how modelling or computations are performed. The workflow is therefore setup transparently to increase the applicability and opens opportunities to other developers to increase the quality of it.

#### **Global Structure module**

- This module of the integral workflow can process a wide variety of geometries and construct the FEM models of the corresponding CLT structures. For instance, one-dimensional folded geometries, two-dimensional folded geometries, and pyramidal folded geometries. But also, randomly oriented geometries are handled by the workflow effortlessly.
- Geometrical and Structural relationships are derived from the Global Structure module that serve as input for the Joint Design module.

#### **Joint Design module**

- Visualizations are generated to give the user insight in the three-dimensional shape of a CTL connection panel.
- The tool that performs the analytical Unity Check's gives the user a reliable initial outline of a CLT connection panel for the structural design.
- From a higher level, the workflow allows for a feedback loop to feed the (spring) stiffness of the joints from the Joint Design back to the Global Structure module. However, no universal methodology is found in this research that determines the stiffness accurately. Several methodologies with different accuracies were tested to determine the stiffness of the joints. Therefore, a designer should ensure one is confident with the accuracy of the applicable methodology. No 100% accurate universal methodology was achieved, which is due to the large size of the panels (> 0.5m x 0.5m) and the orthotropic material properties.
- The three-dimensional outline of a CLT connection panel generated in the Joint Design strongly influences the robotic fabrication process.

#### **Robotic Fabrication module**

- The G- code to produce a CLT connection panel is generated successfully.
- The main relationships from Robotic Fabrication to the other modules of the integral workflow are the affordances and constraints of the fabrication process. These should be carefully considered when

applying the process of customized robotic fabrication on a commercial project. The previous section of this paragraph describes the conclusions regarding these affordances and constraints more into depth.

#### *8.3.3.2 Quantitative conclusions on the developed workflow*

- The computation of the shear- and bending stiffnesses according the shear-flexible beam method is validated successfully.
- The FEM modelling of the joints is validated successfully by a developed tool that performs analytical Unity Check's, based on the applicable codes for CLT structures.
- Design graphs that describe the influence of geometrical parameters of a CLT structure and/or a CLT connection panel on the structural performance of it are derived effortlessly.

#### *8.3.3.3 On an Integral Design Process in general*

- Regardless the geometrical specifications of a project, the affordances and constraints of the robotic fabrication process should be considered for both the global and local preliminar structural design.
- To transform a design process from a linear to an integral process, special attention must be laid on the relationships and (in)dependencies between different modules/stages of the design process.

## 8.4 RECOMMENDATIONS AND FURTHER INVESTIGATIONS

As described in the critical reflections on this thesis, there are several fields of the research that could be investigated or elaborated more into depth.

- The integral workflow is build up in a way that it is suitable for the implementation of a User Interface (UI). This would increase the user-friendliness as well as it consists of three plain Grasshopper scripts now. The UI could be modelled by means of Human UI for instance, a plugin for Grasshopper.
- Optimization could be implemented in the integral workflow, which would increase the quality and integrity of the workflow. For instance, in case of designing a roof of CLT plates, one could optimize toward the optimal size of openings between CLT plates, as these openings influence the amount daylight that comes through the roof. The workflow is setup in a way that it is suitable to perform optimization on designs towards different variables and parameters.
- Right now, the market does not provide any type of CLT that can be applied visibly in the outdoor environment. The reason behind this is that the main demand on CLT flows from residential projects. However, in future the demand to apply CLT in the outdoor environment could rise. An example of this is the project of the bus transferium in Alblasterdam. Therefore, performing investigation on the application of impregnated CLT in the outdoor environment is recommended. Part of the project of the bus transferium could serve as a test-case by monitoring the material behavior of CLT applied outdoor. This data could be used to further utilize the application of impregnated CLT in the outdoor environment.
- The integral workflow is not validated by means of a mock-up study. A validation like this would increase the reliability significantly, as well as the identification of bugs and errors that still might be present in the current workflow.
- During this thesis, no universal methodology was found to determine the (spring) stiffness of the joints with full accuracy. The most accurate methodology as proposed in this thesis however, can be utilized to derive design graphs of influential geometrical parameters on the structural performance of the joints. Nevertheless, if the (spring) stiffness of the joints can be accurately determined, this stiffness could be fed back to the Global Structure module. Therefore, it is recommended to investigate this aspect of the research further into depth.
- Now, the integral workflow does not contain feedback loops across the three modules. For instance, the influence of the milling angle on the structural performance of the screws could be derived from a feedback loop between the Joint Design and Robotic Fabrication module. Further investigation in feedback loops like this will certainly increase the integrity, quality, and reliability of the workflow.
- This thesis left out of scope robotic screwing and assembling of CLT connection panels. However, to elaborate on, and broaden the automation and customization of the design process, these aspects should be investigated further into depth.

## Bibliography

- [1] Aanpak Stikstof. [Online]. 2020. Available from: <https://www.aanpakstikstof.nl/> [Accessed February 10, 2020]
- [2] Cobouw, Annexum. “*Revolutionaire bouwers dolblij met stikstof: ‘Dit kan weleens dé motor van verandering zijn’*” [Online]. 2020. Available from: <https://www.annexum.nl/nieuws-uit-de-markt/revolutionaire-bouwers-dolblij-met-stikstof-dit-kan-weleens-de-motor-van-verandering-zijn/> [Accessed February 9, 2020]
- [3] Faulstick B., Drexel University, “Q+A: *WHY WOOD CONSTRUCTION IS MAKING A COMEBACK*” [Online].; 2019. Available from: <https://newsblog.drexel.edu/2019/01/16/qa-why-wood-construction-is-making-a-comeback/> [Accessed October 5, 2019]
- [4] Mlvander., NC State University, “*CLT: The Future of Residential Timber Construction*”. [Online]. 2019. Available from: <https://cnr.ncsu.edu/fb/news/2019/12/clt-the-future-of-residential-timber-construction/> [Accessed October 7, 2019]
- [5] Spikker L. *Transferium Alblaserdam*. Structuurontwerp Procesdocument. 2019
- [6] Tamke M, Thomsen MR. *Digital Wood Craft*. CAAD Futur. 2009;673–686 p.
- [7] Pasetti Monizza G, Bendetti C, Matt DT. *Parametric and Generative Design techniques in mass-production environments as effective enablers of Industry 4.0 approaches in the Building Industry*. Autom Constr [Online]. 2018;92(June 2017):270–85. Available from: <https://doi.org/10.1016/j.autcon.2018.02.027>
- [8] Naboni R, Paoletti I. *Advanced Customization in Architectural Design and Construction*. 2015. 153–159 p.
- [9] Leveté A., The Plan, “*The Timber Wave*”. [Online]. 2013. Available from: <https://www.theplan.it/eng/webzine/wood-in-architecture/the-timber-wave-wood-en> [Accessed September, 2019]
- [10] Eversmann P, Gramazio F, Kohler M. *Robotic prefabrication of timber structures: towards automated large-scale spatial assembly*. Constr Robot. 2017;1(1–4):49–60.
- [11] Krieg OD, Bechert S, Groenewolt A, Horn R, Knippers J, Menges A. *Affordances of Complexity: Evaluation of a Robotic Production Process for Segmented Timber Shell Structures*. Proc 2018 World Conf Timber Eng. 2018;1–8.
- [12] Bidgoli A. *Towards an integrated design-making approach in architectural robotics*. 2016. 102p.
- [13] Reinhardt D. *Robotic Fabrication in Architecture, Art and Design*. 2016. 190–203 p.
- [14] Gengnagel, C., Kilian, A., Palz, N., Scheurer F. *Computational Design Modelling*. 2011. 239–248 p.
- [15] Blomgren H-E. *Structural Guidance Note. The use of cross-laminated timber, particularly in North America: an introduction*. 2012;29.
- [16] NEN-EN 16351. *Timber structures – Cross laminated timber – requirements*. 1st ed. Delft. NEN; 2015.
- [17] Gagnon S, Pirvu C. *Hand book cross laminated timber Canada*. 2011. 626 p., §2.5.
- [18] Wallner-Novak M, Koppelhuber J, Pock K. *Cross-Laminated Timber Structural Design*. 2014. 191 p.
- [19] Bianconi F, Filippucci M. *Digital Wood Design* [Online]. 2018. Available from: <http://www.springer.com/series/15087>.
- [20] NEN-EN 1995-1-1. *Eurocode 5: Design of timber structures – Part 1-1: General – Common rules and rules for buildings*. NEN; 2005.

- [21] Öberg J, Wiege E. *Moisture risks with CLT-panels subjected to outdoor climate during construction-focus on mould and wetting processes - Fuktrisker på KL-trä som utsätts för yttre klimat under produktion-fokus på mögel och uppfuktning*. 2018; 84p. Available from: <http://www.diva-portal.org/smash/get/diva2:1222631/FULLTEXT01.pdf>
- [22] Scheffer, T.C. and J.J. Morrell. *NATURAL DURABILITY OF WOOD: A WORLDWIDE CHECKLIST OF SPECIES*. Forest Research Laboratory, Oregon State University. 1993. Research Contribution 22. 58p.
- [23] Graham Finch G, Morris P, Rickets D, Thivierge C, Wang J. FPIInnovations. "*Design for Durability: Cross-Laminated Timber (CLT) Construction*". [Online]. 2018. Available from: <http://www.woodusematrix.com/database/rte/files/CLT-Durability%20by%20Design.pdf> [Accessed November 4, 2019].
- [24] Technical guideline for Europe. *Fire safety in timber buildings* [Online]. The Structural Engineer. 2013. 139 p. Available from: [https://eurocodes.jrc.ec.europa.eu/doc/Fire\\_Timber\\_Ch\\_5-7.pdf](https://eurocodes.jrc.ec.europa.eu/doc/Fire_Timber_Ch_5-7.pdf) [Accessed November, 2019].
- [25] Foreco houtproducten, Safewood. [Online]. 2019. Available from: <https://www.foreco.nl/nl/producten/safewood> [Accessed February, 2020].
- [26] Processing-Wood, German Engineering. "*Production processes*". [Online]. 2018. Available from: <https://processing-wood.com/processes/clt/process/steps/> [Accessed September, 2019].
- [27] Sandhaas C. *Timber Engineering - Principles for design*. Karlsruhe. 2017. Scientific Publishing. 658p.
- [28] Multicomfort, SES. "*CLTHouses*". [Online]. 2013. Available from: <https://www.sesagbasel.com/en/prefabricated-houses/technology/> [Accessed October 2, 2019].
- [29] Lever Architecture. "*What is cross-laminated timber*". [Online]. 2017. Available from: [https://leverarchitecture.com/research/what\\_is\\_crosslaminated\\_timber](https://leverarchitecture.com/research/what_is_crosslaminated_timber) [Accessed October 2, 2019].
- [30] NEN-EN 1991-1-1. *Eurocode 1: Belastingen op constructies - Deel 1-1: Algemene belastingen - Volumieke gewichten, eigengewicht en opgelegde belastingen voor gebouwen*. NEN; 2002.
- [31] Buck D, Wang XA, Hagman O, Gustafsson A. *Bending properties of Cross Laminated Timber (CLT) with a 45° alternating layer configuration*. BioResources. 2016;11(2):4633–4644.
- [32] Schwartz T, Bard J, Ganon M, Jacobson-weaver Z, Jeffers M, Tursky R. *Robotic Fabrication in Architecture, Art and Design* [Internet]. Robotic Fabrication in Architecture, Art and Design 2014. 2014. 67-82,373-380 p. Available from: <http://link.springer.com/10.1007/978-3-319-26378-6>. DOI: <https://doi.org/10.1007/978-3-319-26378-6>
- [33] Alison Brooks Architects Ltd. "*The Smile London*" [Online]. 2016. Available from: <http://www.alisonbrooksarchitects.com/project/the-smile>. [Accessed October 2019].
- [34] Rothoblaas. "*Fastening-Brackets and Plates*". [Online]. 2019. Available from: <https://www.rothoblaas.com/products/fastening/brackets-and-plates> [Accessed February 27, 2020]
- [35] Williams B. *An Introduction to Robotics in Catalonia*. Catalònia. 2019. 43p.
- [36] Tamke M, Riiber J, Jungjohann H. *Generated Lamella*. Acadia. 2010;340–347p.
- [37] Wit S De. *Parametric Segmental Timber Shell Structures Combining form-finding with structural analysis and digital fabrication*. 2017. 136p.
- [38] KUKA. "*The KUKA smartPAD: simply more freedom*". [Online]. Available from: <https://www.kuka.com/en-de/products/robot-systems/robot-controllers/smartpad> [Accessed October 2019].
- [39] IRB 4400. ABB. "*IRB-4400*" [Online]. 2019. Available from: <https://new.abb.com/products/robotics/industrial-robots/irb-4400> [Accessed October 2019].

- [40] FANUC. "Large Robot R-200iC". [Online]. Available from: [https://www.fanuc.co.jp/en/product/robot/f\\_r\\_large.html](https://www.fanuc.co.jp/en/product/robot/f_r_large.html). [Accessed October 2019].
- [41] KUKA|prc. Association for Robots in Architecture. "MAKING ROBOTS ACCESSIBLE TO THE CREATIVE INDUSTRY" [Online]. 2015. Available from: <https://www.robotsinarchitecture.org/kuka-prc>
- [42] RAP Technologies. [Online]. 2019. Available from: <https://www.raptech.io/rapcam> [Accessed February 2020].
- [43] PyPi. "RoboDK". [Online]. 2020. Available from: <https://pypi.org/project/robodk/> [Accessed March 2020].
- [44] Estrella GP. *Robotics in Architecture: Potential applications and current limitations*. 2010.
- [45] Hein T. "Robotic systems integration presses forward with Parliament Hill". [Online]. 2015. Available from: <https://www.automationmag.com/canadian-can-do-5477/> [Accessed September 2019].
- [46] O'Neal B. "Silky Concrete Project: Massive Concrete Installation Built by KUKA" [Online]. 2015. Available from: <https://3dprint.com/80490/silky-concrete-project/> [Accessed September 2019]
- [47] KUKA, YouTube. "KUKA Robots for the Welding Industry". [Online]. 2014. Available from: <https://www.youtube.com/watch?v=NJlgQjKDVUg> [Accessed October 2019].
- [48] Zwaluw. CeBIT. "KUKA robotic arm draws portrait". [Online]. 2012. Available from: <https://www.youtube.com/watch?v=Wi0CsWGDnNU> [Accessed October 2019].
- [49] KUKA. "Automatic bending of sheet metal with a KUKA robot". [Online]. 2010. Available from: <https://www.youtube.com/watch?v=Nrea-6JYXmM> [Accessed October 2019].
- [50] ABB Robotics Products AB. *RAPID Reference Manual*. 2011;759p.
- [51] ABB. "Controllers". [Online]. Available from: <https://new.abb.com/products/robotics/controllers> [Accessed October 2019].
- [52] FANUC. "General Catalog". [Online]. Available from: [https://www.fanuc.co.jp/en/product/catalog/pdf/robot/Roboti\(E\)-34.pdf](https://www.fanuc.co.jp/en/product/catalog/pdf/robot/Roboti(E)-34.pdf) [Accessed October 2019].
- [53] KUKA. "Industrial Robots from KUKA" [Online]. 2019. Available from: <https://www.kuka.com/en-be/products/robotics-systems/industrial-robots>. [Accessed September 2019].
- [54] ETHZurich, ETH Zurich ITA Institute of Technology in Architecture. "Robotic Fabrication Laboratory". [Online]. 2016. Available from: <https://ita.arch.ethz.ch/archteclab/rfl.html> [Accessed October 2019].
- [55] Arch20. "Robotization of BIM : How Robots Could Improve BIM Workflow". [Online]. 2019. Available from: <https://www.arch2o.com/robotization-bim-robots-improve-bim-workflow/> [Accessed October 2019].
- [56] Liu B, Zhang F, Qu X. *A method for improving the pose accuracy of a robot manipulator based on multi-sensor combined measurement and data fusion*. Sensors (Switzerland). 2015;15(4):7933–7952p
- [57] Breaz RE, Bologa OC, Racz GS, Oleksik VS, Gîrjob C. *Simulation approach for improving CNC milling machines accuracy for single axis motion*. IEEE Int Symp Ind Electron. 2010;1760–1764p.
- [58] Menges A. *Morphospaces of Robotic Fabrication*. Rob | Arch 2012. 2013;28–47p.
- [59] Krieg D, Menges A, Fleischmann M, Robeller C. University of Stuttgart. "Material systems". [Online]. 2009. Available from: <https://icd.uni-stuttgart.de/?p=3129> [Accessed October 2019].
- [60] Willmann J, Block P, Hutter M, Byrne K, Schork T. *Robotic Fabrication in Architecture, Art and Design 2018*. 2018;406–420p. DOI: <https://doi.org/10.1007/978-3-319-92294-2>
- [61] D'Acunto P, Kotnik T. *AA/ETH Pavilion*. Proc Tensinet Symp 2013. 2013;1–10p.



- [62] Vasey L, Grossman T, Kerrick H, Nagy D. *The hive: A human and robot collaborative building process*. SIGGRAPH 2016 - ACM SIGGRAPH 2016 Talks [Internet]. 2016;1–2p. Available from: <https://www.scopus.com/inward/record.uri?eid=2-s2.0-84986237635&partnerID=40&md5=a6c35010ab90170ee1a6bf0e90e89b1e>
- [63] Menges A, Achimmenges.net. “*Urbach Tower*”. [Online]. 2019. Available from: <http://www.achimmenges.net/?p=21454> [Accessed on October 2019].
- [64] StudioRAP. “*Skilledin Office*”. [Online]. 2015. Available from: <http://studiorap.nl/#/skilledin> [Accessed October 2019].
- [65] Abeysekera I, ARUP. *Modelling CLT for dynamics*. 2018;1-4 p.
- [66] Rothoblaas. “*VGS Fully threaded screw with countersunk or hexagonal head*”. [Online]. 2020. Available from: <https://www.rothoblaas.com/products/fastening/screws/screws-structures/vgs> [Accessed February 2020].
- [67] Gijzen RPT. *Modular cross-laminated timber buildings*. 2017; Available from: <https://repository.tudelft.nl/islandora/object/uuid%3Af687e2cc-86e1-442e-862a-2ceb382f7157>

# Appendices

## Appendix A. Determining $s_0$

$S_0$  for CLT with three layers [24]:

Exposure on	Floors		Walls	
	unprotected	protected <sup>a</sup>	unprotected	protected <sup>a</sup>
Tension side	$\frac{h}{30} + 3,7$ (6.33)	10	— <sup>b</sup>	— <sup>b</sup>
Compression side	$\frac{h}{25} + 4,5$ (6.34)	$\min \begin{cases} 13,5 \\ \frac{h}{12,5} + 7 \end{cases}$ (6.35)	$\frac{h}{12,5} + 3,95$ (6.36)	$\min \begin{cases} 14,5 \\ \frac{h}{12,5} + 7 \end{cases}$ (6.37)

$S_0$  for CLT with five layers [24]:

Exposure on	Floors		Walls	
	unprotected	protected <sup>a</sup>	unprotected	protected <sup>a</sup>
Tension side	$\frac{h}{100} + 10$ (6.38)	For $75 \text{ mm} \leq h \leq 100 \text{ mm}$ : $-\frac{h}{4} + 34$ (6.39) For $h > 100 \text{ mm}$ : $\frac{h}{35} + 6$ (6.40)	— <sup>b</sup>	— <sup>b</sup>
Compression side	$\frac{h}{20} + 11$ (6.41)	18	$\frac{h}{15} + 10,5$ (6.42)	20

$S_0$  for CLT with seven layers [24]:

Exposure on	Floors		Walls	
	unprotected	protected <sup>a</sup>	unprotected	protected <sup>a</sup>
Tension side	For $105 \text{ mm} \leq h \leq 175 \text{ mm}$ : $\frac{h}{6} + 2,5$ (6.43) For $h > 175 \text{ mm}$ : 10	As unprotected	— <sup>b</sup>	— <sup>b</sup>
Compression side	For $105 \text{ mm} \leq h \leq 175 \text{ mm}$ : $\frac{h}{6} + 2,5$ (6.44) For $h > 175 \text{ mm}$ : 13	As unprotected	For $105 \text{ mm} \leq h \leq 175 \text{ mm}$ : $\frac{h}{6} + 4$ (6.45) For $h > 175 \text{ mm}$ : 16	As unprotected

## Appendix B. Bending- and Shear Stiffnesses of CLT

The bending- and shear stiffness according the shear-flexible beam method can be determined according Formulas (1)-(4) [18]

$$(EI)_{ef,0} = \sum_{i=1}^n E_{0,i} * \frac{b * d_{0,i}^3}{12} + \sum_{i=1}^n E_{0,i} * b * d_{0,i} * a_{0,i}^2$$

*Strong direction;0* +

$$\sum_{i=1}^n E_{90,i} * \frac{b * d_{90,i}^3}{12} + \sum_{i=1}^n E_{90,i} * b * d_{90,i} * a_{90,i}^2$$

$$(EI)_{ef,90} = \sum_{i=1}^n E_{90,i} * \frac{b * d_{0,i}^3}{12} + \sum_{i=1}^n E_{90,i} * b * d_{0,i} * a_{0,i}^2$$

*Weak direction;90* +

$$\sum_{i=1}^n E_{0,i} * \frac{b * d_{90,i}^3}{12} + \sum_{i=1}^n E_{0,i} * b * d_{90,i} * a_{90,i}^2$$

$$(GA_s)_{ef,0} = \kappa \left( \sum_{i=1}^n G_{0,i} * b * d_{0,i} + \sum_{i=1}^n G_{90,i} * b * d_{90,i} \right)$$

*Strong direction;0*

$$(GA_s)_{ef,90} = \kappa \left( \sum_{i=1}^n G_{90,i} * b * d_{0,i} + \sum_{i=1}^n G_{0,i} * b * d_{90,i} \right)$$

*Weak direction;90*

For the  $\kappa$ -factor the value depends on the number of layers:

1 layer	3 layers	5 layers	7 layers	9 layers
<i>Of equal thickness</i>				
$\kappa = 0.83$ (5/6)	$\kappa = 0.21$	$\kappa = 0.24$	$\kappa = 0.26$	$\kappa = 0.27$

The difference between the strong- and weak direction lies in the E- and G-moduli that are applied to each layer. Below this is schematically visualized.

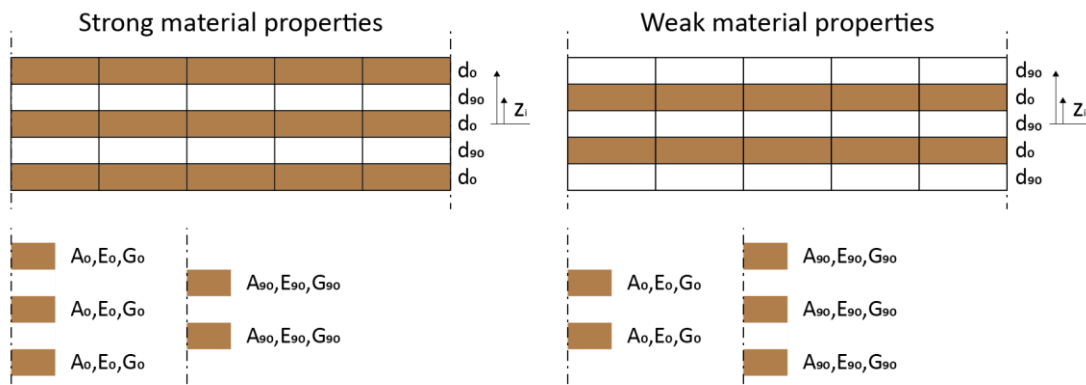


Figure A.1: Relevant properties to compute shear- and bending stiffnesses in strong and weak direction for CLT

## Appendix C. Overview of Robotic Fabrication Purposes

TECHNIQUE	SUB-CATEGORY	MATERIAL	NEEDED TOOL	ADVANTAGES	DEAD/VANTAGES
SUBTRACTIVE	Milling	Foam, Wood, Metal	Milling motor, Milling Tool, Milling grip, tool changer (optional)	Accurate, works for wide range of forms, generate fine details	Slow, need of tool change, needs lubrication and cooling, produce dust
	Hot wire cutting	Foam	Wire frame and wire, Power supply	Fast, silent, leftovers of material is still usable, almost clean while working.	Only works with special forms, may make toxic fumes
	Saw Wire Cut	Stone, wood	Diamond wire saw, saw frame, lubricant pump, water pump	Fast, in some cases, leftovers of materials are still useable	Needs much lubrication and cooling, produce dust
ADDITIVE	3D Print	ABS, Plastic, Clay, Resin	Nuzzle, Nuzzle		
	Pouring		Pouring guide		
	Components Merging Materials	Glass, Wax, Ice	Heater, Hot air blower	Useful when using components that can get together by melting down partially	Hard to control, mostly used as a kind of welding
JOINING	Real Time Casting	Resin, Clay	Nuzzle, Drier, Injector	Create some types of free forms in 3D	Mostly works by adding thin lines of material, takes too long when making complex volumes, hard to calculate the final relaxed form and deformation after pouring material.
	Welding	Metal	Welding Torch or Welding Arc	For connecting metal objects in point or lines	Needs one or two other robots to keep the connecting objects in place
	Gluing	Plastic, Wood	Gluing Nuzzle		
FORMING PROCESS	Bending	Metal bars	CNC Bending tool, or heavy bending frame and strong robotic arm, Welding Torch or Arc	Best for making wire frame 3D forms	Needs a heavy collaboration among a team of robots, cnc machines, and users
	Wood Bending	Plywood	Heavy Gripper, heavy frames or holders	For steam bending of plywood	Very hard to calculate final form of every element
	Punching	Metal	Incremental Forming tool, electric hammer machine	For accurate forming of metal sheets	Loud noise and super slow procedure
	Forming	Metal, Clay	Pressing surfaces, pressing niddle		
	Pressing and pulling	Metal, Clay			
	Defining	Ceramic	Die Cast, Die blades	Good for free form making by resembling human hand form making, good for folding in different direction and angles based upon die cut lines	
	Die Cutting	Metal sheets, Paper Metal, Plastic, Paper	Die Cast, Die blades		
GENERATIVE	Melting	Brick, component-based objects, metal, ...	Gripper (Mechanical, Pneumatic, Vacuum...)	Generate forms from available or costume made component, very use for large scale projects, can be combined with welding, gluing etc. to put them in their exact position	Limited to specific type of form and setup
	Assembling			Can be connected to computer vision and AI	
	Air Pump spray	Ink and Spray	Nuzzle	For making drawings from available or generated graphic, especially in monochrome	Not very accurate, need protection for the robot itself
	Drawing	Ink	Brush, Ink Dropper, Ink batch	For making graphic patterns	Somehow out of control
	Brush	Ink	Brush, Ink batch	For drawing different graphics	Needs changing the brush and cleaning
	Still Image	-	Camera (DSLR), module	For taking pictures in exact position and exact time specially for stop motion and HDRI and merged pic	
	Video	-	Camera (DSLR), module	For generating super accurate movement in the video	
Visualization	Long Exposure and Moving Subject	-	Camera (DSLR), control module	For making an image of moving object like glowing ones, making stop motions and ...	
	Weaving	Rope, Textile, Fabric, Carbon Fiber	Gripper, Camera		

[12]

## Appendix D. Description of the Program of a Robotic System

The first step to let a robot perform a certain program, is to write instructions. This paragraph briefly explains the programming principles for setting up these instructions.

### D.1 INSTRUCTIONS IN GENERAL

On the smallest element level of a program, there are the instructions. Instructions tell the robot *what* to do. They consist of certain arguments. There are two types of instructions: various and general. An example of an instruction is shown below. TPWrite writes text on the controller display. Behind the TPWrite instruction, the arguments are set which complete the instruction.

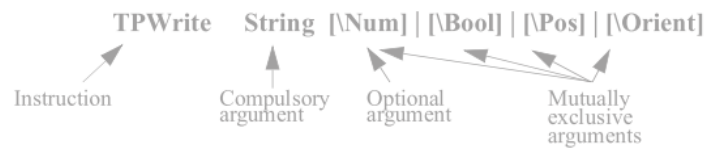


Figure D.1: Arguments of an instruction [50]

#### D.1.1 Instructions for motion

To define the motion of the robot, several motion settings and characteristics are required as arguments to complete the motion instructions. Once these are programmed, the software automatically calculates the final motion from one point to another. A few important motion characteristics that can be used as arguments are:

- The velocity for the robot arms
- The acceleration for the robot arms
- The payload for the robot, and
- The tool data for the Tool Center Point (TCP). The TCP is the point that the robot will be calibrated at. It is the point that the robot will take as a reference to base its position upon.

#### D.1.2 Scopes of instructions

Once the instructions defined, they are grouped in programs and modules. These programs and modules contain routines, which are a set of instructions ordered according to a certain sequence defined by the user.

There are two different scopes that apply to routines to group instructions properly:

1. *Global scope*. This scope enables a routine to include the instructions of other modules.
2. *Local scope*. This scope restrains the routine to only include the instructions of the module that the routine itself is part of.

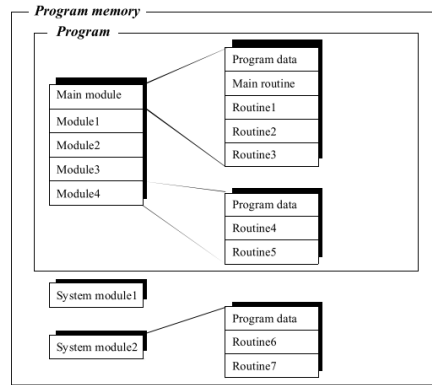


Figure D.2: Global and local scopes of routines [50]

### D.1.3 Sequence of instructions

Now that the instructions are grouped in routines, the sequence of instructions within and between routines should be determined. This sequence can be controlled according five different principles:

1. Calling another routine.
2. Executing instructions depending on whether a certain condition is satisfied.
3. Repeating a sequence of instructions till a certain condition is satisfied.
4. Going to a label/line within the same routine.
5. Stopping program execution.

### Priorities

By default, the robot will execute all instructions one by one according to the set order in the program. However, it is possible to change the priority of one task by putting tasks either to the fore- or background. The background tasks will only execute when the foreground tasks are waiting for other tasks to be performed or have stopped the execution (idle). An example of task priorities is shown below.

Round robin chain 1:

- Tasks 0, 1, and 8 are busy

Round robin chain 2:

- Tasks 0, 3, 4, 5 and 8 are busy tasks 1 and 2 are idle

Round robin chain 3:

- Tasks 2, 4 and 5 are busy tasks 1, 2, 9 and 10 are idle.

Round robin chain 4:

- Tasks 6 and 7 are busy tasks 0, 1, 2, 3, 4, 5, 8 and 9 are idle

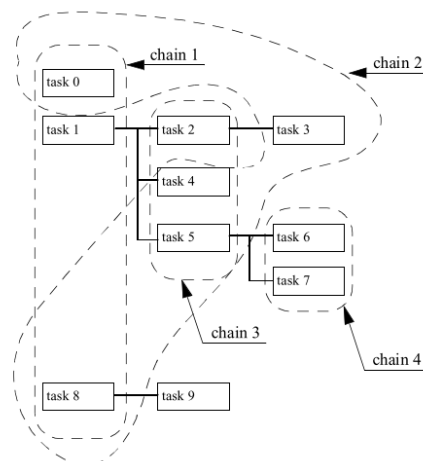


Figure D.3: Prioritizing tasks by chains [50]

## D.2 ROBOTIC PROGRAMS: PERFORMING INSTRUCTIONS

In the previous paragraph the general setup of how to instruct a robot is explained. Now that the instructions are set, the next step is to analyze how a robot physically processes and performs these instructions. This paragraph briefly explains how a robot moves and orients when processing and performing the instructions that are assigned to it.

### D.2.1 Types of motion

A robot moves with the TCP, the Tool Center Point the robot is calibrated at, from one point to another. During this movement, there are different types of motion that a robot can apply.

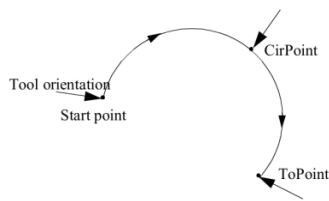


Figure D.4: Circular movement [50]

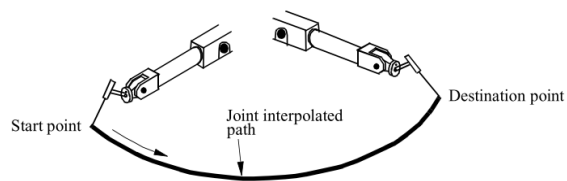


Figure D.5: (Absolute) joint movement [50]

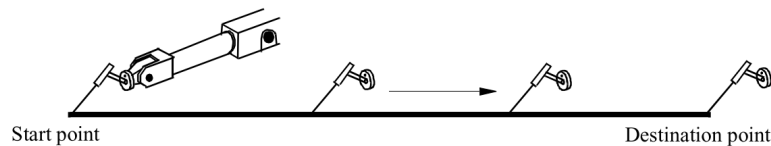


Figure D.6: Linear movement without reorientation of the tool (ABB Robotic Products AB, 2011)

For circular movement the path consists of three different points: starting point, support point, end point. In case of (absolute) joint movement, the tool moves as quick as possible from one point to another. The third type of movement, linear movement, will let the tool move linearly along a path.

### D.2.2 Robot axes

The robot moves by making movements on or around the robot axes. Robots know two types of axes: arm axes and wrist axes. The difference between arm- and wrist axes is that wrist axes move on the axis, while arm axes move around the axis. Most robots applied in the architectural industry are equipped with five or six axes. Examples are shown below.

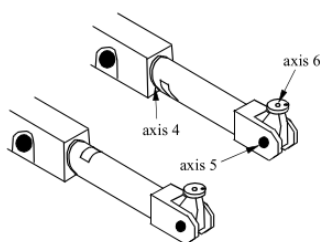


Figure D.7: Arm axis: 5, Wrist axes: 4, 6 [50]

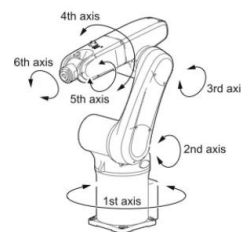


Figure D.8: The axis of a 6 axes robot [50]



### D.2.3 Coordinate systems in general

Finally, a robot uses a coordinate system to orient its position upon. There are seven different coordinate systems a robot can apply for its orientation, which are shown below.

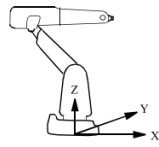


Figure 3: Base coordinate system [50]

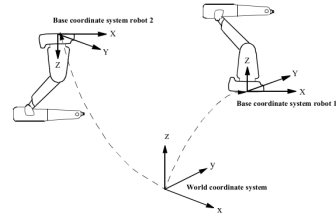


Figure 4: World coordinate system [50]

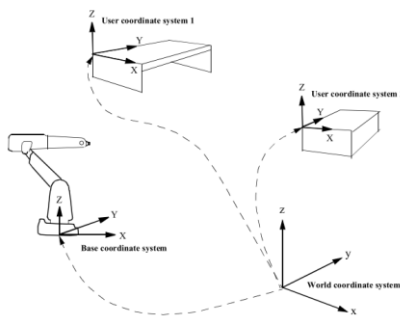


Figure D.9: User coordinate system [50]

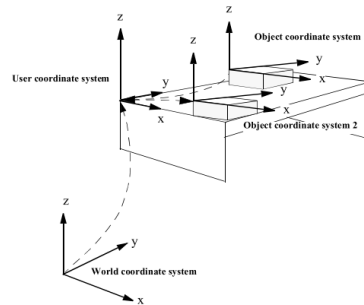


Figure D.10: Object coordinate system [50]

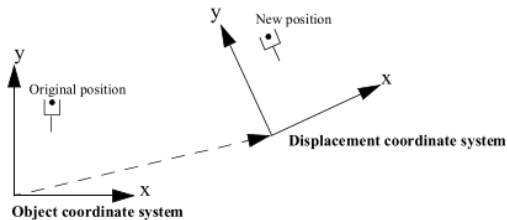


Figure D.11: Displacement coordinate system. All positions are displaced [50]

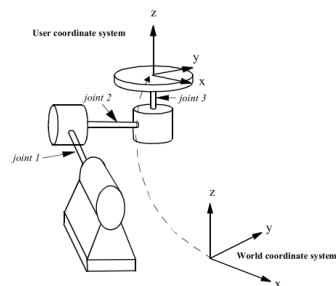


Figure D.12: External axis based on user coordinate system [50]

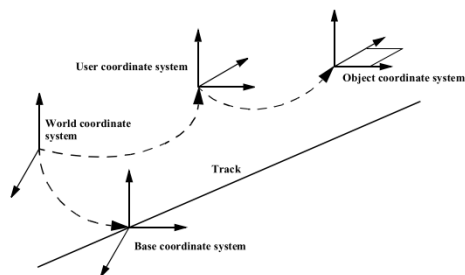


Figure D.13: External axis based on base coordinate system [50]

**i. Base coordinate system**

The base coordinate system is oriented at the base of the robot, which means that the origin is situated at the intersection of axis 1 and the base mounting surface. This type of coordinate system is generally used for simple applications.

**ii. World coordinate system**

A robot does not necessarily have to be floor-mounted but can also be mounted on a ceiling or wall. In these cases, a base coordinate system is not sufficient. The robot should be oriented according to the world coordinate system. Furthermore, if two robots collaborate they can be calibrated according to the same world coordinate system to let them communicate properly.

**iii. User coordinate system**

A robot can work with different fixtures or working surfaces, having different positions and orientations. A user coordinate system can be defined for each fixture. The principle of the user coordinate system is based on the world coordinate system and can be moved among the fixtures or working surfaces.

**iv. Object coordinate system**

In some cases, the robot operates on different fixtures or working surfaces. It is beneficial to create a coordinate system for each working surface or fixture. This enables the robot to work on different objects within one program, even if objects are moving as programmed.

**v. Displacement coordinate system**

Sometimes, the path of the robot should be placed on several places of the object. A displacement coordinate system is advisable in this case. The advantage of this coordinate system is that the positions do not have to be re-programmed for each path, since the coordinate system itself displaces.

**vi. External axes based on the user coordinate system**

In case the object of the external axis is placed on a mechanical (moving) object, an external axis based on the user coordinate system is preferred.

**vii. External axes based on the base coordinate system**

In case the object of the external axis is mounted on for instance a track or gantry, an external axis based on the base coordinate system is preferred.

## Appendix E. Validation of Finite Element Modelling of CLT

This appendix shows the validation of the modelling of orthotropic material properties according the FEM. It concerns an out-of-plane loaded CLT plate that simply supported. First, the numerical FEM model is described and secondly this is validated by an analytical calculation.

### E.1 INPUT FEM - GEOMETRY

**Geometry.** The geometry of the FEM model is set up by a rectangular surface generated in Grasshopper, which is divided into an equally distributed quadratic mesh.

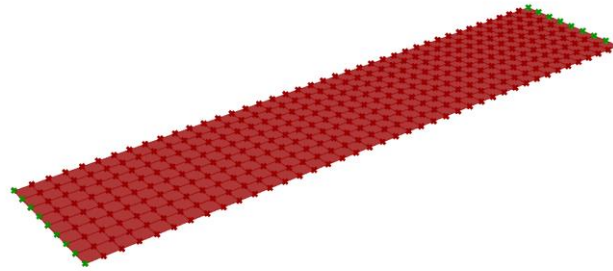


Figure E.1: Grasshopper geometry of a CLT plate equally divided into a quad mesh

**FEM geometry.** The above geometry is baked from Grasshopper into GSA, where the CLT plate is simply supported. The plate is pinned at the left side and hinged by a roller support on the right side.

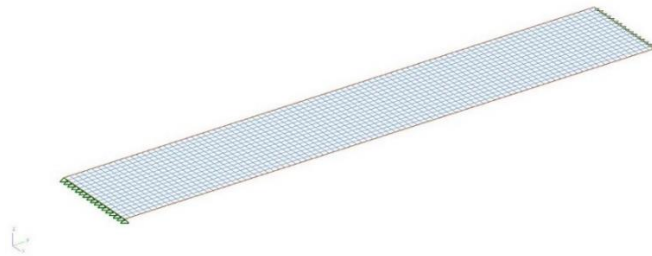


Figure E.2: GSA model of a CLT plate w

**Cross-sectional geometry.** The cross-section of the plate is built up according the following geometry: XLAM 140 L7s (20l-20w-20l-20w-20l-20w-20l)

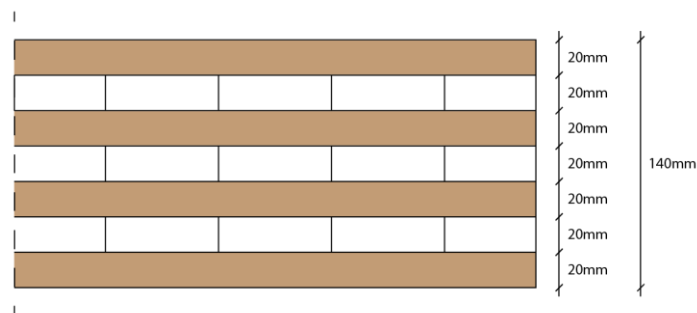


Figure E.3: GSA model of a CLT plate with seven layers of 20mm thick

## E.2 INPUT FEM – MATERIAL PROPERTIES

The first step to correctly model the orthogonal material properties of a CLT element is to determine its strong and weak direction. For an out-of-plane loaded element, this can be done by looking at the most typical load applicable, which is a distributed load.

**Typical loading in bending.** For bending, bending around the x-axis becomes critical as the span in y-direction is larger than in x-direction. Therefore, for bending it is preferable to model the strong direction in the y-direction as this will increase the  $E_y$ -modulus, and subsequently the bending resistance.

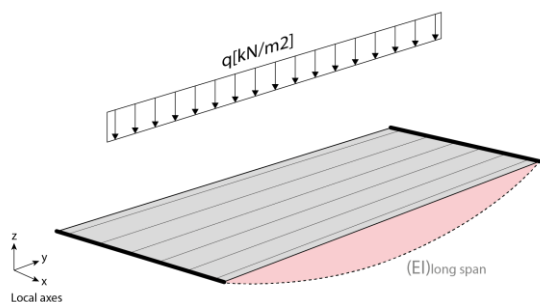


Figure E.4: Bending around the x-axis due to pressure load  $[kN/m^2]$  – supports at thick edges

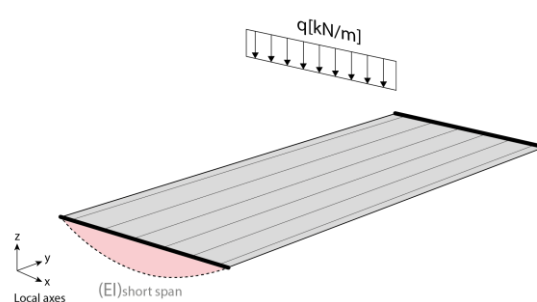


Figure E.5: Bending around the y-axis due to pressure load  $[kN/m^2]$  – supports at thick edges

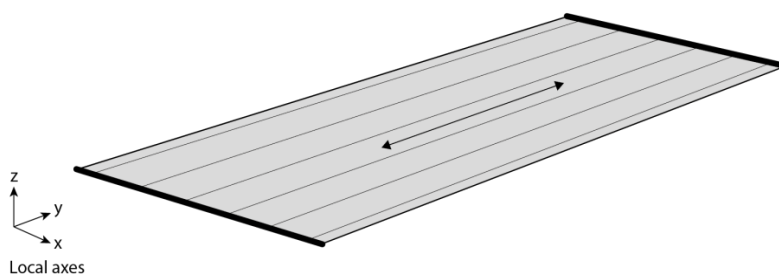


Figure E.6: Preferable strong direction regarding bending, where  $E_y$  is governing as  $I [mm^4]$  is constant – supports at thick edges

**Typical loading in shear.** For shear, one should carefully look at the distribution of the out-of-plane load. The distributed load per meter in the direction of the longest span results in a higher load than the distributed load in the direction of the shortest span. This is shown in Figures E.8-E.9 and in Table E.1.

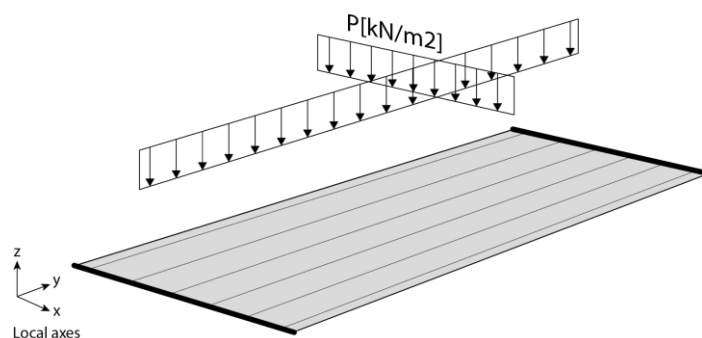


Figure E.7: Out-of-plane loaded CLT element – supports at thick edges

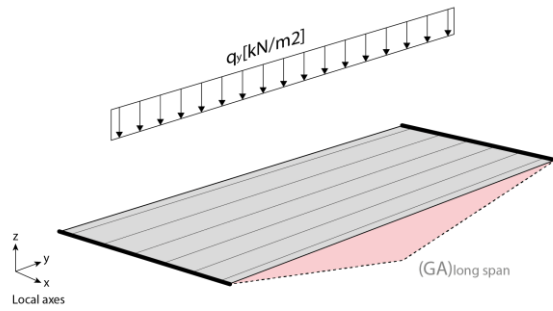


Figure E.8: Shear deformation over longest span– supports at thick edges

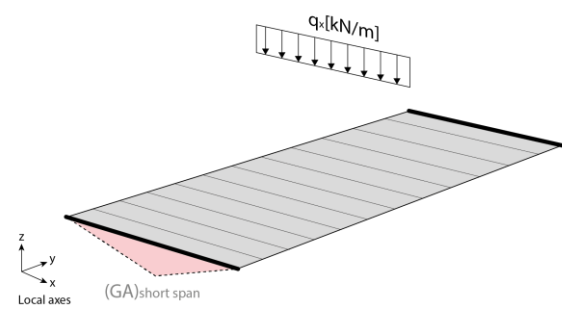


Figure E.9: Shear deformation over shortest span– supports at thick edges

	Span in direction	q	Shear deformation occurs in plane
Longest span	y	$q_y = l_y \cdot P$	xz
Shortest span	x	$q_x = l_x \cdot P$	yz

Table E.1: Overview of shear deformation in both directions of a CLT element

As  $q_{x,y}$  depends on the length of the span, one can conclude that  $q_x < q_y$ . Therefore, the largest shear resistance should occur in the xz-plane. If applying this situation to the theory as described in Chapter 5.2, the  $G_{xz}$  modulus will represent the strong direction, as this parameter relates to the resistance in the yz-plane, and the strong direction will be modelled in the y-direction.

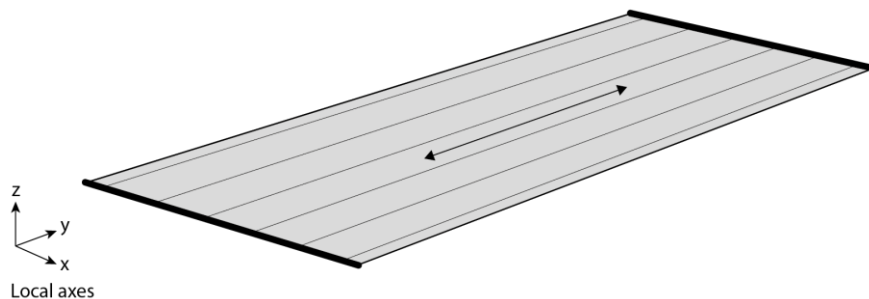


Figure E.10: Shear deformation over shortest span– supports at thick edges

**Conclusion strong and weak direction.** As for both the bending- and shear resistance the preferable strong direction is the local and global y-direction, the strong direction will be modelled in the y-direction and the weak direction will be modelled in the x-direction.

### E.3 INPUT FEM – ORTHOGONAL MATERIAL PROPERTIES

Once the strong and weak direction are determined, the next step is to determine the values of the input material parameters for the FEM model. As stated in Chapter 5.2, the relevant parameters for the orthotropic material that at least must be manually set in the FEM model are:

- Young's moduli:  $E_x, E_y, E_z$
- Shear moduli:  $G_{xy}, G_{yz}, G_{zx}$
- Self-weight:  $\rho = 400\text{kg/m}^2$

**Structural parameters from code.** From the proHolz design guide, the relevant Young's and shear moduli can be determined according the reduced cross-section design philosophy. Applying the formulas as described in the Chapter 1.5 and Appendix B, this theory results in the following cross-sectional parameters:

Parameter	Magnitude	
$(EI)_{ef,strong}$	$1,814 \cdot 10^{12} \text{ [Nmm}^2\text{]}$	Bending stiffness in strong direction
$(GA)_{ef,strong}$	$1,4835 \cdot 10^7 \text{ [N]}$	Shear stiffness in strong direction
$(EI)_{ef,weak}$	$7,862 \cdot 10^{11} \text{ [Nmm}^2\text{]}$	Bending stiffness in weak direction
$(GA)_{ef,weak}$	$1,173 \cdot 10^7 \text{ [N]}$	Shear stiffness in weak direction

Table E.2: Overview of the effective bending- and shear stiffnesses in strong and weak direction

As GSA only accepts specific E- and G-moduli, the above stated values should be translated accordingly.

**Translation of E moduli to FEM parameters.** For the Young's moduli the calculation can be performed by taking the ratio with the moment of inertia over the gross cross-section. The overall moment of Inertia should be calculated as follows:

$$I_{tot} = \frac{1}{12}bh^3 \quad (5)$$

$$I_{tot} = \frac{1}{12} * 1000 * (7 * 20)^3$$

$$I_{tot} = 2.2867 * 10^8 \text{mm}^4$$

For the strong direction,  $E_y$  follows from:

$$E_y = \frac{(EI)_{ef,strong}}{I_{ef,strong}} \quad (6)$$

$$E_y = \frac{1,814 * 10^{12}}{2,2867 * 10^8}$$

$$E_y = 7932 \text{N/mm}^2$$

For the weak direction,  $E_x$  follows from:

$$E_x = \frac{(EI)_{ef,weak}}{I_{ef,weak}} \quad (7)$$

$$E_x = \frac{7,862 * 10^{11}}{2,2867 * 10^8}$$

$$E_x = 3438 \text{N/mm}^2$$

*Note: the  $(EI)_{ef}$  moduli are influenced by the distance of the layers from the neutral axis by applying Steiner's rule. The further away from the neutral axis, the larger the value of  $EI$ , and subsequently the larger the value of the  $E$  moduli as the total moment of Inertia concerns a constant value. Besides, the  $E_z$  modulus is not important as CLT is modelled as two-dimensional mesh elements.*

**Translation of G moduli to FEM parameters.** For the shear moduli the calculation can be done by taking a reduced area  $A_{ef}$  [mm<sup>2</sup>] in both the strong and weak direction. The reduced area can be calculated by applying a factor  $\kappa$ , which is specified in the proHolz design guide. For rectangular cross-sections it is recommended to apply  $\kappa = 5/6$  [-], see also Appendix B. The reduced area can be calculated as follows:

$$A_{ef} = \kappa * A_{tot} \quad (8)$$

$$A_{ef} = \frac{5}{6} * (7 * 20 * 1000)$$

$$A_{ef} = 116.666,67 \text{ mm}^2$$

For the strong direction,  $G_{xz}$  follows from:

$$G_{xz} = \frac{(GA)_{ef, strong}}{A_{ef}} \quad (9)$$

$$G_{xz} = \frac{1,4835 * 10^7}{116.666,67}$$

$$G_{xz} = 127 \text{ N/mm}^2$$

For the weak direction,  $G_{yz}$  follows from:

$$G_{yz} = \frac{(GA)_{ef, weak}}{A_{ef}} \quad (10)$$

$$G_{yz} = \frac{1,173 * 10^7}{116.666,67}$$

$$G_{yz} = 100 \text{ N/mm}^2$$

The in-plane shear,  $G_{xy}$  can be calculated as follows [65]:

$$G_{xy} = 0.36 * G_0 \quad (11)$$

$$G_{xy} = 0.36 * 690$$

$$G_{xy} = 248 \text{ N/mm}^2$$

## E.4 INPUT FEM – OVERVIEW

The following data is used as input for the FEM model:

**Orthogonal material properties.** Table E.3 gives an overview of all orthogonal material properties required by a FEM model. Table E.4 shows the most relevant ones.

Parameter	Unit	Description	Comment
$E_x$	N/mm <sup>2</sup>	E for extension in x direction.	Out of plane bending around the y-axis
$E_y$	N/mm <sup>2</sup>	E for extension in y direction.	Out of plane bending around the x-axis
$E_z$	N/mm <sup>2</sup>	E for extension in z direction	Not relevant for 2D shell elements
$\nu_{xy}$		Poisson's ratio in the xy-plane	Timber is not a poisson's ratio material and G-values need to be explicitly defined. A very small value should be used as input.
$\nu_{yz}$		Poisson's ratio in the xy-plane	
$\nu_{zx}$		Poisson's ratio in the xy-plane	
$\rho$	kg/m <sup>3</sup>		
$\alpha_x$	/°C	Thermal expansivity x	Generally, the thermal expansivity is not of importance in timber design.
$\alpha_y$	/°C	Thermal expansivity y	
$\alpha_z$	/°C	Thermal expansivity z	
$G_{xy}$	N/mm <sup>2</sup>	In plane stiffness	Not important if modeling out of plane behavior (floors) Important if modeling in plane behavior (walls)
$G_{yz}$	N/mm <sup>2</sup>	Shear stiffness in yz-plane	
$G_{zx}$	N/mm <sup>2</sup>	Shear stiffness in zx-plane	
$\zeta$	%	Damping ratio	The damping ratio is not important as damping is explicitly defined in the footfall vibration load case if required.

Table E.3: Overview of required material properties according the FEM for orthotropic materials

Input parameter	Maginitude	Unit
Distributed load P	2	kN/m <sup>2</sup>
Span in y-direction	6	m
Span in x-direction	1	m
$E_x$	3438	N/mm <sup>2</sup>
$E_y$	7932	N/mm <sup>2</sup>
$G_{xy}$	248	N/mm <sup>2</sup>
$G_{yz}$	100	N/mm <sup>2</sup>
$G_{zx}$	127	N/mm <sup>2</sup>

Table E.4: Overview of essential material properties according the FEM



## Geometry and loads

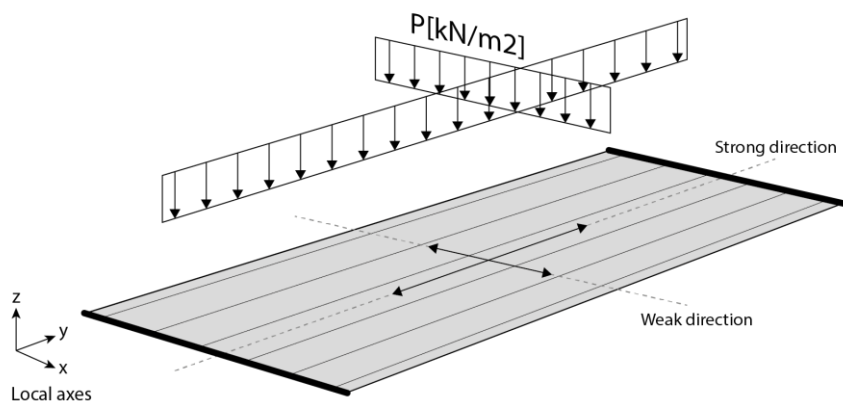


Figure E.11: Geometry of the simply supported CLT plate with strong and weak directions– supports at thick edges

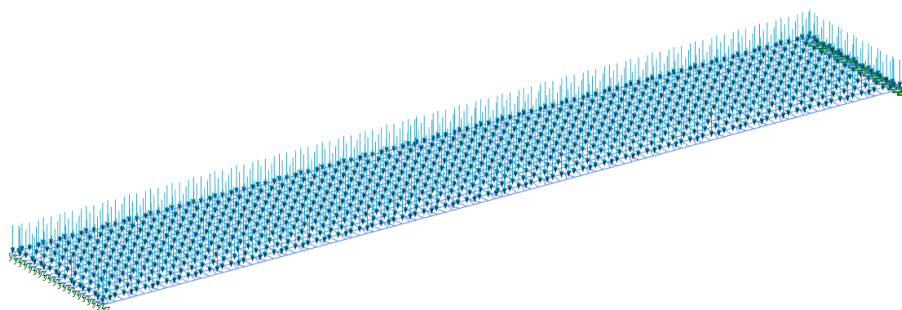


Figure E.12: Perspective view of the geometry and distributed load

## E.5 OUTPUT FEM: RESULTS AND VALIDATION OF THE FINITE ELEMENT MODEL

**Results FEM model – Bending.** The maximum deflection of the model due to bending concerns 18,6mm, and the floor shows a deflected shape as shown in Figure E.13. In this case, the shear moduli are set to infinite to nullify the deflection due to shear.

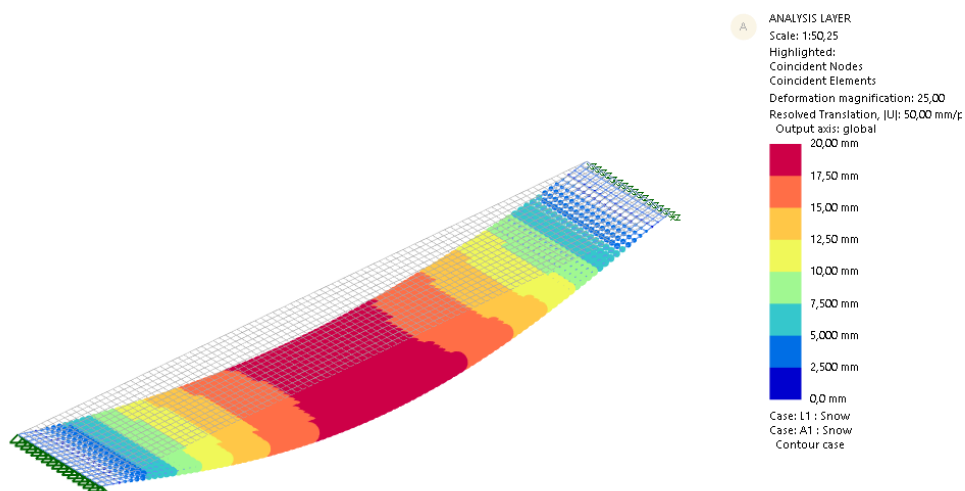


Figure E.13: Deflected shape of an out-of-plane loaded CLT element – maximum deflection due to bending is 18.6mm

**Results FEM model – Shear.** The maximum deflection of the model due to shear concerns 0,606mm, and the floor shows a deflected shape as shown in Figure E.14. In this case, the Young's moduli are set to infinite to nullify the deflection due to bending.

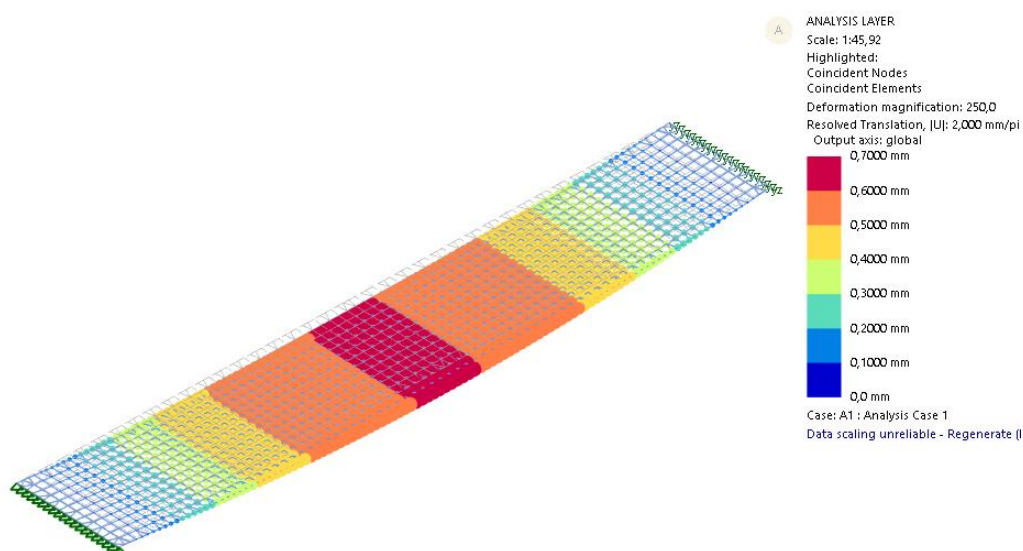


Figure E.14: Deflected shape of an out-of-plane loaded CLT element – maximum deflection due to shear is 0.606mm

**Results FEM model – Bending and shear.** The maximum deflection of the model due to shear concerns 0,606mm, and the floor shows a deflected shape as shown in Figure E.15. In this case, the material properties as presented in previous paragraph are applied.

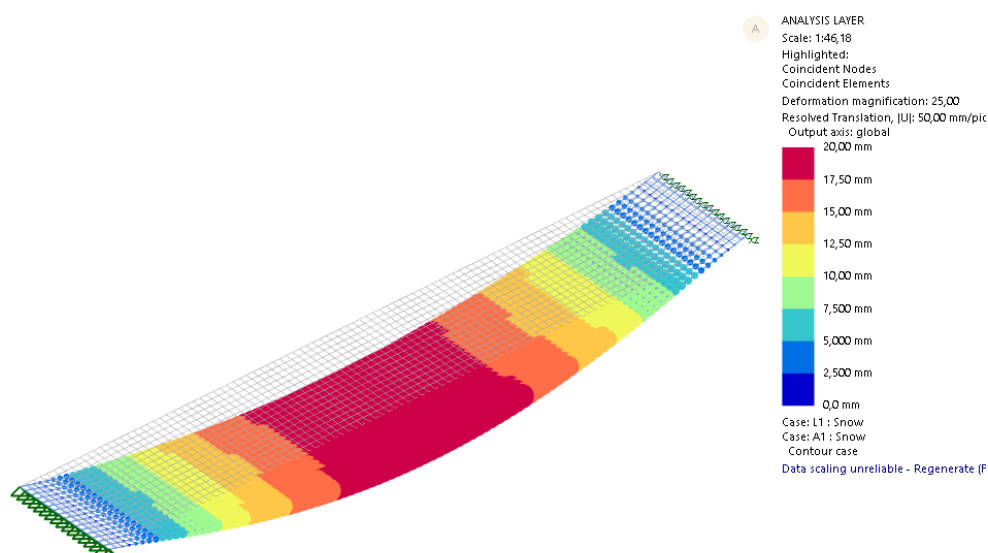


Figure E.15: Deflected shape of an out-of-plane loaded CLT element – maximum deflection due to bending and shear is 19.22mm

**Validation of the FEM model.** The results of the FEM model can be validated by an analytical calculation. The following formulas can be derived from differential equation of a uniformly loaded simply supported beam. Subsequently the results of the FEM model are compared to applying the formulas below.

$$w_{bending} = \frac{5ql^4}{384EI} \quad (12)$$

$$w_{shear} = \frac{ql^2}{8GA} \quad (13)$$

$$w_{tot} = \frac{5ql^4}{384EI} + \frac{ql^2}{8GA} \quad (14)$$

The stiffness parameters that are applied are in the formulas shown in Table E.5, see Chapter E.3.

Parameter	Magnitude	
$(EI)_{ef,strong}$	$1,814 \cdot 10^{12}$ [Nmm <sup>2</sup> ]	Bending stiffness in strong direction
$(GA)_{ef,strong}$	$1,4835 \cdot 10^7$ [N]	Shear stiffness in strong direction

Table E.5: Overview of stiffness parameters for the analytical calculation

This results the following values for deflection due to bending and shear.

	Bending	Shear	Bending and Shear
FEM	18,6 mm	0,606 mm	19,206 mm
Analytical calculation	18,61 mm	0,607 mm	19,217 mm
Deviation	0,053 %	0,06 %	0,057 %

## E.6 CONCLUSION AND DISCUSSIONS

**Conclusions.** As the results deviate with a maximum of 0.06%, the following can be concluded:

- The FEM model is validated successfully.
- The orthogonal material parameters are set correctly in the FEM model.
- It is preferable to model the strong direction of an out-of-plane loaded CLT element in the direction of the longest span.
- The small deviation between the analytical calculation and the FEM model can be caused by one of the following:
  - o The hogging effect of the plate compared to the formulas that apply to a beam, looking at the longitudinal cross-section. There is a small difference between the deflection of the sides of the plate and the center point of the plate.

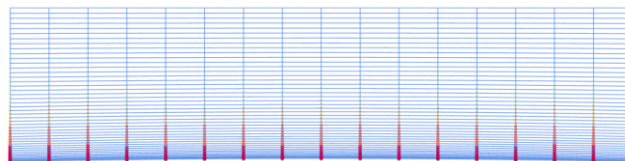


Figure E.16: Hogging effect of a CLT floor according the plates and slabs theory

- o Another reason is the rounding of numbers, which is performed more accurately by GSA than by hand.

**Discussions.** By varying the span of the out-of-plane loaded element, the following graphs can be derived to further investigate the FEM model.

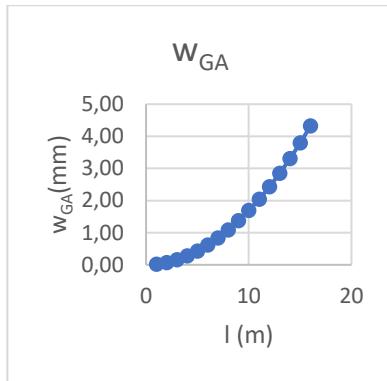


Figure E.17:  $w_{GA}$

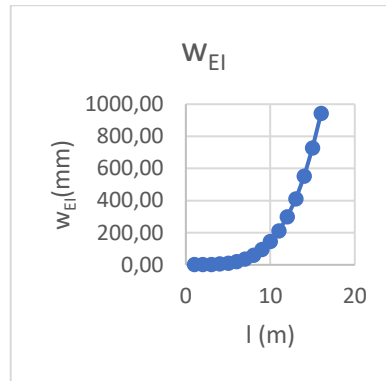


Figure E.18:  $w_{EI}$

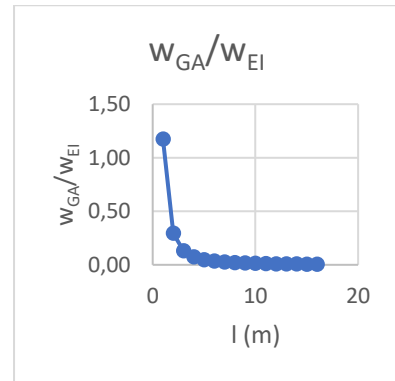


Figure E.19:  $w_{GA}/w_{EI}$

The above graphs in Figures E.17-E.19 show that the deflection is governed by shear in case of a span of the strong direction between 0m-2m, and that the deflection is governed by bending in case of a span of the strong direction larger than 2m. Concluding: short spans in CLT floors are governed by shear, whereas long spans in CLT floors are governed by bending. This is a well-known phenomenon for beams.

Other variants that are investigated are models with varying orthogonal material properties of the model. The model as described in this chapter is taken as the reference model. Figure E.20 shows the results of variants modelled on this reference model. The results are retrieved by setting all material parameters to infinite, except the parameter that is investigated.

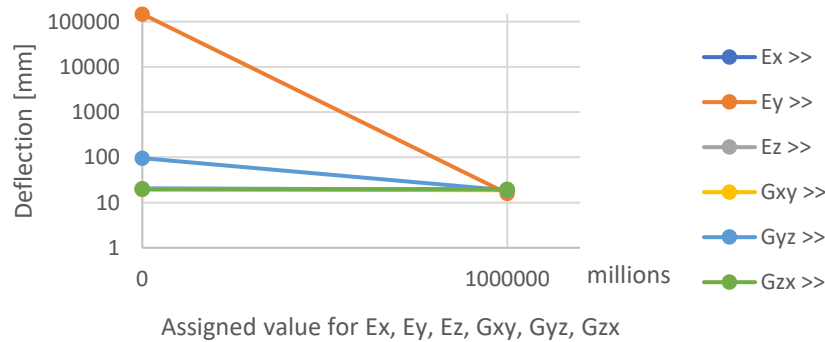


Figure E.20: Influence of orthogonal material properties on the deflection of an out-of-plane loaded CLT element

The results above confirm the influence of the different material properties. As expected,  $E_y$  and  $G_{yz}$  are the most influential factors on the structural behavior of the floor.

# Appendix F. Explanation of Variables for Global Structure

Variable	
a. <b>Surface</b>	<div><div>Description</div><div>The input surface can consist of either a joined surface or separated free surfaces.</div><div>Type</div><div>Geometry</div><div>Examples</div></div>

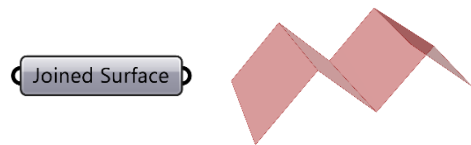


Figure F.1: Grasshopper Component and geometry for joined surface input

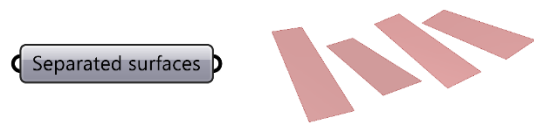


Figure F.2: Grasshopper Component and geometry for separated surface input

b. <b>Width of Joints</b>	<div><div>Description</div><div>In case of a joined surface, the offset between the CLT plates can be varied, which represents the width of the connection panels.</div><div>Type</div><div>Integer</div><div>Examples</div></div>
---------------------------	--

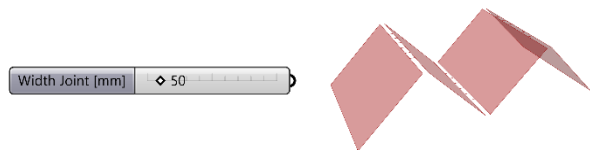


Figure F.3: Grasshopper Component and geometry of small Width of Joints

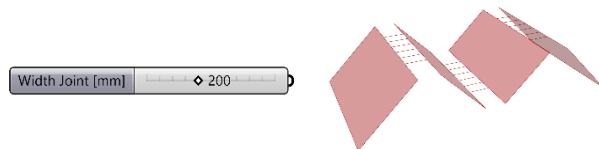


Figure F.4: Grasshopper Component and geometry of large Width of Joints

c. <b>Joined or separate surface</b>	<div><div>Description</div><div>This variable informs the script whether the input surfaces are joined or separated free surfaces.</div><div>Type</div><div>Integer</div></div>
--------------------------------------	---

**d. Number of joints along edge**

*Description* The number of joints along an edge can be varied. The number can either be increased or decreased.

*Type* Integer

*Example*

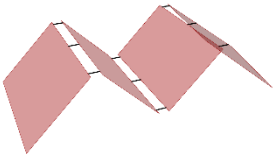


Figure F.5: Grasshopper Component and geometry of small number of joints

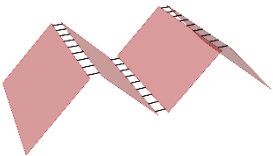


Figure F.6: Grasshopper Component and geometry of large number of joints

**e. Scaled length for joint division**

*Description* The length along which the joints are divided can be varied. This length is scaled along the corresponding edge on a scale from 0.2-1.0[-].

*Type* Number

*Examples*

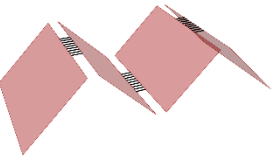


Figure F.7: Grasshopper Component and geometry of small scaled edge length

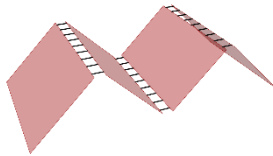


Figure F.8: Grasshopper Component and geometry of large scaled edge length

f. **Joint orientation**

*Description* This parameter allows a user to choose for the orientation of the joints. They can be either oriented perpendicular to the adjacent surface or aligned vertically to the global z-axis.

*Type* Integer

*Examples*

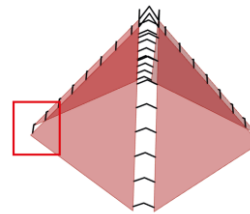


Figure F.9: Example geometry to illustrate the joint orientation in the red-marked rectangle.

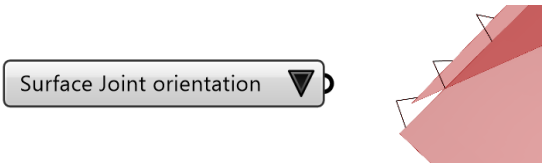


Figure F.10: Grasshopper Component and geometry of joints aligned to surface

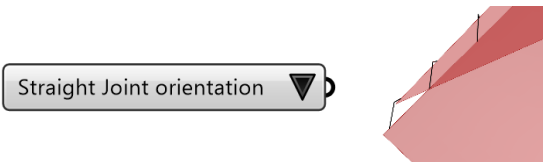


Figure F.11: Grasshopper Component and geometry of joints aligned to z-axis

g. **Joint to analyze**

*Description* This variable selects the joint a user wants to analyze. Only one joint a time can be structurally verified in the Joint Design module, so a user should first select the edge he wants to analyze and subsequently the joint. For example, in case of the geometry as shown in variable b-e, there are three edges a user can select from.

*Type* Integer

h. **Cross-sectional build-up**

*Description* The cross-sectional build-up is a list of all layer thicknesses of the CLT cross-section. To control all layer thicknesses individually, a Genome is used.

*Type* List

*Example*

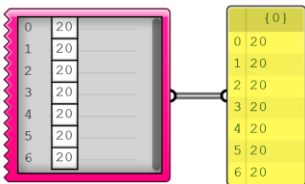


Figure F.12: Cross-sectional build-up (1) provided by a Genome

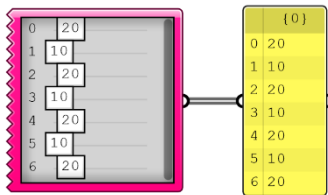


Figure F.13: Cross-sectional build-up (2) provided by a Genome

i. **Wood properties**

*Description* CLT is made of a certain type of wood. Therefore, the wood properties should be a variable:  $E_0$ ,  $E_{90}$ ,  $G_0$ ,  $G_{90}$ ,  $\rho_{CLT}$ . They consecutively result in different stiffness parameters as input for the FEM model.

*Type* Numbers

*Example*

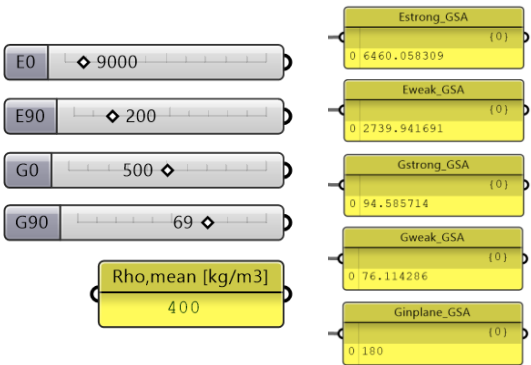


Figure F.14: Grasshopper Component and geometry of wood properties (1)

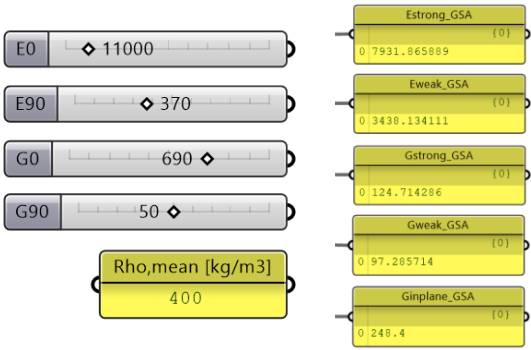


Figure F.15: Grasshopper Component and geometry of wood properties (2)

j. **Orientation of first layer**

*Description* The direction of the strong direction of CLT plates can be manually set. As illustrated in Appendix E, the preferable strong direction is the direction of the longest span. However, a user can modify this property manually if desired.

*Type* Integer

*Example*

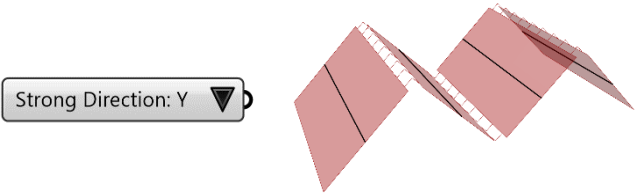


Figure F.16: Grasshopper Component and geometry of local strong direction Y

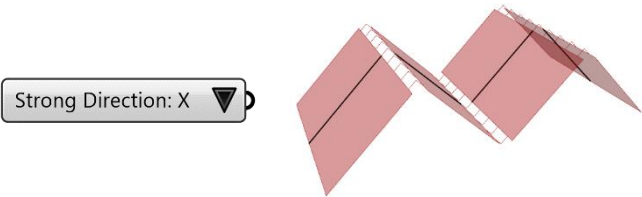


Figure F.17: Grasshopper Component and geometry of local strong direction X



## Appendix G. Python Script for Orthogonal Material Properties

```
1. """Provides a scripting component.
2.     Inputs:
3.         x: The x script variable
4.         y: The y script variable
5.     Output:
6.         a: The a output variable"""
7.
8. __author__ = "arjen.veldhuis"
9. __version__ = "2020.01.07"
10.
11. import rhinoscriptsyntax as rs
12. import math as mt
13. import operator as op
14. import Rhino.Geometry as rg
15.
16. n_layer = len(t_layer)
17. density = rho
18.
19.
20.
21. #Get total thickness
22. Thickness = 0
23. t_partial = []
24. for v in t_layer:
25.     Thickness += v
26.     t_partial.append(Thickness)
27.
28. #Check Total Thickness
29. if Thickness >= 300:
30.     DimCheck = "The total thickness is too large"
31. else:
32.     DimCheck = "Thickness OK"
33.
34. #Check Layer thickness
35. if any(x >= 60 for x in t_layer):
36.     LayCheck = "Check layer dimensions"
37. else:
38.     LayCheck = "Layer dimensions OK"
39.
40.
41.
42. #Calculate material properties
43.
44. #Find arm of each layer to centre
45.
46. #-----METHOD 1-----
47.
48. """
49. t_tot = 0
50. t_cumulative = []
51. t_mod = []
52. for y in t_layer:
53.     t_mod = y/2
54.     t_tot += y
55.     t_cumulative.append(t_tot)
56.
57. t_mod = [int(x/2) for x in t_layer]
58.
59. t_new = map(op.sub, t_cumulative, t_mod)
60.
61. ##print(t_cumulative)
62. #print(t_mod)
```

```

63. #print(t_new)
64. """
65.
66. #-----METHOD 2-----
67.
68. t0 = []
69. t0.append(0)
70. tmem = []
71. tmem.append(0)
72.
73. for i in range(len(t_lay)):
74.     t0.append(t0[i] + tmem[i] + t_lay[i]/2)
75.     tmem.append(t_lay[i]/2)
76. t0.pop(0)
77. e_top = t0
78. e_center = [abs(x-Thickness/2) for x in t0]
79.
80. #print('Thickness =', Thickness)
81. #print('e_top =', e_top)
82. print('e_center =', e_center)
83.
84. #-----Split layers-----
85.
86. #The first comment tells about strong or weak E, G. The second about the strong or weak layer
87.
88. #Split weak and strong direction of arms e
89. estr_str, estr_wk = e_center[:,2], e_center[1:,2]
90. #print('e-strong: Strong e are', estr_str)
91. #print('e-strong: Weak e are', estr_wk)
92.
93. #Split weak and strong direction of Young's moduli E (the L is printed, but doesn't affect the numbers)
94. tstr_str, tstr_wk = t_lay[:,2], t_lay[1:,2]
95.
96. #Calc sum of all strong and weak directions. If lay1 = 0: first layer is vertical. If lay1 = 1: first layer is horizontal.
97. #Change t_A0net in t_Anet_hor
98. #Change t_A90net in t_Anet_vert
99.
100. if lay1 == 0:
101.     t_Anet_hor = tstr_wk
102.     t_Anet_vert = tstr_str
103. elif lay1 == 1:
104.     t_Anet_hor = tstr_str
105.     t_Anet_vert = tstr_wk
106.
107. #Split weak and strong direction of arms e
108. ewk_str, ewk_wk = e_center[1:,2], e_center[:,2]
109. #print('e-weak: Strong e are', ewk_str)
110. #print('e-weak: Weak e are', ewk_wk)
111.
112. #Split weak and strong direction of Young's moduli E (the L is printed, but doesn't affect the numbers)
113. twk_str, twk_wk = t_lay[1:,2], t_lay[:,2]
114.
115.
116. #-----EI and GA Calculation-----
117.
118. #Calculation of EI-STRONG
119.
120.
121. #Estrong: E0*A*estr_str^2
122. Estr_E0_A_e0 = []

```

```

123.     for i in range(len(tstr_str)):
124.         Estr_E0_A_e0.append(tstr_str[i]*E0*1000*estr_str[i]**2)
125.
126.     #Estrong: E90*A*estr_wk^2
127.     Estr_E90_A_e90 = []
128.     for i in range(len(tstr_wk)):
129.         Estr_E90_A_e90.append(tstr_wk[i]*E90*1000*estr_wk[i]**2)
130.
131.     #print('E-Strong: E0*A*e0^2', Estr_E0_A_e0)
132.     #print('E-Strong: E90*A*e90^2', Estr_E90_A_e90)
133.
134.     #For Estrong: E0*I
135.     Estr_E0_I = []
136.     for i in range(len(tstr_str)):
137.         Estr_E0_I.append(E0*1000*(tstr_str[i]**3/12))
138.
139.     #For Estrong: E90*I
140.     Estr_E90_I = []
141.     for i in range(len(tstr_wk)):
142.         Estr_E90_I.append(E90*1000*(tstr_wk[i]**3/12))
143.
144.     EIstrong = sum(Estr_E0_A_e0) + sum(Estr_E90_A_e90) + sum(Estr_E0_I) + sum(Estr_E
145.         90_I)
146.     print('EI-strong =', EIstrong)
147.
148.     #Calculation of EI-WEAK
149.
150.
151.     #Eweak: E0*A*estr_str^2
152.     Ewk_E0_A_e0 = []
153.     for i in range(len(twk_str)):
154.         Ewk_E0_A_e0.append(twk_str[i]*E0*1000*ewk_str[i]**2)
155.
156.     #Eweak: E90*A*estr_wk^2
157.     Ewk_E90_A_e90 = []
158.     for i in range(len(twk_wk)):
159.         Ewk_E90_A_e90.append(twk_wk[i]*E90*1000*ewk_wk[i]**2)
160.
161.     #print('E-Weak: E0*A*e0^2', Ewk_E0_A_e0)
162.     #print('E-Weak: E90*A*e90^2', Ewk_E90_A_e90)
163.
164.     #For Eweak: E0*I
165.     Ewk_E0_I = []
166.     for i in range(len(twk_str)):
167.         Ewk_E0_I.append(E0*1000*(twk_str[i]**3/12))
168.
169.     #For Eweak: E90*I
170.     Ewk_E90_I = []
171.     for i in range(len(twk_wk)):
172.         Ewk_E90_I.append(E90*1000*(twk_wk[i]**3/12))
173.
174.     EIweak = sum(Ewk_E0_A_e0) + sum(Ewk_E90_A_e90) + sum(Ewk_E0_I) + sum(Ewk_E90_I)
175.     print('EI-weak =', EIweak)
176.
177.
178.     #Calculation of GA-strong
179.
180.
181.     #For Gstrong: G0*A
182.     Gstr_G0_A = []
183.     for i in range(len(tstr_str)):
184.         Gstr_G0_A.append(tstr_str[i]*G0*1000)
185.
186.

```

```

187. #For Gstrong: G90*A
188. Gstr_G90_A = []
189. for i in range(len(tstr_wk)):
190.     Gstr_G90_A.append(tstr_wk[i]*G90*1000)
191.
192.
193. GAstrong = 0.25*(sum(Gstr_G0_A)+sum(Gstr_G90_A))
194. print('GA-strong =', GAstrong)
195.
196.
197. #Calculation of GA-weak
198.
199.
200. #For Gweak: G0*A
201. Gwk_G0_A = []
202. for i in range(len(twk_str)):
203.     Gwk_G0_A.append(twk_str[i]*G0*1000)
204.
205. #For Gweak: G90*A
206. Gwk_G90_A = []
207. for i in range(len(twk_wk)):
208.     Gwk_G90_A.append(twk_wk[i]*G90*1000)
209.
210. GAwweak = 0.25*(sum(Gwk_G0_A)+sum(Gwk_G90_A))
211. print('GA-weak =', GAwweak)
212.
213.
214. #-----GSA VALUES-----
215.
216.
217. Itot = 1000/12*Thickness**3
218. Estr_GSA = EIstrong/Itot
219. Ewk_GSA = EIweak/Itot
220. print('E-GSA-strong =', Estr_GSA, 'and E-GSA-weak =', Ewk_GSA)
221.
222. Agsa = k*Thickness*1000
223. Gstr_GSA = GAstrong/Agsa
224. Gwk_GSA = GAwweak/Agsa
225. print('G-GSA-strong =', Gstr_GSA, 'and G-GSA-weak =', Gwk_GSA)
226.
227.
228. #-----Net sections/thicknesses-----
229.
230. #t (A0net)-----
231. t_A0net = sum(tstr_str)
232. #print(t_A0net)
233.
234. #t (A90net)-----
235. t_A90net = sum(tstr_wk)
236. #print(t_A90net)
237.
238. #I0-----
239. Istr_steiner = []
240. for i in range(len(tstr_str)):
241.     Istr_steiner.append(tstr_str[i]*1000*estr_str[i]**2)
242.
243. Istr = []
244. for i in range(len(tstr_str)):
245.     Istr.append(1000*(tstr_str[i]**3/12))
246.
247. I0net = sum(Istr_steiner)+sum(Istr)
248. #print(I0net)
249.
250. #I90-----

```

```

251. Iwk_steiner = []
252. for i in range(len(tstr_wk)):
253.     Iwk_steiner.append(tstr_wk[i]*1000*estr_wk[i]**2)
254.
255. Iwk = []
256. for i in range(len(tstr_wk)):
257.     Iwk.append(1000*(tstr_wk[i]**3/12))
258.
259. I90net = sum(Iwk_steiner)+sum(Iwk)
260. #print(I90net)
261.
262. #S0-----
263. S0 = []
264. for i in range(len(tstr_str[::int(mt.ceil(len(tstr_str)/2))]]):
265.     S0.append(tstr_str[i]*1000*estr_str[i])
266. S0net = sum(S0)
267. #print(S0net)
268.
269. #S90-----
270. S90 = []
271. for i in range(len(tstr_wk[::int(mt.ceil(len(tstr_str)/2))]]):
272.     S90.append(tstr_wk[i]*1000*estr_wk[i])
273. S90net = sum(S90)
274. #print(S90net)
275.
276. lay1 = lay1
277. G0=G0

```

# Appendix H. Input for the FEM of Global Structure

## INPUT: Geometry and supporting conditions.

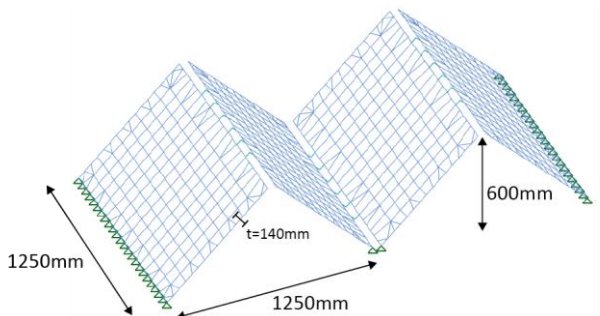


Figure H.1: GSA geometrical input

## INPUT: Beam sections.

The beam sections correspond with the plate material properties as explained in Chapter 5.4.4.

## INPUT: Mesh material properties.

Parameter	Magnitude	Unit	Parameter	Magnitude	Unit
$E_0$	7931	N/mm <sup>2</sup>	$G_{xy}$	248	N/mm <sup>2</sup>
$E_{90}$	3438	N/mm <sup>2</sup>	$G_{yz}$	100	N/mm <sup>2</sup>
$t_{plate}$	140	mm	$G_{zx}$	127	N/mm <sup>2</sup>
$\rho$	400	kg/m <sup>3</sup>			

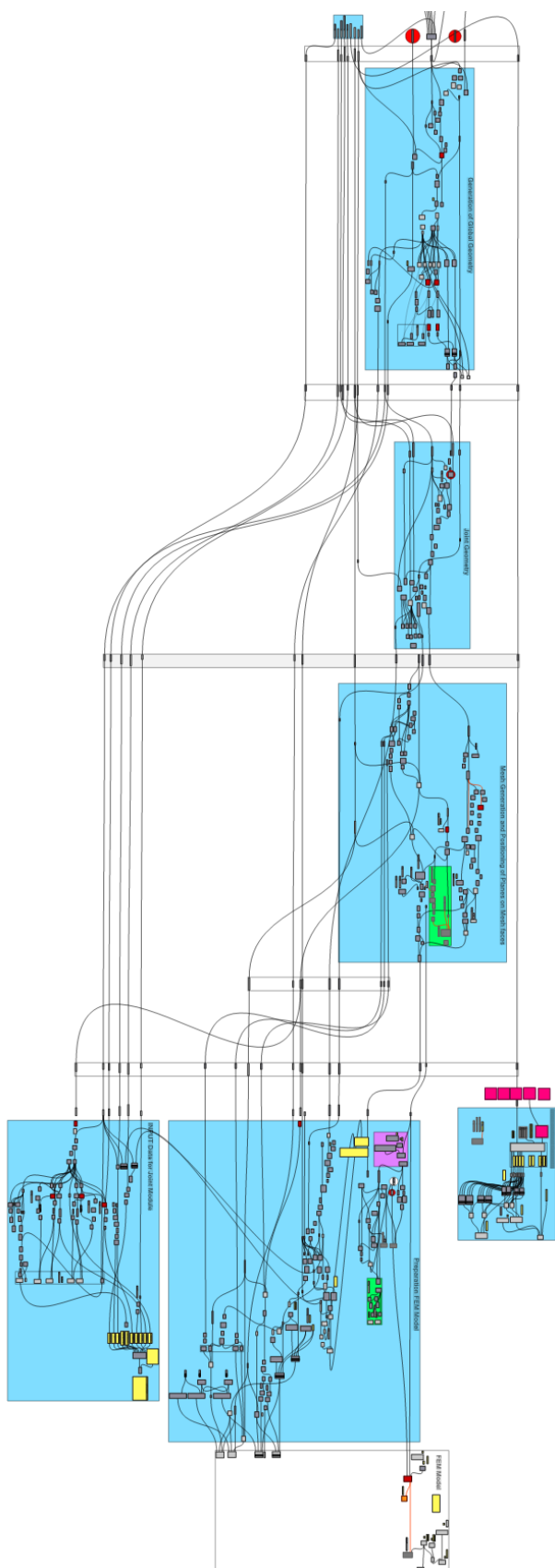
## INPUT: Loading.

	Load case	Magnitude	Unit
LC1	Gravity loading	$G \cdot (\rho \cdot m^3)$	kN
LC2	Variable loading on mesh elements (global z-axis)	-2	kN/m <sup>2</sup>

## INPUT: Analyses task.

Static analyses: LC1 + LC2

## Appendix I. Script for Global Structure module



## Appendix J. Design Graphs Global structure

The yellow highlighted value represents the variable compared to the reference model.

	x	y	z	a	t	n	q	U <sub>max</sub>	F <sub>xjoint</sub>	F <sub>yjoint</sub>	F <sub>zjoint</sub>	
1	1	1250	1250	625	50	140	6	1,5	0,375	0,2701	0,265	0,5046
	2	1500	1250	625	50	140	6	1,5	0,4605	0,3752	0,3138	0,6115
	3	1750	1250	625	50	140	6	1,5	0,5694	0,5424	0,3848	0,608
	4	2000	1250	625	50	140	6	1,5	0,707	0,7432	0,4625	0,6721
	5	2500	1250	625	50	140	6	1,5	0,9173	1,122	0,5596	0,8189
	6	3500	1250	625	50	140	6	1,5	1,278	1,732	0,7207	1,009
2	1	1250	1250	625	50	140	6	1,5	0,375	0,2701	0,265	0,5046
	7	1250	1500	625	50	140	6	1,5	0,5814	0,3391	0,3329	0,599
	8	1250	1750	625	50	140	6	1,5	0,773	0,4099	0,4026	0,9429
	9	1250	2000	625	50	140	6	1,5	0,997	0,4671	0,4589	1,229
	10	1250	2500	625	50	140	6	1,5	1,66	0,6498	0,6393	1,864
	11	1250	3500	625	50	140	6	1,5	2,5	0,8252	0,8128	3,376
3	12	1250	1250	400	50	140	6	1,5	0,72	0,387	0,269	0,8349
	13	1250	1250	500	50	140	6	1,5	0,44	0,3313	0,2827	0,5508
	14	1250	1250	575	50	140	6	1,5	0,3834	0,2927	0,2727	0,5114
	1	1250	1250	625	50	140	6	1,5	0,375	0,2701	0,265	0,5046
	15	1250	1250	650	50	140	6	1,5	0,3643	0,264	0,2636	0,4944
	16	1250	1250	700	50	140	6	1,5	0,3519	0,252	0,2595	0,4857
	17	1250	1250	800	50	140	6	1,5	0,3142	0,2366	0,2584	0,4604
	18	1250	1250	900	50	140	6	1,5	0,304	0,2253	0,2541	0,4186
	19	1250	1250	1000	50	140	6	1,5	0,298	0,2176	0,2515	0,4121
4	1	1250	1250	625	50	140	6	1,5	0,375	0,2701	0,265	0,5046
	20	1250	1250	625	100	140	6	1,5	0,575	0,2875	0,2772	0,5019
	21	1250	1250	625	150	140	6	1,5	0,7355	0,3011	0,2857	0,4833
	22	1250	1250	625	200	140	6	1,5	1,237	0,3487	0,3281	0,4247
	23	1250	1250	625	300	140	6	1,5	2,18	0,4157	0,3848	0,395
	24	1250	1250	625	400	140	6	1,5	3,198	0,4714	0,4302	0,3364
5	25	1250	1250	625	50	35	6	1,5	1,872	0,2361	0,2348	0,4112
	26	1250	1250	625	50	70	6	1,5	0,7365	0,23	0,2275	0,4446
	27	1250	1250	625	50	105	6	1,5	0,487	0,2427	0,2388	0,4755
	1	1250	1250	625	50	140	6	1,5	0,375	0,2701	0,265	0,5046
	28	1250	1250	625	50	175	6	1,5	0,3129	0,303	0,2966	0,5325
	29	1250	1250	625	50	210	6	1,5	0,2715	0,3395	0,3317	0,5597
6	30	1250	1250	625	50	140	3	1,5	0,3617	0,3267	0,319	1,015
	31	1250	1250	625	50	140	4	1,5	0,3749	0,2316	0,2264	0,6481
	32	1250	1250	625	50	140	5	1,5	0,321	0,1826	0,1798	0,5828
	33	1250	1250	625	50	140	6	1,5	0,3432	0,1636	0,1612	0,4558
	34	1250	1250	625	50	140	8	1,5	0,3215	0,1331	0,1311	0,4412
	35	1250	1250	625	50	140	10	1,5	0,3	0,1183	0,1165	0,2915
7	36	1250	1250	625	50	140	6	1	0,2864	0,207	0,2018	0,3843
	1	1250	1250	625	50	140	6	1,5	0,375	0,2701	0,265	0,5046
	37	1250	1250	625	50	140	6	2	0,4662	0,3332	0,3281	0,6249
	38	1250	1250	625	50	140	6	3	0,646	0,4594	0,4543	0,8655
	39	1250	1250	625	50	140	6	5	1	0,7119	0,7068	1,347
	40	1250	1250	625	50	140	6	10	1,9	1,343	1,338	2,55



Varying parameter

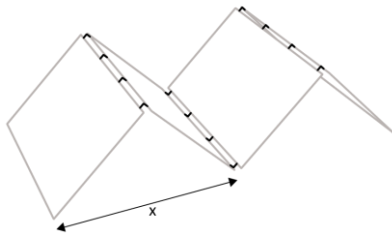


Figure I.1: Varying parameter  $x$

Derived design graph from FE

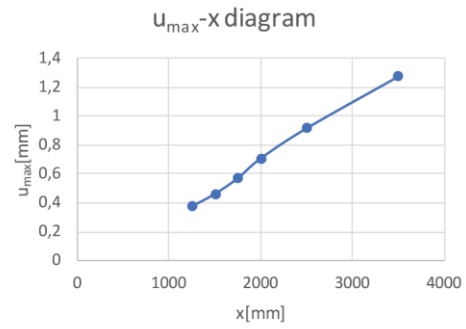


Figure I.2: Design graph for varying parameter  $x$ [mm] versus the maximum displacement[mm] in the FE model

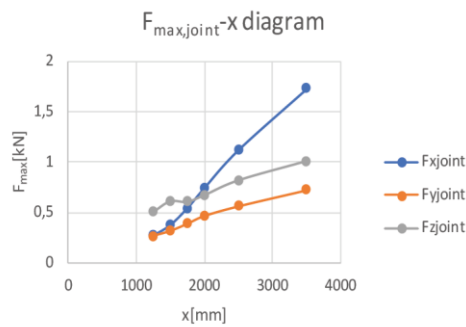


Figure I.3: Design graph for varying parameter  $x$ [mm] versus the maximum occurring force  $F_x$ ,  $F_y$ ,  $F_z$  [kN] in the joints

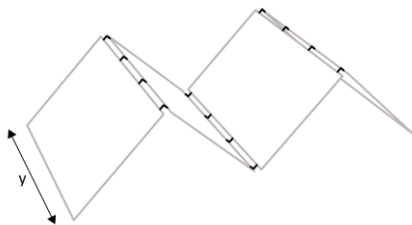


Figure I.4: Varying parameter  $y$

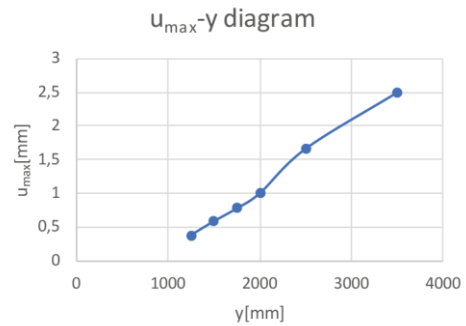


Figure I.5: Design graph for varying parameter  $y$ [mm] versus the maximum displacement[mm] in the FE model

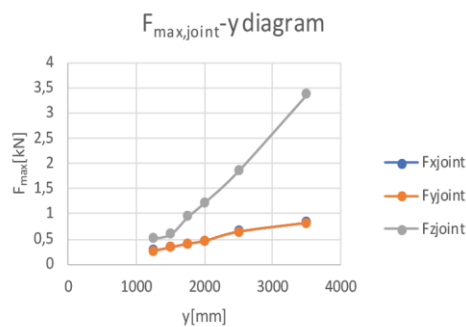


Figure I.6: Design graph for varying parameter  $y$ [mm] versus the maximum occurring force  $F_x$ ,  $F_y$ ,  $F_z$  [kN] in the joints

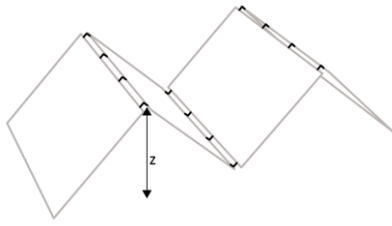


Figure I.7: Varying parameter  $z$

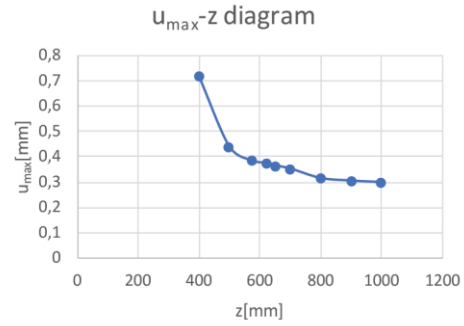


Figure I.8: Design graph for varying parameter  $z$ [mm] versus the maximum displacement[mm] in the FE model

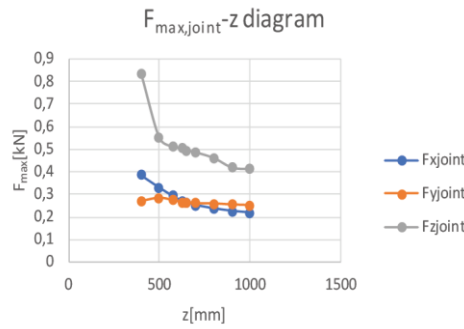


Figure I.9: Design graph for varying parameter  $z$ [mm] versus the maximum occurring force  $F_x$ ,  $F_y$ ,  $F_z$  [kN] in the joints

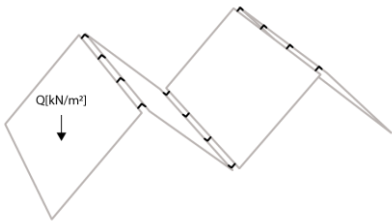


Figure I.10: Varying parameter  $Q$

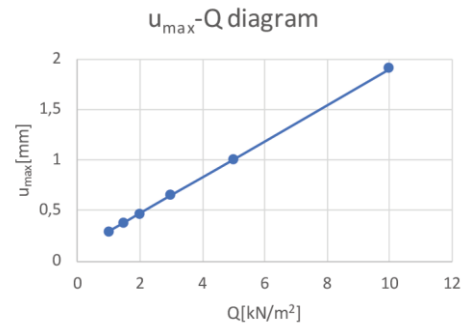


Figure I.11: Design graph for varying parameter  $Q$ [kN/m²] versus the maximum displacement[mm] in the FE model

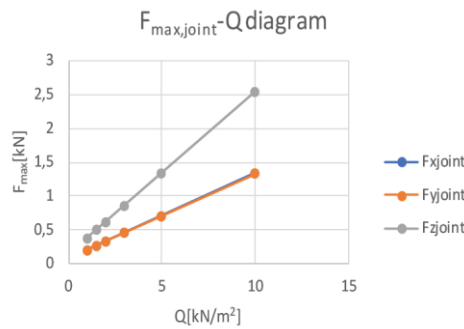


Figure I.12: Design graph for varying parameter  $Q$ [kN/m²] versus the maximum occurring force  $F_x$ ,  $F_y$ ,  $F_z$  [kN] in the joints

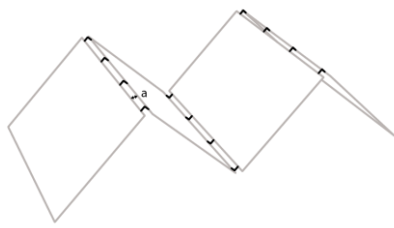


Figure I.13: Varying parameter  $a$

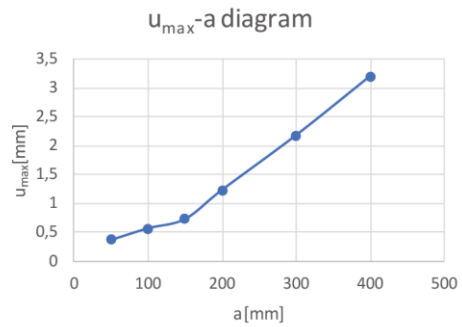


Figure I.14: Design graph for varying parameter  $a$  [mm] versus the maximum displacement [mm] in the FE model

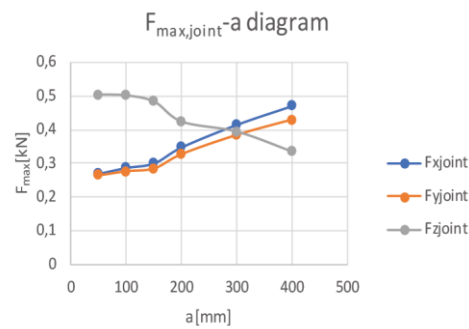


Figure I.15: Design graph for varying parameter  $a$  [mm] versus the maximum occurring force  $F_x$ ,  $F_y$ ,  $F_z$  [kN] in the joints

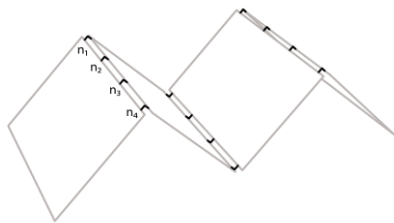


Figure I.16: Varying parameter  $n$

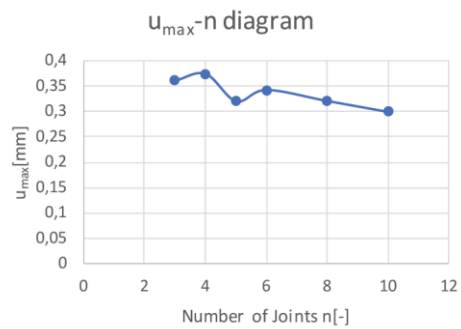


Figure I.17: Design graph for varying parameter  $n$  [-] versus the maximum displacement [mm] in the FE model

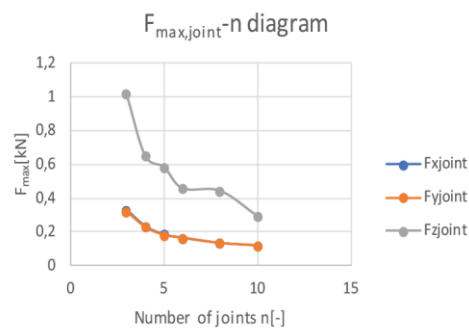


Figure I.18: Design graph for varying parameter  $n$  [-] versus the maximum occurring force  $F_x$ ,  $F_y$ ,  $F_z$  [kN] in the joints

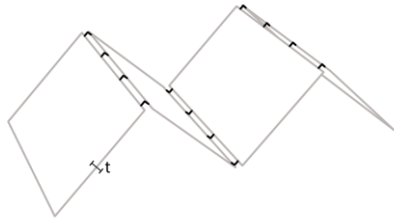


Figure I.19: Varying parameter  $t$

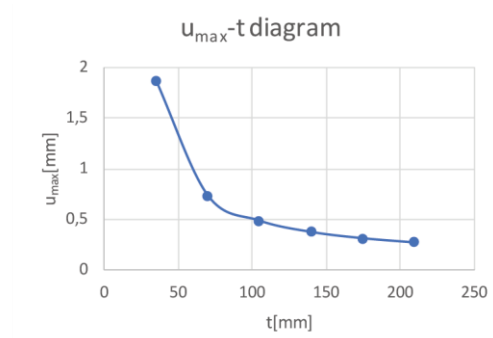


Figure I.20: Design graph for varying parameter  $t$  [mm] versus the maximum displacement [mm] in the FE model

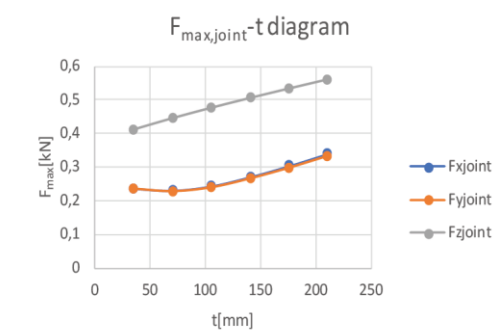


Figure I.21: Design graph for varying parameter  $t$  [mm] versus the maximum occurring force  $F_x$ ,  $F_y$ ,  $F_z$  [kN] in the joints

## Appendix K. Insufficiencies of GeometryGym

After many software updates of GeometryGym through the research, many bugs were fixed by the software developer. However, there is one software bug that still must be bypassed. This concerns the alignment of the planes on the mesh faces, as discussed in Chapter 5. Figure K.2 shows the error of the alignment of the mesh face orientation.

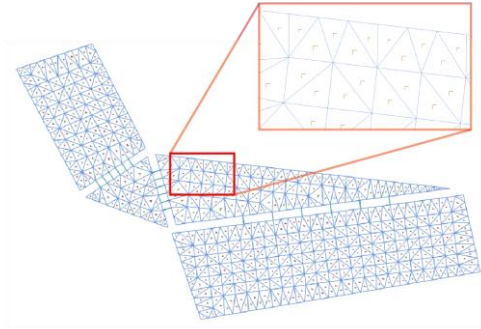


Figure K.1: Correctly aligned planes – with workaround

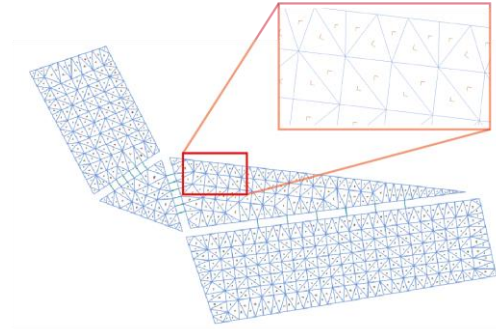


Figure K.2: Misaligned planes – without workaround

The steps to still align the planes correctly in the FEM model are listed and illustrated below.

**Step 1.** The first step is to construct a FE mesh. This mesh is misaligned as this is the bug that should be worked around. The planes can be aligned along the strong direction of the CLT plates by computing the angle between each mesh orientation and the strong direction.

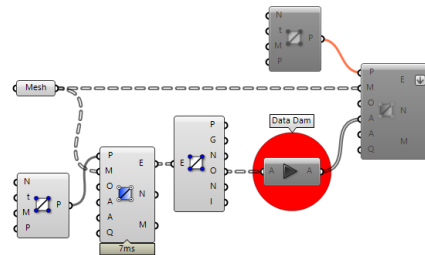


Figure K.3: Step 1. Deconstructing FE mesh and retrieve mesh orientation (O)

**Step 2.** Once the planes are aligned along the strong direction of the CLT plates by rotating them by the computed angle of step 1, the data is fed into a new FE mesh.

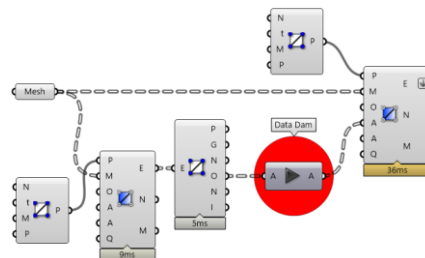


Figure K.4: Step 2. Feeding the orientation (O) into a new FE mesh

**Step 3.** Now the new mesh is constructed and the original mesh should be disabled to prevent duplicate mesh faces in the FEM model.

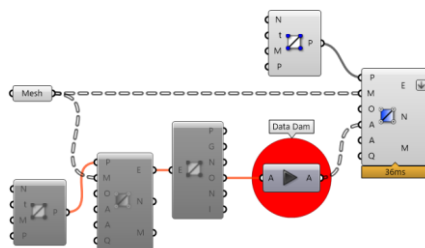


Figure K.5: Step 3. Disabling the misaligned original FE mesh

## Appendix L. Explanation of Variables for Joint Design

- a. Rotation angle of CLT plates ( $^{\circ}$ )**
- Description* The rotation angles of CLT plates are the angles between the appending structure and the CLT connection panel perpendicular to the panel. These can vary from  $[-45^{\circ} < \alpha < 45, -45 < \beta < 45^{\circ}]$ .

*Type* Integers

*Example*

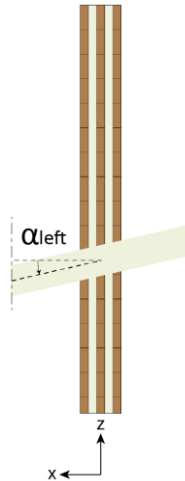


Figure L.1: Rotation angle  $\alpha$  [ $^{\circ}$ ] for appending panel in left slot

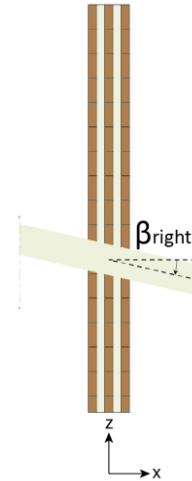


Figure L.2: Rotation angle  $\beta$  [ $^{\circ}$ ] for appending panel in right slot



Figure L.3: Grasshopper component of rotation angles

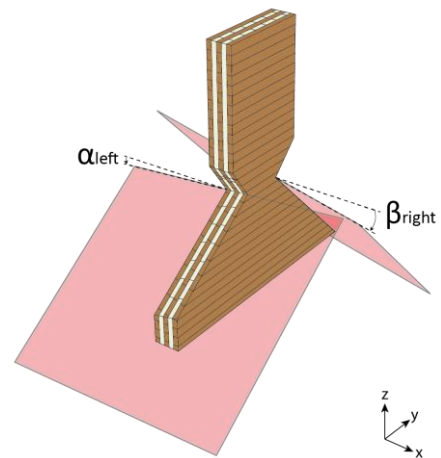


Figure L.4: 3D view for rotation angles  $\alpha$  and  $\beta$  for appending CLT panels

- b. Visualization settings** *Description* The visualization settings enable a user to generate a visualization of the connection panel to be fabricated. A few settings to customize the visualization are implemented in the workflow, to optimally prepare the panel for fabrication.

*Type* Integers

*Example*

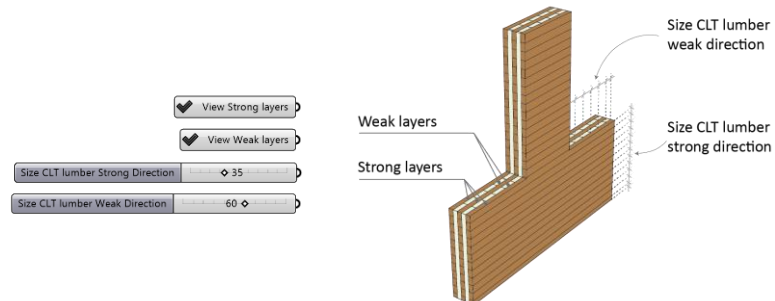


Figure L.5: Grasshopper Component and geometry of visualization settings

- c. Connection Panel Sizes** *Description* The connection panel sizes generate the initial outline of the CLT connection panel. The red ones are set numbers since they are determined by the geometry from the Global Structure module. The grey ones can be manually set by the user.

*Type* Integers

*Examples*

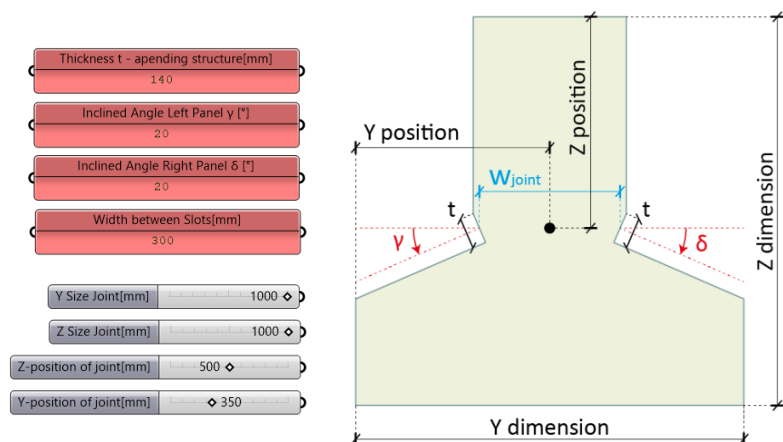


Figure L.6: Grasshopper Component and geometry of connection panel sizes. The red variables are retrieved from the Global Structure module.

- d. Cross-Sectional parameters** *Description* These parameters are the same type as the cross-sectional parameters for the Global Structure module. Therefore, more information about this variable is presented in Chapter 5.4.5 and Appendix F. They concern the following parameters:

- Cross-sectional buildup
- Wood properties
- Orientation of the first layer

*Type* Integers

e. <b>Derived forces from FEM model</b>	<p><i>Description</i> From the FEA performed on the Global Structure, the critical joint(s) force(s) can be derived. These form the input for the analytical Unity Check's in the Joint Design module. The derived local forces concern: <math>F_x</math>, <math>F_y</math>, <math>F_z</math>.</p> <p><i>Type</i> Numbers</p>
---	---

*Example*

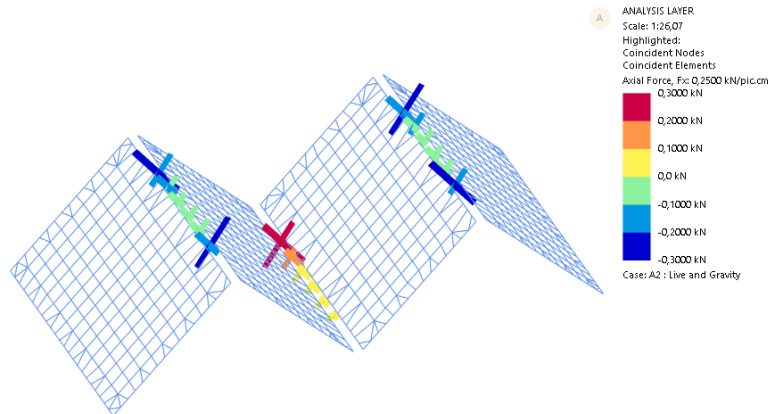


Figure L.7: Grasshopper Component and geometry of small number of joints

f. <b>Spring settings/</b>	<p><i>Description</i> Two principles that must be modelled in the FEM model are represented by springs. These concern the following:</p>
g. <b>Diameter of screws</b>	<ul style="list-style-type: none"> <li>- The <u>contact area</u> between the CLT plates and the Connection panel. This will be represented by compression springs</li> <li>- The <u>screws</u> that connect the CLT plates with the Connection panel. These will be represented by regular spring elements with stiffnesses <math>k_x</math>, <math>k_y</math>, <math>k_z</math>.</li> </ul>

Therefore, the spring settings for the Joint Design concern the following parameters:

- Number of screws
- Number of compression springs
- Diameter of screws

The diameter of the screws also is a separate variable to perform the analytical Unity Checks, but also serves as input to compute the spring settings for the FEM model. Figure L.8 shows this schematically.

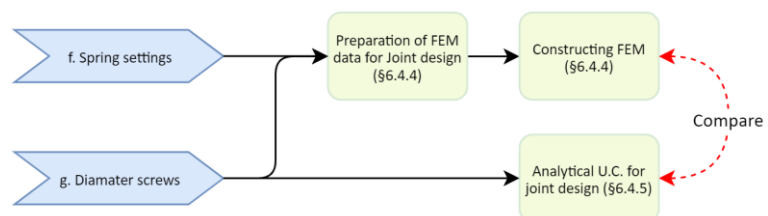


Figure L.8: Callout from the Joint Design workflow – comparison between Joint design according analytical Unity Check and the FEM

*Type* Integers



### Example

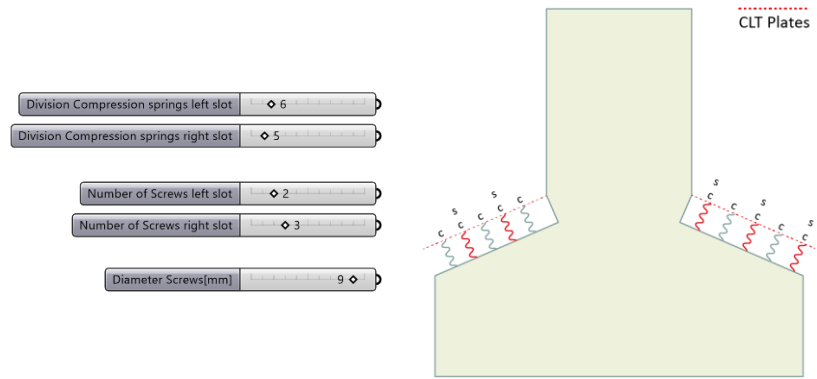


Figure L.9: Grasshopper Component and geometry of spring settings. Red: Screws (s) and compression springs (duplicate springs). Grey: Compression springs (c).

### h. Q-loading

**Description** The magnitude of the Q-loading on the appending structure can be set manually or be derived from the Global Structure module.

**Type** Integer

#### Example

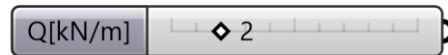


Figure L.10: Grasshopper Component and geometry of small number of joints

### i. Length of appending structure

**Description** The length of the appending structure can be derived from the Global Structure module or can be set manually. It models the appending structure, the CLT plates, as beam elements.

**Type** Integers

#### Example



Figure L.11: Grasshopper Component of the length of the appending structure

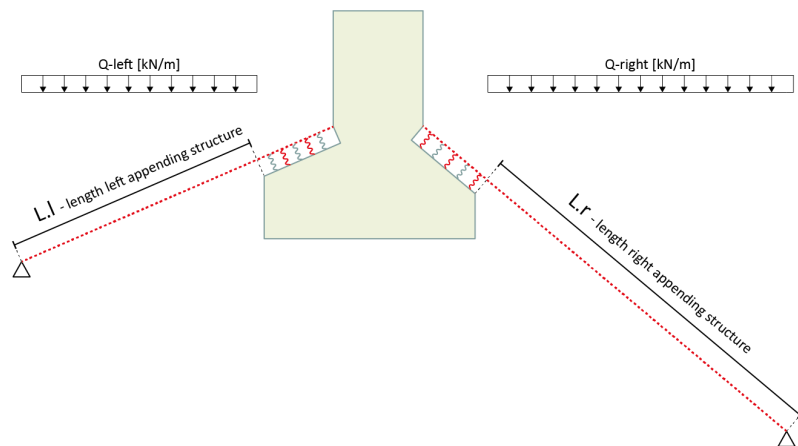


Figure L.12: Schematization of the Global Structure. This figure shows the geometry of the length of the appending structure

## Appendix M. Python Script for Analytical U.C. Cross-sections

```
1. """Provides a scripting component.
2.     Inputs:
3.         x: The x script variable
4.         y: The y script variable
5.     Output:
6.         a: The a output variable"""
7.
8. __author__ = "arjen.veldhuis"
9. __version__ = "2020.01.09"
10.
11. import rhinoscriptsyntax as rs
12.
13. LS_US = 0
14. LS_LS = 1
15. LS_USA = 2
16. LS_LSA = 3
17. LS_BS = 4
18.
19. RS_US = 5
20. RS_LS = 6
21. RS_USA = 7
22. RS_LSA = 8
23. RS_BS = 9
24.
25. MJ = 10
26.
27. #U.C. Compression of the joint-----
28.
29. def UC_fcd(N0d,t_Anet,fc0k,len,lin):
30.     sigma_cd = N0d*1000/(t_Anet*len)                #Compression Parallel
31.     #print sigma_cd
32.     fcd = fc0k*(kmod/Gamma_m)                        #Compression Parallel
33.     #print fcd
34.     if sigma_cd >= fcd:
35.         return [lin,
36.             "U.C. fcd: NOT OK (" +str(round(sigma_cd,2))+ " > " +str(round(fcd,2))+ ")",
37.             1]
38.     else:
39.         return [0,
40.             "U.C. fcd: OK (" +str(round(sigma_cd,2))+ " < " +str(round(fcd,2))+ ")",
41.             0]
42.
43.
44.
45. #U.C. Compression of the plate-----
46.
47. def UC_fcdPlate(N90,t_tot,fc90k,len,lin):
48.     sigma_90dPlate = N90*1000/(t_tot*len)
49.     #print sigma_90dPlate
50.     f_c90dPlate = fc90k*(kmod*Gamma_m)
51.     #print f_c90dPlate
52.     if sigma_90dPlate >= f_c90dPlate:
53.         return [lin,
54.             "U.C. fcd Plate: NOT OK (" +str(round(sigma_90dPlate,2))+ " > " +str(round(f_c
55.             90dPlate,2)),
56.             1]
57.         else:
58.             return [0,
59.                 "U.C. fcd Plate: OK (" +str(round(sigma_90dPlate,2))+ " < " +str(round(f_c90dP
60.                 late,2)),
```

```

59.         0]
60.
61.
62.
63. #U.C. Shear of the joint-----
    -----
64.
65. def UC_fVd(Vd,t_Anet,fVk,len,lin):
66.     tau_vd = Vd*1000/(t_Anet*len)                #Shear stress in section
67.     #print tau_vd
68.     fVd = fVk*(kmod/Gamma_m)                    #Shear resistance of joi
        nt
69.     #print fVd
70.     if tau_vd >= fVd:
71.         return [lin,
72.             "U.C. fVd: NOT OK (" +str(round(tau_vd,2))+ " > " +str(round(fVd,2))+")",
73.             1]
74.     else:
75.         return [0,
76.             "U.C. fVd: OK (" +str(round(tau_vd,2))+ " < " +str(round(fVd,2))+")",
77.             0]
78.
79.
80.
81. #U.C. Bending of the joint-----
    -----
82.
83. def UC_fMd(Mzd,t_A0net,t_A90net,fMk,len,lin):
84.     sigma_mz0d = Mzd*1000000/((t_A0net*len**2)/6)
85.     sigma_mz90d = Mzd*1000000/((t_A90net*len**2)/6)
86.     #print sigma_mz0d
87.     #print sigma_mz90d
88.     fMd = fMk*(kmod/Gamma_m)
89.     #print fMd
90.     if sigma_mz0d >= fMd and sigma_mz90d <= fMd:
91.         return [lin,
92.             "U.C. fMd0: NOT OK (" +str(round(sigma_mz0d,2))+ " > " +str(round(fMd,2))+ " and
",
93.             "U.C. fMd90: OK (" +str(round(sigma_mz90d,2))+ " < " +str(round(fMd,2))+")",
94.             1]
95.     elif sigma_mz0d <= fMd and sigma_mz90d >= fMd:
96.         return [lin,
97.             "U.C. fMd0: OK (" +str(round(sigma_mz0d,2))+ " < " +str(round(fMd,2))+ " and ",
98.             "U.C. fMd90: NOT OK (" +str(round(sigma_mz90d,2))+ " > " +str(round(fMd,2))+")"
",
99.             1]
100.    elif sigma_mz0d >= fMd and sigma_mz90d >= fMd:
101.        return [lin,
102.            "U.C. fMd0: NOT OK (" +str(round(sigma_mz0d,2))+ " > " +str(round(fMd,2))+ "
and ",
103.            "U.C. fMd90: NOT OK (" +str(round(sigma_mz90d,2))+ " > " +str(round(fMd,2))
+ ")",
104.            1]
105.    else:
106.        return [0,
107.            "U.C. fMd0: OK (" +str(round(sigma_mz0d,2))+ " < " +str(round(fMd,2))+ " and
",
108.            "U.C. fMd90: OK (" +str(round(sigma_mz90d,2))+ " < " +str(round(fMd,2))+")"
",
109.            0]
110.
111.     ""-----
    ----- ""
112.

```

```

113. #Strong layer for compression is the vertical layer (for _US and _LS)
114.     #A0net = sum(t_Anet_vert)    (only this one!)
115.
116. #Strong layer for shear is the horizontal layer (for _USA and _LSA)
117.     #A0net = sum(t_Anet_hor)    (only this one!)
118.
119. #Strong layer for bending is the horizontal layer (for _USA and _LSA)
120.     #A0net = sum(t_Anet_hor)
121.     #A90net = sum(t_Anet_vert)
122.
123. """-----
-----"""
124.
125. #0 LS_US
126. #Anet_LS_US_fcd = sum(t_Anet_vert)          #LS_US compression
127. #fcd_LS_US = Vup_l
128.
129. #1 LS_LS
130. Anet_LS_LS_fcd = sum(t_Anet_vert)          #LS_LS compression
131. fcd_LS_LS = Vdown_l
132.
133. #2 LS_USA
134. #Anet_LS_USA_fVd = sum(t_Anet_hor)          #LS_USA shear
135. #fVd_LS_USA = Vup_l
136. #A0net_LS_USA_fMd = sum(t_Anet_hor)          #LS_USA bending
137. #A90net_LS_USA_fMd = sum(t_Anet_vert)        #LS_USA bending
138. #fMd_LS_USA = max(Mup_l,Mdown_l)
139.
140. #3 LS_LSA
141. Anet_LS_LSA_fVd = sum(t_Anet_hor)          #LS_LSA shear
142. fVd_LS_LSA = Vdown_l
143. A0net_LS_LSA_fMd = sum(t_Anet_hor)          #LS_LSA bending
144. A90net_LS_LSA_fMd = sum(t_Anet_vert)        #LS_LSA bending
145. fMd_LS_LSA = max(Mup_l,Mdown_l)
146.
147. #4 LS_BS
148. #Anet_LS_BS_fcd = sum(t_Anet_hor)          #LS_BS compression
149. #fcd_LS_BS = Ncompr_l
150.
151. """-----
-----"""
152.
153. #5 RS_US
154. #Anet_RS_US_fcd = sum(t_Anet_vert)          #RS_US compression
155. #fcd_RS_US = Vup_r
156.
157. #6 RS_LS
158. Anet_RS_LS_fcd = sum(t_Anet_vert)          #RS_LS compression
159. fcd_RS_LS = Vdown_r
160.
161. #7 RS_USA
162. #Anet_RS_USA_fVd = sum(t_Anet_hor)          #RS_USA shear
163. #fVd_RS_USA = Vup_r
164. #A0net_RS_USA_fMd = sum(t_Anet_hor)          #RS_USA bending
165. #A90net_RS_USA_fMd = sum(t_Anet_vert)        #RS_USA bending
166. #fMd_RS_USA = max(Mup_r,Mdown_r)
167.
168. #8 RS_LSA
169. Anet_RS_LSA_fVd = sum(t_Anet_hor)          #RS_LSA shear
170. fVd_RS_LSA = Vdown_r
171. A0net_RS_LSA_fMd = sum(t_Anet_hor)          #RS_LSA bending
172. A90net_RS_LSA_fMd = sum(t_Anet_vert)        #RS_LSA bending
173. fMd_RS_LSA = max(Mup_r,Mdown_r)
174.
175. #9 RS_BS
176. #Anet_RS_BS_fcd = sum(t_Anet_hor)          #RS_BS compression

```

```

177. #fcd_RS_BS = Ncompr_r
178.
179. """-----
-----"""
180.
181. #10 MJ
182. Anet_MJ_fVd = sum(t_Anet_vert) #MJ shear
183. fVd_MJ = abs(Ncompr_l-Ncompr_r)
184.
185. """-----
-----"""
186.
187.
188.
189.
190.
191.
192.
193. #0-----Checking of Left Slot - Upper Side (LS_US)-----
-----
194. #UC_LS_US_fcd = UC_fcd(fcd_LS_US,Anet_LS_US_fcd,fc0k,len[LS_US],lin[LS_US])
195.
196.
197.
198. #1-----Checking of Left Slot - Lower Side (LS_LS)-----
-----
199. UC_LS_LS_fcd = UC_fcd(fcd_LS_LS,Anet_LS_LS_fcd,fc0k,len[LS_LS],lin[LS_LS])
200.
201.
202.
203. #2-----Checking of Left Slot - Upper Shear Area (LS_USA)-----
-----
204. #UC_LS_USA_fVd = UC_fVd(fVd_LS_USA,Anet_LS_USA_fVd,fVk,len[LS_USA],lin[LS_USA])
205. #UC_LS_USA_fMd = UC_fMd(fMd_LS_USA,A0net_LS_USA_fMd,A90net_LS_USA_fMd,fMk,len[LS_USA],lin[LS_USA])
206.
207.
208.
209. #3-----Checking of Left Slot - Lower Shear Area (LS_LSA)-----
-----
210. UC_LS_LSA_fVd = UC_fVd(fVd_LS_LSA,Anet_LS_LSA_fVd,fVk,len[LS_LSA],lin[LS_LSA])
211. UC_LS_LSA_fMd = UC_fMd(fMd_LS_LSA,A0net_LS_LSA_fMd,A90net_LS_LSA_fMd,fMk,len[LS_LSA],lin[LS_LSA])
212.
213.
214.
215. #4-----Checking of Left Slot - Back Side (LS_BS)-----
-----
216. #UC_LS_BS_fcd = UC_fcd(fcd_LS_BS,Anet_LS_BS_fcd,fc0k,len[LS_BS],lin[LS_BS])
217.
218.
219.
220.
221.
222.
223.
224. #5-----Checking of Right Slot - Upper Side (RS_US)-----
-----
225. #UC_RS_US_fcd = UC_fcd(fcd_RS_US,Anet_RS_US_fcd,fc0k,len[RS_US],lin[RS_US])
226.
227.
228.
229. #6-----Checking of Right Slot - Lower Side (RS_LS)-----
-----
230. UC_RS_LS_fcd = UC_fcd(fcd_RS_LS,Anet_RS_LS_fcd,fc0k,len[RS_LS],lin[RS_LS])

```

```

231.
232.
233.
234.  #7-----Checking of Right Slot - Upper Shear Area (RS_USA)---
      -----
235.  #UC_RS_USA_fVd = UC_fVd(fVd_RS_USA,Anet_RS_USA_fVd,fVk,len[RS_USA],lin[RS_USA])
236.  #UC_RS_USA_fMd = UC_fMd(fMd_RS_USA,A0net_RS_USA_fMd,A90net_RS_USA_fMd,fMk,len[RS_
      _USA],lin[RS_USA])
237.
238.
239.
240.  #8-----Checking of Right Slot - Lower Shear Area (RS_LSA)---
      -----
241.  UC_RS_LSA_fVd = UC_fVd(fVd_RS_LSA,Anet_RS_LSA_fVd,fVk,len[RS_LSA],lin[RS_LSA])
242.  UC_RS_LSA_fMd = UC_fMd(fMd_RS_LSA,A0net_RS_LSA_fMd,A90net_RS_LSA_fMd,fMk,len[RS_
      LSA],lin[RS_LSA])
243.
244.
245.
246.  #9-----Checking of Right Slot - Back Side (RS_BS)-----
      -----
247.  #UC_RS_BS_fcd = UC_fcd(fcd_RS_BS,Anet_RS_BS_fcd,fc0k,len[RS_BS],lin[RS_BS])
248.
249.
250.
251.
252.
253.
254.  #10-----Checking of Middle Joint (MJ)-----
      -----
255.  UC_MJ_fVd = UC_fVd(fVd_MJ,Anet_MJ_fVd,fVk,len[MJ],lin[MJ])
256.
257.
258.
259.
260.  #11-----Checking of Plate-----
261.  UC_Plate_Vdown_l = UC_fcdPlate(Vdown_l,t_tot,fc90k,len[LS_LS],lin[LS_LS])
262.  UC_Plate_Vdown_r = UC_fcdPlate(Vdown_r,t_tot,fc90k,len[RS_LS],lin[RS_LS])
263.
264.
265.
266.  print 'Netto t_Area horizontal layers is ', sum(t_Anet_hor)
267.  print 'Netto t_Area vertical layers is ', sum(t_Anet_vert)

```

## Appendix N. Python Script for Analytical U.C. Screws

```
1. """Provides a scripting component.
2.     Inputs:
3.         x: The x script variable
4.         y: The y script variable
5.     Output:
6.         a: The a output variable"""
7.
8. __author__ = "arjen.veldhuis"
9. __version__ = "2020.01.13"
10.
11. import rhinoscriptsyntax as rs
12. import math as mt
13.
14. LS_US = 0
15. LS_LS = 1
16. LS_USA = 2
17. LS_LSA = 3
18. LS_BS = 4
19.
20. RS_US = 5
21. RS_LS = 6
22. RS_USA = 7
23. RS_LSA = 8
24. RS_BS = 9
25.
26. MJ = 10
27.
28. #U.C. Against shearing off of screws-----
29.
30. def UCscrews_Vd(N,d,Rvk,len,lin):
31.     n_shear = mt.ceil((len-7*d-
32.         12*d)/(10*d)) #Check minimum distances of screws
33.     print 'n_shear =', n_shear
34.     neff = mt.ceil(n_shear**0.85)
35.     Rvkd = neff*Rvk
36.     if N >= Rvkd:
37.         return [lin,
38.             "Number of screws: "+str(neff),
39.             "U.C. screws: NOT OK (" +str(round(N,2))+" > " +str(round(Rvkd,2))+" )",
40.             1]
41.     else:
42.         return [0,
43.             "Number of screws: "+str(neff),
44.             "U.C. Screws: OK (" +str(round(N,2))+" < " +str(round(Rvkd,2))+" )",
45.             0]
46.
47.
48. #U.C. Against withdrawal of screws-----
49.
50. def UCscrews_Raxd(Nax,d,Raxk,len,lin):
51.     n_wd = mt.ceil((len-7*d-
52.         12*d)/(10*d)) #Check minimum distances of screws
53.     print 'n_wd =', n_wd
54.     Raxd = n_wd*Raxk
55.     if Nax >= Raxd:
56.         return [lin,
57.             "Number of screws: "+str(n_wd),
58.             "U.C. screws: NOT OK (" +str(round(Nax,2))+" > " +str(round(Raxd,2))+" )",
59.             1]
```

```

59.     else:
60.         return [0,
61.                 "Number of screws: "+str(n_wd),
62.                 "U.C. Screws: OK (" +str(round(Nax,2))+ " < " +str(round(Raxd,2))+")",
63.                 0]
64.
65.
66. #U.C. against withdrawal of left side
67. UC_LS_Raxd = UCscrews_Raxd(Vup_l,d,Raxk,len[LS_LS],lin[LS_LS])
68.
69.
70.
71. #U.C. against withdrawal of right side
72. UC_RS_Raxd = UCscrews_Raxd(Vup_r,d,Raxk,len[RS_LS],lin[RS_LS])
73.
74.
75.
76. #U.C. against shearing off of left side
77. Vy_l = max(Vypos_l,Vyneg_l)
78. UC_LS_RVd = UCscrews_Vd(Vy_l,d,RVk,len[LS_LS],lin[LS_LS])
79.
80.
81.
82. #U.C. against shearing off of right side
83. Vy_r = max(Vypos_r,Vyneg_r)
84. UC_RS_RVd = UCscrews_Vd(Vy_r,d,RVk,len[RS_LS],lin[RS_LS])

```



## Appendix O. Spring Stiffnesses for Screws

This appendix describes all actual values for spring stiffnesses for screws and the contact area between CLT plates and the CLT connection panel.

For the **screws**, resistances in the following local directions are modelled:

- x-direction: withdrawal resistance [kN]
- y-direction: shear resistance [kN]
- z-direction: shear resistance [kN]

The resistances are retrieved from product sheets of manufacturers. An example is the VGS fully threaded screw from Rothoblaas [66]. In case the shear resistances are not provided in the product sheet, these are calculated by Formula (15), according the NEN 1995-1-1 (7.1) [20]. The data for the screw resistances is retrieved from Rothoblaas and a thesis about modular cross-laminated timber buildings. [67]

$$K_{ser} = \frac{\rho_m^{1.5} * d}{23} \quad [\text{N/mm}] \quad (15)$$

$\rho_m$  = Density of CLT [kg/m<sup>3</sup>]  
 $d$  = Diameter of the screw [mm]



For this research, the following data is used:

$\rho_m$  = 400 kg/m<sup>3</sup>  
 $d$  = 9 mm

CHARACTERISTICS	
FOCUS	42° connections, lifting and reinforcements
HEAD	countersunk with ribs for L < 600 mm hexagonal for L > 600 mm
DIAMETER	9.0   11.0   13.0 mm
LENGTH	from 100 mm to 3200 mm

$k_{ser,y}$  (shear) = 3130 N/mm [20]  
 $k_{ser,z}$  (shear) = 3130 N/mm [20]  
 $K_{ser,x}$  (tension) = 17600 N/mm [67]

For the **contact area**, springs are modelled as compression-only springs. The total contact area between the CLT plates and the connection panel is divided by the number of modelled springs. As the contact area is represented by compression-only springs, the stiffness can be derived from Formula (16).

$$K_{compr} = K_x = \frac{E_{CLT} * A_{spring}}{l_{spring}} \quad [\text{N/mm}] \quad (16)$$

$E_{CLT}$  = E-modulus of CLT [N/mm<sup>2</sup>]  
 $A_{spring}$  = Area distributed to spring [mm<sup>2</sup>]  
 $l_{spring}$  = Length of the spring [mm]

For this research, the following data is used:

$E_{CLT}$  =  $E_{strong}$  N/mm<sup>2</sup>  
 $A_{spring}$  = Depending on geometry mm<sup>2</sup>  
 $l_{spring}$  =  $t_{CLT,appending} / 2$  mm  
 $k_{ser,x}$  = Depending on geometry N/mm  
 $k_{ser,y}$  = 0 N/mm  
 $k_{ser,z}$  = 0 N/mm

# Appendix P. Input for the FEM of Joint Design

## INPUT: Geometry and supporting conditions.

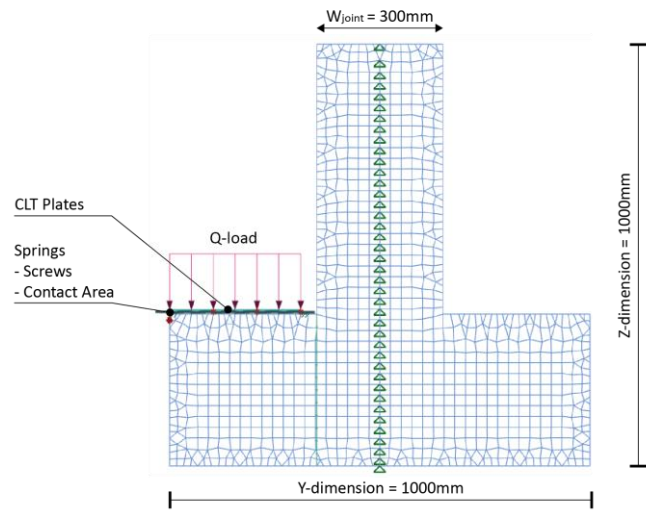


Figure P.1: GSA geometrical input

## INPUT: Beam sections.

The beam sections correspond with the plate material properties as explained in Chapter 6.4.4.

## INPUT: Mesh material properties.

Parameter	Magnitude	Unit	Parameter	Magnitude	Unit
$E_0$	7931	N/mm <sup>2</sup>	$G_{xy}$	248	N/mm <sup>2</sup>
$E_{90}$	3438	N/mm <sup>2</sup>	$G_{yz}$	100	N/mm <sup>2</sup>
$t_{plate}$	140	mm	$G_{zx}$	127	N/mm <sup>2</sup>
$\rho$	400	kg/m <sup>3</sup>			

## INPUT: Spring properties

Element	$k_x$	$k_y$	$k_z$
Screws*	17.600 kN/m	3.130 kN/m	3.130 kN/m
Contact Area	Variable kN/m	0 kN/m	0 kN/m

(Compression-only)

The magnitude of the spring stiffnesses that represent the screws is elaborated in Appendix P.

## INPUT: Loading.

	Load case	Magnitude	Unit
LC1	Variable loading on mesh elements (global z-axis)	-6	kN/m <sup>2</sup>

## INPUT: Analyses task.

Static analyses: LC1

## Appendix Q. Validation of FEM Joint models

For the analytical U.C., the shear force and -stress are calculated by Formulas (17) and (18). The shear force from the FE models are retrieved through a constructed assembly along the highlighted cross-section. The results of the occurring forces in these assemblies are shown hereafter.

$$F_V = q * l_{beam} \quad (17)$$

$$\tau_V = \frac{F_V}{A_{net}} \quad (18)$$

### Q.1 GEOMETRY 1.YL.ZH

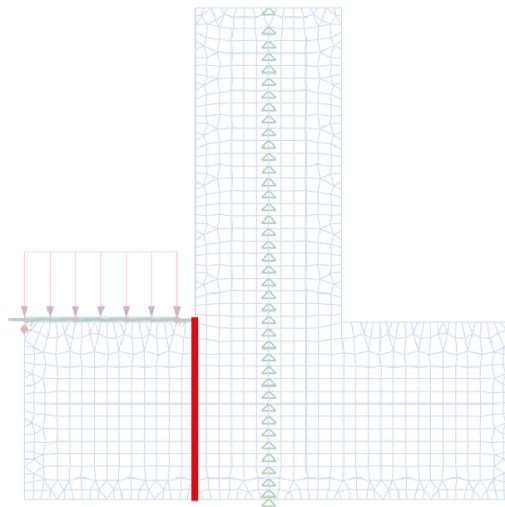


Figure Q.1: Cross-section of the joint along which the shear force and -stress are measured

#### Grasshopper Parameters

Width between slots:	300 mm
Z-position of joint:	570 mm
Y-position of joint:	350 mm
Number of screws:	3 [-]
Mesh res.	50 [-]
Z dimension	1000 mm
Y dimension	1000 mm
t <sub>plate</sub>	140 mm

#### Geometrical/structural parameters

t <sub>net</sub>	80 mm
h <sub>SA</sub>	360 mm
q	6 kN/m
l-beam	312 mm
A <sub>net</sub>	28800 mm <sup>2</sup>
V	1872 N
□-FEM	0,062487 N/mm <sup>2</sup>
□-U.C.	0,0650 N/mm <sup>2</sup>
Deviation	0,0025 N/mm <sup>2</sup>

#### Results

Model	Shear Force $F_V$	Shear stress $\tau_V$
Analytical U.C.	1,872 kN	0.065 N/mm <sup>2</sup>
FEM	1,79963 kN	0,062487153 N/mm <sup>2</sup>
Deviation	3.87 %	

Q.2 GEOMETRY 2.YL.ZL

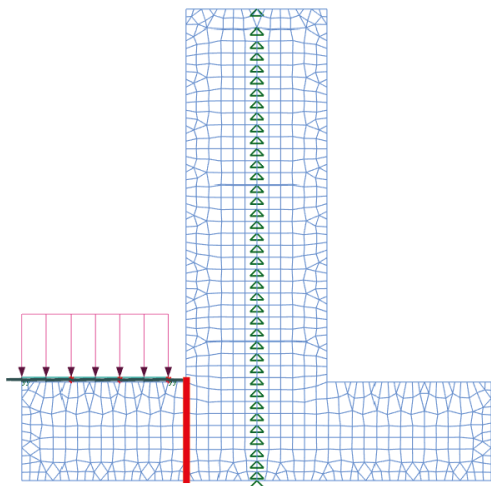


Figure Q.2: Cross-section of the joint along which the shear force and -stress are measured

Grasshopper Parameters

Width between slots:	300 mm
Z-position of joint:	720 mm
Y-position of joint:	350 mm
Number of screws:	3 [-]
Mesh res.	50 [-]
Z dimension	1000 mm
Y dimension	1000 mm
t_plate	140 mm

Geometrical/structural Parameters

t_net	80 mm
h_SA	210 mm
q	6 kN/m
I-beam	312 mm
Anet	16800 mm2
V	1872 N
□-FEM	0,09902321 N/mm2
□-U.C.	0,11142857 N/mm2
Deviation	0,01240536 N/mm2

Results

Model	Shear Force $F_v$	Shear stress $\tau_v$
Analytical U.C.	1,872 kN	0,11142857 N/mm <sup>2</sup>
FEM	1,66359 kN	0,09902321 N/mm <sup>2</sup>
Deviation	11,1 %	

Q.3 GEOMETRY 3.YS.ZH

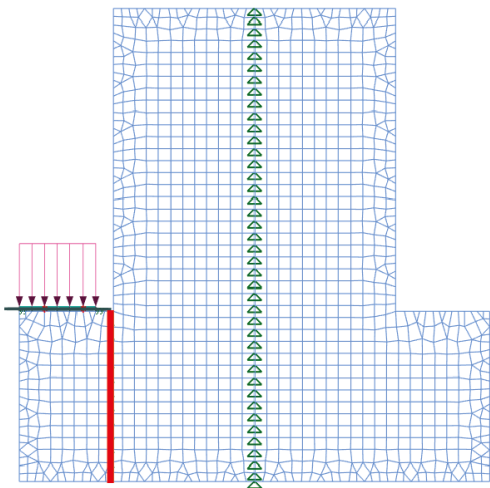


Figure Q.3: Cross-section of the joint along which the shear force and -stress are measured

Grasshopper Parameters

Width between slots:	600 mm
Z-position of joint:	570 mm
Y-position of joint:	200 mm
n:	2 [-]
Mesh res.	50 [-]
Z dimension	1000 mm
Y dimension	1000 mm
t_plate	140 mm

Geometrical/structuralParameters

t_net	80 mm
h_SA	360 mm
q	6 kN/m
I-beam	162 mm
Anet	28800 mm2
V	972 N
□-FEM	0,03069 N/mm2
□-U.C.	0,03375 N/mm2
Deviation	0,00306 N/mm2

Results

Model	Shear Force $F_v$	Shear stress $\tau_v$
Analytical U.C.	0,972 kN	0,03375 N/mm <sup>2</sup>
FEM	0,883862 kN	0,03069 N/mm <sup>2</sup>
Deviation	9,1 %	

Q.4 GEOMETRY 4.YS.ZL

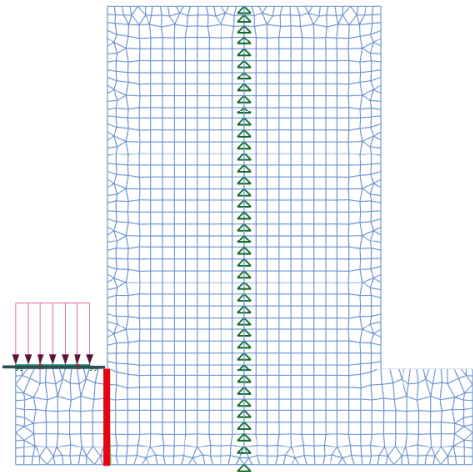


Figure Q.4: Cross-section of the joint along which the shear force and -stress are measured

Grasshopper Parameters

Width between slots:	600 mm
Z-position of joint:	720 mm
Y-position of joint:	200 mm
n:	2 [-]
Mesh res.	50 [-]
Z dimension	1000 mm
Y dimension	1000 mm
t_plate	140 mm

Geometrical/structural Parameters

t_net	80 mm
h_SA	210 mm
q	6 kN/m
I-beam	162 mm
Anet	16800 mm2
V	972 N
□-FEM	0,056359 N/mm2
□-U.C.	0,057857 N/mm2
Deviation	0,001498 N/mm2

Results

Model	Shear Force $F_V$	Shear stress $\tau_V$
Analytical U.C.	0,972 kN	0,057857 N/mm <sup>2</sup>
FEM	0,946828 kN	0,056359 N/mm <sup>2</sup>
Deviation	2,6 %	

## Appendix R. Methodologies to determine Spring Stiffness

### R.1 M-PHI RELATIONSHIP OF A CLT CONNECTION PANEL

The first step in determining the correct representative rotational spring stiffness, is to investigate the relationship between the applied moment at a joint and the occurring nodal rotation of it. Figure R.1 shows the geometry that was used to investigate this. The joint is clamped at the extended intersection of the two plates and a unit moment (1kNm) was applied at the end of the left plate.

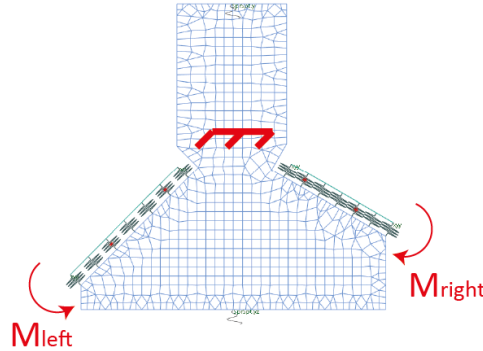


Figure R.1: Geometry to investigate the M-phi relationship

The result of this quick study is shown below. The M-phi relationship shows to behave linearly. Therefore, the first methodology is to apply a unit moment (1kNm) at the edge of the plates. The rotational stiffness can subsequently be determined by Formula (19).

$$K_r = \frac{M}{\phi} = \frac{1kNm}{\phi} \quad (19)$$

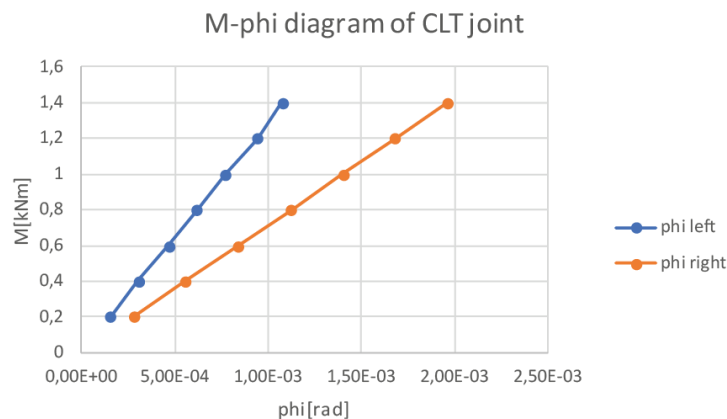


Figure R.2: Resulting M-phi diagram

## R.2. METHODOLOGY 1

Figure R.3 shows a schematization of the first methodology. The right half of the joint is clamped, and the occurring rotation is measured under a loading of a unit moment (1kNm).

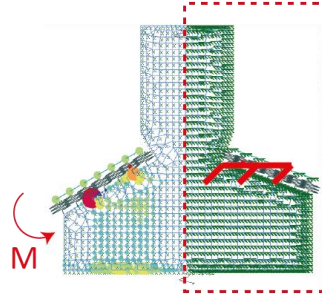


Figure R.3: Schematization of methodology 1 to determine spring stiffness

**Results.** Based on the linear relationship found between the applied moment  $M$  and the occurring rotation  $\phi$ , the results did not converge to the full model. The deviation was large, and the rotational spring model behaved too stiff.

## R.3. METHODOLOGY 2

Given the fact that clamping side of the joint resulted in too stiff behavior of the springs, the second method only clamped the joint at the edge of the non-loaded plate. Figure R.4 shows a schematization of this situation.

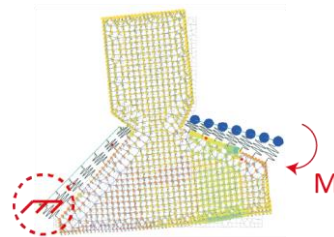


Figure R.4: Schematization of methodology 2 to determine spring stiffness

**Results.** The rotational spring model and the full model showed a finer match than with the first methodology. The springs did not behave too stiff, and the deviation was reduced to 30.64%. However, 30.64% is still much deviation. Therefore, methodology 3 is introduced.

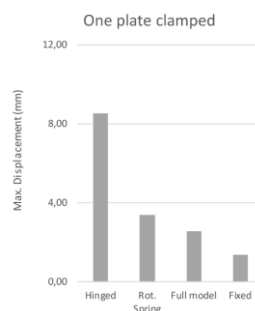


Figure R.5: Results of methodology2 to determine the spring stiffness of the joint



## R.4. METHODOLOGY 3

As the representative springs behaved too stiff in the second methodology, spring supports are introduced. This will force the joint to resist the momentum forces by itself, instead of by the clamped connections. However, the unit moment (1kNm) should be applied at both ends of the plates to let the model converge to an equilibrium. Figure R.6 shows a schematization of this situation.

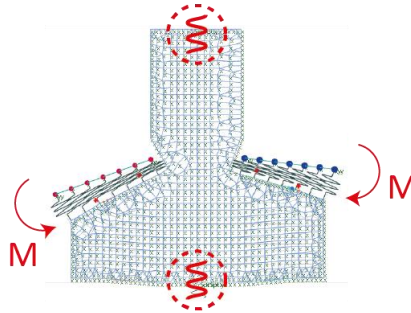


Figure R.6: Schematization of methodology 3 to determine spring stiffness

**Results.** This methodology showed a finer convergence than the methodologies 1 and 2. It only deviated 5.38% from the full model. Figures R.7-R.8 show this result.

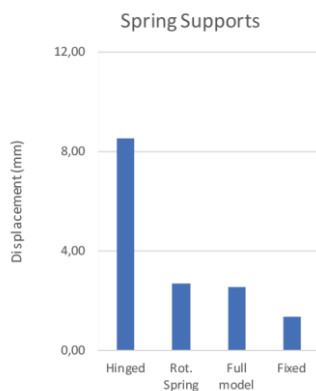


Figure R.7: Results of methodology 3 to determine the spring stiffness of the joint

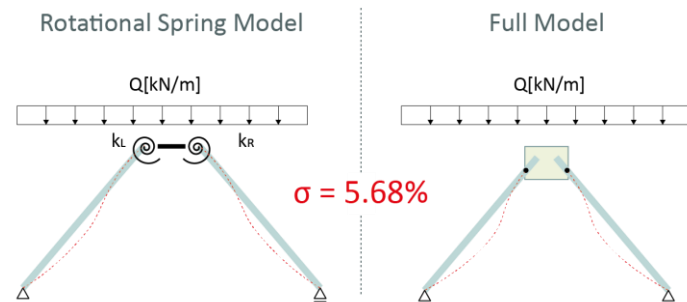


Figure R.8: 5.38% deviation between the representative spring model and the full model

**Further elaboration of Methodology 3.** Based on the result shown above, this methodology is further elaborated. Due to the relative large dimensions of the connection panel, there is uncertainty about the distribution of the bending moment within the panel. Therefore, it is assumed to model the rotational springs in the middle of the CLT plates in the slotted hole. This is shown in right picture. In between the rotational springs an infinite stiff beam is modelled as the connection panel itself is very stiff regarding bending in-plane as well. These assumptions result in the following rotational spring model as shown in Figure R.10.

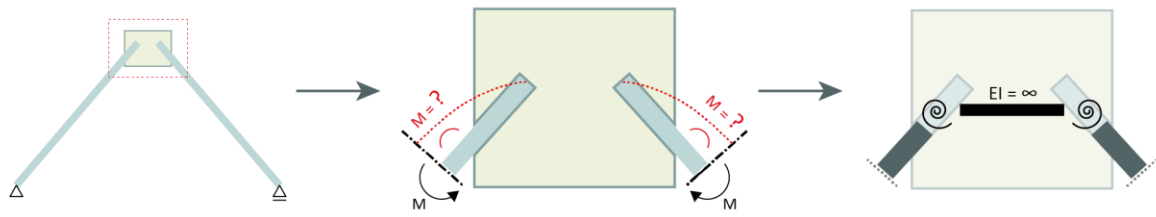


Figure R.9: Left: full model. Middle: uncertain distribution of the bending moment along the CLT plates. Right: proposed simplified modelling of rotational springs in the middle of the slotted holes.

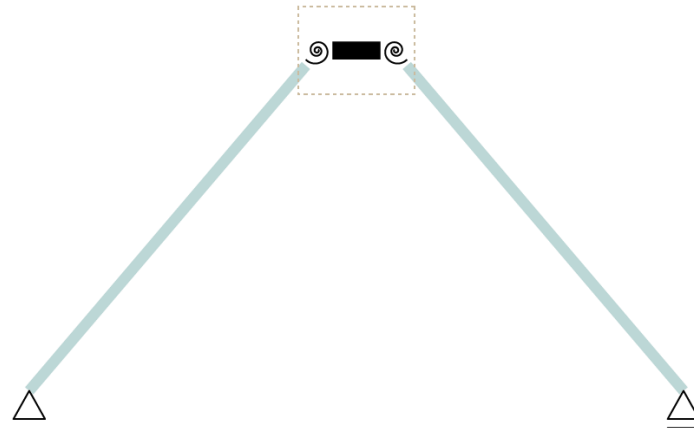


Figure R.10: Simplified Rotational spring model

Based on the result and assumptions as described above, variants were set up to further verify the methodology. The following parameters were varied among different models.

<ul style="list-style-type: none"> <li>- <u>J</u>oint Size: <ul style="list-style-type: none"> <li>o <u>S</u>mall JS</li> <li>o <u>L</u>arge JL</li> </ul> </li> <li>- <u>A</u>ngles: <ul style="list-style-type: none"> <li>o <u>F</u>lat AF</li> <li>o <u>S</u>teep AS</li> </ul> </li> <li>- Appending Structure: <ul style="list-style-type: none"> <li>o <u>S</u>ymmetrical SS</li> <li>o <u>A</u>symmetrical SA</li> </ul> </li> <li>- <u>L</u>oad Intensity: <ul style="list-style-type: none"> <li>o <u>L</u>ow L-L</li> <li>o <u>H</u>igh L-H</li> </ul> </li> <li>- <u>L</u>oad symmetry: <ul style="list-style-type: none"> <li>o <u>S</u>ymmetrical L-S</li> <li>o <u>A</u>symmetrical L-A</li> </ul> </li> </ul>	→	JS_AS_SS_L-LS	1
		JS_AS_SS_L-LA	2
		JS_AS_SS_L-HS	3
		JS_AS_SS_L-HA	4
		JS_AS_SA_L-LS	5
		JS_AS_SA_L-LA	6
		JS_AS_SA_L-HS	7
		JS_AS_SA_L-HA	8
		JS_AF_SS_L-LS	9
		JS_AF_SS_L-LA	10
		JS_AF_SS_L-HS	11
		JS_AF_SS_L-HA	12
		JS_AF_SA_L-LS	13
		JS_AF_SA_L-LA	14
		JS_AF_SA_L-HS	15
		JS_AF_SA_L-HA	16
		JL_AS_SS_L-LS	17
		JL_AS_SS_L-LA	18
		JL_AS_SS_L-HS	19
		JL_AS_SS_L-HA	20
		JL_AS_SA_L-LS	21
		JL_AS_SA_L-LA	22
		JL_AS_SA_L-HS	23
		JL_AS_SA_L-HA	24
		JL_AF_SS_L-LS	25
		JL_AF_SS_L-LA	26
		JL_AF_SS_L-HS	27
		JL_AF_SS_L-HA	28
		JL_AF_SA_L-LS	29
		JL_AF_SA_L-LA	30
		JL_AF_SA_L-HS	31
		JL_AF_SA_L-HA	32

**Final results.** The variants all show some deviation, and the average deviation across all variants is 48.1%, which is too large to create a reliable representative spring model. Further investigation of convergence of the results towards the full model is elaborated in Methodology 4.

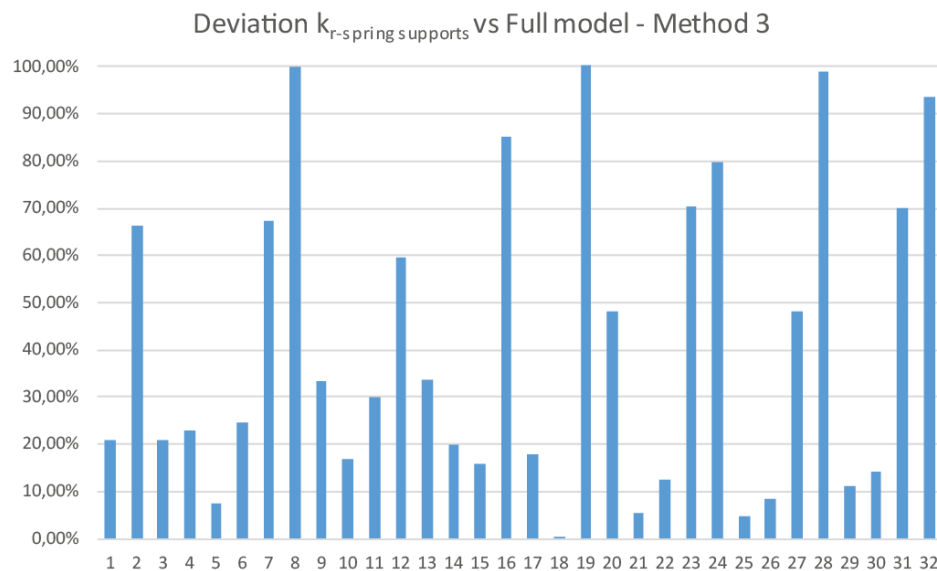


Figure R.11: Deviation between the rotational spring model and the full model among different variants, modelled according methodology 3.

## R.5. METHODOLOGY 4

Even though in the beginning of this chapter it was stated that there is a linear relationship between the applied moment  $M$  and the occurring rotation  $\phi$ , this methodology does consider a unit moment (1kNm) as the applied force at the joint. However, the normal, shear and moment sectional forces derived from the global structure model are applied on the joint. The occurring rotation will be measured and divided by the moment applied. Figure R.12 shows this principle.

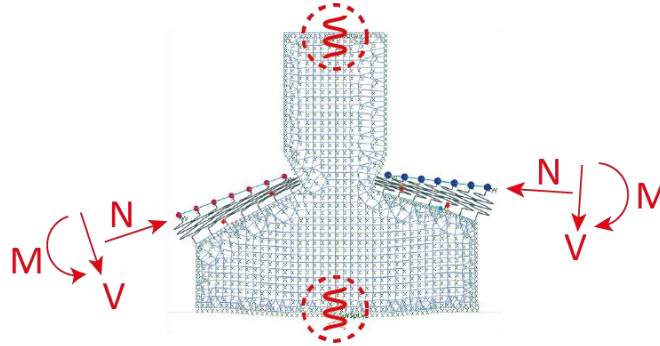


Figure R.12: Schematization of methodology 4 to determine spring stiffness

Briefly stated, there are four steps involved in this methodology:

1. Retrieve sectional force from the Global structure, as described in Chapter 5.6
2. Induce these forces as loading on a separate joint model and determine the rotational stiffness by  $k_r = M/\Phi$
3. Feed the stiffness back to the rotational spring model
4. Verify with the full model

**Results.** The same 32 variants are processed as the ones in methodology 3. However, the results still show an average deviation of 31.9%. This still is too much to generate a feedback loop that feeds a representative spring stiffness to the joints in the global structure.

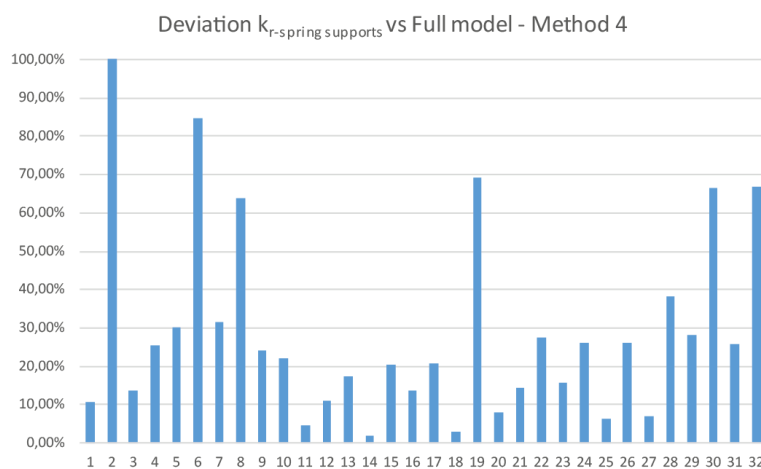


Figure R.13: Deviation between the rotational spring model and the full model among different variants, modelled according methodology 4.

The following graph can be obtained if looking at the deviation of the results of methodology 4.

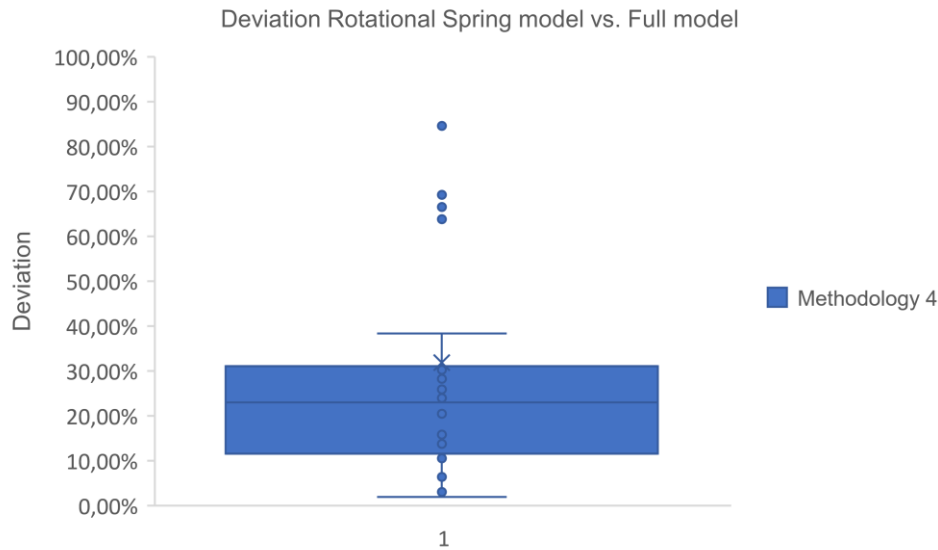


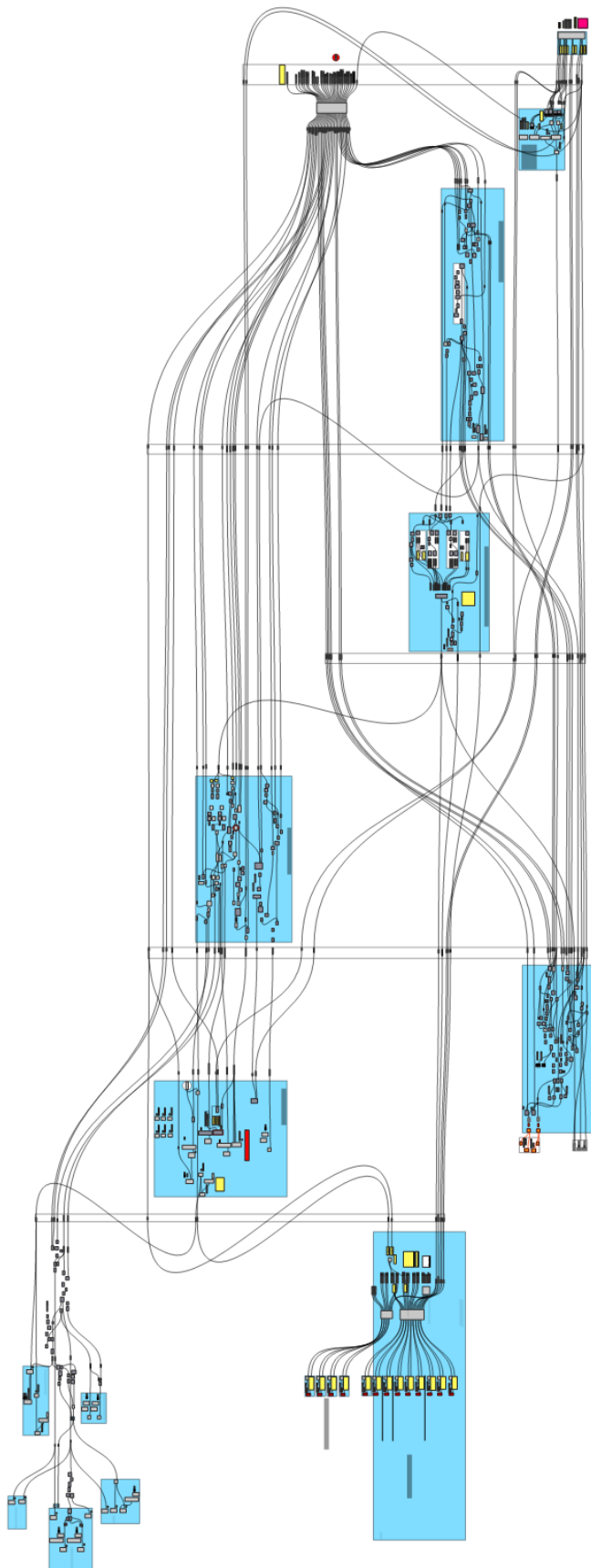
Figure R. 14:: Deviation between the rotational spring model and the full model among different variants, modelled according methodology 4.

**Conclusion.** After analyzing the results and applying different methodologies, it was concluded there is no universal methodology with 100% accuracy found, to determine the exact representative (spring) stiffness. This presumably relates to the following reasons:

- The size of the joint is too large to catch the entire behavior in one or two rotational springs.
- The appending CLT plates can barely bend and rotate in the slotted hole of the connection panel, in case of the full model. However, in the representative spring model, they are only restricted to bend or rotate by the rotational springs.
- The iterations the full model undergoes due to the modelling of the compression-only springs. This behavior and result cannot be covered or simulated in a representative spring model.

After all, the workflow does allow for a feedback loop of the spring stiffness back to the Global Structure module. However, different methodologies relate to different levels of accuracy. At this moment, no universal method is found with 100% accuracy. Therefore, a designer should carefully evaluate the desired level of accuracy to implement a feedback loop with the spring stiffness, to get a more reliable understanding of the global structural performance. Besides, determining the stiffness of joints should be utilized to determine correlations between the normalized magnitude of the stiffness of the joints and different design parameters of the connection panel. Chapter 6.7 and 6.8 illustrate these correlations.

## Appendix S. Script for Joint Design Module



# Appendix T. Design Graphs for Joint Design

Varying parameter

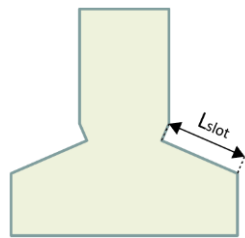


Figure T.1: Varying parameter  $L_{slot}$

Derived design graph from FE

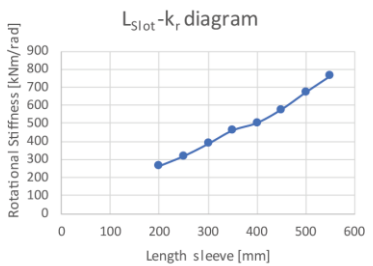


Figure T.2: Design graph for varying parameter  $L_{slot}$  [mm] versus the corresponding spring stiffness of the joint

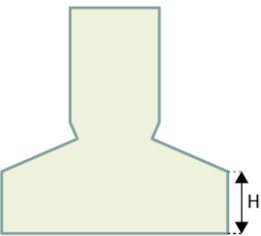


Figure T.3: Varying parameter  $H$

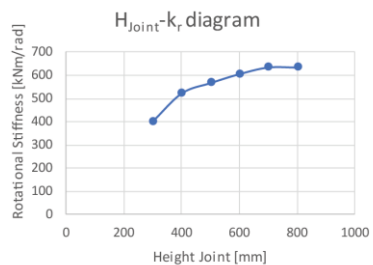


Figure T.4: Design graph for varying parameter  $H$  [mm] versus the corresponding spring stiffness of the joint

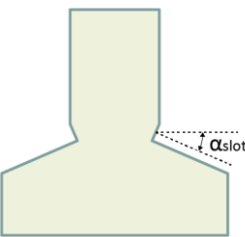


Figure T.5: Varying parameter  $\alpha_{slot}$

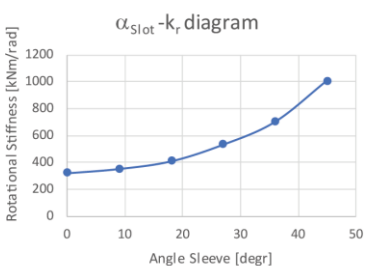


Figure T.6: Design graph for varying parameter  $\alpha_{slot}$  [mm] versus the corresponding spring stiffness of the joint

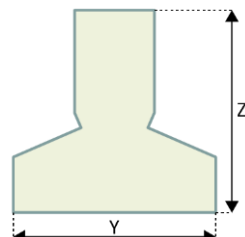


Figure T.7: Varying parameter Size

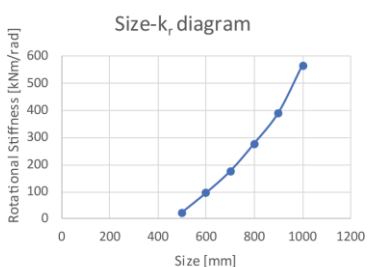


Figure T.8: Design graph for varying parameter Size  $y,z$  [mm] versus the corresponding spring stiffness of the joint

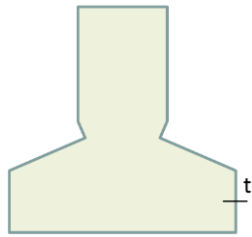


Figure T.9: Varying parameter thickness

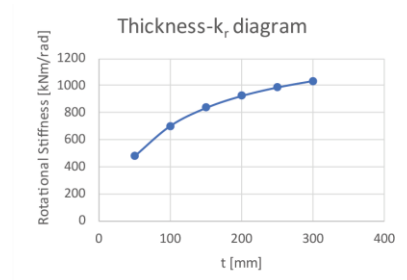


Figure T.10: Design graph for varying parameter thickness [mm] versus the corresponding spring stiffness of the joint

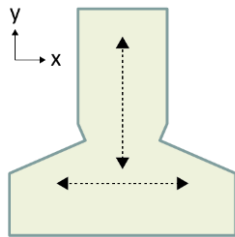


Figure T.11: Varying parameter Layer orientation

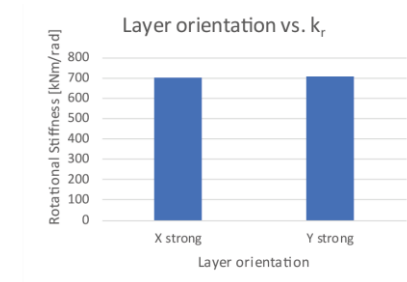


Figure T.12: Design graph for varying parameter layer orientation [mm] versus the corresponding spring stiffness of the joint



## Appendix U. Explanation of Variables for Robotic Fabrication

*Variable*

*Explanation*

### a. Layer height of Toolpath

*Description*

A robot mills a geometry in different layers. The larger the height of a single layer, the longer the toolpath and the greater the accuracy. A user can set the layer height of the toolpath manually.

*Type*

*Number*

*Example*

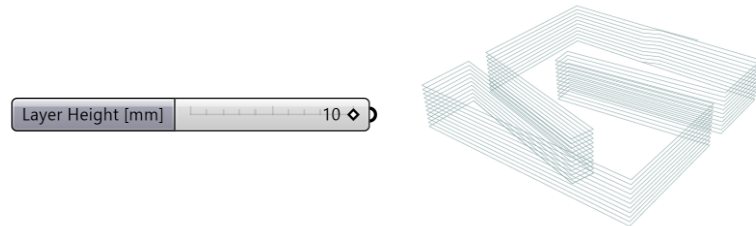


Figure U.1: Grasshopper Component and geometry of layer height of toolpath



Figure U.2: Layer height of the toolpath

### b. Ramp length (start/stop) toolpath

*Description*

The ramp length is used to construct the beginning and ending of the toolpath. It aligns with the toolpath before the actual fabrication (milling) starts.

*Type*

*Number*



Figure U.3: Ramp length Grasshopper component

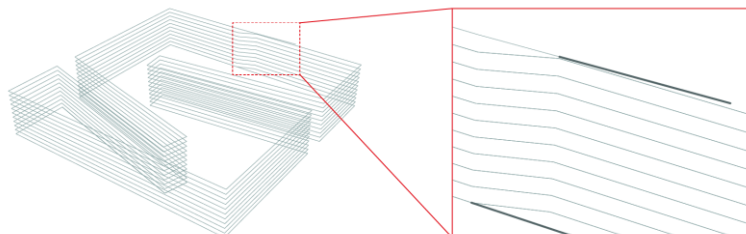


Figure U.4: Ramp length Grasshopper geometry

**c. Simulation settings**

*Description* The robotic fabrication process can be simulated for which the following input is required: the distance between the object (CLT panel) and the Tool Center Point (TCP), orientation planes for the robot and tool, and the simulation step a user wants to simulate. The entire toolpath is unitized from 0 to 1. Therefore, a simulation step  $x$  should be within the domain of  $0 < x < 1$ .

*Type* Numbers and planes

*Example*

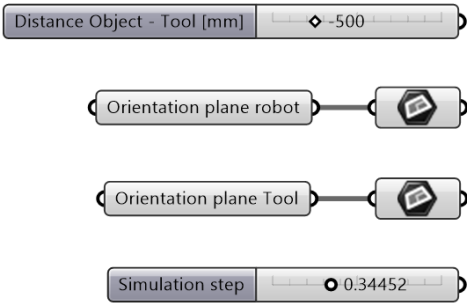


Figure U.5: Grasshopper Component and geometry of robot simulation

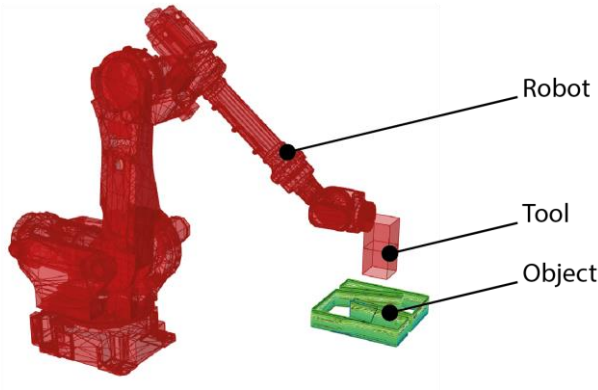


Figure U.6: Grasshopper Component and geometry of robot simulation

Appendix V. Script for Robotic Fabrication

